NATL INST OF STAND & TECH R.I.C.
A11104 123436
NIST
PUBLICATIONS

NISTIR 5256

National Institute of Standards and Technology Conference On

Reducing the Cost of Space Infrastructure and Operations

Part 2: Topical Papers

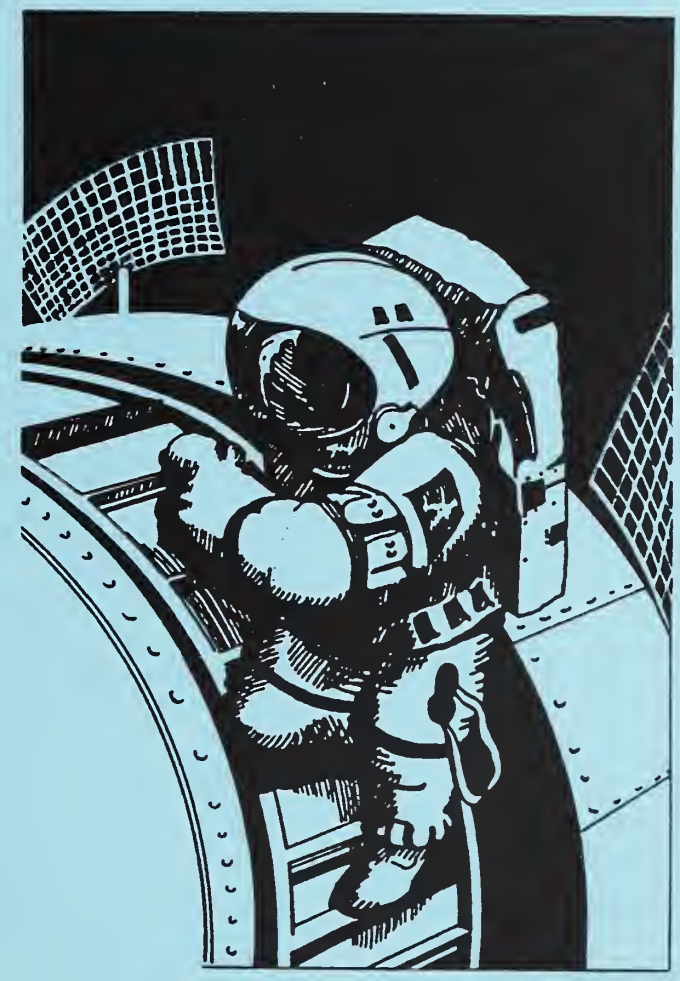

QC
100
.U56
#5256
1993

Building and Fire Research Laboratory
Gaithersburg, Maryland 20899

United States Department of Commerce
Technology Administration
National Institute of Standards and Technology

NISTIR 5256

National Institute of Standards and Technology Conference On

Reducing the Cost of Space Infrastructure and Operations

Part 2: Topical Papers

William C. Stone, Ed.

August 1993
Building and Fire Research Laboratory
National Institute of Standards and Technology
Gaithersburg, MD 20899

U.S. Department of Commerce
Ronald H. Brown, *Secretary*
Technology Administration
Mary L. Good, *Under Secretary for Technology*
National Institute of Standards and Technology
Arati Prabhakar, *Director*

Abstract

A conference was held from November 20-22, 1989 at the National Institute of Standards and Technology in Gaithersburg, Maryland for the purpose of discussing methods for reducing the cost of space infrastructure and operations. This was a multi-disciplinary group that included invited speakers from both within and outside of the traditional aerospace community. Specific comparison was made in the case of habitats and extravehicular activity with commercially successful undersea operations on earth which operate daily under more severe environmental conditions and with operating budgets on the order of 1/1000 that of orbital analogs. Other topical areas included chemical and advanced launch systems and institutional aspects including insurance and differences between top-down control and performance-based development of space infrastructure. The proceedings are published in two separate reports. Part 1, **Oral Presentations and Discussion**, contains edited transcriptions of the invited lecture presentations and of the discussion which followed each presentation and is available as a separate NISTIR report. Part 2, **Topical Papers**, is contained in the present publication and includes prepared manuscripts which were submitted in advance of the conference.

Keywords: advanced propulsion; cost reduction; unit cost; launch insurance; NIST conference; orbital habitats; space infrastructure; space suits; space transportation

List of Acronyms

ALS	Advanced Launch System
ASAT	Anti-Satellite Device
CFD	Computational Fluid Dynamics
DARPA	Defense Advanced Research Project Agency
DOC	Department of Commerce
ECLSS	Environmental Closed Life Support System
EMU	Extra Vehicular Mobility Unit
ETCO	External Tanks Corp.
EVA	Extra Vehicular Activity
FDU	Fairleigh Dickinson University
FTS	Flight Telerobotic Servicer
GD	General Dynamics Corp.
GPS	Global Positioning System
GSO	Geo Stationary Orbit
GTO	Geostationary Transfer Orbit
ICBM	Intercontinental Ballistic Missile
ISF	Industrial Space Facility
IVA	Intravehicular Activity
Isp	Specific Impulse (seconds)
JSC	Johnson Space Center, NASA
LEO	Low Earth Orbit
LRT	NOAA Launch and Recovery Transport
LSB	Life Support Buoy
MITI	Ministry of International Trade and Industry, Japan
MMU	Manned Maneuvering Unit
NASA	National Aeronautics and Space Administration
NASP	National Aerospace Plane
NBS	National Bureau of Standards
NIST	National Institute of Standards and Technology
NOAA	National Oceanic and Atmospheric Administration
OAST	Office of Aeronautics and Space Technology, NASA
OSC	Orbital Sciences Corporation
OTA	Office of Technology Assessment, United States Congress
OTV	Orbital Transfer Vehicle
RMS	Robot Manipulator System
ROV	Remotely Operated Vehicle
SDI	Strategic Defense Initiative
SDIO	Strategic Defense Initiative Office, Department of Defense
SSI	Space Studies Institute
SSME	Space Shuttle Main Engine
STEP	Space Transportation Engine Program
UDMH	Unsymmetrical Dimethyl Hydrazine

Table of Contents: Part 2

The Industrial Space Facility
Max A. Faget, Space Industries, Inc 1

The SPACE PHOENIX Program
Thomas F. Rogers, The External Tanks Corp and The Sophron Foundation 17

External Tank Habitat
Allan S. Hill, A&K Consultants 29

External Tank Work at NIST:

A Numerical Procedure for the Evaluation of Drag and Aerodynamic Torque for Convex Shells of Revolution in Low Earth Orbit
William C. Stone and Christoph Witzgall, NIST 45

Autonomous Propulsion System Requirements for Placement of an STS External Tank in Low Earth Orbit
William C. Stone and Geraldine S. Cheok, NIST 76

EVA Life Cycle Cost Issues Summary
Paul F. Marshall, NASA 89

Flight Opportunity for Small Payloads
Patrice Larcher, Arianespace 94

Commercial Launch Vehicles Using Hybrid Propulsion
Jay Kniffen, AMROC 103

Novel Integration Concepts
Edward H. Bock, General Dynamics 110

Payload Sensors
Carl F. Schueler, Hughes Santa Barbara Research Center 118

Cost Comparison Between the Space Flight and the Commercial Catalog Models of a Cesium Atomic Clock Module
Helmut Hellwig, NIST 135

Laser Propulsion Work at Lawrence Livermore National Laboratory

Pulsed-Laser Propulsion for Low Cost, High Volume Launch to Orbit
Jordin Kare, LLNL 146

Laser Propulsion and Possible Missions to Mars
Jordin Kare, LLNL 154

The Ram Accelerator as a Space Cargo Launcher
A. Hertzberg and A.P. Bruckner, Univ. of Washington 166

Appendix A: List of Conference Participants 228

The Industrial Space Facility

Dr. Max A. Faget
Space Industries, Inc.
711 W. Bay Blvd., Suite 320
Webster, Texas 77598-4001

THE INDUSTRIAL SPACE FACILITY

Near the end of the Apollo program, NASA started giving a considerable amount of attention to follow-on programs. Primary among these was a space station. For numerous reasons, various space station proposals waxed and waned during the years until the early 1970s. At that time, it was recognized that a serious commitment to a space station would also require a transportation system, preferably of a reusable nature. Consequently, the shuttle program was started and, because of financial reasons, further considerations of a space station were put aside until completion of the shuttle program. As the name implies, the primary purpose of the shuttle has always been to provide transportation service between the earth and some place in space.

Starting in 1983, Space Industries began serious studies of a man-tended, free-flyer that would be serviced by the shuttle and would, consequently, provide a place in space to which the shuttle would go. The Industrial Space Facility (ISF) has been designed strictly from a commercial perspective; that is, to be more cost effective with focus on providing power, duration and flexibility of use. Initially, it was primarily intended to be a facility wherein commercially marketable material could be processed in the space environment. The shuttle program never reached its launch rate goal in the early 1980s and was out of service over two and one-half years during the later part of the decade. As a result, the opportunities to develop materials that might have market appeal were diminished to nearly zero. Consequently, we at Space Industries

have focused our attention on research in the microgravity environment and other uses for the ISF.

Figure 1 -- Figure 1 shows the Industrial Space Facility which is a man-tended free-flyer that will be operational after one launch. The ISF is stabilized by a gravity-gradient boom. The arrangement of the gravity-gradient boom and the solar array is such that the naturally stable attitude in orbit will be upright with one solar array leading and one trailing. It will be permanently deployed in space and will be launched and serviced by the shuttle. It will be operationally compatible with Space Station Freedom. To this end, we intend to locate it in the same orbit as Freedom--either slightly ahead or behind. It will also employ a docking system that should be operationally compatible with Freedom.

It is intended that the ISF will be privately owned and operated. Standard user interfaces will be provided. For instance, user accommodation interfaces within the ISF racks will provide the same services and volume as the space station racks. Presently the ISF is on the shuttle manifest for an initial launch in early 1994.

Figure 2 -- Figure 2 illustrates the varied elements of the ISF. The main element is the Facility Module which will provide full accommodation for shirt-sleeve operation in a pressurized volume. The internal volume of 2500 cubic feet will also

house most of the user's equipment in racks or modular containers. Consequently, this equipment will be available for easy servicing during the period the ISF is docked to the shuttle. The Facility Module has a port on either end and also two side ports. These ports may be used for docking with the shuttle or to accommodate externally attached elements that would provide additional volumes accessible to the crews. The Auxiliary Module represents such an element which may be attached to these ports. Auxiliary Modules will provide up/down capabilities for resupply of consumables or changeout of payload (i.e., new racks and modular containers). An Auxiliary Module may also provide more on-orbit volume that could house additional racks and modular containers. The Auxiliary Module may also be outfitted with specialized payloads in an assembly that would not ordinarily be compatible with racks or modular containers.

Finally, Space Industries will provide a Docking System for the shuttle since none will exist at the time we plan the initial deployment of the ISF. It is our intention to construct the Docking System in a manner that would make many elements of the Docking System useful to NASA during operation of Space Station Freedom. The ISF Docking System will include a small payload container which can house two modular containers. By carrying some payload elements in the Docking System, we will be able to provide users with the opportunity for late insertion of experiment hardware prior to shuttle launch and also early access to down-transported material shortly after landing.

Figure 3 -- ISF user accommodations are illustrated in Figure 3. The users can be accommodated with racks, modular containers or external ports. These are illustrated in the figure with pertinent data as to the power, cooling and other services. It should be noted that the power capacity listed represents the power level for which the particular rack or modular container will have been wired. However, during the mission, the maximum power to all users for a sustained period will not normally exceed 7 kW. For short periods, the batteries can be drained to produce higher power levels, and for this purpose one or two racks labeled "High Power" will be equipped with heavier power circuits. The power to the various users will be scheduled to stay within the power generating capacity of the facility. The racks will be designed, insofar as possible, to be similar to space station racks. The Boeing Company is under contract to Space Industries to provide rack design and construction. Since they are also designing the racks for the space station, we feel that a high degree of similarity can be maintained. This is important since equipment that might fly on the ISF would be easily integrated onto space station racks with a minimum of design changes. The modular containers are also designed with four trays--each sized to accommodate shuttle mid-deck locker inserts. Thus, equipment which was initially developed in the shuttle mid-deck or perhaps the Spacehab may easily be reused in an ISF mission. The ISF will have three user ports that can accommodate the Auxiliary Modules or special purpose modules. ISF utilities will be made available with the berthing port locations so that such modules can obtain these services.

Figure 4 -- Figure 4 summarizes the ISF capabilities to the users, which have been discussed and illustrated in prior figures.

Figure 5 -- Figure 5 provides a comparison between the ISF and other orbiting facilities. Shown on the figure are pertinent performance and operation parameters for SpaceLab, Eureca and Space Station Freedom, as well as those for the ISF. It should be noted that with the exception of full-time manning, the ISF compares well with these other microgravity facilities.

Figure 6 -- Up until now, the ISF has been discussed primarily in terms of its performance and utilities as a microgravity laboratory. However, we feel that the ISF provides a number of other interesting applications. It can be viewed as a powered LDEF, providing a test bed for both space technology and operations. It could also find applications as a space science platform for both cosmic and earth-looking measurements. As a bridging program to Space Station Freedom, it provides an opportunity for developing numerous operations and perhaps a facility that could participate in the build-up of the space station itself. Finally, for processing commercially useful material, the ISF will undoubtedly provide the lowest cost facility that could provide the requisite volume, environment and isolation that may be required for a space factory.

I now would like to discuss the implications of transportation cost. Material processing activity in space is unique in that it requires transportation from orbit back down to earth in addition to up transportation. Thus, transportation cost is a significant factor in facilities employed for microgravity processing. In the case of the ISF, we have made an estimate of the total life cycle cost of the program, which would include operating the ISF, its acquisition cost, and cost of transportation including the resupply transportation. The estimated transportation cost was the dominant cost and might amount to two-thirds the cost of the entire program. If NASA were to charge the full cost of operating the shuttle instead of its current commercial rates, the transportation costs would be an even more significant factor.

The ISF can be classified as a space-based platform as opposed to terrestrial-based. Terrestrial-based platforms would include such things as Spacelab and the Eureca. Eureca provides a duration far greater than that of the Spacelab, but it does so at the additional cost of an additional shuttle mission to retrieve it from orbit. Terrestrial-based platforms must also include the cost of transporting the entire processing equipment plus the housing facility including its utilities in a round-trip to space. The total transportation cost for these facilities is significantly greater than that for a space-based platform which requires only part of the equipment to be transported to and from orbit for any given process or experiment. On the other hand, terrestrial-

based platforms have the advantage of being accessible to much more manpower for servicing, modifications, etc., than would a space-based platform. The point of all of this discussion is that even for platforms employing the most cost-effective transportation system (such as the ISF) the transportation cost dominates the total cost.

The cost of space transportation and the cost of equipment transported into space are interrelated. The reason that equipment transported into space is so expensive is because the cost of getting that equipment there is expensive and, consequently, the equipment must be designed to be as light as possible and reliable as possible for its intended function. At the same time, the transportaiton systems are designed to carry very expensive hardware into space and as a result must be made extremely reliable and, consequently, expensive. Since inception of space flight, great strides have been made to improve the reliability of launch systems with only casual attention to reducing cost, and as a matter of fact, we may argue that the cost of launch vehicles may indeed be higher in inflation adjusted dollars than the earlier versions which had very high failure rates. Certainly the achievement of the higher reliability is commendable, however, more attention need be placed on reducing transportation cost.

Figure 7 -- Figure 7 illustrates the economic considerations that would probably result if cost of space transportation could be significantly reduced. Two effects would happen. There would be a direct effect of decreasing the cost of space products and

services that would result from the reduced transportation cost. In addition, with lower transportation cost, the premium for light weight designs would be moderate, resulting in a decrease in the cost of the orbiting facility, further reducing the cost of space products and services. As a result of lowering the cost of space products and services, there would then result an increase in the variety and quantity of products and services that could be produced in a cost effective manner. This would result in an increase in the market demand for space transportation. With a larger market which affects both competition and the benefits of scale, the costs of space transportation would be further decreased. As you can see, this process, once started, will continue to reduce the cost of products and services as utilization of space increases. Clearly, a significant reduction in the cost of space transportation is the key to opening the door for wide spread commercial activity in space.

SPACE INDUSTRIES INTERNATIONAL INC.

What is the Industrial Space Facility?

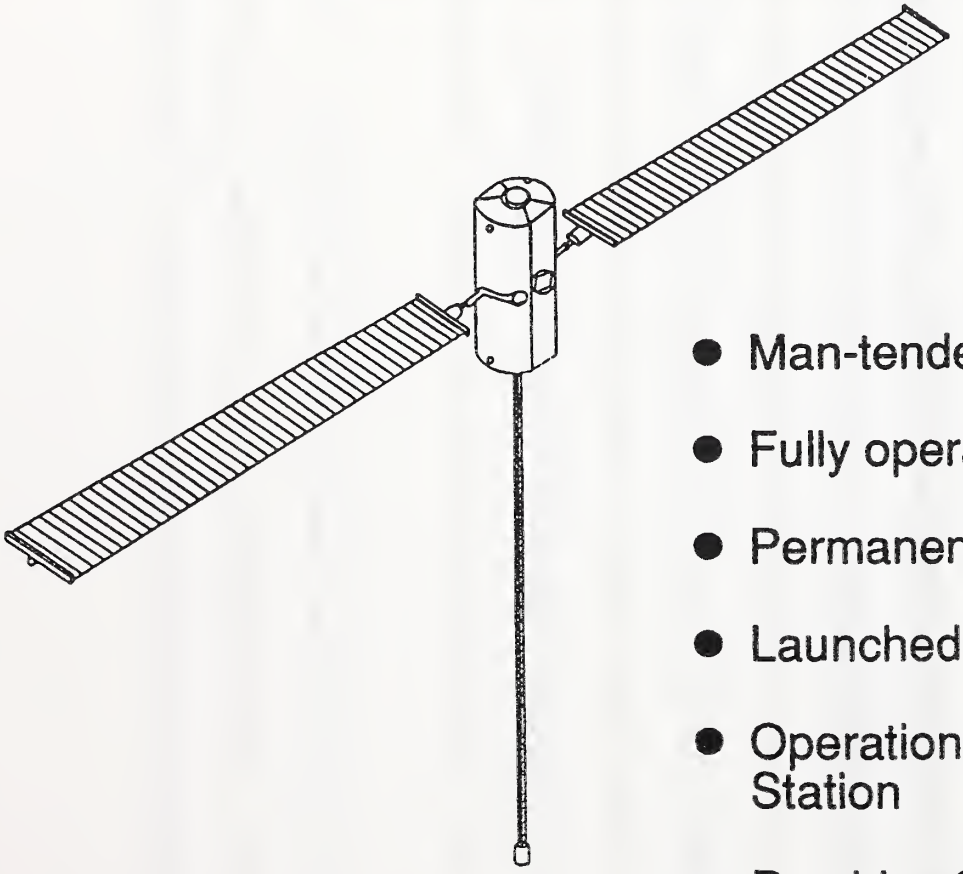

- Man-tended free-flyer
- Fully operational with one launch
- Permanently located in space
- Launched and serviced by NASA Space Shuttle
- Operationally compatible with International Space Station
- Provides Standardized user interfaces
- Manifested for Shuttle launch: February 1994
- Privately-owned and operated

Orbital Data

- 28.45° Inclination
- 291 to 500 km Altitude

89008901b:111689MAF

Figure 1

SPACE INDUSTRIES INTERNATIONAL INC.

ISF Flight Elements

Facility Module

- Man-Tended
- Remains on Orbit
- High Quality Microgravity
- Internal and External Payload Attachments

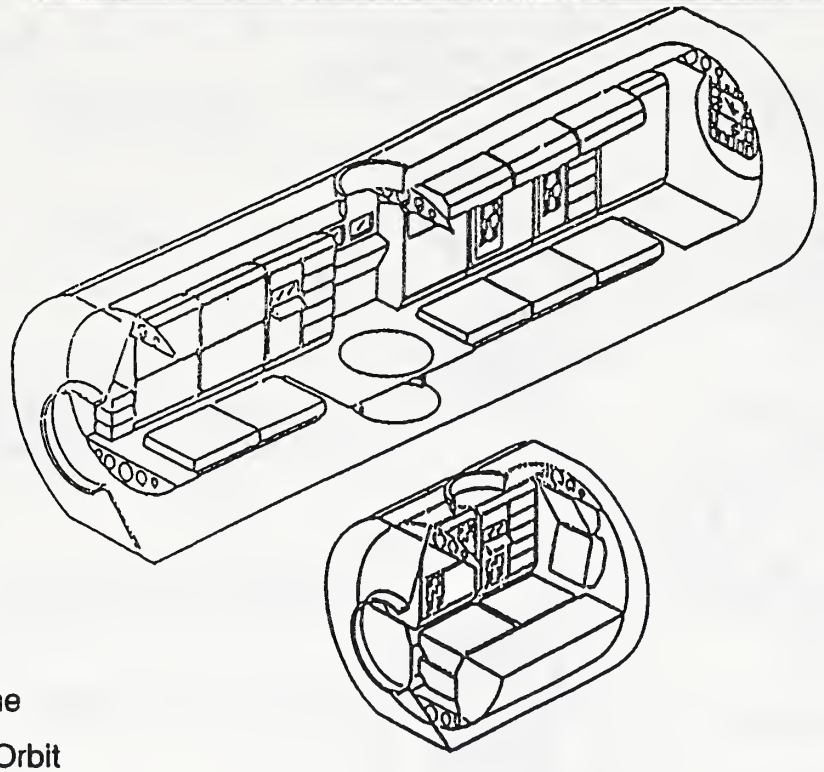

Weight:	14, 825 kg
Volume:	70.8 m^3
Length:	10.7 m
Diameter:	4.2 m
Power To User	
Continuous:	7 kW
Peak:	50 kW
User Accomm.:	7 Racks
	6 Modular Containers
	3 External Ports

Auxiliary Module

- Operational Flexibility
- Consumables Resupply
- Payload Changeout
- Additional On-orbit Volume
- Transported to and from Orbit by Shuttle

Weight:	7,063 kg
Volume:	28.3 m^3
Length:	10.7m
Diameter:	4.2m
User Accomm.:	4 Racks
	6 Modular Containers

Docking System

- Facilitates Revisit
- Provides for Payload Transfer
- Accommodates EVA
- Remains on Shuttle

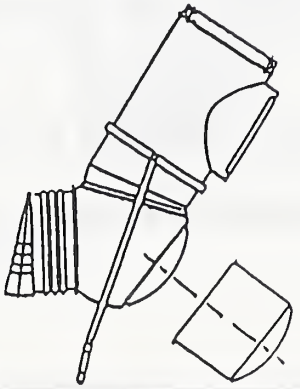

Weight:	1134 kg
User Accomm.:	2 Modular Containers

89008901c:111589MAF

Figure 2

SPACE INDUSTRIES INTERNATIONAL INC.

ISF User Accommodations

Common Racks and Mountings

- Tilt out for Easy Wall Access
- Common Interface Plate
- Replacement Unit Interface
- Complies with Space Station Envelope

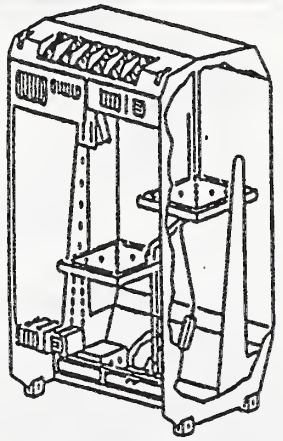

Payload Capacity:

Weight:	662 kg
Volume:	1.5 m^3
Power - Standard:	4 kW, 6 kW Peak
- High Power:	10 kW
Cooling:	5.5 kW Continuous
	16 kW Peak
Vacuum Venting:	Yes
Command and Telemetry:	Yes

Common Modular Containers

- Accommodate Middeck Locker Inserts
- Common Interface Plate

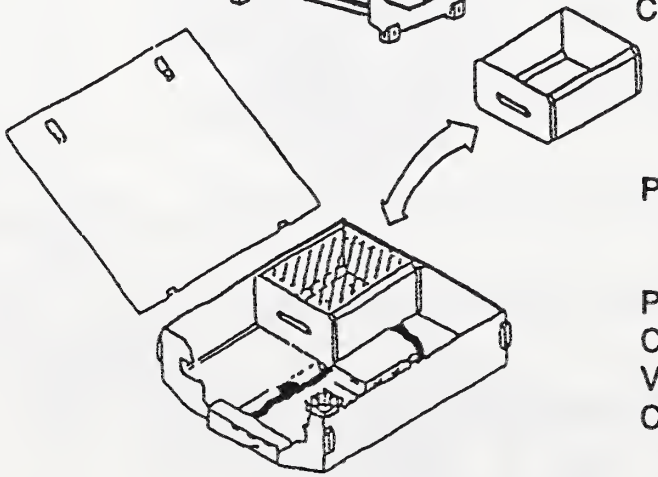

Payload Capacity

Weight:	170 kg
Volume:	0.3 m^3
Power:	0.8 kW, 1.0 kW Peak
Cooling:	1.5 kW
Vacuum Venting:	No
Command and Telemetry:	Yes

External Ports

- Flexible Interface for Mounting External Payloads
- Accomodate Special-Purpose Modules

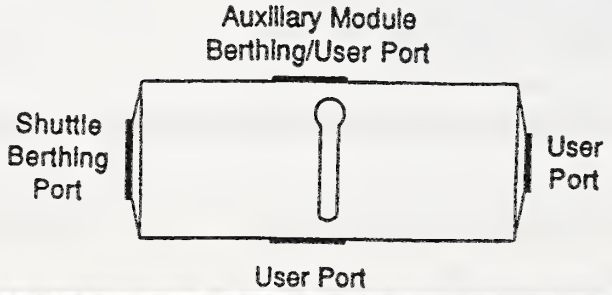

Power:	7 kW
Cooling:	4 kW
Vacuum Venting:	Yes
Command and Telemetry:	Yes

Figure 3

SPACE INDUSTRIES INTERNATIONAL INC.

ISF Capabilities to Users

RESOURCES	CAPABILITIES
7 Racks	1.5 cubic meters per rack 662 kilogram per rack (max)
6 Modular Containers	0.3 cubic meters per modular container 170 kilograms per modular container (max)
Mission Duration	120 - 180 days
3 Attachment Ports	Accommodation of external payloads
Continuous Power (average)	7 kW
Energy per Mission	12,000-17,000 kW-hrs.
Level of Microgravity	10^{-6} g up to 0.1 Hz; 10^{-5} g up to 1 Hz

Figure 4

SPACE INDUSTRIES INTERNATIONAL INC.

Characteristics Comparison

Spacelab	Eureca	ISF	International Space Station/ Columbus
-	Long Duration	Long Duration	Long Duration
-	-	High Power	High Power
Large Pressurized Volume	-	Large Pressurized Volume	Large Pressurized Volume
-	Highest Quality Microgravity	Highest Quality Microgravity	Microgravity Subject To Disturbances
Manned	-	Man-tended	Manned
-	-	Remains On Orbit	Remains On Orbit
-	Automation Emphasis	Automation Emphasis	Automation Emphasis
-	-	Station Compatible	N/A
-	-	Continuous Operations	Continuous Operations
1989	1991	1994	Late 1990s

89008901f:111689MAF

Figure 5

SPACE INDUSTRIES INTERNATIONAL INC.

ISF General Applications

- A microgravity laboratory (10^{-5} to 10^{-6} g)
- An on-orbit testbed for:
  - Technology
  - Operations
- A space sciences platform for:
  - Observation
  - Measurements
- An International Space Station support platform
- A processing/manufacturing facility

Figure 6

SPACE INDUSTRIES INTERNATIONAL INC.

Space Commercialization: Economic Considerations

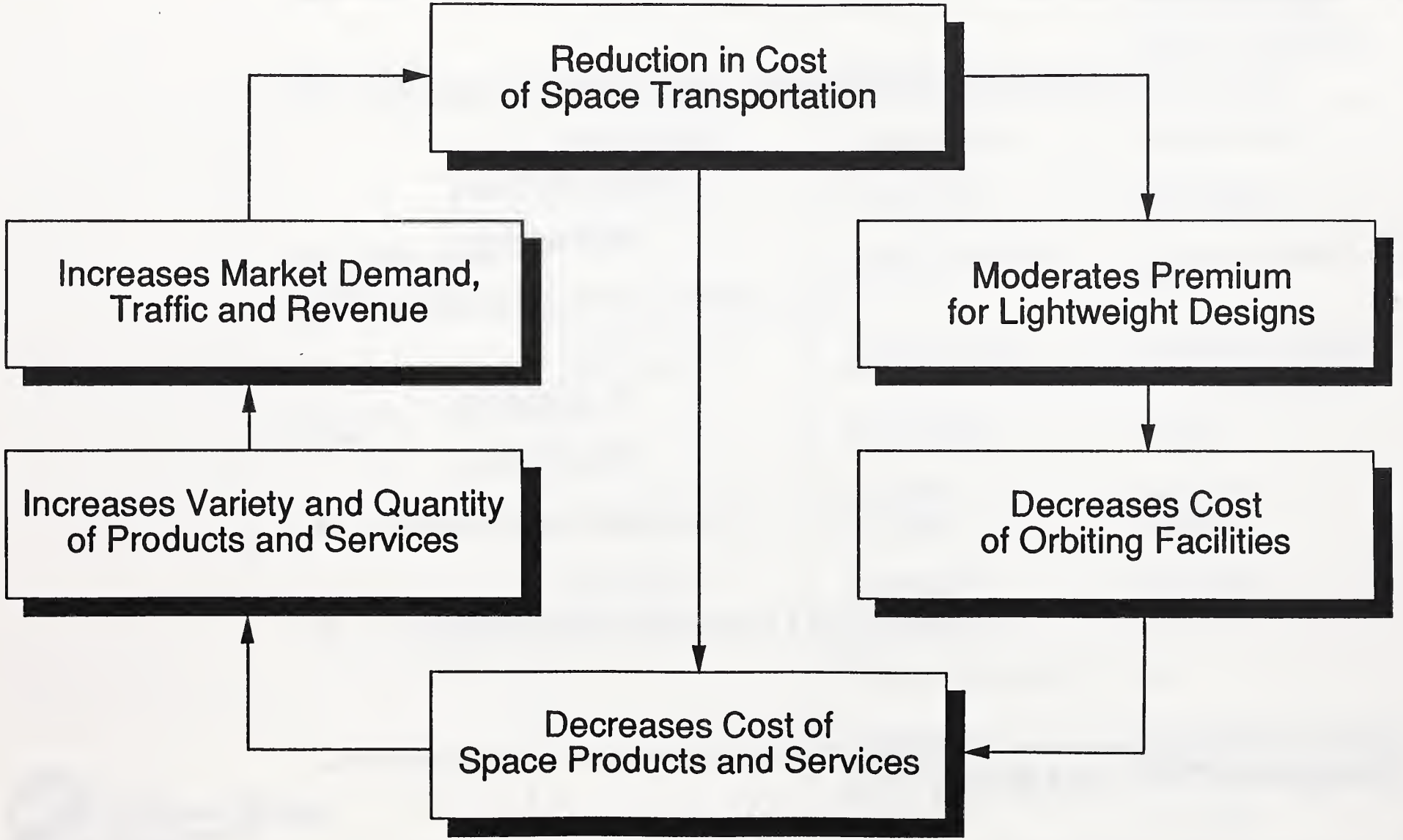
Reduction in Cost of Space Transportation
Increases Market Demand, Traffic and Revenue
Moderates Premium for Lightweight Designs
Increases Variety and Quantity of Products and Services
Decreases Cost of Orbiting Facilities
Decreases Cost of Space Products and Services

89008901a:111589MAF

Figure 7

The SPACE PHOENIX Program

Thomas F. Rogers
The External Tanks Corp. and The Sophron Foundation
7404 Colshire Drive
McLean, Virginia 22102

There are four fundamental reasons that can be advanced for placing assets in space and conducting activities there: (a) Social, (b) Cultural, (c) National Security, and (d) Economic.

As to each:

(a) To date, there are no purely Social reasons;

(b) There are the valid Cultural reasons of scientific research and exploration and, just as the public supports symphony orchestras, parks, sculptors, etc., it supports these kinds of activities -- but at a relatively modest continuing level;

(c) In the Post-Sputnik and Post-Gagarin era, i.e., during and since the Mercury, Gemini, Apollo days, by far the most important reason for the large and continuing public support of the civil space area has been that of National Security. But now it is clear that "The Russians are NOT coming" -- the military and political threat of the Soviet Union is, per se, no longer a reason for the conduct of civil space activities of important scale; and

(d) Therefore many continue to look to the Economic reason for spending large sums re space. But, except for somewhat improved weather forecasting, the only large-scale economic return on the some $500 billion [inflation-adjusted 1989 dollars, inclusive of an opportunity cost of modest rate] that the American public has obtained in the civil space area is that of satellite communications -- and that fine example is over a quarter of a century old. And now (to modify the observation in (b), above) "The Russians ARE coming in the space area -- in a diligent search throughout the world for space business."

[Study of our own planet from space is in a special category, inasmuch as such studies can combine elements of all four of the above reasons.]

Why have we failed to secure an adequate economic return on our great civil space public investment? By far the most important reason is the enormous costs of space assets and space activities, and the inability of our space industry and our space government offices to bring them down.

Whatever else can be said about civil space assets and activities, it must be said that they are extraordinarily costly. Relative to their earthly analogues, space costs continue to be higher by factors of 100X-10,000X. To the potential space businessman, such unit costs are simply numbing to contemplate. It's no wonder that, in spite of the earnest striving by many within our business and government sectors to "commercialize" space (and, again, with satellite communications excepted) we have simply failed to see private investments attracted to the civil space area on a large scale and to see space usefully exploited for Economic reasons.

In this context it is most important that attention be paid to the unexpected and historic political events commencing in Poland and the Soviet Union a very few years ago, spreading to the latter's Baltic republics, then to Hungary, and accelerating rapidly during just the past month to encompass the German Democratic Republic and Bulgaria. These have been the long hoped-for culmination of the four and a half decades of political, military, and economic "containment" of the Soviet Union and its Eastern Bloc and other allies by the United States of America and the other member nations of the North Atlantic Treaty Organization. But this grand international political advance has been purchased at a terrible, terrible, cost of blood and treasure. And some of the impacts of these economic costs upon our society are hardly yet recognized, let alone appreciated.

To one significant figure, the United States of America alone has probably spent some 20,000,000,000,000 (1989) dollars, i.e., $20,000 billion, in this long global containment effort. This is the sum spent by our Department of Defense, the Central Intelligence Agency, the nuclear weapons section of the Department of Energy, and for foreign military and other assistance, etc., to contain the international thrusts of Communism over the past two generations, awaiting the day when this year's earthshaking geopolitical events would take place.

This fact -- the spending of such an almost unimaginable sum by our Federal Government for national security purposes -- is central to the circumstances that now permeate our civil space area, that prompted the creation of the SPACE PHOENIX Program, and that led, indirectly, to the calling of this Conference by the National Institute of Standards and Technology (N.I.S.T.).

For the influence of this enormous, multi-generational, Federal Government spending has created a space industry of a most peculiar character when viewed from the perspective

of the long term economic interests of the United States of America. It has warped the economic character of the civil space area to zero order. The spending of such a large sum over such a long time under circumstances of fear, haste, political influence, and little if any relationship between cost and economic value, has resulted in our having a space industry and its related government offices of truly great defense accomplishment -- but just as great economic inefficiency. And now the United States and, especially nearly all of our space scientists and engineers, and their managers and government financial supporters, must begin to climb down from this anti-economic "addiction" after having been on it for all of their professional lives. (See the Appendix.)

An excellent example of this professional "warping" in the space industry has just been provided by the American Institute Of Aeronautics And Astronautics (A.I.A.A.). It conducted a wide-ranging study on "space commercialization" that was reported under the title of: "Issues in Strategic Planning for Commercial Space Growth". Consider that, today, a person may travel the 200 miles between New York City and Washington, D.C., for some $100 or less, while the cost to the Government (i.e., to all of us) of sending an astronaut up to a 200 mile orbit is some $100 million; that we can purchase electricity for home use at a cost of less than 10 cents per kilowatt-hour, while in low Earth orbit it costs some $100 per kilowatt-hour; etc., etc. Yet, while making some very brief and general statements about cost, when the A.I.A.A. came to listing the specific "Issues" in the matter of increasing private sector activity in space (see its report's "Issues and Barriers" section which lists eight items as "Specific concerns" -- among them such unusual inhibitions as "Conflicting voices among various government agencies", "Excessive government red tape", and "the fickleness of government commitments") the A.I.A.A. didn't even mention the matter of space costs at all !

The pacing element in the exploitation of space for Economic purposes is space transportation. For instance, the true unit cost of placing anything into Low-Earth-Orbit with the Shuttle fleet is some $10,000 per pound. If the civil space area is ever to prosper in the business sense, the unit cost of space transportation simply must be reduced, and reduced sharply. Unfortunately, no one now knows specifically how to do this.

Whenever the cost of space transportation is spoken to, almost invariably the cost referred to is that of its ongoing Operations and Maintenance, i.e., O.& M., cost. Hardly ever mentioned is the cost to acquire the vehicle fleet.

But note that the cost of designing, engineering, producing, testing, and correcting for early system weaknesses in, the Shuttle fleet was some $40 billion (in 1989 dollars and inclusive of an opportunity cost of modest rate). Amortizing this acquisition cost over a few decades at today's Government borrowing rate suggests an annual acquisition charge of some $4 billion per year. And note also that, during each of the two years immediately prior to the Challenger disaster the total, military plus civilian, payload launched to orbit by the U.S.A. was some 600,000 pounds.

Therefore, if any other new space transportation vehicle-fleet costing the same amount as the Shuttle were to launch, say, 2/3 of this payload in the future (the remaining 1/3 would be launched by E.L.V.s) than the unit cost of doing so would be at least $4 billion/400,000 #s = $10,000 per pound -- i.e., even if the O.& M. costs were to be reduced to <u>zero</u> the total unit cost of space transportation would not be reduced at all!

And the burden of proof is upon anyone in the space industry who would say that his/her organization could provide a next generation vehicle-fleet with essentially the same or better weight/volume/reliability as the Shuttle fleet at a cost of, say, 1/10th of $40 billion. (A willingness to accept a fixed price contract with penalty clauses to do so would be an acceptable initial proof.)

Thus, if the unit cost of space transportation is to come down sharply, other means than today's government-space industry methods and means will have to be used, and/or the total payload to be launched per year will have to be increased sharply. And the payload will have to be privately paid-for payload.

This is the <u>raison d'etre</u> of the SPACE PHOENIX Program: the Program seeks to provide large amounts of habitable infrastructure in L.E.O. at a very low unit cost so as to allow, and stimulate, a large market for the conduct of a wide variety of civil space activities. It envisions a space market so large and evident that, eventually, it should prompt a fundamental reassessment of the space transportation area, and a concentration by the aerospace industrial-Government community on private, large volume, passenger carrying, vehicle-fleet capabilities.

In essence, the SPACE PHOENIX Program is concerned with the creation in space of large amounts of what, at the Earth's surface, would be described as "raw land" at a very low unit cost. In space, the absence of a breathable atmosphere requires that the "raw land" be provided in the

form of pressurized volume so that human life can be supported there.

Each Shuttle trip sees a very large External Tank (ET) carried up nearly to orbit, where, at main engine cut-off, the ET is released from its people-carrying Orbiter and falls back toward the Earth to destruction. Each ET consists of an oxygen pressure vessel, a much larger hydrogen pressure vessel, and a smaller unpressurized intertank volume separating the two. Placed into orbit, each 150 foot long, 28 foot wide, ET would provide some 70,000 cubic feet of pressurized, and some 5,000 cubic feet of unpressurized, volume.

Program studies conducted to date suggest that an ET could be safely delivered to a high long-term storage orbit for less than $10 million. That is, the Program would obtain a discarded, but potentially very valuable space asset, without having to pay either its cost of some $30 million or the cost of $ several hundreds of millions to place it into orbit.

Other Program studies suggest that, with imagination, determination, and large volume operations, each of a series of ETs could be stabilized, modified, and outfitted with basic life-support capability at an additional cost of some $100 million each. These studies also suggest that, unconstrained by government assistance and financial limitations, a first test-demonstration ET could be orbited in some 3 years from the time that a decision were made to do so. And a follow-on ET inhabitable laboratory facility could be made available in L.E.O. to supplement the Government's Extended Duration Orbiter and Space Station scientific research capabilities some two years thereafter.

The SPACE PHOENIX Program is organized around three organizations:

a) The University Corporation for Atmospheric Research (U.C.A.R.), a not-for-profit organization that sees nearly 60 Universities and other senior research groups conducting scientific research on weather and climate;

b) Its not-for-profit U.C.A.R. Foundation, charged with realizing financial income from the intellectual property that continues to be created by the U.C.A.R. professionals; and

c) The External Tanks Corporation (E.T.C.O.), a private Corporation that is charged by U.C.A.R., its majority stockholder through its Foundation, to provide the financial,

business, and technical resources required to see the ETs of the Shuttle fleet employed in space for scientific and commercial purposes.

U.C.A.R. and the Federal Government, specifically the National Aeronautics and Space Administration (N.A.S.A.), signed a Memorandum of Understanding in 1987 attesting to the shared interest of both parties in seeing the concept of additional in-space use made of the Shuttle fleet's ETs explored. And, last year, U.C.A.R. and N.A.S.A. signed a Memorandum of Agreement which positions U.C.A.R. and E.T.C.O. to employ the unpressurized intertank volume of five ETs on one-hour suborbital spacetrips.

E.T.C.O. has obtained some $1 million of equity money and has been conducting ET related technical and operating studies. U.C.A.R. is now in negotiations with the Federal Government that would see U.C.A.R. obtain access to the first ETs in orbit, and is searching out an increased equity base in the financial community.

The SPACE PHOENIX Program is continuing to advance toward its objectives of seeing ET mass, physical and chemical properties, unused fuel, surface, unpressurized and pressurized volume, and nearby space employed for widespread scientific and commercial purposes in a businesslike fashion. The Program's first ET orbital facility is now expected to be a laboratory, to be followed by others that will have private uses remote from those of science and technology.

The SPACE PHOENIX Program welcomes the entry of the Department of Commerce's N.I.S.T. into the civil space area. It is particularly welcome inasmuch as it will concentrate upon by far the most important problem faced by the United States as it continues to seek a satisfactory economic return on its great, and continuing, public investment in the civil space area. Working with and for American commercial and industrial interests, our Federal Government's National Institute of Standards and Technology could be most helpful as, together, we all tackle the fundamental inhibition to the creation of a large new space business: reducing, sharply and soon, the unit cost of basic space assets and activities.

Summary Observations

Considering the papers presented to the Conference and the discussions which they prompted, the following appear to be reasonable observations to the Department of Commerce and its National Institute of Standards and Technology.

1. The profoundly altered international situation has now removed any national security consideration as an important justification for the conduct of a large publicly funded civil space program. That is, there is no likely threat on the part of the Soviet Union or countries closely allied to it that would prompt a large civil space response on the part of the United States of America. A, perhaps the, major thrust in the civil space area now must become economic.

No country is particularly well positioned to mount such an economic space thrust because the costs of space assets and activities are so enormous as to require that they be met from the public purse. Consequently, throughout the world support of most space activities still develops essentially for political, not economic, reasons and there is a paucity of ideas about what kinds of businesses could be conducted in and re space. Apparently, and ironically, only the Soviet Union is mounting a thrust whose undisguised purpose is to do commercial space business on a global basis.

Under these fundamentally changed circumstances the Department of Commerce clearly should play a leading role in seeing the United States now move out in space for economic reasons, and the Secretary of Commerce might well reassess his responsibilities and opportunities in the space area.

2. The economic prospects of the United States civil space area would be markedly enhanced if the technology-related professional talents and experience of N.I.S.T. could be addressed to the most basic problem now facing the civil space area: the absolute necessity of reducing the unit cost of basic in-space infrastructure and activities. If N.I.S.T. were to do so, it would be valuable in its own right, and it would also prompt a re-thinking of the space transportation field from a high volume operation, unit cost-reduction, perspective. If unit costs could be reduced by a large factor, and there is now clear evidence to suggest that this is the case, a whole new space commercial-industrial business area of large potential dimension could be opened. Therefore, N.I.S.T should feel encouraged to lead in studies in

this area -- an area basic to the general interests of the Department of Commerce.

And, of course, when space unit costs are reduced in the private sector, the influence thereof would soon be felt in the government sector as well. Keeping in mind that the government sector now spends over $25 billion per year on space goods and services, N.I.S.T. could well become a direct and important friend of the American taxpayer.

3. Specifically, N.I.S.T. should draw upon two areas of long term and particular interest to the Department of Commerce:

a) It should draw upon the unique experience gained in the N.O.A.A. "Aquarius" acquisition and operation programs, and the related private deep sea diving business, to see that the technologies developed and operating experience already obtained therein are transferred to the space area as quickly, broadly, and prudently as possible.

Much of today's undersea habitable infrastructure, human pressure suits, human-assisting robot equipments and vehicles, and undersea "E.V.A.", are remarkably similar in many basic respects to their in-space analogues, but the cost of undersea assets and activities is less by some three orders of magnitude.

And, as well, N.I.S.T. excells in the application of human-assisting automation and robotic advances to the conduct of human activities under particularly difficult environmental circumstances.

b) It should draw upon its long and direct experience with the design and testing of large, habitable, civil structures, and their safe and satisfactory operation under difficult environmental circumstances, to learn how large habitable pressure vessels could be placed into Low Earth Orbit safely and economically, and modified and outfitted so as to support people therein in the conduct of a wide variety of space business activities. It could do so by studying the additional in-space use of the so called External Tank space qualified pressure vessels, with their valuable residual gases, which could be made available in space as a by-product of the ordinary operation of the U.S. Government's Shuttle fleet.

The United States could see a large number of ETs placed into long-term orbit where they would be the space equivalent of very rare "raw land", i.e., the only "land"

between the Earth and the Moon a quarter of a million miles away. Many of the skills and experiences of N.I.S.T. could address the matter of seeing "betterments" applied to this land in such a fashion that it could be made available to United States business interests at a relatively very low unit cost -- "land" that is not available to any other country than the Soviet Union.

Analogous unit cost reduction studies could also be made for other, more specialized, habitable, space pressure vessels of the type now being considered for use in such private sector business programs as the Industrial Space Facility and Spacehab.

Appendix

Let me illustrate by touching upon my own professional career:

Throughout all of my life through the completion of undergraduate studies, I, my family, and all of my acquaintances had to be very careful about the spending of about every bit of money that we possessed.

In December, 1944, I undertook my first professional employment in a secret university laboratory supported by the Federal Government that was devoted to the defeat of the German and Japanese military radar capabilities. I was immediately provided with all of the instruments, materials, tools, books, and technical and administrative support that my work required, essentially upon request -- I could even be given amounts of cash to make quick local purchases. The question of cost never arose: there was a war on; people were being killed, wounded, and imprisoned; we were working to hurl back the totalitarian darkness.

With World War II over, by the end of 1945 I was working in the private sector as an electronics engineer on television receiver design, and all of my "economic signals" were reversed. Hardly a day went by in which I was not reminded about costs, for costs were related to prices, and prices were related to sales, and sales were related to profits, and profits to the health of my company and to my continued employment and income.

By 1948 I was again working in a secret (Government) laboratory now supporting our airlift to a beleaguered Berlin cut off from the West by Soviet military forces deep within East Germany. My "economic signals" were reversed again: now, for a second time, cost hardly mattered.

Thereafter, for more than the two decades I worked on a series of very high technology military projects, so-called "crash projects": the arctic Distant Early Warning line, the SAGE air defense system, the Atlas intercontinental ballistic missile, the Polaris strategic nuclear system, and various strategic command and control systems. Cost was of little concern: there was a "cold war" on; people were being terrorized, imprisoned, and killed; the very existence of our Country and western civilization was at stake.

And then, in 1964, at the very end of a meeting with the (then) Secretary of Defense, he informed me that he was

completely satisfied with the characteristics of what was to become the world's first global satellite communications system that I had just described to him, but that he wouldn't approve of it because it would cost too much. I was taken aback -- of all the things that I might have expected him to say, that my plans might be seen to be too expensive to obtain his support had never entered my head! But, within little more than a month I was able to go back to him with a system design of equivalent performance and a program cost reduced by 70% !

I never forgot that. Twenty years after my television engineering experience I had been unexpectedly told again that cost really mattered. And I very quickly found out that our aerospace universe was composed largly of financial "water" -- costs that, with determination and imagination, could be squeezed out without sacrificing basic operational performance.

My professional experience suggests that today, unless he or she has entered the civil space community from a position in an ordinary commercial-industrial organization, any space engineer or manager younger than some 60 years of age will have had little if any useful experience dealing with the true economic costs associated with the development and exploitation of advanced technology. Thus, nearly all of our present space industry professionals will have to learn a whole new way of professional life. And it will do them little good to communicate with each other about how to do so, or with Federal Government space offices, for all of these professionals are "in the same boat".

External Tank Habitat

Allan S. Hill
A&K Consultants, Inc.
11204 SE 286th St.
Kent, Washington 98031

EXTERNAL TANK HABITAT

Allan S. Hill

1. Background

This presentation summarizes a study conducted for the Sophron Foundation to evaluate the technical feasibility and operational approaches for using STS expended external tanks (ET) for orbital missions. The study was charged specifically with answering the questions posed in Table 1.

A detailed study report of approximately 170 pages was prepared and submitted to the Sophron Foundation with considerably more programmatic, technical and cost detail than is presented in this paper and should be consulted for substiating technical analyses, cost and schedule data, study constraints, assumptions and ground rules. In addition, the report defines specific areas for further study that deserve consideration by this audience.

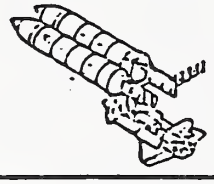

Table 1. Study Direction/Requirements

(a) From an engineering viewpoint, how can the Shuttle ET's be brought together in orbit, stabilized, purged, interconnected, modified, tested and made ready for use at very low initial and on-going cost?

(b) What would be the major phases of such an engineering assembly, modification and test program and how long would it be expected to take?

(c) What are the significant engineering, assembly, modification and testing problems that require further detailed consideration? Do any of them appear to require either a priori surface or in-orbit development?

(d) What are the weaknesses of the basic concept?

(e) What are the important cost and schedule drivers?

(f) What are the overall initial and on-going costs likely to be, to one significant figure?

2. Introduction

In this brief presentation I'm going to describe the design and operational features of the system concept defined in our study, discuss some key technical problems and their proposed solution and summarize preliminary schedule and cost analyses. Figure 1 shows the overall configuration developed[1].

First of all, the context of this study must be understood. We are not discussing a fully outfitted, totally operational, complex space station. This was not an exercise in using ET's as an alternative to the NASA Space Station program. This was a study to develop an on-orbit "warehouse" concept. Perhaps a terrestrial analogy is appropriate: a commercial developer here on Earth acquires land, obtains financing and architecture - engineering services, erects an empty building, ties in the utilities, paves the parking lot, hangs up a "For Rent" sign and markets the buildings space. The concept we studied took expended ET's delivered to orbit, captured and stabilized them, provided the necessary thermal and micrometeoroid protection and attached Control Modules with all required support subsystems, i.e., the "utilities". We then had a habitable, but empty, basic on-orbit facility to be utilized by someone as he/she sees fit. We didn't provide the "For Rent" sign - that's Tom Roger's job.

Figure 1. Dual ET Baseline Configuration

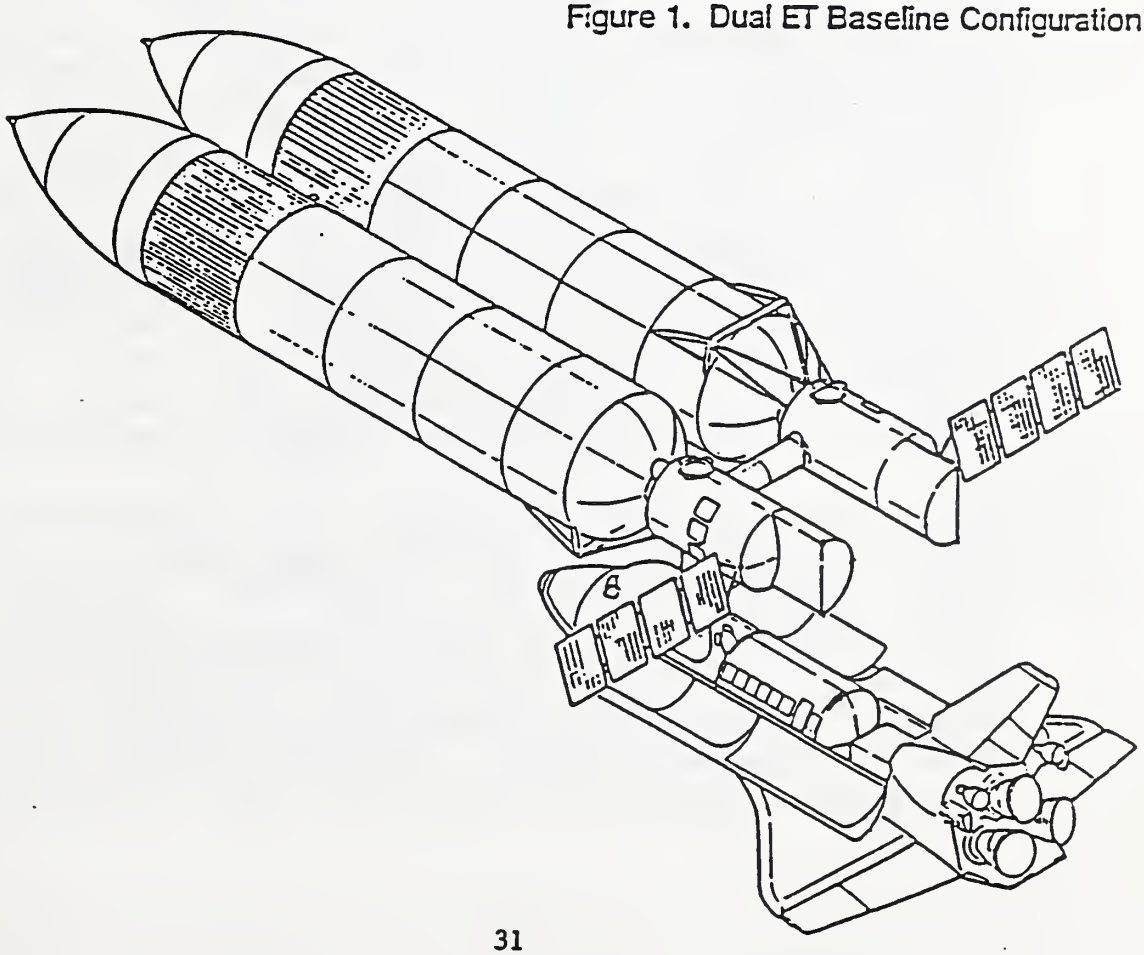

3. Technical Features.

As you might imagine, there are a number of exciting ideas and many interesting engineering challenges associated with adapting ET's for use on orbit. NASA, Martin Marietta (the ET fabricator) and others have studied these in detail and there are considerable data published addressing some approaches.[2-6] Let me briefly highlight the more critical problems and note the solutions we developed.

a. ET Modifications. The ET, being a propulsion system element, has some particular features that must be modified to allow its use on orbit. Table 2 summarizes the problems and the fixes required. Typically, these are redesigns that must be incorporated, probably by Martin, into the ET prior to launch. They are not major projects, but certainly are not insignificant changes. Martin has already looked at these under contract to MSFC and has defined their design solutions and cost impact.[7] We assumed in our study that we were working with ET's incorporating these changes.

A word about residual propellants - when separated from the shuttle, the ET still contains some 12,000 pounds of residual LOX and LH_2 in the form of liquid and gas in the tanks and trapped propellants in the lines. It has been suggested that these propellants be retained and used on orbit for ET maneuvers, attitude control or in fuel cells for power generation. Other studies are underway to define techniques for "capturing" the residuals and using them. (By the way, this is not an easy job in engineering terms). In our study we considered the residuals to be undesirable contaminants and our approach was to fully vent and then purge the tanks prior to sealing them and initializing the life support system. Other approaches, if deemed possible, can certainly be incorporated.

b. On-orbit Stabilization and Control. When jettisoned from the Shuttle the basic ET will tumble randomly because of tip-off forces, aerodynamic drag, solar pressure, etc. Capturing the massive ET after that event would be extremely difficult, risky and costly. In our study we developed the concept shown in Figure 2 whereby the ET is stabilized by the Shuttle on orbit during the initialization process. The Control Module containing the support subsystems is carried into orbit in the Shuttle

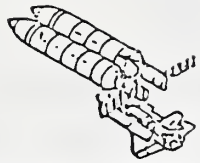

Table 2. Prelaunch ET Modifications Required

Item	Existing Conditions	Mods Required
Tumble Value	Pyro operated; opens to vent LO_2 tank perpendicular to tank center line to impart tumble for reentry debris footprint control.	Deactivate or remove for missions intended for on–orbit use of ET.
ET to Shuttle Latches	Not designed to positively release with zero relative velocity.	Redesign latches and provide for positive ET/shuttle separation for missions intended for on–orbit use of ET.
Intertank and ET Bulkhead Hatches	Permanently bolted, load carrying hatch covers.	Provide for on–orbit disassembly or redesign hatches to accommodate hinged, unlatchable covers.
Range Safety System	Destroys LO_2 and LH_2 with linear shaped charge upon receipt of destruct command.	Deactivate after launch for missions intended for on–orbit use of ET.

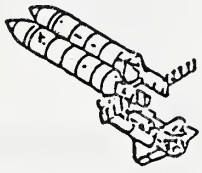

Figure 2. Selected Initialization Concept

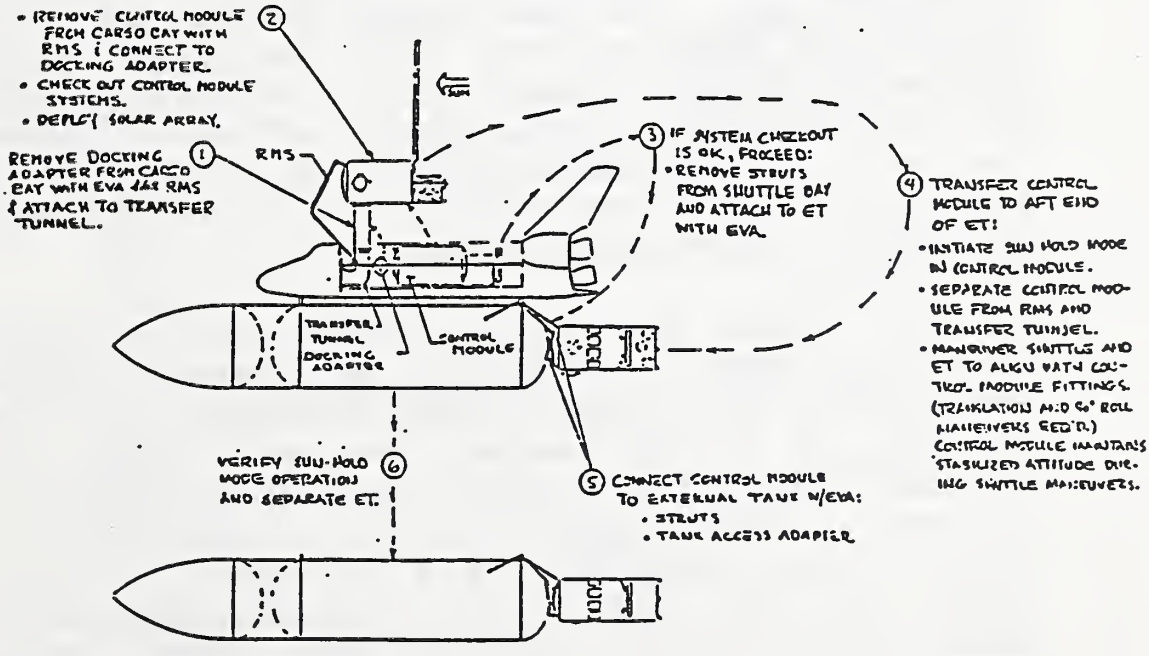
• REMOVE CONTROL MODULE FROM CARGO BAY WITH RMS & CONNECT TO DOCKING ADAPTER.
• CHECK OUT CONTROL MODULE SYSTEMS.
• DEPLOY SOLAR ARRAY.
2
REMOVE DOCKING ADAPTER FROM CARGO BAY WITH EVA AID RMS & ATTACH TO TRANSFER TUNNEL.
1
RMS
3 IF SYSTEM CHECKOUT IS OK, PROCEED:
• REMOVE STRUTS FROM SHUTTLE BAY AND ATTACH TO ET WITH EVA.
4 TRANSFER CONTROL MODULE TO AFT END OF ET:
• INITIATE SUN HOLD MODE IN CONTROL MODULE.
• SEPARATE CONTROL MODULE FROM RMS AND TRANSFER TUNNEL.
• MANEUVER SHUTTLE AND ET TO ALIGN MATH CONTROL MODULE FITTINGS. (TRANSLATION AND 90° ROLL MANEUVERS REQ'D.)
CONTROL MODULE MAINTAINS STABILIZED ATTITUDE DURING SHUTTLE MANEUVERS.
TRANSFER TUNNEL
DOCKING ADAPTER
CONTROL MODULE
VERIFY SUN-HOLD MODE OPERATION AND SEPARATE ET.
6
5 CONNECT CONTROL MODULE TO EXTERNAL TANK W/EVA:
• STRUTS
• TANK ACCESS ADAPTER

cargo bay, deployed, checked out and attached to the ET by use of the Remote Manipulator System and EVA activities. Upon activation of the ET Control Module attitude control system and verification of its proper operation, the ET is separated in a stabilized and controlled manner. Another launch would bring a second tank and Control Module into orbit for attachment to the first ET to produce the dual tank configuration of our baseline concept.

In our study we looked at a number of on-orbit attitude control modes and selected a constant sun pointing scheme as the baseline. As noted in Figure 3, it is simple to implement, allows a fixed solar array, provides an easily analyzed thermal control condition and results in a constant solar pressure torque. We recognize this would not always be an acceptable mode for all potential users, but it is responsive to the study guidelines of assuredly stabilizing an ET on orbit, at relatively low cost. For specific missions where other modes are required, i.e., constant earth orientation or long term celestial pointing, conventional subsystem changes would be incorporated to meet user needs.

c. Environmental Protection. The existing ET design provides neither thermal control nor micrometeoroid protection for long term use in space. The boost heating insulation (SOFI) was analyzed and shown to have totally inadequate on-orbit performance. Figure 4 indicates that heat loss from the current ET would be so great it is not habitable without modifications. Even improving the insulation efficiency by a factor of 10 is insufficient. Only the use of space qualified thermal blankets provides the heat retention necessary.

The proposed design solution derived from our analyses is shown in Figure 5. It combines an 0.040-inch aluminum micrometeroid shield with conventional aerospace multi-layer insulation for a highly reliable, but relatively low cost protection system. These blankets would be pre-fabricated in segments on earth, carried into orbit on the Shuttle and wrapped around the ET using EVA techniques. Periodically spaced stand-offs would provide the 4-inch micrometeroid shield spacing necessary. The design details, blanket sizes and shapes, cutouts for access, thermal closeout provisions, etc. all

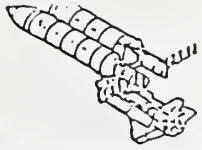

Figure 3. Attitude Control Trades

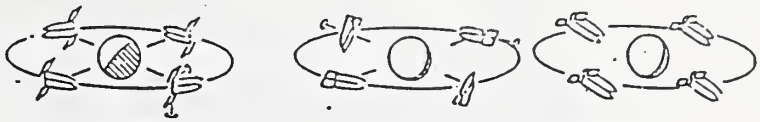

CHARACTERISTIC	LOCAL VERTICAL ACTIVE	LOCAL VERTICAL PASSIVE	EARTH POINTING W/ SUN STEERING	CONSTANT SUN POINTING
Earth viewing	Constant	Constant	Intermittent	Intermittent
Drag make-up	Any time	Separate mode	Separate mode	Separate mode
Thermal	Variable	Variable	Variable	Variable
Solar array	2-axis	Fixed	1-axis artic.	Fixed
Gravity Grad.	Zero	Zero	Constant	Zero
Solar torque	Variable	Variable	Variable	Constant
Aero drag	Constant	Constant	Variable	Variable
Control Modes: Number	Operations Docking Drag make-up	Operations Docking Drag make-up	Operations Docking Drag make-up	Operations Docking Drag make-up
Complexity	Medium	Low	High	Low
Control Limits Operations	Naturally Loose	Naturally Loose	Medium	Medium
Docking	Tight	Tight	Tight	Tight
Drag make-up	Medium	Medium	Medium	Medium
Disturbances	Minor	Minor	More Variable	Medium
Expendables	Low	Low	High	Medium
Make-up ΔV	Separate	Separate	Integral	Integral

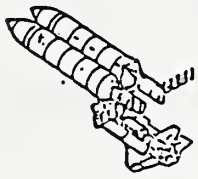

Figure 4. Orbital Thermal Analysis Results

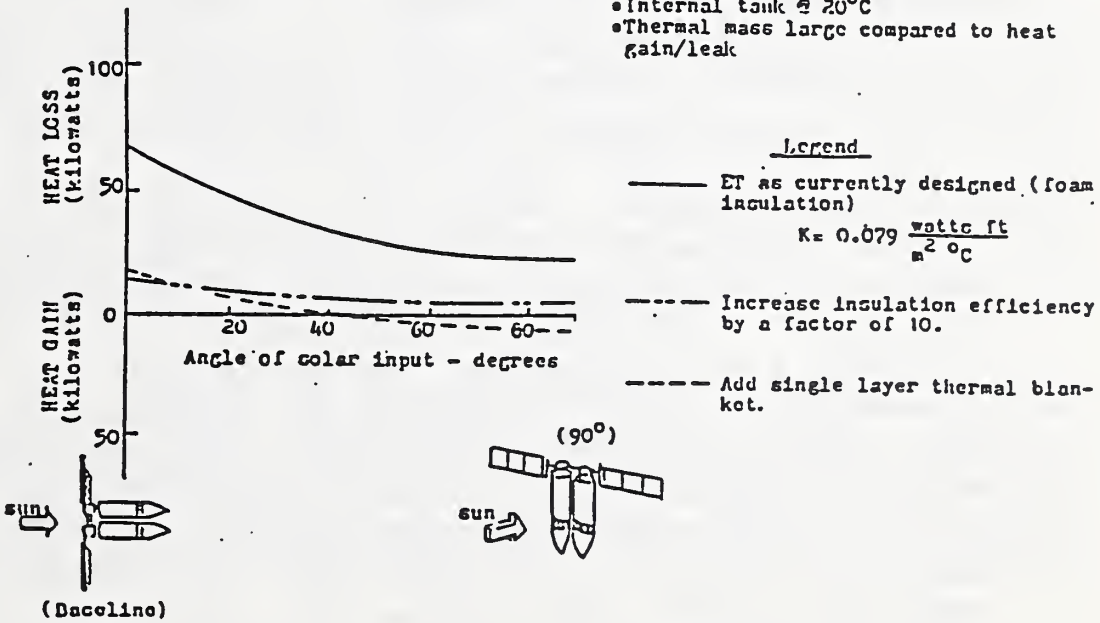

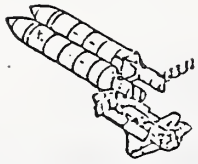

Figure 5. Combined MLI/Micrometeroid Protection

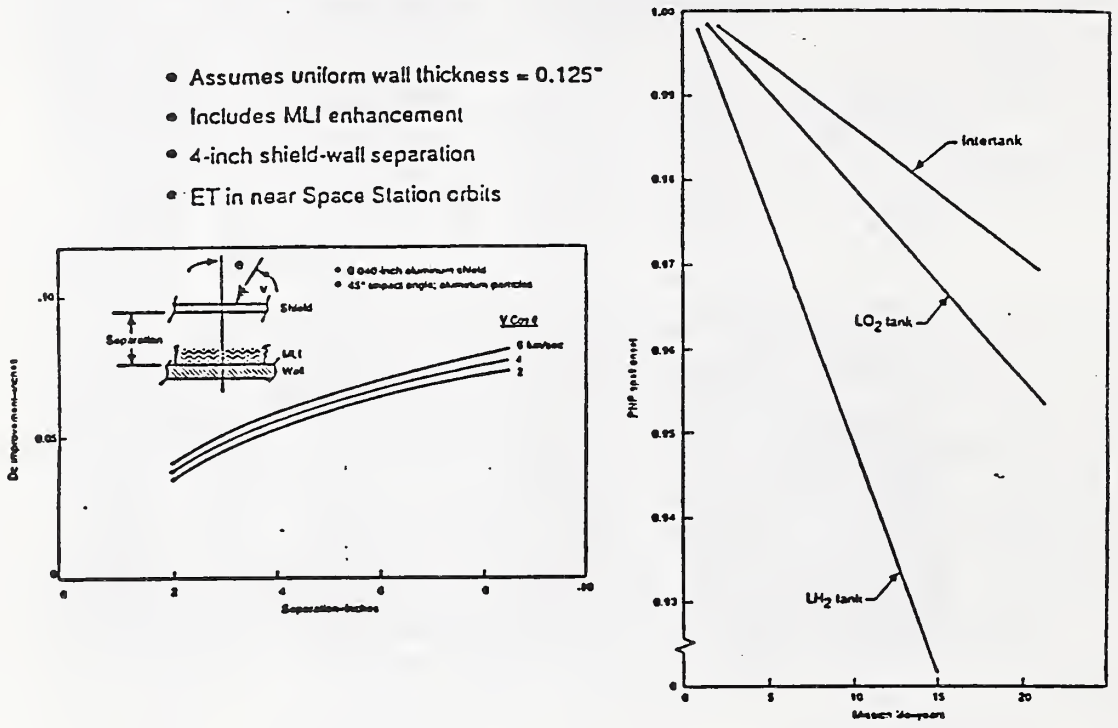

have to be developed in detail, but are not considered difficult problems.

Our analysis showed this system would provide approximately 0.95 probability of no spall[2] onset in the ET hydrogen tank for a 10-year mission life assuming the current NASA Space Station micrometeroid and space debris model[8]. The probability is greater for the oxygen tank and intertank structure primarily because of their smaller external area.

d. Orbital Lifetime. The large size of the ET and the low altitudes associated with nominal Shuttle launches prompted a study of aerodynamic drag on ET's in orbit and an estimation of propulsion requirements to maintain circular orbits[9]. Figure 6 provides a summary overview. As expected, ΔV is strongly dependent on the solar cycle and the ET orientation on orbit, i.e., broadside vs. "nose into the wind". For long duration missions during solar max conditions it can be shown that total ΔV can be reduced by approximately 65% by maneuvering the ET to altitudes of at least 450 km. We concluded that operational altitude, orbital lifetime and maneuver propulsion will be very important considerations in planning ET missions in the future.

Figure 6. Orbital Altitude Maintenance

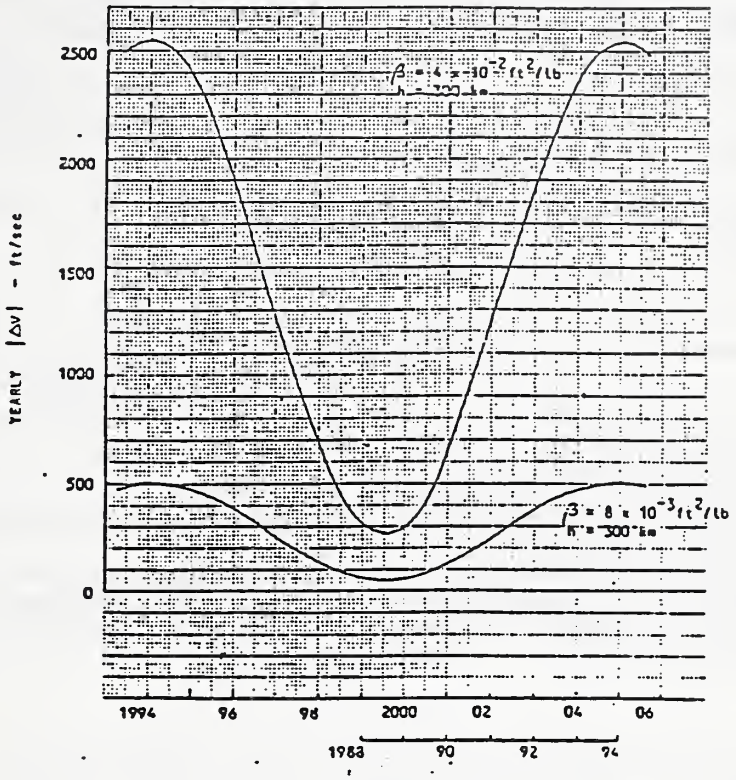

4. Development Schedule.

If we assume our feasibility study is equivalent to a Phase A Concept Definition, then to fully implement an ET warehouse on-orbit requires the equivalent of a Phase B Design Definition study and the equivalent of a Phase C/D Full Scale Implementation program. Figure 7 shows the program master schedule derived in our study for the assumptions and groundrules noted. The Phase B study would define and select specific components and subsystems from those available within the industry permitting early placement of procurement orders upon Phase C/D authority to proceed.

This schedule was developed based on an assessment of the conceptual baseline design, which emphasizes a high degree of equipment availability, and the assumption that the program is organized and managed in a cost-effective, "commercial" manner consistent with previous programs in the study team's experience base.

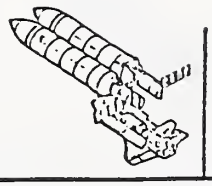

Figure 7. Program Master Schedule

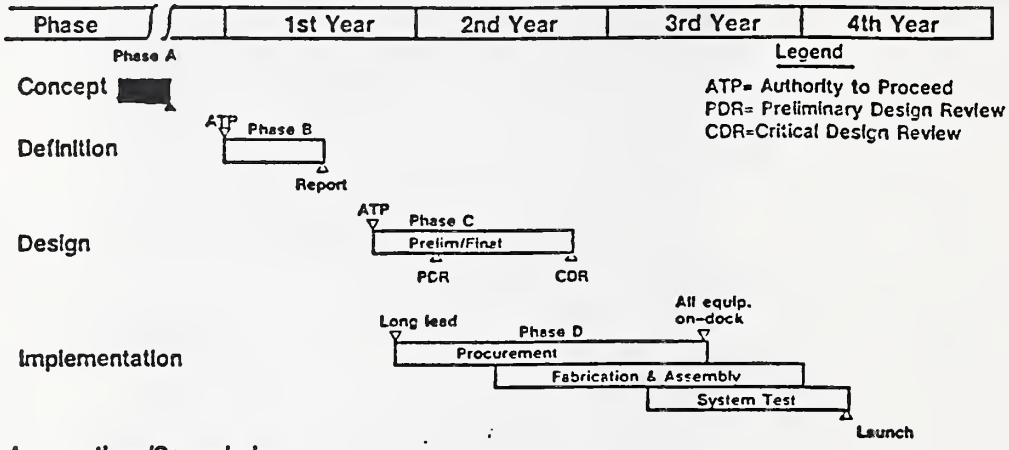

Assumptions/Groundrules:

1. Schedule is not constrained by fiscal funding limits.
2. Design and implementation Phases are authorized simultaneously although they are phased as shown.
3. Ground support equipment is available to support the flight hardware.
4. Basic program is 5-day week, 1-shift basis with nominal overtime.
5. Mission and system requirements do not change after acceptance of the phase B final report.

As in all programs, there are key schedule drivers that must be successfully managed to achieve the desired schedule milestones. And, as discussed below, these schedule drivers can have a significant impact on program cost if not controlled. Table 3 briefly summarizes these drivers and associated issues. Potential control measures addressing these drivers are discussed in our report.

5. Cost Analysis.

The program cost for putting an ET into orbit and providing a basic "warehouse" capability consists of many elements as summarized in Table 4.

Prelaunch mods are assumed to be designed and implemented by Martin Marietta under contract to NASA. We did not presume to estimate these costs. I understand they have been developed by Martin and quoted to potential ET developers. Whether NASA intends to fund these costs or pass them on is beyond the scope of this study.

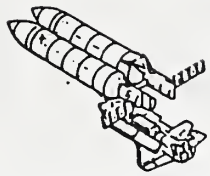

Table 3. Schedule Drivers and Issues

Driver	Schedule Issue
Design Changes	• Engineering repetition of analyses, simulations, specifications, drawings, etc.
Equipment Procurement	• Lead time for supplier fab, assembly and test for non-off-the-shelf items.
Late Subcontractor Deliveries	• Introduces delays, workarounds, inefficient phasing and/or retesting.
Integration/Test Failures	• Inefficient workarounds, program rephasing and/or retesting
Funding Constraints	• Inefficient scheduling and phasing. • Stop-work and/or phase-down modes. • Restart inefficiencies

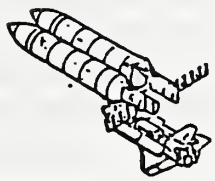

Table 4. First Order Cost Estimates

Element	ROM Cost	Remarks/Assumptions
ET Prelaunch Mods.	(No est.)	To be completed by Martin Marietta under NASA contract.
Organizational and Financing	(No est.)	Beyond scope of study.
Shuttle Launch and On-Orbit Activities	$75/launch	NASA tariff dependent. Requires further analysis when specific missions are defined.
Control Module Design Development and Fab.	$67M	Low cost commercial approach with off-the-shelf subsystems.
Operational and On-Orbit Maintenance	$1.2M/yr.	Cost of basic facility-excludes unique user requirements.

Organizational and financing costs including facilities, personnel, overhead, marketing, etc. associated with the ET developer and/or user entity were likewise not estimated in this study. That's in Tom Roger's area.

Shuttle launch and on-orbit activities cost to initialize the ET are dependent on NASA tariffs at the time of mission formalization and are subject to negotiated agreement with potential ET developers. It is a function of the EVA time required, shared launch with other payloads and NASA commercialization policies. Our estimate is intended only to provide an indication of the expected magnitude of this cost and does not represent a detailed analysis.

The Control Module design, development and fabrication cost was estimated assuming implementation of a high degree of cost-effective commercial practices: low cost design and management approaches with a minimally sized team, non-involvement of NASA engineers except for safety related items, absolute minimum of documentation, design reviews and subcontracting, use of existing state-of-the-art components and subsystems, a protoflight test and integration concept[10], rapid recycle spares philosophy and (as previously noted) premodified ET's to provide required Control Module physical and functional interfaces.

A breakout of the Control Module costs as estimated is shown in Table 5. It is assumed a "prime contract" would be implemented either at the ET developer or through an award process with a large percentage of the components and subsystems procured through subcontracts.

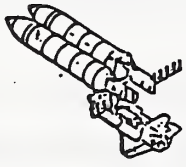

Table 5. Control Module Cost Breakout

Item	Prime	Subs	Total	Notes
Program Management	$1.3M	$0.6M	$1.9 M	
Engineering	6.9	3.8	10.7	
Manufacturing and Integration Lists	7.8	–	7.8	Excludes facilitization costs if any.
Procurement	1.8	25.5	27.3	Components/subsystems
Other & Indirect	1.1	1.6	2.7	
Travel, Fees, Etc.	1.5	1.6	3.1	
Contingency	5.1	8.3	13.4	Approximately 25%
Total	$25.5	$41.4	$66.9	

• For baseline dual tank configuration. Cost for a single ET with control Module is $42M.

The achievement of the cost estimated for the Control Module depends on success in implementing the assumed management and design approach, adherence to the development schedule discussed above and availability of existing components and subsystems which can be successfully integrated into the design. Toward this end, our study identified key top level cost drivers (both programmatic and technical), the cost issue/impact and potential control measurers recommended for management implementation. Tables 6 and 7 briefly summarize these cost drivers and issues. I will not discuss them in detail here because of time limitations; they are treated extensively in our report.

6. Conclusion.

In summary, our 1984 study showed that acquiring a "Spartan" on orbit ET facility is feasible with the implementation of certain ET design changes to accommodate orbital operations, and that the development of an on-orbit habitable "warehouse" with basic performance capabilities is achievable in 3 years time frame for approximately $42M first unit cost (excluding Shuttle launch and EVA costs) using available off-the-shelf components/subsystems and low cost commercial practices.

Today, five years later, considerable progress has been made in achieving the reality of using ET's on-orbit, especially with the recent agreement between UCAR and NASA. While our Control Module concept may not be the eventual way the ET's are used, other interesting approaches are merging. Effective utilization of ET's on orbit is becoming an exciting engineering challenge for those lucky enough to be involved.

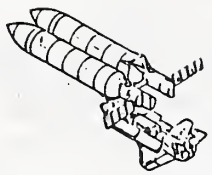

Table 6. Programmatic Cost Drivers and Issues

Driver	Cost Issue
Schedule and Schedule Adherence	• Schedule duration and task phasing. • Schedule changes due to program redirection and/or design changes. • Schedule compliance by all organizational elements.
Design/Management Approach	• Total understanding of program philosophy by all organizational elements. • Design emphasis on producibility, maintainability, simplicity and cost-effectiveness.
Component/Subsystem Selection	• Utilization of truly available equipment. • Suitability of low cost commercial components. • Elimination of redesign and associated requalification testing.

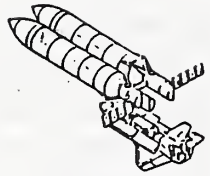

Table 7. Technical Cost Drivers and Issues

Driver	Cost Issue
Power level and regulation	• Solar array size and power subsystem complexity.
Attitude control pointing accuracy	• Subsystem equipment selection and availability. • Design and test complexity. • Software development, validation and verification.
Habitation requirements	• Size of worker complement and associated provisioning. • Emergency, safety and rescue modes. • Resupply and transportation needs.
Communication data rates and frequencies	• Subsystem equipment selection and availability. • Design and test complexity. • Antenna sizing and articulation. • Impact on power subsystem.

References and Notes

1. A dual tank configuration is shown to indicate the feasibility of multi-ET arrangement possibilities. The design analyses apply equally well to a single ET configuration.

2. Gimarc, J. A., Space Shuttle External Tank Applications, Space Studies Institute, Princeton, NJ, December 1985.

3. California Space Institute, Utilization of the External Tanks of the Space Transportation System, Univ. of California at San Diego, April 1983.

4. Nein, M. ET Orbital Applications, ET Utilization Workshop, Boulder, Co, August 1987.

5. Davis, B.G., ET-GRIT Study Overview, ET Utilization Workshop, Boulder, CO, August 1987.

6. Morgenthaler, G.W., Programmatic, Scientific and Commercial Uses of Orbiting Space Shuttle External Tanks, University of Colorado, Boulder, CO, March 1987.

7. Prince, R.L., Preflight Modifications to Enchance On-orbit Utilization of Space Shuttle External Tanks, Martin Marietta Aerospace, Denver, CO, August 1987.

8. Hill, A. S., Micrometeoroid and Space Debris Penetration of Orbiting Shuttle External Tanks, October 1987. (In publication)

9. Hill, A.S., Velocity Make-up Requirements due to Aerodynamic Drag on Orbiting Shuttle External Tanks, October 1987. (In publication)

10. A Protoflight development concept is characterized by the fabrication, test and launch of a single unit. There are no ground test units, "hanger queens" or development units. In this approach, the hardware is typically exposed to flight qualification levels for acceptance test durations during environmental testing.

External Tank Work at NIST:

A Numerical Procedure for the Evaluation of Drag and Aerodynamic Torque for Convex Shells of Revolution in Low Earth Orbit

William C. Stone and Christoph Witzgall
National Institute of Standards and Technology
Bldg 226/B168, Gaithersburg, MD 20899

and

Autonomous Propulsion System Requirements for Placement of an STS External Tank in Low Earth Orbit

William C. Stone and Geraldine S. Cheok
National Institute of Standards and Technology
Bldg 226/B168, Gaithersburg, MD 20899

A Numerical Procedure for the Evaluation of Drag and Aerodynamic Torque for Convex Shells of Revolution in Low Earth Orbit

by
William C. Stone and Christoph Witzgall
Research Structural Engineer and Mathematician, respectively,
National Institute of Standards and Technology, Gaithersburg, Maryland 20899 [1]

Abstract

A numerical procedure is described in which the aerodynamic drag and torque are calculated for convex shells of revolution for any given angle of attack based on free molecular flow theory. Assumptions are that the center of gravity lies on the axis of revolution and that there are no significant appendages. The contours of the shells are considered to consist of strictly concave ascending and descending portions connecting smoothly to an optional horizontal middle section. Each portion is described by a series of parametric equations. The system is discretized into circular cross sections perpendicular to the axis of revolution, which yield a series of ellipses when projected according to the given angle of attack. The drag profile, that is, the projection of the entire shell is approximated by the convex envelope of those ellipses. The area of the drag profile, that is, the drag area, and its center of area moment, that is, the drag center, are then calculated and permit determination of drag force and aerodynamic torque. For a given shell, the functional dependence of drag area and aerodynamic eccentricity on the angle of attack can be expressed to a high degree of accuracy in the least squares sense by polynomials of low degree which may be suitable for processing in real time.

Keywords: aerodynamic drag, aerodynamic torque, attitude control, external tank, free molecular flow, low Earth-orbit, perpendicular projection, shell of revolution, Space Shuttle

Introduction

Within the next ten years it is anticipated that a significant number of structures exhibiting very large drag profiles will be placed in low earth orbit (LEO). Large orbital structures

[1]Work of the U.S.Government and not subject to copyright protection in the United States. Trade or company names mentioned in this text do not constitute endorsement by the National Institute of Standards and Technology.

are not new: the Echo I experimental inflatable satellite had a projected drag area of some 725 square meters [6]. What is new is that the facilities planned for the 1990's will be at substantially lower altitude than Echo I (300 – 500km vs 1000km) and of such mass (in excess of 30 metric tons) that random re-entry cannot be permitted on grounds of safety. Significant engineering problems arise when attitude (orientation) control and δV (altitude change) motors must be provided for positive control of such craft. For asymmetrical structures as much as an order of magnitude difference can exist in the amount of fuel required for orbit maintenance depending on the spacecraft orientation with respect to its velocity vector. This is of particular concern to entrepreneurial commercial space companies seeking financing for the placement of such structures on orbit, since it presently costs approximately $3000 per pound in transport costs to LEO alone.

Of particular interest to the present study is the external tank for the Space Shuttle, that is, the U.S. Space Transportation System (STS). The external tank is currently the only non-reuseable component of the STS. On a typical launch to an orbit inclined 28.5° with respect to the equator (a due east launch from Cape Kennedy) these tanks reach approximately 98% of orbital velocity at an altitude of about 100 kilometers [1]. It is possible for the shuttle to take these tanks into relatively low orbit for only a modest penalty in terms of reduced shuttle payload capacity for most missions and at no penalty on some missions which are limited by weight and balance considerations [1]. Given that the amortized cost of taking an object of similar mass to orbit would be well in excess of $200 million, there is a compelling argument to consider making use of these tanks, rather than allowing them to re-enter the earth's atmosphere following main engine cut-off (MECO) as is present practice.

The economies of employing such "used" equipment on orbit were recognized as early as 1976 [14] and several detailed studies concerning various uses for external tanks were carried out in the early 1980's [1,18]. Recently it was observed that two external tanks "will make an ideal concrete plant" in a lunar environment [8].

An agreement signed in December 1988 between the University Corporation for Atmospheric Research (UCAR) and NASA [17] grants approval to instrument five STS external tanks for sub-orbital flights within the next three years. These sub-orbital missions will constitute tests of flight hardware eventually to be used to place external tanks in long-term stable orbits. The control of such tanks, which weigh more than 30 metric tons and which have a total exterior surface area about half that of a football field, poses a considerable challenge. Considering the potentially broad impact that the availability of such assets on orbit will have on commercial space enterprises, NIST has undertaken a program to study the problems surrounding the control and conversion of such structures to habitable facilities on orbit at the lowest possible cost while maintaining safety.

The problem of controlling an earth-orbiting spacecraft may be divided into the following four components: orbit determination, attitude determination, attitude control, and altitude control. Four principal disturbing forces acting on objects in low earth orbit must be quantified in order to determine the control requirements described above. These are gravity-gradient torque, solar radiation pressure (and induced torque), aerodynamic drag (and induced torque), and magnetic disturbance torque [16]. The aerodynamic component is dominant at altitudes below 400 kilometers, and a numerical method which quantifies that component for convex shells of revolution is the subject of this paper. Documentation of the

computer code which underlies the numerical results reported in the paper will be found in a forthcoming technical report [11]. A short description of the method and applications to the LO_2 and LH_2 component tanks are contained in [12].

Under the assumptions of free molecular flow theory [9] no boundary layer is formed. Molecules reemitted from a surface do not collide with free stream molecules until far away from the body. One may thus neglect distortions of the free stream velocity distribution due to the presence of the body, and assume that aerodynamic drag force is entirely due to impact of atmospheric molecules on the spacecraft surface. For hypersonic flows impinging on cool surfaces the momentum of molecules leaving the surface may be neglected. The impact of molecules in the incident stream may thus be modeled as inelastic without reflection, that is, the incident particle's energy is completely absorbed [3]. It is also assumed that attitude changes are slow compared to the translational velocity of the spacecraft.

Given these conditions, the problem of determining the disturbing forces reduces to the determination of the projected surface area, or "shade" area, of the spacecraft onto a plane perpendicular to the velocity for any given angle of attack and roll angle, and the determination of the center of area moment for this projected area. Exact formulas for free molecular aerodynamic forces and moments on simple shapes were determined in the 1960's. Methods developed in the 1970's [4,13] relied on the superposition of projected areas of elementary shapes (e.g. sphere, cylinder, rectangular flat plate) to determine the extent to which various leeward-facing spacecraft components were obscured, or shaded, by forward-facing components. These methods were both computationally intensive and limited by the geometrical models for which closed form solutions were known. A more recent approach [10] has been

developed in which computer aided design (CAD) software is used to partially automate the process for shade determination for spacecraft described by many elementary shapes. This latter procedure still requires significant user interaction in order to determine which primitive components are to be removed from the shade model presented on the computer screen for a given projection.

As part of an effort to develop a simulator for orbiting Space Shuttle tanks at NIST, our first step was that of developing a robust stand-alone algorithm for determining the aerodynamic drag and torque acting on a tank in low Earth orbit that could be inserted into the simulator. This ruled out all of the previously described approaches. Furthermore the substantial curvature of the tank cannot be accurately reproduced by superposition of simple primitive shapes. The approach which follows avoids this drawback, also.

Drag Area and Aerodynamic Eccentricity

Let $\mathbf{v}$ denote the unit vector in the direction of the translational velocity V of the center of gravity of the spacecraft relative to the incident stream, and let $\mathbf{i}$ be the attitude vector, that is, the unit vector in the direction of the axis of revolution, oriented from rear to to front of the spacecraft. The angle between the velocity vectorv and the attitude vector $\mathbf{i}$ is the angle of attack θ, where

$$0° \leq \theta \leq 180°.$$

Consider the plane $\mathbf{P}$ (see Fig.1) which is perpendicular to the velocity vector $\mathbf{v}$ and passes through the center of gravity of the body. The projection of the shell surface in the direction of $\mathbf{v}$ into plane $\mathbf{P}$ will be referred to as the drag profile. Due to the rotational symmetry of

the surface, the shape and the size of the drag profile depend solely on the angle of attack. The drag force $\mathbf{F}_{aero}$ and the aerodynamic torque $\mathbf{N}_{aero}$ are determined by the area A_{drag} – referred to as the drag area – and the center of area moment – referred to as the drag center – of the drag profile.

The differential drag force $d\mathbf{F}_{aero}$ acting on a surface element dA with outward unit normal $\mathbf{n}_s$ is given by

$$d\mathbf{F}_{aero} = -\frac{1}{2}\rho C_{drag} V^2 (\mathbf{n}_s \cdot \mathbf{v})\mathbf{v}\, dA,$$

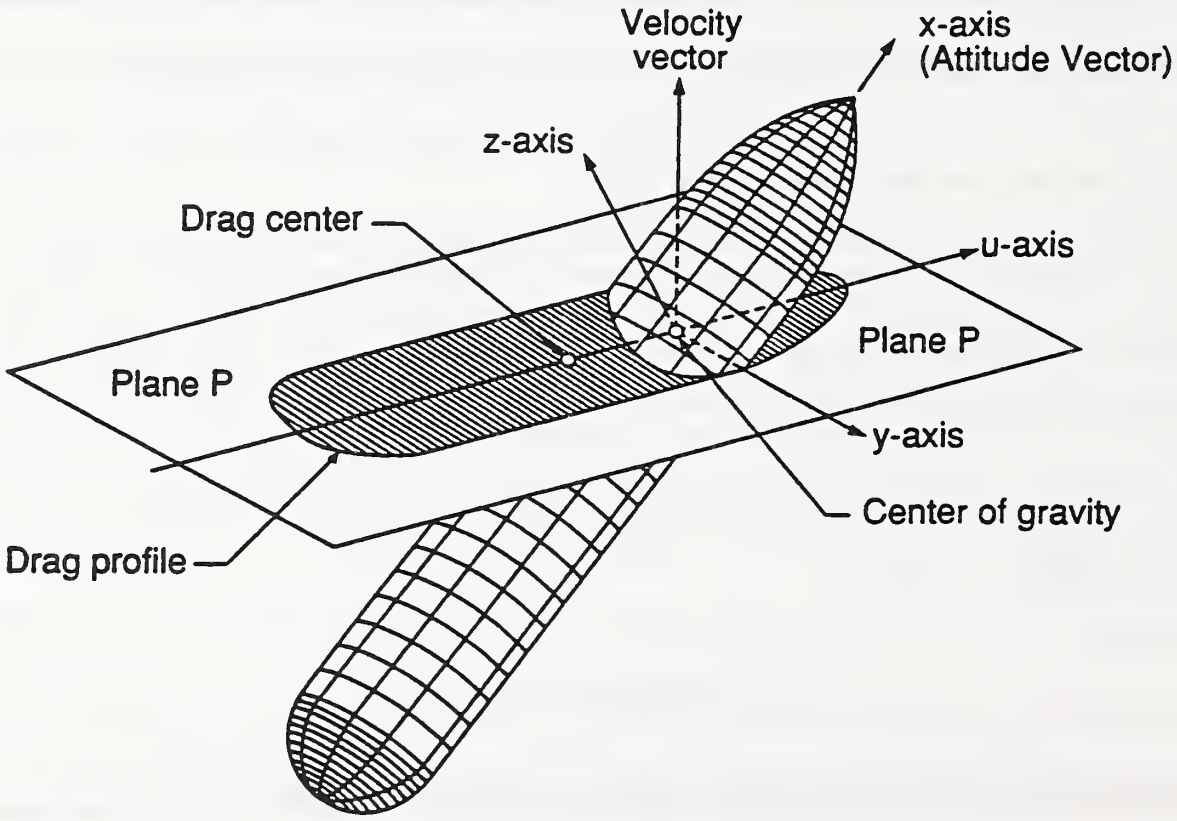

Fig. 1: Definition of coordinate systems and principal variables used to describe the drag profile and aerodynamic eccentricity for a given angle of attack.

where ρ is the atmospheric density [16]. Analytical models for the atmosphere up to an altitude of 110 kilometers [5] and for altitudes above 90 kilometers [7] are available which provide seasonal (as affected by solar activity) and latitudinal values of ρ. The parameter C_{drag} is the drag coefficient and is, in general, a function of the surface structure. In the limiting hypersonic case, only forward-facing surface elements contribute to drag and for these the value $C_{drag} = 2.0$ [9] is suggested.

Note that the factor $(\mathbf{n}_s \cdot \mathbf{v})\, dA$ in the above expression for the differential drag force $d\mathbf{F}_{aero}$ represents the projection of the surface element dA in the direction of $\mathbf{v}$ onto plane $\mathbf{P}$. Total drag force $\mathbf{F}_{aero}$ is obtained by integrating the contributions from all forward-facing exterior surface elements of the spacecraft. The projections of these surface elements exactly cover the projection of the total surface, that is, the drag profile. In other words,

$$\int (\mathbf{n}_s \cdot \mathbf{v})\, dA \;=\; A_{drag}.$$

The total drag force vector may thus be expressed as:

$$\mathbf{F}_{aero} \;=\; -\frac{1}{2}\rho C_{drag} V^2 \mathbf{v} A_{drag}.$$

The aerodynamic torque $\mathbf{N}_{aero}$ acting on the spacecraft due to the differential force $d\mathbf{F}_{aero}$ is given by the integral:

$$\mathbf{N}_{aero} \;=\; \int \mathbf{R}_s \times d\mathbf{F}_{aero}$$

where $\mathbf{R}_s$ is the vector from the spacecraft's center of gravity to the surface element dA. The integral is over the spacecraft surface for which $(\mathbf{n}_s \cdot \mathbf{v})$ is positive. Substituting for the differential drag force $\mathbf{F}_{aero}$ yields:

$$\mathbf{N}_{areo} \;=\; -\frac{1}{2}\rho C_{drag} V^2 \int (\mathbf{R}_s \times \mathbf{v})(\mathbf{n}_s \cdot \mathbf{v})\, dA.$$

In order to evaluate the integral in the above expression, we recall that $(\mathbf{n}_s \cdot \mathbf{v})\, dA$ is the projection of surface element dA onto the surface element of plane $\mathbf{P}$. Since that plane contains the center of gravity of the body, and since the vector $\mathbf{R}_s$ originates at that center, the vector $\mathbf{R}_s \times \mathbf{v}$ leads – within plane $\mathbf{P}$ – from the center of gravity to the projected surface element. The integral in question thus reduces in plane $\mathbf{P}$ to a familar expression: when divided by area over which the integration extends, it indicates the location of the center of area moment of the drag profile, namely, the drag center, with respect to the common origin of vectors $\mathbf{R}_s$, namely, the center of gravity of the body. Denoting by $\mathbf{R}_{cg}$ the eccentricity vector which leads from the center of gravity to the drag center we thus have:

$$\int (\mathbf{R}_s \times \mathbf{v})(\mathbf{n}_s \cdot \mathbf{v})\, dA \;=\; A_{drag}\mathbf{R}_{cg},$$

and

$$\mathbf{N}_{aero} \;=\; -\frac{1}{2}\rho C_{drag} V^2 A_{drag}\mathbf{R}_{cg} = \mathbf{R}_{cg} \times \mathbf{F}_{aero}.$$

The aerodynamic eccentricity is a scalar whose absolute value is the length of the eccentricity vector $\mathbf{R}_{cg}$. It is positive if the drag center leads the center of gravity in the direction of the attitude vector $\mathbf{i}$:

$$e_{aero} \;=\; \mathrm{sign}(\mathbf{R}_{cg} \cdot \mathbf{i})\|\mathbf{R}_{cg}\|.$$

Due again to the rotational symmetry of the shell and because its center of gravity lies on the axis of revolution, the eccentricity depends only on the angle of attack θ. The remainder of this paper is devoted to the description of a numerical procedure for the determination of the drag area A_{drag} and the drag center, needed to find the aerodynamic eccentricity e_{aero},

for convex shells of revolution under a specified angle of attack θ.

Description of Shells of Revolution

The present software implementation of our method is restricted to a particular category of convex shells of revolution. The geometric shape of the Space Shuttle external tank falls into that category. We assume the shells to be embedded in x, y, z-space with the x-axis as the axis of revolution directed from rear to front (see Fig.1). Each shell is characterized by its "contour", that is, the graph of a function

$$z \;=\; r(x) \geq 0$$

over a closed interval $[\underline{x},\ \bar{x}]$ (see Fig.2). The longitudinal section of the shell in the x, z-plane,

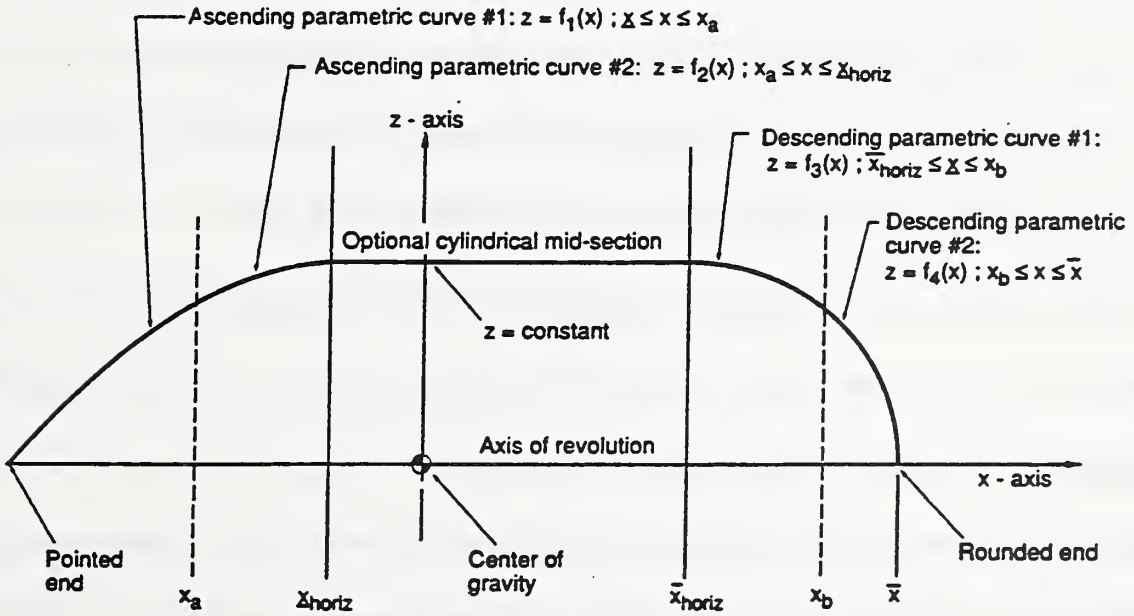

Fig. 2: Definition of parametric equations describing a generic shell of revolution and the coordinate plane in which they must be described. Any number of such segmented equations may be used to describe a given shell.

whose rotation sweeps the volume of the shell, is then bounded above by $+r(x)$ and below by $-r(x)$. Typically, the domain $[\underline{x},\ \bar{x}]$ will be partitioned into a series of intervals in each of which the contour function will be expressed by a suitable parametric equation.

For the shell of revolution to be convex it is necessary and sufficient that the contour function be concave. Beyond this property, we will require that the contour function consists of (see Fig.2):

1. To the left, an ascending strictly concave function with unique tangents which starts with a value of zero, $r(\underline{x}) = 0$, and terminates with a horizontal tangent, $r'(\underline{x}_{horiz}) = 0$;

2. In the middle, an optional horizontal line at maximum function value r_{max} (corresponding to an optional cylindrical middle section of the shell) which starts at the end of the previous function, $r(\underline{x}_{horiz}) = r_{max}$;

3. To the right, a descending strictly concave function with unique tangents which starts at the end $r(\bar{x}_{horiz}) = r_{max}$ of the cylindrical portion – provided such is present – with a horizontal tangent, $r'(\bar{x}_{horiz}) = 0$, and terminates with a value of zero, $r(\bar{x}) = 0$.

Here $\underline{x}_{horiz} \leq \bar{x}_{horiz}$ denote the left and right ends of the horizontal portion; $\underline{x}_{horiz} = \bar{x}_{horiz}$ if there is none present. By "strictly concave" it is meant that there is a continual change of the tangent direction and therefore no straight line segments in the graph of the function to which the term is applied. Thus the horizontal straight line representing the optional cylindrical middle section is the only straight line segment presently permitted in the contour. Since the above left portion of the contour function terminates at its right with a horizontal tangent and the above right portion starts with a horizontal tangent to its left, each point of the

entire contour function has a unique slope. The contour function is therefore differentiable everywhere in the interior of the domain. The above partitionability of the contour function into an ascending, a descending and, optionally, a horizontal portion does not mean that only three parametric equations are permitted for the description of the contour function: any number of such equations can be used as long as the resulting function meets the above requirements.

At the the endpoints $\underline{x}$ and $\bar{x}$ of the domain of the contour function, we permit infinite values for its derivatives. That is, $r'(\underline{x}) = +\infty$ and/or $r'(\bar{x}) = -\infty$ may hold, indicating vertical end tangents. In those cases, the ends $(\underline{x}, 0, 0)$ and $(\bar{x}, 0, 0)$, respectively, of the shell of revolution are "rounded". They are "pointed" at those ends if the corresponding end tangents are nonvertical. For instance, the shell of revolution generated by the contour depicted in Figure 2 has a pointed left end and a rounded right end.

For the applications considered here, it will be convenient to locate the origin of the coordinate system at the center of gravity of an empty external tank, or a tank with a uniform pressurized internal atmosphere such as might exist following on-orbit modifications to create a shirt-sleeve workshop. The effects of residual fuel sloshing and dynamically shifting the location of the center of gravity are beyond the scope of this paper.

In the previous section, a velocity vector $\mathbf{v}$ was introduced. Because of the rotational symmetry, we may assume that this vector lies in the vertical z, x-plane. The angle θ between the velocity vector $\mathbf{v}$ and the x-axis is the angle of attack. The vector $\mathbf{v}$ also determines the plane $\mathbf{P}$ which is perpendicular to it and contains the origin of the x, y, z-coordinate system, that is, the center of gravity as shown in Figure 1. This plane contains the y-axis. The

intersection of $\mathbf{P}$ with the z,x-plane yields a line that is perpendicular to the y-axis, and can be selected as the u-axis of a u,y-coordinate system in that plane $\mathbf{P}$. We direct the u-axis so that its angle with the x-axis lies between 0° and 90°. The perpendicular projection, that is, the shade cast in the direction of the velocity vector $\mathbf{v}$ by the shell of revolution onto the plane $\mathbf{P}$ is the drag profile, whose shape, area A_{drag}, and center of area moment, the drag center $(u_{drag}, 0)$, are at issue. Since both $+\mathbf{v}$ and $-\mathbf{v}$ yield the same drag profile in the same plane $\mathbf{P}$, we may assume without loss of generality that the angle of attack θ lies between zero and ninety degrees: $0° \leq \theta \leq 90°$. If $\theta = 0°$, then the drag profile is given by the circular cross section of largest diameter. We will therefore assume in the next two sections that θ is positive:

$$0° < \theta \leq 90°.$$

Discretization of Shells of Revolution

Our method for determining the drag profile is based on approximating the contour function $z = r(x)$ in a piecewise linear fashion: select a finite sequence of points,

$$\underline{x} = x_1 < x_2 < \ldots < x_i < \ldots < x_n = \bar{x},$$

from its domain $[\underline{x}, \bar{x}]$, and connect adjacent points $(x_i,\ z_i = r(x_i))$, $(x_{i+1},\ z_{i+1} = r(x_{i+1}))$ in the graph of the contour function by straight line segments. The resulting shell of revolution consists of a sequence of slices of circular cones or of cylinders, the circular top of one forming the base for the next. The perpendicular projection of such a "piecewise conical" shell of revolution can be described in closed form as described below. A different way of looking at the same procedure is as a discretization method that approximates the given shell of

revolution by a finite sequence of circular cross sections, which project into a sequence of similar and parallel ellipses. The drag profile is then approximated by the convex envelope, that is, the smallest convex set enclosing those ellipses.

The approximate drag profile is thus determined by a sequence of ellipses $\mathbf{E}_i$, $i = 1, ..., n$. The centers of these ellipses are located on the u-axis of plane $\mathbf{P}$ with coordinates $u_i = x_i sin\theta$. The major axes $a_i = r(x_i)$ are in the direction of the y-axis. The minor axes lie on the u-axis, their length given by $b_i = a_i \cos\theta$. The equation of ellipse $\mathbf{E}_i$ is therefore:

$$\left(\frac{u - u_i}{b_i}\right)^2 + \left(\frac{y}{a_i}\right)^2 = 1.$$

The first and the last of these ellipses may be degenerate, $a_i = b_i = 0$, and consist of a single point.

If any ellipse in the above sequence is contained in a neighboring one, then such an ellipse can be deleted without changing the convex envelope. This usually happens at the beginning and the end of the sequence of ellipses. More precisely, there is a largest index $\underline{i}$ such that ellipse $\mathbf{E}_{\underline{i}}$ contains all previous ellipses $\mathbf{E}_i$, $i < \underline{i}$. Analogously, there is a smallest index $\bar{\imath}$ such that ellipse $\mathbf{E}_{\bar{\imath}}$ contains all subsequent ellipses $\mathbf{E}_i$, $i > \bar{\imath}$

$$1 \leq \underline{i} \leq \bar{\imath} \leq n.$$

Since none of the ellipses $\mathbf{E}_i$ with $\underline{i} \leq i \leq \bar{\imath}$ contains any of the others, all that is necessary in order to delineate their convex hull is to join subsequent ellipses by their common tangents. We should clarify that we mean those common tangents which have the ellipses on same rather than different sides.

As a result, the approximate drag profile is described in the u,y-plane $\mathbf{P}$ by a concave function $y = p(u)$ over a domain $[\underline{u},\ \bar{u}]$ with zero values at the endpoints. That domain is partitioned into segments in which the graph of this function is represented, in alternating fashion, either by a straight line or by an elliptical arc (see Fig.3). The first and last segments are elliptical segments. Thus $\underline{u}$ is the left minor axis point of ellipse $\mathbf{E}_{\underline{i}}$, whereas $\bar{u}$ is the right minor axis point of ellipse $\mathbf{E}_{\bar{i}}$. This yields for the endpoints of the approximate drag profile:

$$\underline{u} \ = \ u_{\underline{i}} - b_{\underline{i}}, \ \ \bar{u} \ = \ u_{\bar{i}} + b_{\bar{i}}.$$

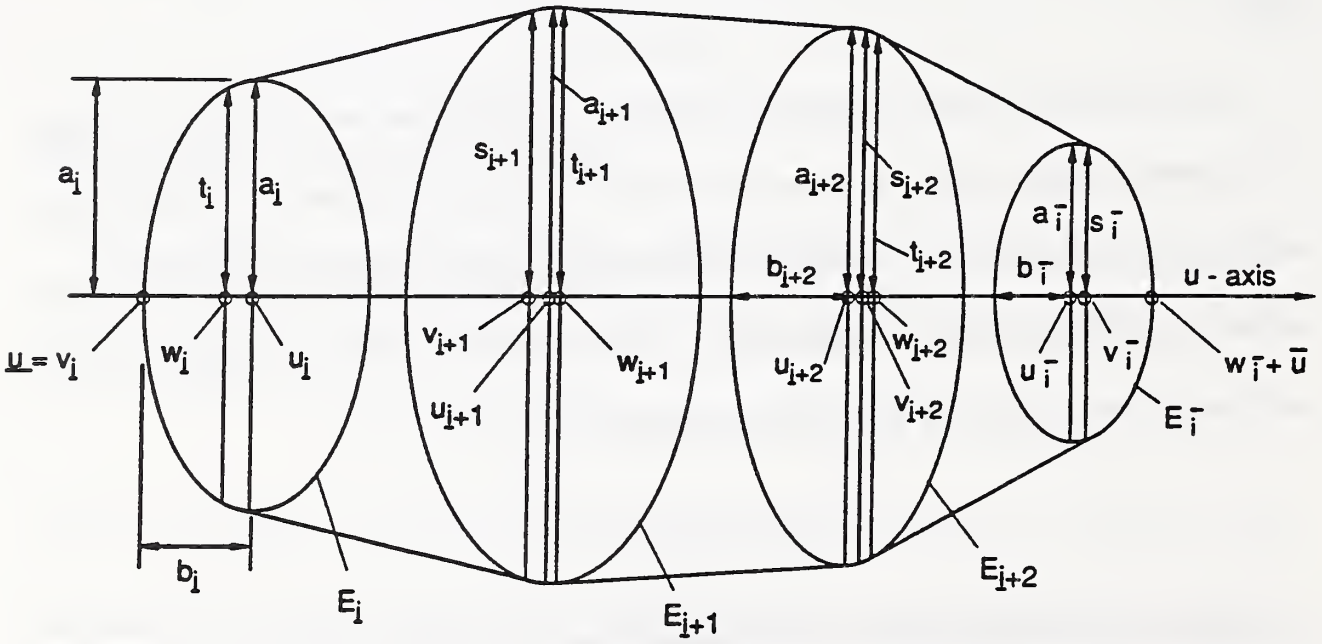

Fig. 3: Definition of discrete parameters used for determining the contribution of each "slice" of the spacecraft to the drag area and aerodynamic eccentricity. Underscored symbols indicate reference with respect to the left end of the spacecraft; symbols with bar overstrikes are relative to the right end.

We denote the breakpoints for the partition into straight and elliptic segments by:

$$\underline{u} = v_{\underline{i}} \leq w_{\underline{i}} < \ldots < v_i < w_i < \ldots < v_{\bar{\imath}} \leq w_{\bar{\imath}} = \bar{u}.$$

The possibility that $v_{\underline{i}} = w_{\underline{i}}$ and $v_{\bar{\imath}} = w_{\bar{\imath}}$ reflects the fact that, the ellipses $\mathbf{E}_{\underline{i}}$ and $\mathbf{E}_{\bar{\imath}}$ at the beginning and the end of the approximate drag area may be just single points. The corresponding segments are then of zero length.

The determination of the breakpoints v_i, w_i is the key to the description of the drag profile. The following quantities, which are independent of the angle of attack θ, play a role in deriving expressions for those breakpoints:

$$\Delta_i = \frac{a_{i+1} - a_i}{x_{i+1} - x_i}.$$

It will be shown in the last section that:

$$v_i = u_i - b_i \left[\frac{a_i - a_{i-1}}{u_i - u_{i-1}}\right] \cos\theta = u_i - b_i \frac{\Delta_{i-1}}{\tan\theta}, \quad \underline{i} < i \leq \bar{\imath},$$

$$w_i = u_i - b_i \left[\frac{a_{i+1} - a_i}{u_{i+1} - u_i}\right] \cos\theta = u_i - b_i \frac{\Delta_i}{\tan\theta}, \quad \underline{i} \leq i < \bar{\imath}.$$

For the corresponding y-coordinates we find using the equation of ellipse $\mathbf{E}_i$:

$$s_i = p(v_i) = a_i \rho_{i-1}, \quad t_i = p(w_i) = a_i \rho_i,$$

where

$$\rho_i = \sqrt{1 - \left(\frac{\Delta_i}{\tan\theta}\right)^2}.$$

In general, the elliptical arcs will be much smaller than the straight line segments except for the first and last elliptical arcs which may well be longer. We therefore recommend to replace all intermediate elliptic arcs by their chords while keeping elliptic arcs at the ends.

The total approximate size A_{tot} of the drag area A_{drag} is the sum

$$A_{drag} \approx A_{tot} = A(v_{\underline{i}}, w_{\underline{i}}) + \ldots + A(v_i, w_i) + A(w_i, v_{i+1}) + \ldots + A(w_{\bar{i}-1}, v_{\bar{i}}) + \ldots + A(v_{\bar{i}}, w_{\bar{i}})$$

of the areas of the vertical "strips", above and below the u-axis, into which the drag profile has been divided. All such strips with the possible exception of the first and last ones are trapezoids that are symmetric about the u-axis. Those strips which were originally bounded by elliptical arcs have area:

$$A(v_i, w_i) = (w_i - v_i)(s_i + t_i) = a_i b_i (\rho_{i-1} + \rho_i) \frac{\Delta_{i-1} - \Delta_i}{\tan\theta}, \quad \underline{i} < i < \bar{i}$$

since

$$w_i - v_i = u_i - b_i \frac{\Delta_i}{\tan\theta} - u_i + b_i \frac{\Delta_{i-1}}{\tan\theta} = b_i \frac{\Delta_{i-1} - \Delta_i}{\tan\theta}.$$

For those strips which were trapezoidal from the beginning, we find:

$$A(w_i, v_{i+1}) = (v_{i+1} - w_i)(t_i + s_{i+1}) = \rho_i^3 (a_{i+1} + a_i)(u_{i+1} - u_i), \quad \underline{i} \le i < \bar{i},$$

since

$$\begin{aligned} v_{i+1} - w_i &= u_{i+1} - b_{i+1} \frac{\Delta_i}{\tan\theta} - u_i + b_i \frac{\Delta_i}{\tan\theta} = (u_{i+1} - u_i) \left(1 - \frac{b_{i+1} - b_i}{u_{i+1} - u_i} \frac{\Delta_i}{\tan\theta}\right) \\ &= (u_{i+1} - u_i) \left(1 - \left(\frac{\Delta_i}{\tan\theta}\right)^2\right) = (u_{i+1} - u_i)\rho_i^2. \end{aligned}$$

The two elliptic end-strips have areas

$$A(v_{\underline{i}}, w_{\underline{i}}) = a_{\underline{i}} b_{\underline{i}} \left(sin^{-1}\rho_{\underline{i}} - \rho_{\underline{i}} \frac{\Delta_{\underline{i}}}{\tan\theta}\right), \quad A(v_{\bar{i}}, w_{\bar{i}}) = a_{\bar{i}} b_{\bar{i}} \left(sin^{-1}\rho_{\bar{i}-1} - \rho_{\bar{i}-1} \frac{\Delta_{\bar{i}-1}}{\tan\theta}\right).$$

Due to the symmetry of the drag area about the u-axis, the drag center lies on the u-axis, and its y-coordinate y_{drag} is therefore zero. Let $c(v_i, w_i)$, $c(w_i, v_{i+1})$ denote the centers of

area moment of their respective strips. For the u-coordinate u_{drag} of the drag center, we find approximately

$$u_{drag} \approx \frac{1}{A_{tot}}(A(v_{\underline{i}}, w_{\underline{i}})c(v_{\underline{i}}, w_{\underline{i}}) + \ \ldots \ + \ A(v_i, w_i)c(v_i, w_i) + \ A(w_i, v_{i+1})c(w_i, v_{i+1}) + \ \ldots \ + A(v_{\bar{\imath}}, w_{\bar{\imath}})c(v_{\bar{\imath}}, w_{\bar{\imath}})).$$

Again we consider the two kinds of trapezoidal strips. For those that were elliptical originally, we find for $\underline{i} < i < \bar{\imath}$:

$$\begin{aligned} c(v_i, w_i) &= \frac{1}{s_i + t_i}\left(\frac{2s_i + t_i}{3}v_i + \frac{s_i + 2t_i}{3}w_i\right) \\ &= u_i - \frac{b_i}{\rho_{i-1} + \rho_i}\left(\frac{2\rho_{i-1} + \rho_i}{3}\frac{\Delta_{i-1}}{\tan\theta} + \frac{\rho_{i-1} + 2\rho_i}{3}\frac{\Delta_i}{\tan\theta}\right). \end{aligned}$$

For the strips bounded by common tangents, we have for $\underline{i} \leq i < \bar{\imath}$

$$\begin{aligned} c(w_i, v_{i+1}) &= \frac{1}{t_i + s_{i+1}}\left(\frac{2t_i + s_{i+1}}{3}w_i + \frac{t_i + 2s_{i+1}}{3}v_{i+1}\right) \\ &= \frac{1}{a_i + a_{i+1}}\left(\frac{2a_i + a_{i+1}}{3}(u_i - b_i\frac{\Delta_i}{\tan\theta}) + \frac{a_i + 2a_{i+1}}{3}(u_{i+1} - b_{i+1}\frac{\Delta_i}{\tan\theta})\right), \end{aligned}$$

and for the elliptic end-strips,

$$c(v_{\underline{i}}, w_{\underline{i}}) = u_{\underline{i}} - \frac{2a_{\underline{i}}b_{\underline{i}}^2\rho_{\underline{i}}^3}{3A(v_{\underline{i}}, w_{\underline{i}})}, \quad c(v_{\bar{\imath}}, w_{\bar{\imath}}) = u_{\bar{\imath}} + \frac{2a_{\bar{\imath}}b_{\bar{\imath}}^2\rho_{\bar{\imath}}^3}{3A(v_{\bar{\imath}}, w_{\bar{\imath}})}.$$

Selecting Cross Sections

The next question concerns the selection of the cross sections, that is, of the locations x_i. Clearly we want to include the end points of the contour curve: $x_1 = \underline{x}$, $x_n = \bar{x}$. If a cylindrical middle section is present, then cross sections are needed only at the beginning $\underline{x}_{horiz}$ and the end $\bar{x}_{horiz}$ of that section. Indeed, intermediate cross sections in the cylindrical portion clearly do not contribute to the convex envelope.

As to selecting cross sections in the ascending or descending portions, the density of the cross sections should increase with the curvature of the contour function. A straightforward way to achieve this is to select according to equal increments δ of tangential angles as follows. For a positive integer m consider the angles (see Fig.4)

$$\alpha_k = 90° - (k-1)\delta \quad \text{for} \quad k = 1, 2, ..., 2m+1$$

with angle increment

$$\delta = \frac{90°}{m}.$$

Then we select those x-coordinates for which the contour function $z = r(x)$ has the prescribed tangential angles α_k and place the cross sections there. Determining the x-coordinates at which given angles α_k are assumed is by a straightforward bipartition scheme based on the derivatives of the given parametric equations.

In addition, we link the choice of the integer m, which determines the above angle increment δ, to the angle of attack θ so that it occurs among the tangential angles α_k. In that case, both ends $\underline{u}$, $\bar{u}$ of the approximate drag profile are exactly the ends of the actual drag profile. This is because the two x-coordinates at which tangents of angles $\pm\theta$, respectively, touch the graph of the contour function can be found among the selected coordinates x_i. The ensuing conceptual simplification of the methodology, together with numerical advantages, justifies the minor additional effort of placing the cross section coordinates according to equal increments of tangential angles. It usually has to be done only once for a series of angles of attack θ.

Care must be taken in the case of pointed ends. For $k = 1$ the corresponding vertical

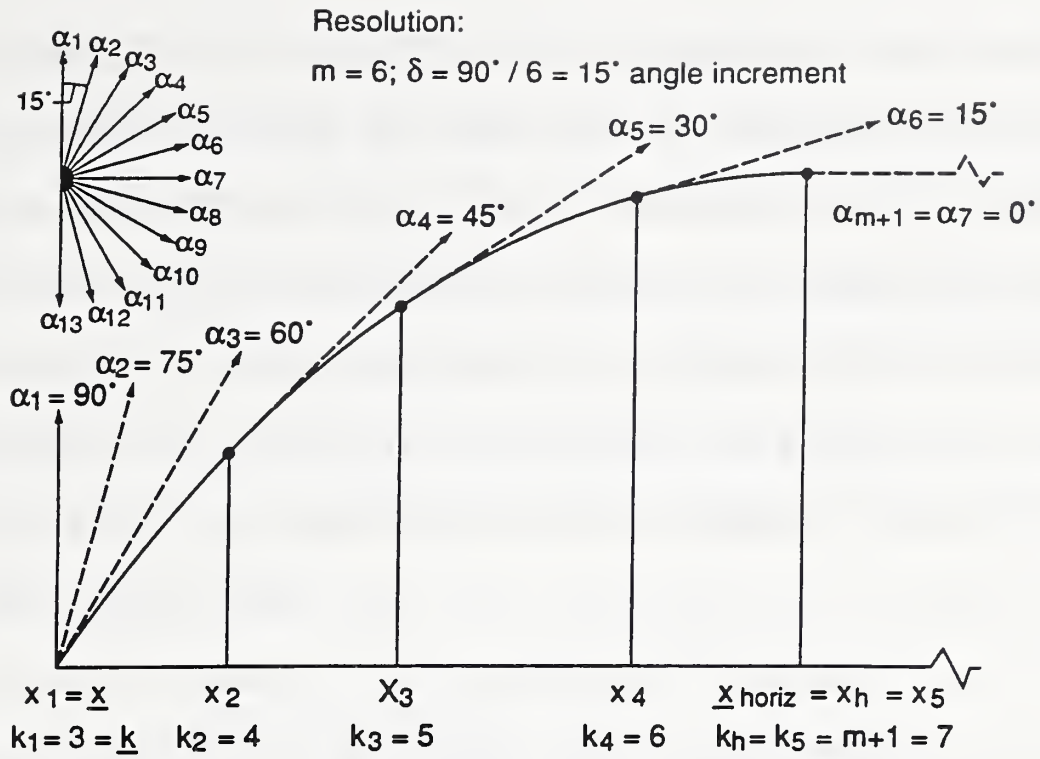
Resolution:
m = 6; δ = 90° / 6 = 15° angle increment
α1 α2 α3 α4 α5 α6 α7 α8 α9 α10 α11 α12 α13
15°
α5 = 30°
α6 = 15°
α4 = 45°
αm+1 = α7 = 0°
α3 = 60°
α2 = 75°
α1 = 90°
x 1 = x
x 2
X3
x 4
x horiz = xh = x5
k1 = 3 = k
k2 = 4
k3 = 5
k4 = 6
kh = k5 = m+1 = 7

Fig. 4a: Ascending profile curve with pointed end. Cross-section placements at points x_k according to an angle decrement of 15°.

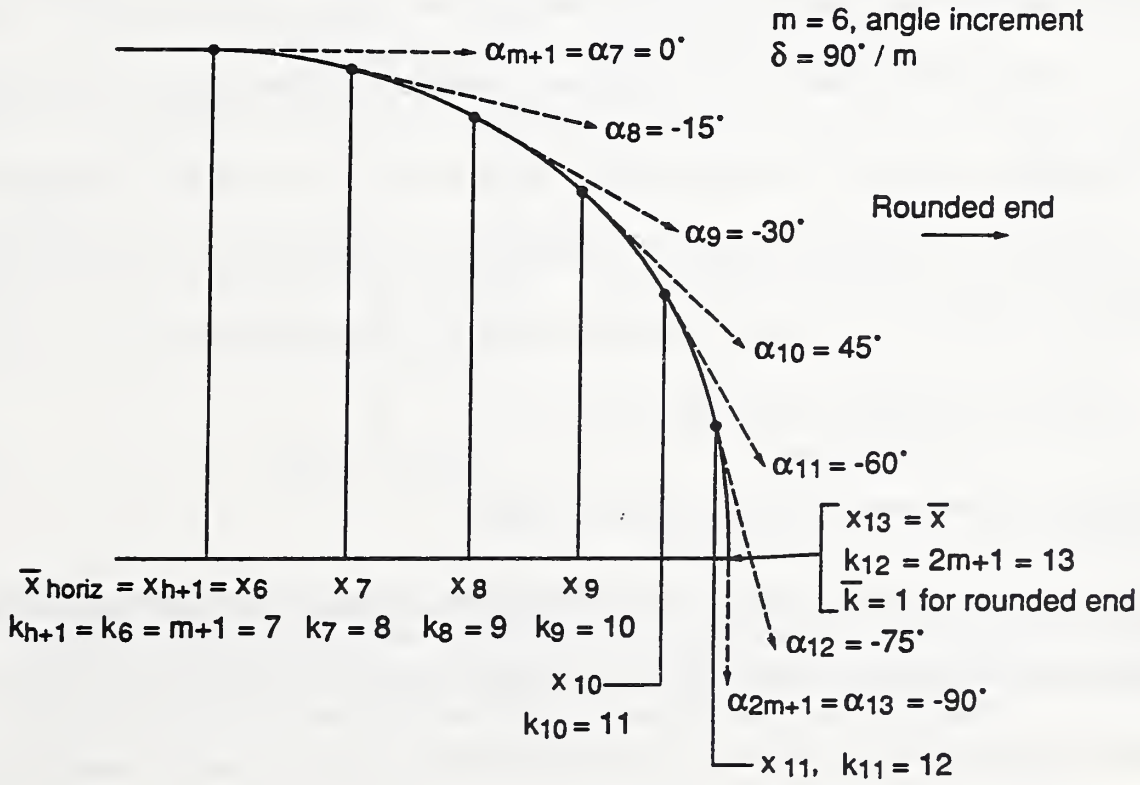

Fig. 4b: Cross-section placements for a descending profile curve with rounded end.

tangent touches the left endpoint of the contour function. If the left end of the shell of revolution is pointed, then the contour tangent with angle α_2 may still touch at the same endpoint. In fact it will continue to do so for higher values of k until α_k becomes smaller than the limit angle $\underline{\lambda}$ at the left end of the contour function (see Fig.4). Let $\underline{k}$ be the largest value of k for which the corresponding tangent still touches at $\underline{x}$. We will associate that value of k with the selection $x_1 = \underline{x}$ and put $k_1 = \underline{k}$. We then let x_2 be the x-coordinate of the subsequent point of tangential contact, associated with $k_2 = \underline{k} + 1$. The horizontal tangent corresponds to $k = m + 1$, and so, for $h = m + 2 - \underline{k}$, we select $x_h = \underline{x}_{horiz}$ with $k_h = m + 1$ and, if $\underline{x}_{horiz} \neq \bar{x}_{horiz}$, $x_{h+1} = \bar{x}_{horiz}$ with $k_{h+1} = m + 1$. Subsequently, the angles α_k become negative and decrease until, for the first time, the right end of the contour function is the tangential point of contact, giving rise to the selection $x_n = \bar{x}$ with $k_n = 2m + 2 - \bar{k}$ where $\bar{k}$ denotes the number of values k whose corresponding tangents touch the contour function at its right end $\bar{x}$. If both ends are rounded, then $\underline{k} = \bar{k} = 1$. Also $n = 2m + 3 - \underline{k} - \bar{k} + d$ and $k_n = n + \underline{k} - 1 - d$, where $d = 1$ if a horizontal portion is present, and $d = 0$ otherwise.

The index bounds $\underline{i}$, $\bar{\imath}$, for which $\underline{u} = v_{\underline{i}}$ and $\bar{u} = w_{\bar{\imath}}$, are now readily characterized. If $k(+\theta)$ and $k(-\theta)$ are such that $\alpha_{k(+\theta)} = +\theta$ and $\alpha_{k(-\theta)} = -\theta$, then $k(+\theta) + k(-\theta) = 2m + 1$. If $k(+\theta) \leq \underline{k}$ then $\underline{i} = 1$. Else $\underline{i}$ is such that $k_{\underline{i}} = k(+\theta)$. Symmetrically, if $k(-\theta) \geq \bar{k}$ then $\bar{\imath} = n$. Else $\bar{\imath}$ is such that $k_{\bar{\imath}} = k(-\theta)$.

Analysis of the Space Shuttle External Tank

There are small differences between individual external tanks for the Space Shuttle. Measurements, parametric equations and location of center of gravity were derived for a generic approximation derived from engineering drawings [15] and personal communication

[2]. Our purpose is to demonstrate general feasibility of the method rather than to produce results for a particular application. The measurements and parametric equations used for the prototype external tank are shown in Figure 5. Appendages such as the LO_2 feedline and the forward and aft orbiter connection truss assemblies have not been included in our analysis due to the present limitation of being able to handle only one shell of revolution at a time. However, the above mentioned appendages are relatively small, with respect to the area of the overall tank, and should not greatly affect the results for orbital lifetime and station-keeping fuel calculations.

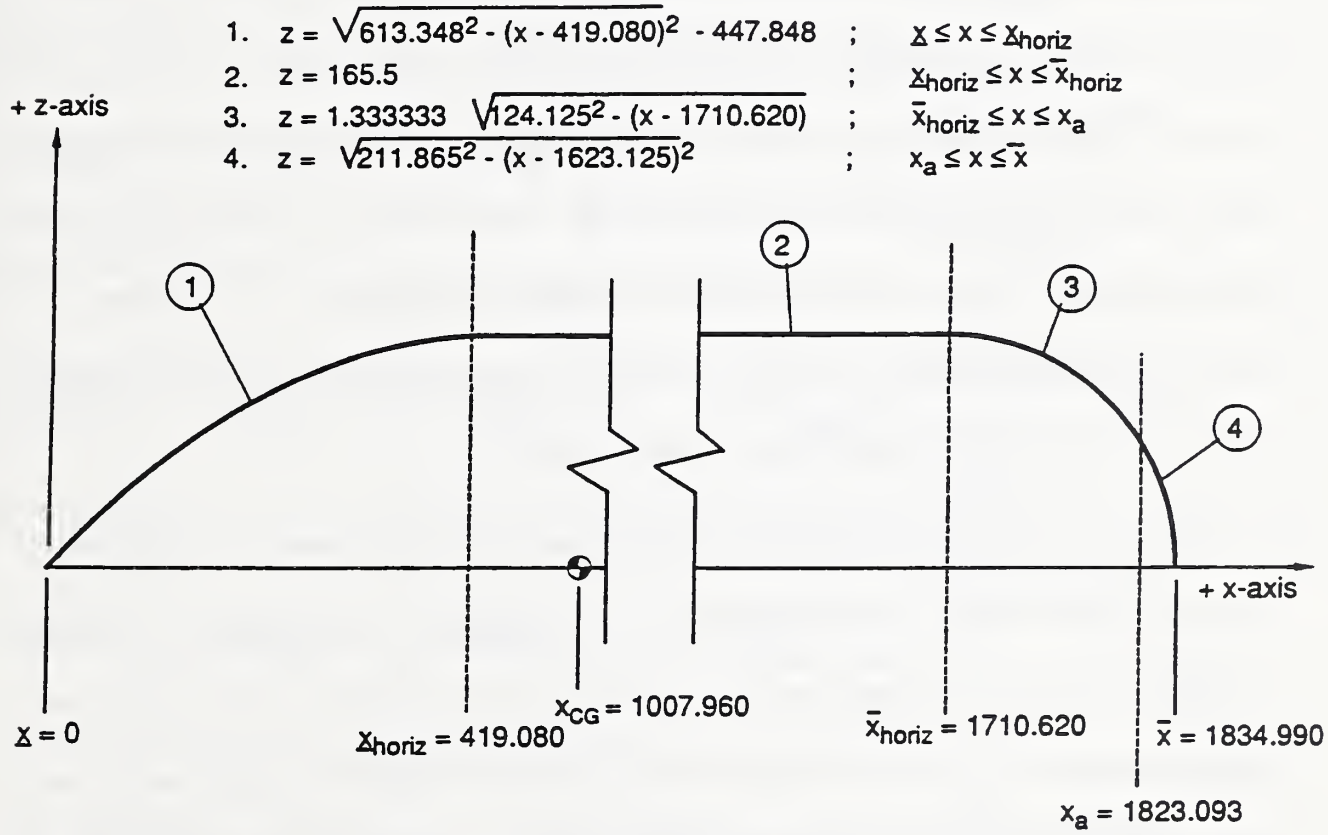
1. $z = \sqrt{613.348^2 - (x - 419.080)^2} - 447.848$; $\underline{x} \le x \le \underline{x}_{horiz}$
2. $z = 165.5$; $\underline{x}_{horiz} \le x \le \bar{x}_{horiz}$
3. $z = 1.333333\ \sqrt{124.125^2 - (x - 1710.620)}$; $\bar{x}_{horiz} \le x \le x_a$
4. $z = \sqrt{211.865^2 - (x - 1623.125)^2}$; $x_a \le x \le \bar{x}$
+ z-axis
1
2
3
4
+ x-axis
$\underline{x} = 0$
$\underline{x}_{horiz} = 419.080$
$x_{CG} = 1007.960$
$\bar{x}_{horiz} = 1710.620$
$\bar{x} = 1834.990$
$x_a = 1823.093$

Fig. 5: Parametric representation of the Space Shuttle external tank. Curve 1 represents the exterior (exposed) curved portion of the LO_2 tank; curve 2 represents the intertank and cylindrical mid-section of the LH_2 tank; curve 3 represents the ellipsoidal portion and curve 4 the spherical portion, respectively, of the H_2 tank.

Figure 6 presents the results of an analysis of the external tank at six representative angles of attack. The projected kinematic profiles are shown under the column marked "shape." These and other numerical experiences [11] indicate that the algorithm is sufficiently robust to handle all possible angles of attack from 0° to 90° degrees.

Some comments are in order concerning the general numerical performance and mathematical accuracy of the method. By mathematical accuracy we mean the accuracy of the results for the shell of revolution as described by the parametric equations without accounting for errors inherent in the parametric equations themselves due to approximations and assumptions in their derivation. The choice of the angle increment guides the selection of the cross sections: the smaller δ, the larger the number of cross sections. As one might expect, accuracy grows with the number of cross sections. Typically for discretization methods, however, there are limits beyond which further refinement of the discretization yields no improvement. This is due to the finite wordlength of the computer – calculations were carried out in single precision – as well as subsidiary computations such as the determination of cross section location by prescribed tangential angles.

For our calculations concerning the external tank, the limit appears to be reached for angle increment $\delta = 0.2°$. With this limitation, the algorithm achieves an accuracy of about six significant digits for the drag area, and about four for the eccentricity. The latter is more sensitive because, in the case of external tank, the center of gravity and the center of area moment tend to be close. The table in Figure 7 shows, for several values of the angle of attack θ, the various degrees of accuracy achieved as the angle increment δ is decreased.

In order to represent the drag area and the aerodynamic eccentricity of the external tank

Angle of Attack (degrees)	Drag Area (10^3 sq. in.)	Eccen-tricity (inch)	Shape (u-axis oriented toward left)
0	86.049	0.00	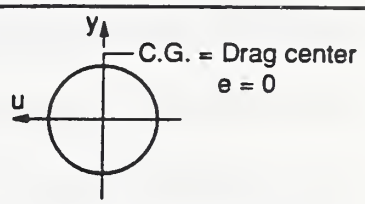
5.125	128.42	-4.54	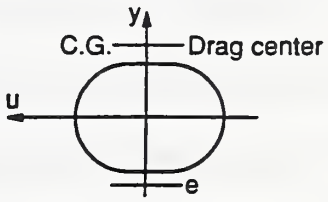
11.25	171.31	-7.04	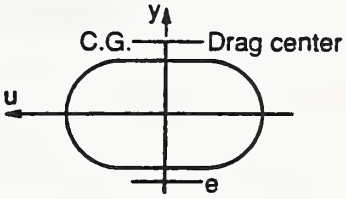
22.50	256.78	-6.28	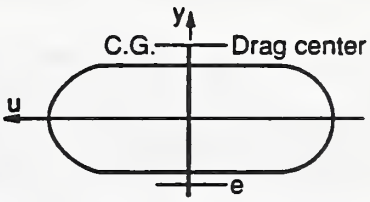
45.0	412.01	12.06	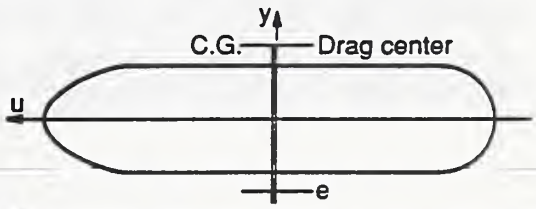
90.0	555.08	40.89	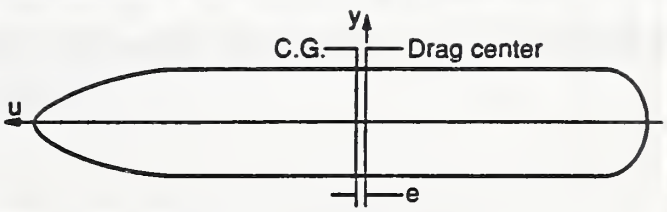

Fig. 6: Drag profile for Space Shuttle External Tank for Angles of Attack between 0° and 90°.

as a function of the angle of attack θ, the above quantities of interest have been evaluated at suitable intervals in preparation of fitting suitable regression equations. Certain inherent properties of these functions, however, should be preserved. Thus the value A_0 of the drag area for $\theta = 0°$ is exactly the area of the circular cross section of maximum diameter. That value should be precisely reproduced. In addition, the drag area function has a maximum with horizontal tangent at $\theta = 90°$. Analogously, the aerodynamic eccentricity vanishes for $\theta = 0°$ and also has a horizontal tangent at $\theta = 90°$. These two considerations suggest fits of the functional form $A_0 + P(\sin\theta)\sin\theta$ and $Q(\sin\theta)\sin\theta$, respectively, with polynomials P and Q determined by the regressions:

$$P(\sin\theta) \sim \frac{A_{drag} - A_0}{\sin\theta}, \quad Q(\sin\theta) \sim \frac{e_{aero}}{\sin\theta}.$$

	drag area (square inches)			*eccentricity (inches)*		
	$\theta = 10°$	$\theta = 20°$	$\theta = 30°$	$\theta = 10°$	$\theta = 20°$	$\theta = 30°$
$\delta = 90°/18$	161648.3	237828.5	311757.0	−6.82970	−7.35425	−2.44331
$\delta = 90°/36$	161726.6	237930.6	311891.8	−6.75525	−7.24731	−2.29323
$\delta = 90°/72$	161747.3	237956.7	311925.9	−6.66586	−7.08309	−2.05549
$\delta = 90°/144$	161752.7	237963.4	311934.5	−6.66063	−7.07611	−2.04601
$\delta = 90°/288$	161754.0	237965.0	311936.7	−6.65928	−7.07434	−2.04363
$\delta = 90°/576$	161754.4	237965.5	311937.2	−6.65893	−7.07390	−2.04303

Fig.7: Drag Area and Eccentricity of the External Tank under Successive Refinement of Discretization.

Such regressions were obtained for the external tank, based on 18 evaluations with θ ranging from 5° to 90° at intervals of 5°. For these evaluations, the cross sections were placed according to an angle increment $\delta = 0.25°$. The equation for drag area as a function of angle of the attack θ is:

$$A_{drag} = 86049 + 425680.2 \sin\theta + 62195.0 \sin^2\theta - 18409.5 \sin^3\theta.$$

The units for A_{drag} are square inches. Similarly, the aerodynamic eccentricity can be represented as follows:

$$e_{aero} = -55.805 \sin\theta + 94.439 \sin^2\theta + 35.210 \sin^3\theta - 32.966 \sin^4\theta.$$

The units for e_{aero} are inches. Both equations are valid for

$$0° \leq \theta \leq 180°.$$

where θ denotes the angle of attack. Should a value of θ between 180° and 360° be specified, then it should be replaced by $360° - \theta$. Both equations are plotted in Figure 8 against the 18 data points. The plots indicate agreement within at least two significant digits.

Expressing the eccentricity e_{aero} as a polynomial in $\sin\theta$ is natural for further reason: if the shell of revolution has a center of symmetry, then the eccentricity is a pure sine wave.

Derivation of the Breakpoint Formulas

We will now address the derivation of the expressions used in the fourth section for the breakpoints v_i, w_i. We will prove that for $\underline{i} \leq i < \bar{\imath}$:

$$w_i = u_i - b_i \left[\frac{a_{i+1} - a_i}{u_{i+1} - u_i}\right] \cos\theta = u_i - b_i \frac{\Delta_i}{\tan\theta}, \quad \Delta_i = \frac{a_{i+1} - a_i}{x_{i+1} - x_i}.$$

Here a_i, a_{i+1} are the major axes, b_i, b_{i+1} the minor ones, and $u_i = x_i \sin\theta$, $u_{i+1} = x_{i+1}\sin\theta$ the u-coordinates of the centers of two consecutive ellipses $\mathbf{E}_i$ and $\mathbf{E}_{i+1}$.

Proof: There are, in general, two pairs of common tangents. Here we are only concerned with those common tangents which leave both ellipses on the same side. Such tangents exist if one ellipse does not contain the other. If both ellipses are of the same size, $a_i = a_{i+1}$, then the above formulas are obviously correct. Thus we are left with the case $a_i \neq a_{i+1}$. In this case there exists a center of similarity $(u_{sim},\ y_{sim}) = (u_{sim}, 0)$ on the u-axis such that the scale to which the ellipses are drawn is proportional to their distance from that center. For the major axes a_i, a_{i+1} that implies:

$$\frac{a_{i+1}}{a_i} = \frac{u_{i+1} - u_{sim}}{u_i - u_{sim}}.$$

From this

$$u_{sim} = \frac{a_{i+1}u_i - a_i u_{i+1}}{a_{i+1} - a_i}, \quad u_{sim} - u_i = -a_i\left[\frac{u_{i+1} - u_i}{a_{i+1} - a_i}\right] = -\frac{a_i \sin\theta}{\Delta_i}.$$

It is also clear that any straight line connecting similar points of the two ellipses, respectively, must pass through the center of similarity. The points of equal slope above – and also those below – the u-axis on each ellipse are such similar points. The two common tangents, in particular, intersect therefore at that center. It follows that the vertical line $u = w_i$, which connects the points of contact of those tangents, is the polar of the center of similarity with respect to ellipse $\mathbf{E}_i$ and must thus agree with the line described by the well-known formula for the polar:

$$\frac{(u - u_i)(u_{sim} - u_i)}{b_i^2} + \frac{y y_{sim}}{a_i^2} = \frac{(u - u_i)(u_{sim} - u_i)}{b_i^2} = 1.$$

Thus, and since $b_i = a_i \cos\theta$,

$$w_i = u_i + \frac{b_i^2}{u_{sim} - u_i} = u_i + \frac{b_i a_i \cos\theta}{u_{sim} - u_i}.$$

An expression for $u_{sim} - u_i$ has been derived above and, upon substitution yields the desired expression for w_i.

Conclusions

Plans are presently underway by university and industry groups to make use of the Space Shuttle external tank in low earth orbit for several purposes, including a low-cost laboratory/residence, as a container for storage of propellants, and as raw material for the on-orbit construction of more advanced spacecraft. The orbital lifetime for an exceptionally large structure, such as the external tank, is highly dependent upon the attitude of the tank with respect to the velocity vector, particularly at altitudes below 400 kilometers where aerodynamic drag is the dominant disturbing force. This paper details a general numerical procedure capable of calculating the aerodynamic drag and torque on such shells of revolution for arbitrary angles of attack. The procedure is suitable for use as a subroutine in an orbital lifetime and reaction control simulation package. For a given shell, the functional dependence of drag area and aerodynamic eccentricity on the angle of attack can be expressed to a high degree of accuracy in the least squares sense by polynomials of low degree which may be suitable for processing in real time for the purposes of altitude and attitude control.

The method extends naturally to shells of revolution which are not members of the category treated in this paper. We are planning to extend software capabilities accordingly to permit straight line segments in the contour other than the horizontal one, and to relax

the requirement for unique tangents at each point along the shell. We expect that small appendages can be treated , and that the above analysis can be extended – if aerodynamic interaction effects are assumed – to the case of unions of convex shells of revolution whose axes are parallel.

List of Symbols

$\mathbf{i}$	=	attitude unit vector
V	=	translational velocity (scalar)
$\mathbf{v}$	=	velocity unit vector
θ	=	angle of attack
$\mathbf{F}_{aero}$	=	drag force vector
$\mathbf{N}_{aero}$	=	aerodynamic torque
$\mathbf{P}$	=	plane of projection; perpendicular to $\mathbf{v}$
A_{drag}	=	drag area; area of drag profile
C_{drag}	=	drag coefficient
ρ	=	atmospheric density
$\mathbf{R}_{cg}$	=	eccentricity vector
e_{aero}	=	aerodynamic eccentricity; size of $\mathbf{R}_{cg}$
$x-$axis	=	axis of revolution
$z-$axis	=	perpendicular to $x-$axis so that $x,z-$plane contains $\mathbf{v}$
$y-$axis	=	perpendicular to $x,z-$plane; lies in $\mathbf{P}$
$u-$axis	=	perpendicular to $y-$axis in $\mathbf{P}$
$\underline{x}$, $\bar{x}$	=	coordinates of maximum longitudinal extension of shell
$\underline{x}_{horiz}$, $\bar{x}_{horiz}$	=	coordinates of maximum longitudinal extension of cylindrical portion
x_i	=	locations of cross sections marked on axis of revolution
δ	=	increment of tangential angle by which x_i are selected
$\underline{u}$, $\bar{u}$	=	coordinates of maximum longitudinal extension of drag profile
$\mathbf{E}_i$	=	ellipse projected into $\mathbf{P}$ from circular cross section at x_i
a_i, b_i	=	major, minor axes of $\mathbf{E}_i$
u_i	=	$u-$coordinate of center of $\mathbf{E}_i$
v_i, w_i	=	$u-$coordinates dividing drag profile into strips
s_i, t_i	=	$y-$coordinates of drag contour at v_i, w_i
Δ_i	=	inverse differences of contour values a_i at x_i
ρ_i	=	auxiliary quantities from Δ_i, θ

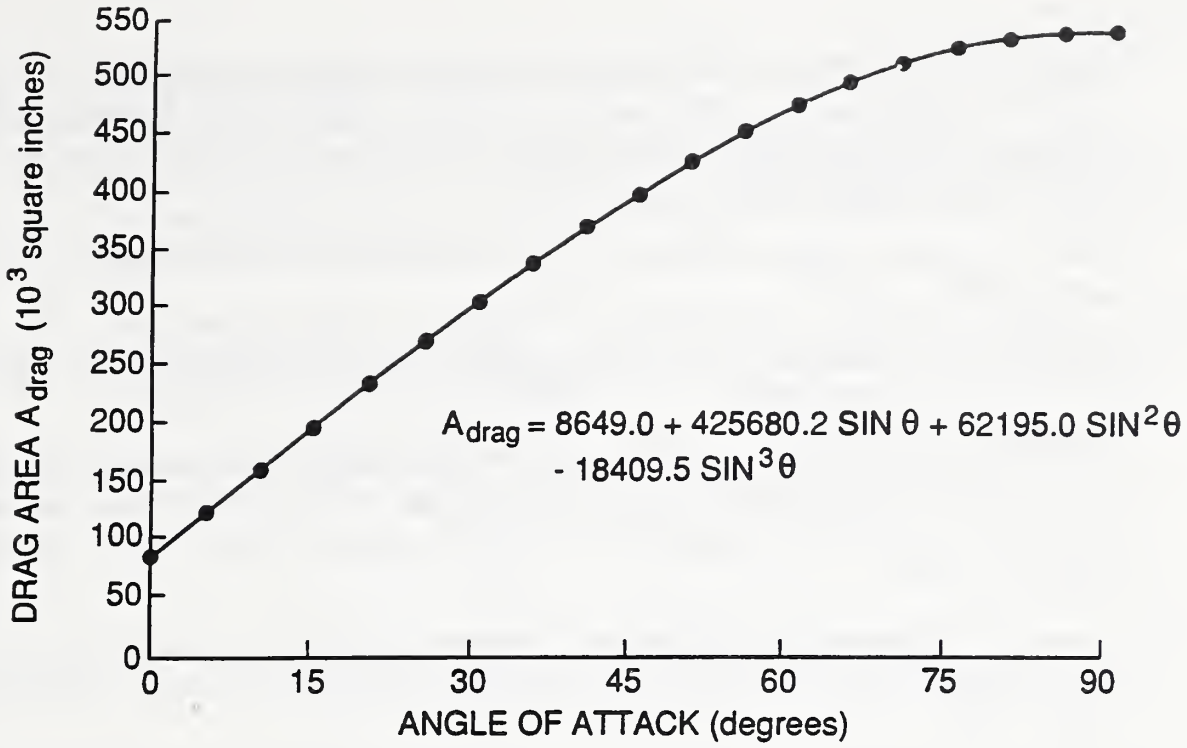

Fig. 8a: Drag area (10^3 square inches) as a function of angle of attack (degrees) for the Space Shuttle external tank.

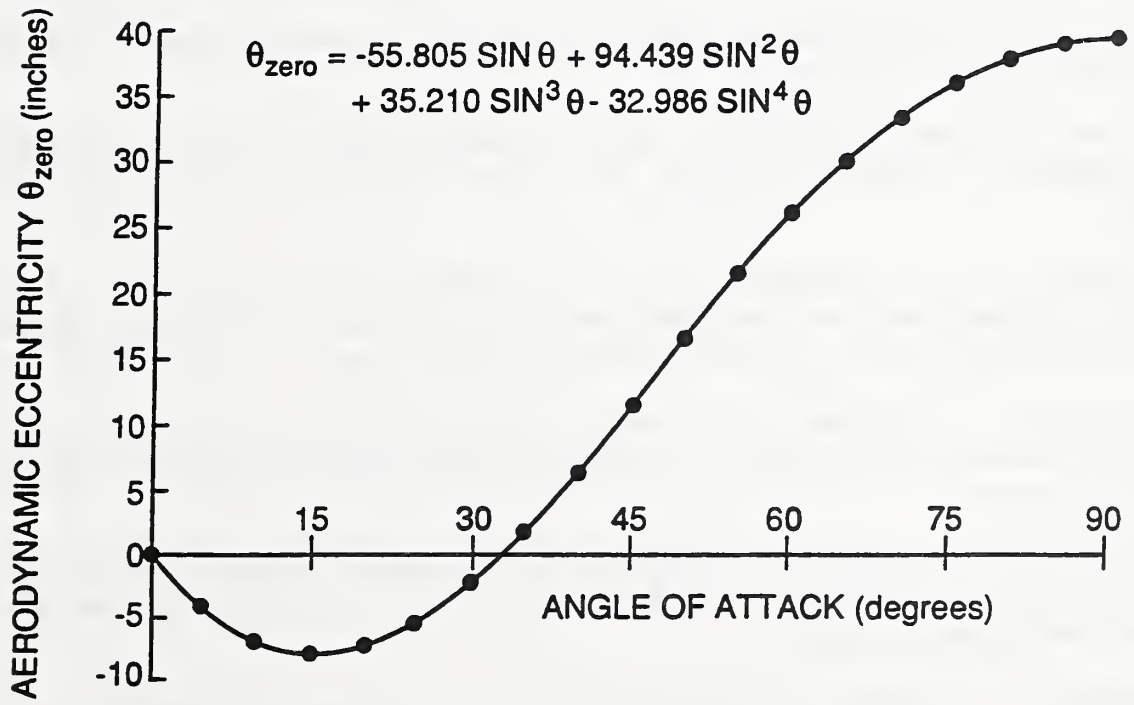

Fig. 8b: Aerodynamic eccentricity (inches) as a function of angle of attack (degrees) for the Space Shuttle external tank.

References

1. Arnold, J.R., et.al., "The Process of Space Station Development Using External Tanks," Report by the External Tank Working Group of the California Space Institute, Scripps Institution of Oceanography, to the Office of Technology Assessment, Space Station Review Project, March 1983.

2. Baillif, F., Martin Marietta Office of Advanced Programs, personal communication, January 1989.

3. Beletskii, V.V., "Motion of an Artificial Satellite About its Center of Mass," NASA publication TT F-429, 1966.

4. Gottlieb, D.M., Gray, C.M., and Hotovy, S.G., "An Approximate Shadowing Technique to Augment the Aerodynamic Torque Model in the AE-C Multi- Satellite Attitude Prediction and Control Program (MSAP/AE)," Computer Science Corp., 3000-257-01TM, Oct. 1974.

5. Groves, G.V., "Seasonal and Latitudinal Models of Atmospheric Temperature, Pressure, and Density, 25 to 110 km," Air Force Cambridge Research Laboratories Report 70-0261, 1970.

6. Hoerner, S.F., "Fluid Dynamic Drag," Chapter 18: *Drag Characteristics at Hypersonic Speeds* 1965. Library of Congress Catalog Card #64-19666.

7. Jacchia, L.G., "Revised Static Models of the Thermosphere and Exosphere with Empirical Temperature Profiles," SAO Special Report 332, 1971.

8. Lin, T.D., et al., "Concrete Lunar Base Investigation," Journal of Aerospace Engineering, Vol. 2, pp. 10-19, 1989.

9. Schaaf, S.A., and Chambre, P.L., "Flow of Rarefied Gases," Number 8, Princeton Aeronautical Paperbacks, Princeton, New Jersey, Princeton University Press, 1961. 55pp.

10. Sedlund, C.A., and Sentman, L.H., "A CAD Method for the Determination of Free Molecule Aerodynamic and Solar Radiation Forces and Moments," 27^{th} AIAA Aerospace Sciences Meeting, Reno, Nevada, January 9-12, 1989. Paper No. AIAA-89-0455, 9pp.

11. Stone, W.C., and Witzgall, C., "A Computer Program for Determining the Projection and its Associated Quantities for a Convex Shell of Revolution," NIST Technical Report in preparation.

12. Stone, W.C., and Witzgall,C., "Evaluation of Aerodynamic Drag and Torque for External Tanks in Low Earth Orbit," Proceedings of the 9th Princeton Conference on Space Manufacturing, 1989.

13. Tidwell, N.W., "Modeling of Environmental Torques of a Spin-Stabalized Spacecraft in Near-Earth Orbit," Journal of Spacecraft, Vol. 7, pp.1425-1435, 1970.

14. "External Tank Utilization for Early Space Construction Base," Marshall Space Flight Center, Dec. 1976.

15. "Space Shuttle External Tank (Light Weight Model): System Definition Handbook," Volume II, Martin Marietta, Michoud Division, New Orleans, La., Document # NAS8-30300 REV. A, April 1983.

16. "Spacecraft Attitude Determination and Control," James R. Wertz, ed., D. Reidel Publishing Co., Boston, U.S.A., 1986. Distributed by Kluwer Academic Publishers, 101 Philip Dr., Norwell, MA 02061.

17. "Utilization of Space Shuttle External Tanks," NASA MOU # 1560-001, Dec. 1988.

Acknowledgements

Dr. Ronald G. Rehm contributed to the initial discussions of the procedure, and Ms. Geraldine Cheok helped iron out last minute problems. The assistance of these coworkers at NIST is much appreciated.

Autonomous Propulsion System Requirements for Placement of an STS External Tank in Low Earth Orbit

by

William C. Stone
and
Geraldine S. Cheok

Abstract

This paper discusses the findings of an extensive series of computer simulations carried out at the National Institute of Standards and Technology to investigate the requirements for powered flight of the external tank through the thermosphere following separation from the Shuttle orbiter at main engine cutoff (MECO). The object of the investigation was to determine the minimum thrust and fuel requirements for an autonomous exterior propulsion package attached to the external tank in order to avoid re-entry on the critical first orbit, and to place the tank in a short term stable orbit from which customary orbit maintenance procedures may be carried out. Descriptions are given for the differential equations of motion, and the atmospheric drag and propulsion models used in the solution.

Introduction

Significant interest has developed during the past two years for the on-orbit utilization of the external tank for the Space Shuttle, that is, the U.S. Space Transportation System (STS). The external tank is currently the only non-reusable component of the STS. On a nominal "standard insertion" launch these tanks, which carry cryogenic oxygen and hydrogen to fuel the three main shuttle engines, reach approximately 98% of orbital velocity at an altitude of about 105 kilometers, after which they separate from the orbiter and are left to re-enter the earth's atmosphere. Each tank measures 8.4 m in diameter by 46.5 m in length and contains an enclosed volume of 2069 cubic meters which is structurally capable of handling internal pressures necessary for human habitation. Potential commercial uses of these tanks in space include, among others, low-cost manned orbital workshops and man-tended manufacturing platforms [Sophron 1984]; fuel storage depots [Arnold, 1983]; and as building blocks for low-cost lunar spacecraft [King, 1989]. Although it is possible on most missions for the Space Shuttle to take the external tank into orbit [NASA, 1988], this has not yet been attempted for several reasons. First, the shuttle cargo bay payload capacity (already a premium) or the maximum mission altitude would generally have to be reduced to accommodate the increased amount of propellant needed to boost the external tank to orbit. Secondly, after achieving orbit, safety issues arise relating to the control of the tank in the vicinity of a manned orbital vehicle (i.e. the Shuttle orbiter), and in particular to the question of uncontrolled random re-entry ("Skylab Syndrome").

Because of these concerns it is desirable to consider the development of an economical means for autonomous placement of the tanks in long term stable orbits following the current separation sequence of the tank from the Shuttle orbiter.

Because of the potentially high payoff, in terms of enhanced on-orbit capability at vastly reduced cost, to U.S. companies seeking to conduct business in space, the National Institute of Standards and Technology has undertaken a research program to resolve the engineering questions relating to the placement, stabilization, and pressurization of Space Shuttle external tanks in low earth orbit. In this paper we discuss the requirements for powered flight of the external tank through the thermosphere following separation from the Shuttle orbiter at main engine cutoff (MECO).

For the reader who is not familiar with shuttle operations, reference to Figure 1 will be of use. This shows a typical time sequence from launch to orbit for the STS for what is known as a "Nominal (or Standard) Insertion" mission, which is by far the most difficult case to solve in terms of propulsion requirements for an external tank. The methods which will be subsequently described apply equally well to "Direct Insertion" missions [see NASA, 1988]. In both cases solid rocket booster staging occurs approximately 2 minutes into launch, after which the orbiter and external tank continue to a predefined altitude of approximately 105 kilometers. There main engine cutoff (MECO) occurs and the external tank is jettisoned. On a Nominal Insertion launch the external tank will then trace an elliptical orbit with an apogee altitude of approximately 159 kilometers and a

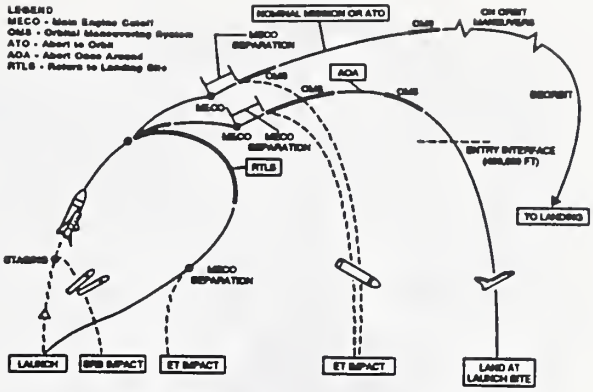

Figure 1: Standard Space Shuttle Launch Scenarios

perigee altitude of about 7 kilometers. It is generally recognized that a spacecraft which descends into the atmosphere below an altitude of approximately 70 kilometers will shortly re-enter and burn up, unless specific steps are taken to increase its tangential velocity. For the external tank this point is reached approximately 45 minutes beyond MECO, after which atmospheric drag increases exponentially, leading to the destruction of the tank. Of particular interest, then, is the determination of the minimum thrust and fuel required to avoid re-entry of the external tank during the critical first orbit.

Orbital Dynamics

For the purposes of solving the problem described above, it is sufficient to consider the problem of orbital mechanics in two dimensions, as shown in Figure 2. Perturbations due to the asphericity of the earth are not considered. Given an initial set of conditions such as the altitude of the external tank at MECO, the altitude at apogee, and the altitude at perigee [as provided in NASA, 1988], it is possible to determine both the location and velocity of the tank from orbital mechanics as follows:

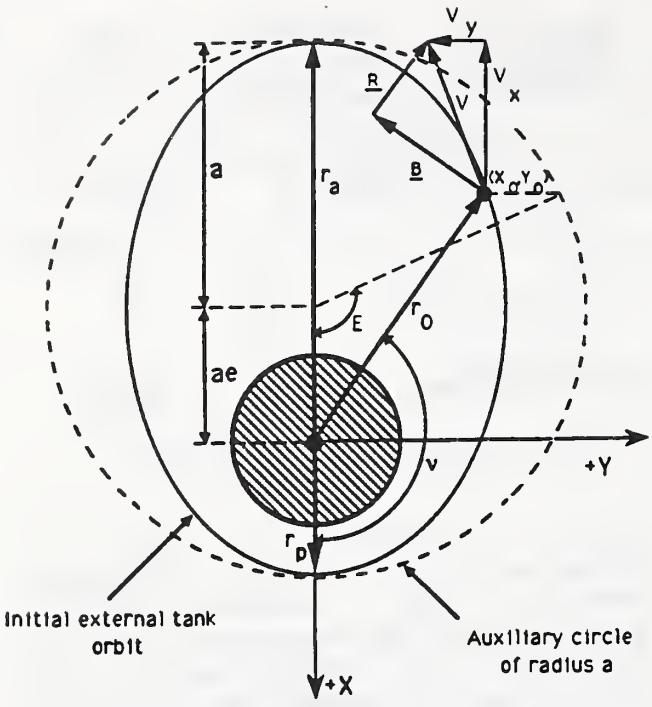

Figure 2: Orbital Mechanics Variables for External Tank Motion

First, the orbital radii at MECO (r_0), apogee (r_a), and perigee (r_p) are determined by adding 6378 km (the average radius of the earth) to the respective altitude figures already given. The orbit is described by an ellipse with a semi-major axis length, a, given by:

$$a = \frac{r_a + r_p}{2} \qquad (1)$$

The eccentricity, e, for this orbit is given by:

$$e = \frac{r_a}{a} - 1 \qquad (2)$$

The eccentric anomaly, E, in radians, measured counterclockwise from the positive X-axis (see Figure 2), is given by:

$$E = \cos^{-1}\left[\frac{a - r_0}{ae}\right] \qquad (3)$$

At this point it is convenient to establish a cartesian coordinate system which can be used to describe both the position and velocity components of the external tank. The positive X-axis, with an origin at the center of the earth, is arbitrarily chosen to be parallel to the semi-major axis of the initial orbit ellipse in the direction of perigee. The initial tank coordinates at MECO are given by:

$$X_0 = a(\cos(E) - e) \qquad (4)$$

$$Y_0 = a\sqrt{(1-e^2)}\ \sin(E) \qquad (5)$$

The determination of the initial cartesian velocity components, V_{x0} and V_{y0}, begins with the calculation of the velocity components parallel and perpendicular to the initial radius vector r_0. These are, respectively:

$$\underline{R} = \frac{\sqrt{\mu a}\ e \sin(E)}{r_0} \qquad (6)$$

$$\underline{B} = \frac{\sqrt{\mu a\ (1-e^2)}}{r_0} \qquad (7)$$

Where μ = 398600 $Km^3/second^2$, and is the gravitational parameter for a spacecraft in near earth orbit. The true anomaly, ν, represents the counterclockwise angle, in radians, from the positive X-axis to the radius vector r_0 in Figure 2. The sine and cosine of the true anomaly are given by:

$$\cos(\nu) = \frac{a(\cos(E) - e)}{r_0} \qquad (8)$$

$$\sin(\nu) = \frac{a\sqrt{(1-e^2)}\,\sin(E)}{r_0} \qquad (9)$$

Using equations 6 through 9 the initial cartesian velocity components may be recovered directly as:

$$V_{x0} = \underline{R}\cos(\nu) - \underline{B}\sin(\nu) \qquad (10)$$

$$V_{y0} = \underline{R}\sin(\nu) + \underline{B}\cos(\nu) \qquad (11)$$

The velocity magnitude at any time may be determined as:

$$V = \sqrt{V_x^2 + V_y^2} \qquad (12)$$

And the proportional fractions of the velocity at any time in the X and Y directions are given by:

$$\tau_x = \frac{V_x}{V} \qquad (13)$$

$$\tau_y = \frac{V_y}{V} \qquad (14)$$

Perturbing Accelerations

During the critical post-MECO period, the external tank will be acted upon by two disturbing forces which in turn produce perturbing accelerations which must be accounted for in the differential equations describing the motion of the tank. These disturbing forces are aerodynamic drag and the thrust produced by the propulsion package. Disturbing forces typically included in long duration orbital lifetime calculations, such as solar radiation pressure, represent second order effects for spacecraft at altitudes below 500 kilometers and are therefore not considered in this analysis. The aerodynamic deceleration per unit mass is given by:

$$T_a = -\frac{C_d\, A_d\, \rho\, V^2}{2m} \qquad (15)$$

where:

C_d = drag coefficient, taken as 2.0 for the external tank, a dimensionless quantity.

A_d = projected drag area perpendicular to the velocity vector, in square meters.

ρ = atmospheric density in kg/m^3.

m = mass of the empty external tank plus any residual hydrogen and oxygen following MECO, plus the weight of any external propellants (which vary with time as the ΔV motor is fired), storage vessels, and propulsion hardware, in kg.

A few comments are in order regarding the above. Accurate closed form solutions are now available for external tank drag area for any given angle of attack (Stone and Witzgall, 1989). The minimum and maximum drag areas are 55.51 and 358.12 square meters for angles of attack of 0 and 90 degrees, respectively. The atmospheric density, ρ, used in this study is described by the National Standard Atmosphere (NOAA, 1976) for

altitudes between 60 and 85 kilometers and by (Tobiska, 1989) for altitudes above 85 kilometers. Both the solar maximum and solar minimum conditions were considered in the analyses, since the atmospheric density may vary by as much as an order of magnitude during the 11 year solar cycle. Presently Solar Maximum is predicted to occur sometime in 1990 with Solar Minimum in 1997. These can represent real launch constraints if the mass of the external tank propulsion package is to be minimized.

It is assumed that a suitable attitude control system is provided which is capable of maintaining the longitudinal axis of the tank parallel to the velocity vector. This is essential to any practical application involving the tanks below an altitude of approximately 500 kilometers, since the drag area for a 90 degree angle of attack is nearly six and one half times that for the head-on configuration and would lead to premature re-entry. The thrust may be either positive or negative. The latter case applies specifically to the problem of de-orbiting the external tank, which is of considerable importance if the tank must be made to safely re-enter and land in a specific, uninhabited location on the earth's surface. The thrust acceleration (or deceleration) is given by:

$$T_f = \frac{F}{m} \qquad (16)$$

where F is the thrust in Newtons of the propulsion system and m has units of kilograms. It should be noted that during an engine burn m is constantly changing since the propellant mass is decreasing. The overall spacecraft mass is thus given by:

$$m = M_{tank} + M_{fuel} - \frac{Ft}{I_{sp} g_0} \qquad (17)$$

where:

M_{tank} = the structural mass of the external tank plus any residual cryogens (hydrogen and oxygen) not used for the propulsive maneuver, plus the structural weight of the propulsion module.

M_{fuel} = the mass of fuel <u>initially</u> available for use by the propulsion module.

t = the cumulative time of operation of the propulsion module at full rated thrust, in seconds.

I_{sp} = the Specific Impulse of the fuel used in the propulsion system, in seconds. Generally, the higher the value of I_{sp}, the higher the performance of the rocket motor. Gaseous hydrogen oxygen thrusters have an I_{sp} near 400s; solid rocket motors, about 200s.

g_0 = acceleration due to gravity at the earth's surface.

It should be noted that quantity

$$M_{fuel} - \frac{Ft}{I_{sp} g_0} \qquad (18)$$

represents the usable fuel reserve. In the results described below it is assumed that once the motor is fired, it will continue firing until the fuel reserve allotted for the initial burn is expended, after which the tank will coast until further authority to fire at some later time is received. In the analysis the

value of T_f is set to zero when equation (18) reaches zero. This is distinctly different from Hohmann Transfer theory (Kaplan, 1981), which assumes all velocity change to occur instantaneously. For a system having a very low thrust level and a large quantity of available fuel, the burn arc, or arc angle of an orbit through which the motor is firing, can be significant. Numerical integration, therefore, is the only means of accurately tracing the resulting motion of the tank. It should be noted that the location of ΔV burn initiation will also significantly affect the path of the tank, and the available time in orbit.

The sum of equations 15 and 16 gives the cumulative perturbing acceleration acting upon the external tank:

$$T = T_f - T_a \qquad (19)$$

Differential Equations of Motion

The motion of the external tank in two dimensions can be completely described by four differential equations, two containing derivatives of the velocity components V_x and V_y and two containing derivatives of the position vectors X and Y, as follows:

$$\frac{dV_x}{dt} = -\frac{\mu}{r^3} X + \tau_x T \qquad (20)$$

$$\frac{dV_y}{dt} = -\frac{\mu}{r^3} Y + \tau_y T \qquad (21)$$

$$\frac{dX}{dt} = V_x \qquad (22)$$

$$\frac{dY}{dt} = V_y \qquad (22)$$

The initial conditions for the above system are given in equations 4,5,10, and 11. The solution was carried out using single precision arithmetic on a Convex C-120 computer using the SDRIV numerical integration package (Kahaner, 1979) as an internal subroutine in the main program, ET_ORBIT, which consisted of 12,000 lines of Fortran 77 code. Single precision accuracy was determined through simulation to be adequate for the results reported below, which represent a relatively brief time on orbit. Off-the-shelf software, which operates in double precision, presently exists for long duration orbital lifetime calculations but these do not permit examination of powered flight.

Results

The objective of this study was to determine the smallest values for the propulsion system thrust and fuel mass required to avoid re-entry for a period sufficient to permit subsequent orbital optimization burns. For the sake of limiting computational time, the required orbital duration for a "successful" boost was set to 30 orbits, or approximately 2 days. During this time the propulsion system will be required to carry out an additional series of burns in order to boost the tank to a parking orbit with sufficient altitude to allow for storage periods of up to 30 years, depending upon the desired use. One recent study (NASA, 1988) has indicated that such a long term parking orbit would have an altitude in the vicinity of 500 kilometers.

To solve the differential equations, certain additional initial conditions must be specified such as the spacecraft mass (structural mass and residual fuel not available for propulsion), the ΔV burn initiation point, the aerodynamic drag model (which includes the specification of solar maximum or minimum and the angle of attack), and the specific impulse, I_{sp}, of the propellant. It may be appreciated that no single optimum design will exist for all users, owing to the availability of an appropriate launch window, safety considerations which may affect where a ΔV burn may be initiated, and budget constraints which may limit a smaller company to consideration of a lower performance propulsion package. The results presented below, therefore, cover a wide spectrum of variables which present a range of options to the user.

Apogee Burn

From an analytical point of view, a propulsive maneuver may be initiated at any time following separation from the shuttle (MECO). From a practical point of view, a minimum separation distance must be allowed between the shuttle orbiter and the external tank in order to maintain safety for the orbiter and its crew. Thus one insertion scenario for the external tank would consist of firing the exterior propulsion package as soon after MECO as safety permits. The alternative would be to allow the tank to coast to its initial apogee (approximately 159 km vs 105 km at MECO) before initiating the burn. This would be the location of choice for a conventional boost intended to raise the perigee altitude.

The apogee-boost case represents the most conservative opportunity for placement of an external tank in orbit at minimum cost. "Conservative" in this context refers to the lack of sensitivity of the resulting motion of the tank to errors in the thrust magnitude and direction. Other scenarios discussed below can be more efficient, but at the price of sensitivity to propulsion system thrust level and attitude vector alignment variations. Figures 3 and 4 show families of curves in which the X-axis represents ΔV motor thrust and the Y-axis represents the time until re-entry in hours. An ascending curve which has been terminated at 43 hours indicates that the tank is still in orbit, and has therefore undergone a successful boost. The mass of the vehicle has been assumed to be 74,000 lbm (33,596 kg), which includes a 5,000 lbm (2,270 kg) budget for residual cryogens in the liquid hydrogen (LH_2) and liquid oxygen (LO_2) tanks and support structures for the propulsion package. This can be considered representative of the vehicle mass during most missions although the residual cryogen mass can be substantially higher, depending on the particular mission. The effect of changing vehicle mass is discussed below. The vehicle mass does not include the fuel used by the propulsion system, which is accounted for separately in the calculations since it is a dynamic quantity. An I_{sp} of 400 seconds (oxygen/hydrogen) has been assumed; the performance for different values of specific impulse is subsequently discussed.

Both figures 3 and 4 indicate that a threshold value of approximately 400 lbf (1800 N) exists for the thrust level necessary to achieve orbit regardless of the amount of fuel available or the prevailing solar flux. This threshold can be viewed as the aerodynamic drag compensation thrust. From an engineering standpoint it will be necessary to

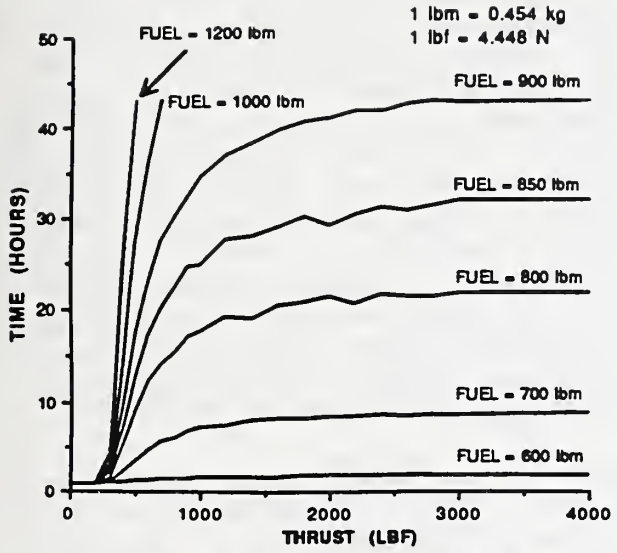

Figure 3: TIME IN ORBIT VS. ENGINE THRUST
Vehicle Mass = 74,000 lbm
ISP = 400 s, Burn at apogee
Solar minimum, Angle of attack = 0°

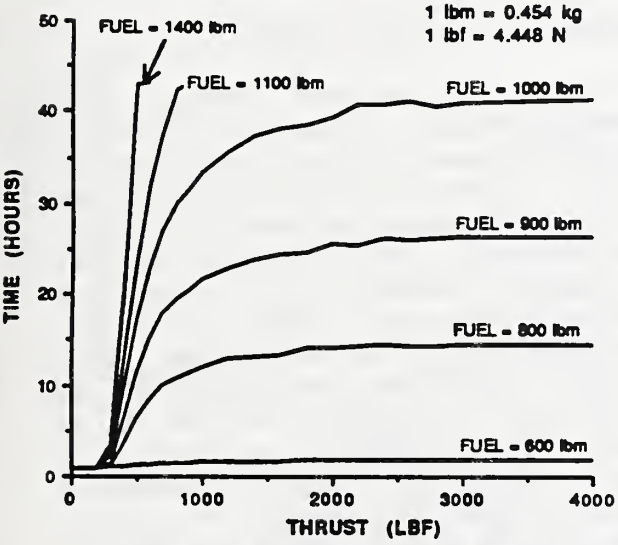

Figure 4: TIME IN ORBIT VS. ENGINE THRUST
Vehicle Mass = 74,000 lbm
ISP = 400 s, Burn at apogee
Solar maximum, Angle of attack = 0°

have sufficient reserve thrust to ensure attainment of orbit despite any problems which might arise, for example in the pointing accuracy of the reaction control system or a decrease in engine performance. A reasonable value of thrust would appear to be approximately 1000 lbf (4450 N). Such a thrust level could be obtained from a variety of off-the-shelf components and is in the range of the larger reaction control units presently employed on the space shuttle orbiter.

Figures 3 and 4 indicate that in order to achieve an initial 40 hour period on orbit (during which additional altitude boost maneuvers would be carried out) a propulsion fuel budget of 1100 lbm (454 kg) is needed under solar maximum conditions. For an oxygen/ hydrogen thruster running a mixture mass ratio of 6:1 (oxidizer: propellant), this amounts to a storage requirement of only 374 liters LO_2 and 1023 liters LH_2.

MECO Burn

The apogee burn scenario described above was termed "conservative", because the time available on-orbit increases monotonically for increasing levels of thrust and amount of propellant. This is not the case when the burn is initiated close to MECO, as shown in figures 5 and 6. Here it is seen that the threshold thrust level to achieve orbit is approximately 200 lbf (900 N). However, there is wide variation in the time in orbit, depending upon the chosen thrust level and fuel mass. Furthermore, thrust levels above 500 lbf (2200 N) lead to significantly decreased time in orbit. The performance depicted in figures 5 and 6 can be better appreciated when one considers the following rule of thumb in conjunction with figure 2, which shows the initial orbit parameters for the external tank at MECO: an instantaneous thrust impulse at any point in an orbit will have the

effect of raising the orbital altitude at a point 180 degrees opposite the point where the impulse was initiated. When low levels of thrust are applied continuously, the effect is generally to increase the orbital altitude at a point approximately 180 degrees opposite the center of the "burn arc". For the MECO burn scenario just described, high levels of thrust, combined with the relatively small quantities of fuel shown, represent nearly impulsive loading, which raises the initial orbital perigee only a small amount, compared with that for a smaller engine which burns over a much longer arc, indeed almost to initial apogee, before expending the same mass of fuel.

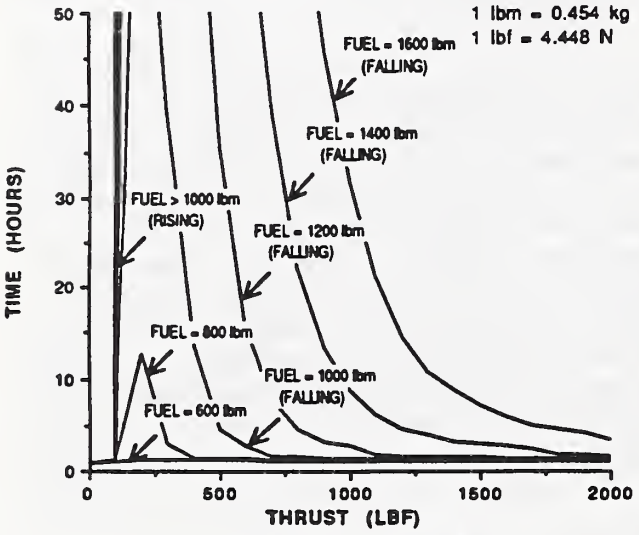

Figure 5: TIME IN ORBIT VS. ENGINE THRUST

Vehicle Mass = 74,000 lbm
ISP = 400 s, Burn at MECO
Solar minimum, Angle of attack = 0°

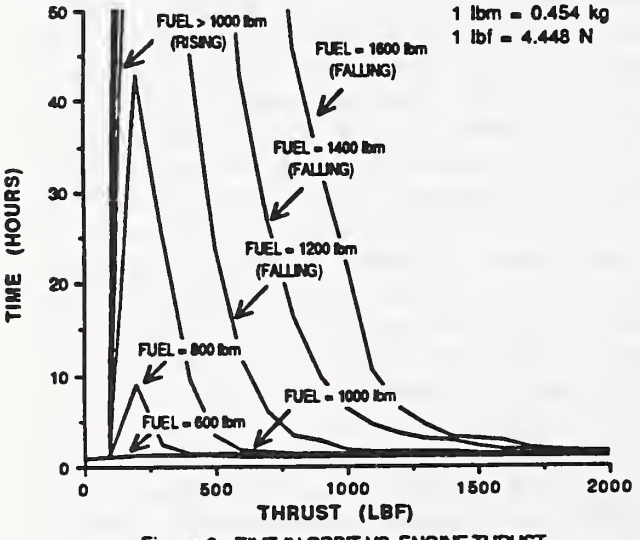

Figure 6: TIME IN ORBIT VS. ENGINE THRUST

Vehicle Mass = 74,000 lbm
ISP = 400 s, Burn at MECO
Solar maximum, Angle of attack = 0°

Despite the benefits indicated by figures 5 and 6, if one could achieve the peak performance shown, the MECO burn scenario represents a risky proposition, because minor variations in the level of thrust or drag would result in vastly reduced time in orbit.

Effect of Specific Impulse

So far, it has been assumed that oxygen/hydrogen thrusters (I_{sp}=400s) would be used to boost the external tank. Other propellants could be used with varying degrees of reduced performance. Bipropellants, such as Nitrogen Tetroxide (N_2O_4) and Mono Methyl Hydrazine (MMH) are non-cryogenic and have an I_{sp} of about 300 s. Solid rocket motors are available in a wide variety of thrust and duration levels and have I_{sp} values between 200-250s. Figures 7 and 8 show the effect of specific impulse on time in orbit for varying quantities of fuel mass. The thrust level, using the apogee burn scenario, has been set at 1000 lbf (4448 N). Figures 7 and 8 indicate that time in orbit is approximately proportional to I_{sp}. A solid rocket motor with twice the mass of the liquid propellant for the oxygen/hydrogen engine would be needed to achieve the same time in orbit.

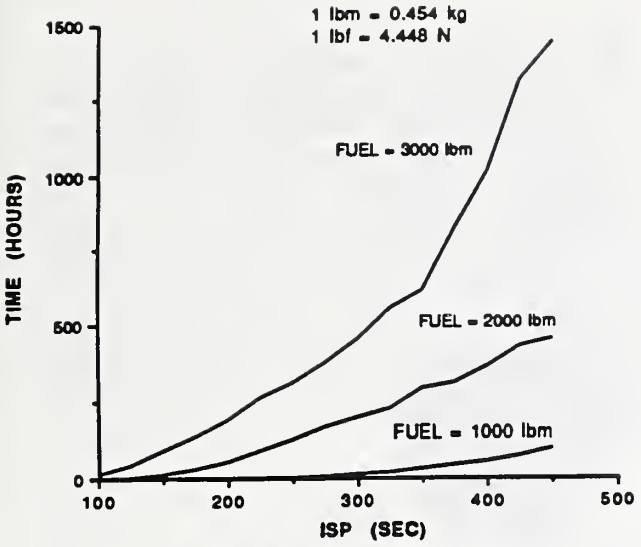

Figure 7: TIME IN ORBIT VS. SPECIFIC IMPULSE
Vehicle Mass = 74,000 lbm
Thrust = 1000 lbf, Burn at apogee
Solar minimum, Angle of attack = 0°

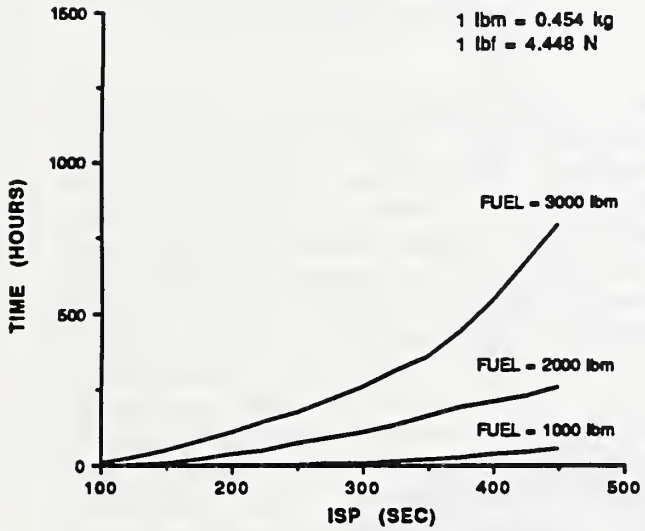

Figure 8: TIME IN ORBIT VS. SPECIFIC IMPULSE
Vehicle Mass = 74,000 lbm
Thrust = 1000 lbf, Burn at apogee
Solar maximum, Angle of attack = 0°

Effect of Spacecraft Mass

Figures 9 and 10 show the time in orbit for an external tank equipped with a 1000 lbf (4448 N) propulsion package as a function of overall vehicle mass (propellant mass for the indicated burn excluded). The important aspect of these figures is that while all curves show decreasing performance for increasing vehicle mass, the penalty for additional mass, in terms of time in orbit following the initial boost, is small. This indicates that additional payload mass could be

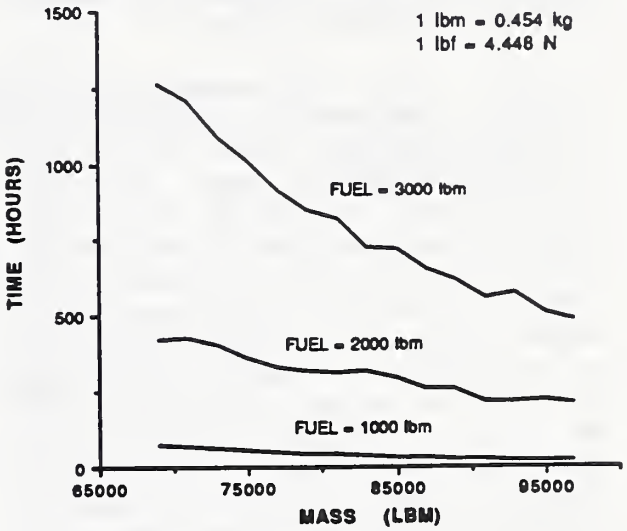

Figure 9: TIME IN ORBIT VS. VEHICLE MASS
Thrust = 1000 lbf
ISP = 400 s, Burn at apogee
Solar minimum, Angle of attack = 0°

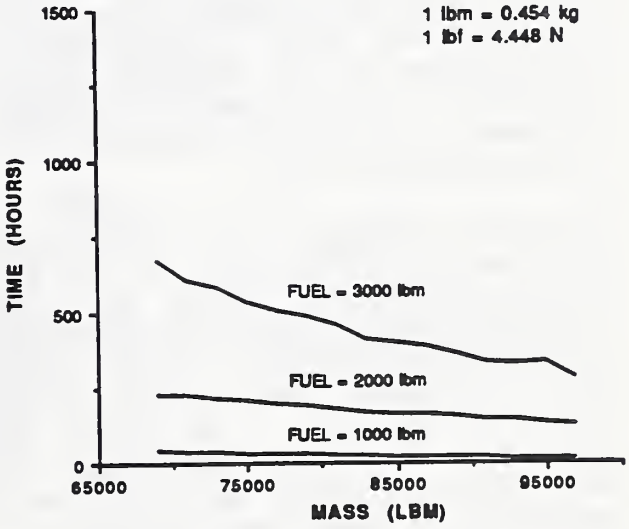

Figure 10: TIME IN ORBIT VS. VEHICLE MASS
Thrust = 1000 lbf
ISP = 400 s, Burn at apogee
Solar maximum, Angle of attack = 0°

taken to orbit by the external tank-- perhaps inside the hollow Intertank structure -- with no significant re-scaling of the exterior propulsion package; provided that the overall shuttle system payload capacity was under-manifested.

Overall Propellant Budget for Orbital Storage of External Tanks

It has been recommended that a suitable long term circular orbit storage altitude would be in the vicinity of 500 km [NASA, 1988]. If, as previously suggested, a 1100 lbm (500 kg) apogee burn is carried out by the tank propulsion system using a 1000 lbf (4450 N) hydrogen/oxygen engine, then the resulting orbit is as described in figure 11a. This orbit has an apogee altitude of 218.3 km and a perigee altitude of approximately 159 km. If no further action is taken to boost the tank to a higher orbit, or if no other orbit maintenance burns are carried out, then the orbit will progressively decay due to atmospheric drag, as shown in figure 11b, ultimately ending with the re-entry of the tank 56.5 hours (38.6 orbits) after the initial apogee burn. Clearly, it is advantageous to act early to boost the tank, as the apogee altitude decreases by a greater amount with each successive orbit.

An initial estimate of the additional fuel required to achieve a 500 km altitude circular orbit may be obtained using Hohmann transfer theory [Kaplan, 1981]. At least three additional burns are required for this maneuver. The first, a circularization burn carried out at the apogee altitude of 218.3 km, involves a velocity change of 18 m/s. The next burn, which may take place anywhere along the circular orbit, places the tank into a transfer ellipse with an apogee altitude of 500 km and a perigee altitude of 218.3 km. The third burn takes place at apogee of the transfer ellipse and results in the final 500 km altitude circular storage orbit. The combined velocity change for these two burns is 160 m/s. This, added to the initial circularization burn amounts to 178 m/s. The propellant mass required to achieve this change may be determined from the standard rocket equation as:

$$Q = m\left(1 - e^{-\Delta V / I_{sp} g_0}\right) \qquad (23)$$

where:

Q = mass of propellant required.
ΔV = velocity change (m/s)

For a spacecraft mass of 74,000 lbm (33,596 kg) this velocity change requires 3285 lbm (1,491 kg) of propellant. Thus, the total post-MECO fuel budget comes to 4537 lbm (2059 kg) or, in terms of volumetric storage requirements, 54 cu.ft. (1542 liters) LO_2 and 149 cu.ft. (4219 liters) LH_2. This is, coincidentally, quite close to the estimates [NASA, 1988] of the minimum residual cryogens suitable for propulsion which remain in the tank following MECO. The calculations thus far have counted this as deadweight and have assumed that all propellants would be carried in exterior tanks which comprise the autonomous velocity change propulsion package. Effective utilization of residual cryogens would essentially eliminate any launch constraints which might exist due to Space Shuttle cargo bay manifesting. This paper has dealt solely with the subject of the initial boost requirements for placing external tanks in long term storage orbits. Other key facets of

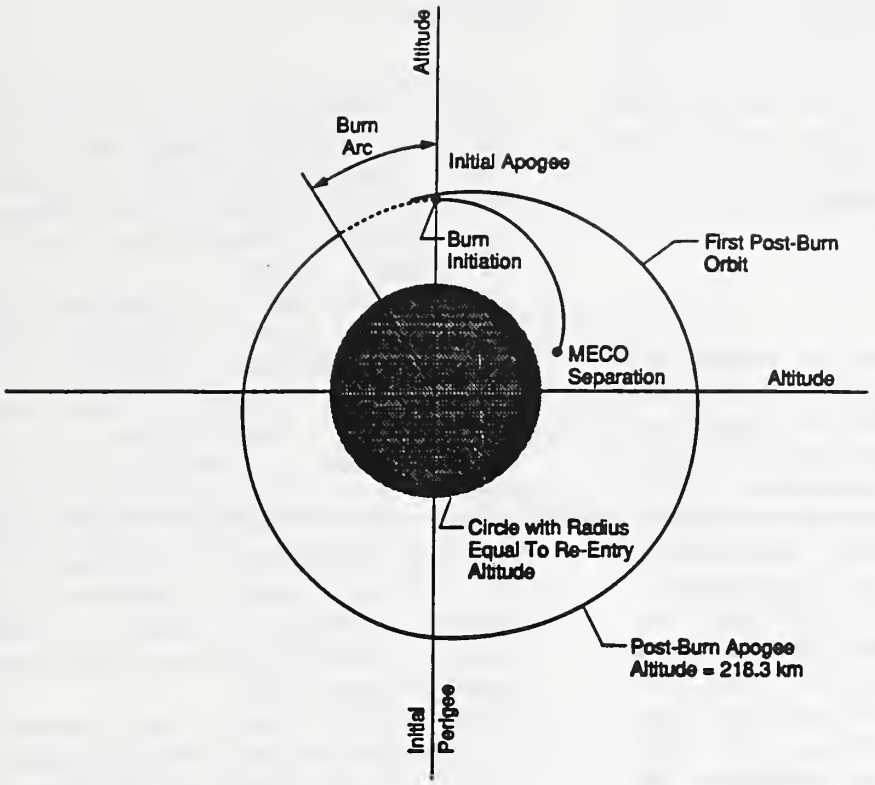

Figure 11a:

First Orbit Following Apogee Burn

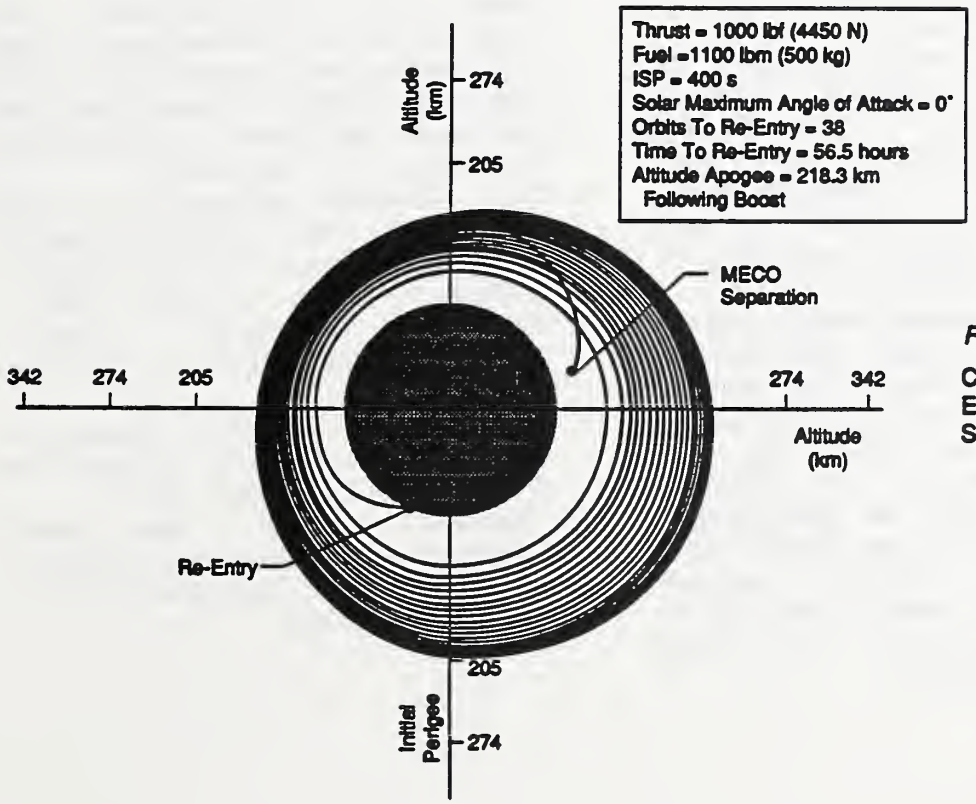

Figure 11b:

Complete Decay Trace For External Tank Following Single Apogee Burn

the problem include orbit maintenance propellant budget determination and the assessment of an appropriate deboost system should the tank need to be brought down in a controlled fashion. These subjects will be discussed in future papers.

Conclusions:

On the basis of extensive numerical simulations it was calculated that the space shuttle external tank can be boosted to a short term stable orbit following standard MECO separation from the shuttle orbiter, and without any direct interaction nor detriment to orbiter performance. An exterior propulsion package for the external tank equipped with a minimum thrust capacity of 1000 lbf (4448 N), a propellant mass of 1100 lbm (500 kg), and an I_{sp} of 400s appears sufficient to achieve an initial time in orbit of nearly two days under solar maximum conditions, provided the burn is made at initial apogee and the angle of attack is maintained near zero degrees by an onboard attitude control system. It is assumed that additional velocity change burns will take place following the initial burn which will place the tank in a circular orbit between 400-500 km altitude for long term storage. Initial estimates of the total fuel required to achieve a 500 km circular storage orbit come to 4537 lbm (2059 kg) based upon Hohmann transfer theory following the initial apogee burn. All calculations assumed 5000 lbm (2270 kg) of residual cryogens in the external tank following MECO as deadweight. Recovery and use of these propellants by the exterior propulsion package would lead to a dramatic increase in the time in orbit above the values reported in this paper.

References:

1. "The Feasibility of Using the Shuttle External Tank as a low Cost Warehouse-Workshop-Residence in Low Earth Orbit," Final Report, The Sophron Foundation, McLean, VA, August, 1984
2. "Utilization of the External Tanks of the Space Transportation System," Arnold, J.R., ed., California Space Institute, Scripps Institution of Oceanography, La Jolla, CA, April 1983.
3. King, C.B., et.al., "A Lunar Habitat Configuration Derived from a National Space Transportation System External Tank," NASA Langley Research Center Technical Paper, June, 1989.
5. "Preliminary Data for On-orbit Utilization of the External Tank," Special Publication of the Program Development Office, NASA George C. Marshall Space Flight Center, Huntsville, Al., April 1988.
6. Stone W.C., and Witzgall, C., "Evaluation of Aerodynamic Drag and Torque for External Tanks in Low Earth Orbit," Proceedings, 9th Conference on Space Manufacturing, Princeton, NJ, May 1989.
7. U.S. Standard Atmosphere, 1976, NOAA, NASA, USAF joint document, U.S. Government Printing Office, Washington, D.C., October, 1976
8. Tobiska,K., Ph.D. Thesis, University of Colorado, Boulder, 1989
9. Kaplan, M.H., "Modern Spacecraft Dynamics and Control," John Wiley & Sons, New York, NY, 1981
10. Kahaner, Moler, and Nash, "Numerical Methods and Software," Prentice Hall, Englewood-Cliffs, NJ., 1989, p295.

EVA Life Cycle Cost Issues Summary

Paul F. Marshall
NASA Headquarters
600 Independence Ave. SW
Washington, D.C.20546

EVA LIFE CYCLE COST DRIVERS

WEIGHT TO ORBIT

- o LAUNCH COSTS/ORBIT RETURN COSTS
- o ON-ORBIT USE LIFE
- o CONSUMABLES USAGE/COST OF CONSUMABLES

GROUND PROCESSING/TRAINING

- o ON-ORBIT USE LIFE (ON-ORBIT SPARES/STORAGE)
- o GROUND TRAINING DEMAND

IVA OVERHEAD

- o TIME - TO - VACUUM
- o MAINTENANCE/SERVICING TIME
- o ON-ORBIT TRINING/IVA OBSERVER TIME

EVA OVERHEAD

- o EFFICIENCY/EFFECTIVENESS IN PERFORMING TASKS
- o MINIMUM SORTIES TO ACCOMPLISH OBJECTIVES

AMOUNT OF EVA REQUIRED

- o HARDWARE DEMAND
- o IMPACT ON OTHER VEHICLE HARDWARE OR "WORK SYSTEMS" (TASK SIMPLIFICATION)

ACQUISITION COSTS

- o TECHNOLOGY MATURITY
- o MANUFACTURABILITY

EMU LIFE CYCLE COST DESIGN SENSITIVITY

WEIGHT – TO – ORBIT

- o CONSUMABLES USAGE: REGENERABLE VS NON–REGENERABLE
- o GROUND REFURBISHMENT LIFE CYCLE (ON–ORBIT STAY TIME)
- o RELIABILITY/MAINTAINABILITY
- o UNIT WEIGHT

GROUND PROCESSING

- o ON–ORBIT USE LIFE: RELIABILITY, # LIMITED LIFE COMPONENTS
- o MAINTAINABILITY/MODULARITY
- o SIMPLIFIED CHECKOUT/SIZING

IVA OVERHEAD

- o PREBREATHE REQUIREMENTS (CABIN PRESSURE, SUIT PRESSURE, R)

EVA OVERHEAD

- o CREW COMFORT (MANEUVERABILITY, DEXTERITY, TEMPERATURE, FATIGUE, ETC...)
- o LIGHTING, RESTRAINTS, SAFETY PROVISIONS

AMOUNT OF EVA REQUIRED

- o CONSUMABLES USAGE
- o RELIABILITY
- o # SORTIES BEFORE REFURBISHMENT

EMU LIFE CYCLE COST DESIGN SENSITIVITY (CONTINUED)

ACQUISITION COSTS

- o DESIGN MATURITY/TECHNOLOGY SELECTION
- o NUMBER OF UNITS REQUIRED
- o MANUFACTURABILITY
- o SPARES QUANTITY REQUIRED

AMES AX-5

Hard Suit

Multiple Bearing Joints

Low Torque Sealed Bearings

Universal Fit Torso

Torso Length Sizing Rings

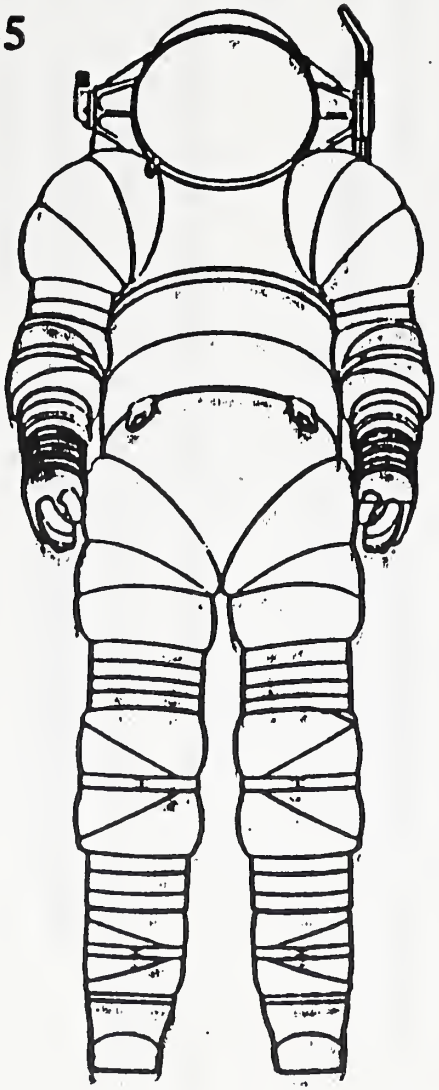

MARK 3

Rolling Convolute Waist

Rolling Convolute Shoulder

Fabric Arm

Hard Brief

3-Bearing Hip

Fabric Leg

Fabric Boot

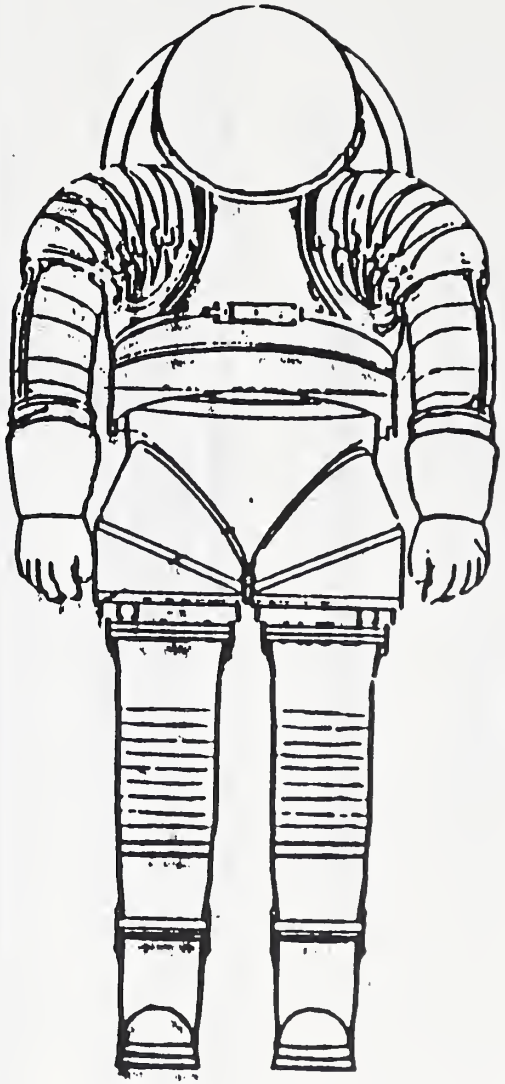

Flight Opportunity for Small Payloads

Patrice Larcher
Arianespace
1747 Jefferson Davis Highway
Suite 601, Arlington, VA 22202

Presentation by Patrice Larcher, Marketing, Arianespace
at Esrin, Italy (8-10 Feb 1989)
Flight Opportunity for small payloads.

Mr. Chairman , Ladies and Gentlemen

This paper, described in somewhat abbreviated form, the natural line of reasoning which has brought us to design launch structures, and establish the basic principles of an appropriate service contract with its entitlements and obligations, designed specifically for the "small payload" to be launched by Arianespace using the European Ariane launcher.

Instead of the back tracking in time - which in our case would take us back to 1973, and the decision to design and produce a European launcher under ESA responsability subsequently delegated to CNES, the first Ariane flight in 1979, the formation of Arianespace in 1980, and operational qualification of the Ariane launcher in 1982 - we shall take a more global look at the present situation.

I would like to draw your attention more particularly to six key points, which now enable us to make a favourable response to world demand in the "lightweight" field, without perturbing the "heavyweight" sector.

Point 1

Europe possesses a qualified, reliable operational launcher in Ariane, with a past history of 28 launches including 4 qualification flights. Ariane has successfully placed 34 commercial satellites ("heavyweights") and 4 small payloads ("lightweights") in orbit,

These include: -The Indian Space Research Organization's APPLE satellite

- The amateur radio OSCAR 10 and AMSAT IIIC payloads,

and the VIKING satellite for the Swedish Space Corporation.

With its modular structure, the Ariane launcher can be tailored precisely to commercial market demand, catering for satellite payloads in the 1.2 to 1.4 T or 1.6 to 1.8 T class, and currently the 2.2 to 2.8 T class, and even payloads of 3.6 T, or in exceptional cases 4 T. A geostationary transfer orbit, or sun-synchronous or escape orbit mission can include one, two or even three satellites in its total payload.

However, at this point we must ask a number of questions :

Do we have spare capacity to carry a 4th, 5th and 6th satellite or more inside the faring, is the necessary volume and performance available, and is all this possible without affecting the launcher?

Point 2

Europe has made a good start in meeting current demand, while planning for the future with the even more powerful Ariane 5 version, and its increased technical and commercial performance.

Returning for the moment to our proverb "he who can do more, can also do less", we are indeed confident, since what has been decided and is operational with Ariane 4, will naturally be compatible with Ariane 5. The 1995/1997 Ariane 5 version will show a 50% increase in performance, giving extended capacity for carrying small payloads.

In this way, our entire policy of today is compatible with the European space sector of tomorrow. Small payloads have a place in our space adventure, in both present and future contexts.

Point 3

With Arianespace, Europe has a company offering a comprehensive spacecraft launch service. The company has been operational in a number of areas for nearly 10 years. These are:

- The funding and management of the complete Ariane launcher manufacturing programme involving the European space industry. Nearly 10,000 engineers and technicians are engaged in this programme.

- Promotion and marketing of payload launch services throughout the world.

- and Ariane launch operations using the Kourou complex.

In other words, Arianespace, a private company, has total responsibility for funding and management of the Ariane product, and marketing and execution of actual launch services.

So far, Arianespace has won nearly 70 launch contracts for "heavyweight" satellite payloads, and we have responded favourably to six requests for "lightweight" launches.

Backed with nearly 10 years experience, we have been able to adapt our marketing approach to achieve compatibility with the structures and resources of universities and amateur organizations, without in any way perturbing our priority objective of winning and holding over 50% of the world commercial market.

Point 4

The world commercial market exists and continues to develop, and we must meet this deman.

- Over the last few years, the average launch rate for commercial satellites successfully placed in orbit by the Europeans and Americans has been 10 per year. Annual figures on the screen show a maximum of 17 satellites in 1985, and a minimum of 5 in the "black year" of 1987. Note that the 11 commercial satellites launched in 1988 were all carried by the European Ariane launcher.

- In the short term, the average rate will increase to 18 to 20 satellite launches per year, then oscillating between 17 and 24 per year in the longer term. Beyond the 1995 horizon, a new market will open up with Colombus, Hermes, the sapce station and the launching of associated structural, equipment and supply payloads.

This market is extremely sensitive and vulnerable, and this situation will be steadily aggravated as a result of very severe competition with three American launchers at the present time, and the appearance of other foreign launchers in the near future. Arianespace is responsible to Europe as a whole, and its shareholders in particular, and must not, on any account, allow any disruption of its commercial, financial, manufacturing and operational activities, which would adversely affect its position in the world market for large satellite launch services.

Consequently, the"lightweights" must integrate and harmonize with our basic activities. There can be no question of adding additional burdens to our structure or management, at the risk of impairing our commercial and financial results.

Point 5

As we have clearly seen throughout this workshop, a small satellite activity already exists.

- Since 1964, the Soviet Union has launched two or three clusters of 8 small satellites, with unit masses of 40 to 50 kg, providing message acquisition, storage and transmission functions.

- The USA has been engaged in experiments in this area since 1974.

- As we now know, Dr. Sweeting and his team of students from Surrey University, successfully launched the first UOSAT satellite back in 1981. Two satellites of the 50/60 kg class are now in orbit, executing scientific, educational and technological missions, and offer the practical possibility of operating a "mail" service between selected points on the globe.

- In 1988, DARPA initiated the "Lightsats" research programme in the USA. Among other functions, this type of small satellite is designed to monitor and observe all kinds of abnormal situations, such as radio transmissions and changes in the structure of the terrain, in other words providing a discreet, practically invulnerable detection function, and at low cost by comparison with the large, powerful satellites, although these are still essential for high-precision listening and observation missions.

In addition, large numbers of "Lightsats" could transmit mail to any point on the globe, using ultra-light, easy-to-use equipment.

The existence of these operational achievements and other concrete projects have opened our eyes to the future.

Point 6

A market for "lightweight" payloads is emerging.

Looking into the future, and bearing in mind the strong demand from a number of sources, we must examine both the quality and quantity of the launch services market for the "Lightweights", "Small payloads", "Lightsats", "Piggy back" and "Get away special" configurations, "secondary passengers" and so on. The list of new denominations seems endless !

Following an initial study of the market, and faced with this multiplicity of terms, we have adopted a single expression to describe this type of satellite. This is:

"Auxiliary Payload"

and we hope that this term will be generally adopted in Europe.

Very quickly, our definition of an Auxiliary Payload is as follows :

An Auxiliary Payload can be classified in one of four categories, as we see on the screen:

- Microsatellites
- Technological payloads
- Minisatellites
- Retrievable capsules.

The term "technological payload" is used to describe a payload which must be secured to a space-borne mechanical structure, and remains coupled to this structure. A technological payload is not autonomous, and does not require ejection in the same way as a microsatellite, minisatellite or capsule, each of which has a fully autonomous in-orbit existence.

In contrast to a microsatellite or minisatellite, a capsule is recovered at sea or on land at the end of its time in orbit.

The distinction we make between microsatellites and minisatellites is based purely and simply on mass. Maximum mass for a microsatellite is of the order of 50 kg, with a volume of the order of 50 litres. A minisatellite ranges from around 100 kg to a maxiumum of 600 kg. Irrespective of Auxiliary payload type, the vast majority of these payloads are placed in low earth orbit at an altitude of 200 to 600 km, or in sun-synchronous orbit. Insofar as the microsatellite market is concerned, we invite your comments on our initial estimate, shown in this table. On the basis of three periods around 1990, 1993 and 1995, we anticipate an initial predominance of scientific and amateur radio applications, which will be largely replaced by military applications by about 1995. The share taken by commercial satellites should remain small. Consequently, we anticipate annual launch rates of ten and then twenty payloads, rising to over 30 microsatellites to be launched per year in or around 1995.

I hope you won't ask me to run a similar quantification exercise for minisatellites! We are currently monitoring a number of tentative design projects with interest, although nothing concrete has been achieved so far. We believe that this type of satellite will remain highly specific, and will only be used for special missions.

As for microgravity applications using retrievable capsules, experimental work will continue, involving a number of flights each year, whicle awaiting more suitable carrier structures such as Colombus, Eureca, and the spaceplanes and space stations.

The technological payload category will develop according to the availability of launch facilities and suitable carrier structures. We think it likely that demand will become fairly substantial.

For each enquiry we receive for microsatellite, minisatellite, technological payload and capsule launch services, we must determine the degree of seriousness and the level of know-how involved, in this way detecting the level of credibility of the project as rapidly as possible. The space sector involves hi-tech and complex systems, and there is no place for way-out schemes, which would perturb and contaminate the quality of the launch services activity which all professional operators in the world have come to expect from Arianespace.

To sum up:

Firstly: Europe has an operational launcher catering for today's market, and has designed the next generation launcher for the market of tomorrow.

Secondary: Europe has a payload space launch Service Company which provides comprehensive launch services.

Thirdly: A commercial market exists and is expanding. The Product - Ariane - and the Service - Arianespace - provide a precision response to market demand.

Fourthly: An Auxiliary payload activity also exists, and the outline of a future market is emerging.

We can adopt two axioms: "an Auxiliary payload has its place on-board Ariane in the same way as a heavy satellite" and "an Auxiliary payload will be carried by Ariane, provided it meets the technical, technological and management standards involved, in the same way as those applying to heavy satellites".

In this way, the entitlements and obligations for an Auxiliary payload will be clearly defined in the launch services contract.

- A small payload will be accepted as an Auxiliary payload, provided its space-related character can be clearly identified.

- The Auxiliary payload will participate in a commercial mission which has already been programmed, and where available spare performance capacity exists.

- The Auxiliary payload must be transparent with respect to the main mission scheduled by Arianespace, in line with the launch services contract or contracts signed with one or more commercial customers.
  This involves:

  - Technical transparency: the design of the Auxiliary payload must not introduce any constraint (relating to mass, volume, vibration, separation, wiring, transmission and so on), apart from integration with the main passengers.

- Time schedule transparency: the management authority responsible for the Auxiliary payload must ensure that the payload is ready by the "earliest" date and can also wait up to the "latest date", and must be in a position to supply a "dummy" payload, to ensure, among other reasons, that the global mission is not delayed.

- Risk transparency : the Auxiliary payload customer must provide proof that the payload introduces no additional risk for the basic mission, and must take out additional third-party liability insurance cover as appropriate. The Auxiliary payload must meet all safety constraints in full.

- Operational transparency: the Auxiliary payload must be managed throughout the launch programme, in such a way that it does not perturb the launch programme for the other passengers in any way, with particular reference to telemetry and telecommand functions. The Auxiliary payload must stay silent until after separation of the ASAP platform in the case of a microsatellite, or the upper part of the SPELDA for the ARTEP structure, or the APEX system for a minisatellite.

These various points may sound like constraints, but provided these conditions are met, Auxiliary payloads will have the advantage of extremely attractive financial terms for Ariane launch services. To give a general idea, a multiple launch for up to six microsatellites using an ASAP platform, will come out at a total cost of less than one million dollars. A minisatellite launch requiring a change of launcher version, could cost of the order of ten million dollars, while the price for launching a retrievable capsule, where more substantial constraints are involved, would be around twenty million dollars.

Obviously, these are only approximate figures. Each project will be examined individually by the Arianespace Sales Division, which will determine - on the basis of the technical file submitted by the customer - the feasibility of carrying the Auxiliary payload on Ariane, the actual mission or type of mission in which it could be integrated, and the additional cost generated by including the specific Auxiliary payload in question. The only financial objective of Arianespace under these circumstances, will be to recover additional expenses resulting from the management and analytical functions involved, the launch programme, and the change of Ariane version where this is necessary.

Commercial Launch Vehicles Using Hybrid Propulsion

Jay Kniffen
Amroc
847 Flynn Road
Camrillo, CA 93010

National Institute of Standards and Technology

Conference on Reducing the Cost
of Space Infrastructure and Operations

November, 1989

COMMERCIAL LAUNCH VEHICLES USING HYBRID PROPULSION

Prepared by the American Rocket Company
847 Flynn road
Camarillo, California 93010
U.S.A.

INTRODUCTION

The limited availability and high cost of transportation to low Earth orbit (LEO) has seriously restricted civil space research and produced a barrier to the effective development and growth of commercial space ventures. The high costs and long program schedules inherent in existing launch systems cannot be significantly reduced. Several approaches are being pursued to remedy this serious problem, including both reusable and expendable systems.

Fully or partially reusable launch systems, i.e, the United States, French, and Soviet shuttle programs, the United States NASP, and the British HOTOL design, have obvious appeal and may, in the long run, justify the significant development costs. To date, however, the promise of reduced cost through reusable launchers has not been realized and will probably not soon be achieved.

Improved variants of existing expendable launch vehicles (ELVs) are not capable of significantly reducing launch costs. Although most ELVs rely on existing, proven technology, designs have so far been technically demanding, time consuming to produce, and relatively fragile to operate.

Sponsors of present launch-system development efforts also represent barriers to adequate service. Most current efforts are under the auspices of governments or traditional aerospace firms. For legal and organizational reasons, neither government agencies nor established aerospace prime contractors are likely to develop truly low-cost launch vehicles. Historically, government-sponsored services have been difficult for commercial and institutional customers to use, and the inherent complexities of operation increase costs and introduce significant schedule uncertainties and delays. The traditional aerospace firm, accustomed to producing high-performance, high-cost systems under contract, is uncomfortable with any less expensive approach, and is unwilling to invest its own capital in anything more risky than adapting the familiar, expensive, long-lead systems to commercial applications.

The need, of course, is for a genuinely low-cost, reliable, and readily available commercial launch service unencumbered by the obstacles and costs of government management or subsidy and traditional views of what it takes to develop, produce and offer a service.

In response to this need, the privately-financed American Rocket Company has undertaken the development of a family of low-cost, industrially produced, and commercially operated launch vehicles which utilize the unique attributes of hybrid rocket propulsion technology.

AMERICAN ROCKET'S APPROACH

AMROC's technical approach combines industrial manufacturing processes and modern high performance materials to produce reliable low cost space transportation elements. For this strategy to be effective, careful selection of processes and materials is required to produce the minimum cost while maintaining adequate performance. AMROC has found that balancing the high performance of modern materials with reduced performance requirements, results in a system with moderate performance and low production and operating costs. Through careful selection of system configuration, a simple, rugged vehicle results. This simplicity combined with the safe production and handling characteristics of hybrid motors considerably reduces the cost and complexity of launch operations.

HYBRID ROCKET MOTOR ADVANTAGES

Cost reduction is the ultimate goal in producing a commercially competitive space transportation system. Some of the advantages of hybrid rocket motors contribute directly to reducing overall system costs. Among these advantages are: safety; low development costs; low production costs; and simplified operation.

SAFETY

A major cost driving factor is safety. Safety issues create many of the stringent specifications which increase the costs of vehicle components, manufacturing quality assurance, vehicle assembly, transportation, and launch operations. But in spite of ever increasing safety vigilance, catastrophic failures still occur with significant frequency, contributing not only to the cost of the individual incident, but to even greater safety assurance and schedule costs.

Safety of Operation

Hybrid rocket motors use a solid hydrocarbon fuel and a separate liquid oxidizer and, therefore, cannot detonate or support an uncontrolled burn. Mixing of the fuel and oxidizer before planned ignition is also not possible. The non-toxic propellents used in AMROC's hybrid designs are insensitive to minor production flaws and fuel-grain cracks. De-bonding of the fuel and insulation from the case, the cause of a recent spectacular Titan booster failure, is not a serious concern for hybrid systems.

Safety of Manufacture, Handling and Storage

The intimate contact between the fuel and oxidizer in a solid rocket motor is an invitation to disaster during manufacture and storage. The propellant is extremely sensitive to electrostatic discharge, impact, and internal pressures. Also, fuel from a ruptured tank of a liquid rocket motor can easily ignite in open air if exposed to a spark or heat, resulting in a fire and possible explosion of the remaining fuel. The Challenger explosion, although started by the solid rocket booster field-joint leak and subsequent burn through, was ultimately due to a rupture of the fuel tank and ignition of the hydrogen fuel.

Non-toxic, non-explosive hybrid fuels, on the other hand, permit ease and safety of manufacture and storage in an industrial environment. They may be cast in a light manufacturing facility using standard commercial chemical mixing equipment—no need for expensive remote operations. AMROC's fuel employs a standard industrial-grade polybutadiene elastomer produced by a number of industrial chemical manufacturers in quantities far in excess of projected booster demand.

Safety of Launch Operations

The hazards and associated costs of solid and liquid propellants extend beyond the manufacturing environment. Safety requirements also significantly affect the cost of final vehicle assembly and test on the pad. A truly safe system is not possible when liquid or solid propellants are present. Personnel who must approach the vehicle during these times are literally risking life and limb. Thus, access to the pad is greatly restricted when "live" propellants are present. The associated costs of protecting people, payloads and the vehicle are substantial. The relatively safe hybrid rocket, on the other hand, significantly reduces the risks and thus the costs related to launch operations.

LOW DEVELOPMENT COSTS

Development of large hybrid motor units should cost less than 25% of a comparable thrust liquid engine, and less than 60% of a comparable solid. This cost advantage is largely due to the "soft" non-catastrophic failure modes of hybrids which leave test hardware and equipment intact for analysis and reuse. Also, test motors can be constructed from "off the shelf" industrial equipment which can be reused numerous times.

LOW PRODUCTION COST

The combination of benign failure modes and relative insensitivity to fuel grain cracks, mix variation, and other minor production flaws, allow wider production tolerances to be applied, enabling more common commercial/industrial production practices and sources to be used effectively and reliably.

Rapid expansion of capacity during times of increased use or national emergency is possible using non-traditional commercial aerospace sources. If design goals permit, the hybrid can effectively use materials that would otherwise be considered substandard by conventional aerospace practice.

SIMPLIFIED OPERATION

With a hybrid it is practical to idle a booster at a low thrust level on the pad while checking out operational performance prior to committing the vehicle to flight. Should a fault be detected, the motor is simply shut off. Unlike solid motors, in-flight abort shutdown is easily accomplished by turning off oxidizer flow. This attribute, in combination with a payload return system, would make it possible to safely return the payload in the event of an in-flight failure. This would help to lower the cost associated with insurance by reducing the risk of destroying a payload.

Wide variations in ambient temperature produce no significant change in burning rate. This environmental insensitivity eases launch operations, handling, and performance predictions. This advantage, along with innovative vehicle designs, could reduce the cost of launch delays associated with weather constraints. In addition, the combustion by-products of AMROC's safe hybrid propellants, unlike perchlorate loaded solid motors, are benign and non-toxic, resulting in minimum environmental impact.

The flexibility, speed, and low cost of industrial processes, the use of high performance materials balanced against reduced performance requirements, the simplicity of vehicle design, and the use of hybrid propulsion, all contribute to a rugged AMROC vehicle that is safer, more reliable, and less expensive to produce and operate than other launch systems currently in operation.

STATUS OF HYBRID TECHNOLOGY

The hybrid rocket motor was studied extensively in this country during the 1960s. Early research attempted to characterize basic hybrid combustion processes from experiments with sub-scale motors and laboratory bench burners. Programs ended, however, as NASA's interest shifted to the higher performance of liquid oxygen/hydrogen motors and the military pursued all-solid propulsion to attain maximum storability with minimum maintenance and launch preparation. The history of hybrid research thus ended with testing of a few moderate-size developmental motors but no large-scale flight-weight motors. The understanding of some aspects of hybrid combustion and motor scaling was incomplete. The literature of the period generally ends with the lament that more time and money were required to fully understand these problems.

American Rocket Company, founded in 1985, has revived hybrid motor development for commercial launch vehicles and a considerable portion of the Company's resources over four years has been dedicated to refining earlier research using full-scale hardware to come to a more complete understanding of hybrid motor operation.

AMROC has successfully designed, produced and tested the largest hybrid rocket motors (75,000 lbf) ever fired. Enroute, over 30 motor designs have been explored, and problems not anticipated during the 1960s have been encountered and overcome.

AMROC is currently pursuing several hybrid motor development projects including small orbital maneuvering motors for satellite applications, high performance upper stage motors, and very low cost motors for sounding rocket applications. In addition, conceptual studies are underway for larger hybrid motors to be used on new launch vehicles as well as to retrofit solid strap-on boosters used on existing launch vehicles.

THE GOVERNMENTS ROLE

Historically, government agencies have been the principal customers for space transportation services and have operated their own launch vehicle fleets which have carried both civil and government payloads. Recently, commercial launch operations have begun and the federal government has moved to stimulate the fledgling commercial launch industry by contracting for payload launch services rather than for launch vehicle procurement. This should prove to be a highly effective tool for stimulating cost reductions by allowing launch vehicle operators to develop standards appropriate for competitive commercial operation rather than conforming to the standards developed for government hardware procurements.

Future government customers operating in an environment where commercial launch services are available need not specify how booster hardware is built or strive to determine which launch vehicle configuration the taxpayer will support. They need only specify what performance is required, and select the commercial space transportation service which best suites their needs.

REFERENCES

McKinney, B. C., and French, J. R., "Hybrid Rocket Engines for Low Cost Space Transportation", AIAA paper 87-1795 (1987)

McKinney, B. C., and Kniffen, Jay, R., "Hybrid Boosters Alternatives for Future Low Cost Launch Vehicles", AIAA paper 88-3125 (1988)

Novel Integration Concepts

Edward H. Bock
General Dynamics Space Systems Division
3636 Mt. Laurence Drive
San Diego, CA 92117

Novel Integration Concepts - A presentation for NIST

by Edward H. Bock
General Dynamics Space Systems Division

The integration concepts I'll discuss today are all basic tenants of the Advanced Launch System, or ALS. The ALS is being developed by an Air Force / NASA / Contractor team as America's next generation space transportation system. The basic goal of ALS is to meet a broad range of our 21st century cargo launch needs with a more reliable, much more operable, and significantly lower cost system. (Fig 1)

How broad a payload range? Encompassing current ELV/Shuttle capability (~40 klb) to as much as half-a-million pounds.

How reliable? If the cost of failure is included, a launch vehicle reliability of 0.98 to 0.99 is required to obtain a minimum cost system. Current U.S. ELVs have demonstrated reliabilities of 0.94 to 0.96.

How much more operable? Current launch vehicles require a minimum of 9 months to integrate and launch a payload. ALS is to do it within one month. Vehicle time on the pad is not to exceed five days.

How much less expensive? Congress has mandated a goal of $300 per pound of payload to low earth orbit, an order of magnitude reduction compared to current launch systems.

The challenge presented by these goals is not trivial. To meet them we must certainly be innovative, and perhaps our approach even has to be revolutionary. We obviously must make a substantial departure from our current methods. The basic CULTURE of launching rockets must change. (Fig 2)

- Vehicle integration and most checkout must be accomplished in a "factory" under process control conditions.
- The distance between the "factory" and launch pad must be small to eliminate concern regarding the vehicle's condition following its transfer.
- On-pad checks must be simplified and automated, and performed without intrusion into the vehicle's operating systems. Don't repeat factory checks.
- The quantity of people involved in launch site operations must be significantly reduced. Routine automated events and checkouts must replace "tests". We must eliminate "rocket scientists" at the launch site.
- Use a clean launch pad (no service tower) to reduce refurbishment between flights.
- A "test conductor" should not launch the vehicle. Launch must be a routine event, not a test.

- In summary, launch vehicles must be operated more like airplanes in terms of the support people and procedures required - - - and those people's attitudes.

Fine. These are all lofty concepts, but how to we achieve them with a system as complex as todays launch vehicle? By consciously designing the system to be a lot simpler. And in certain instances, elegantly simple.

Many of you probably remember the Big Dumb Booster proposed by Aerospace Corporation in the late 50's. (Fig 3) The basic idea was that a very large vehicle could be cost effective if its basic design was sufficiently simple. Simple as in pressure fed engines, steel plate propellant tanks, etc. ALS has adapted the BDB's approach by designing for low cost rather than high performance, but has updated it to take advantage of technology matured and proven during the intervening 30 years.

Technology such as liquid hydrogen and liquid oxygen propellants used for all vehicle stages. These inherently high performance propellants provide the flexibility needed to incorporate cost reducing design and processing changes into engines, valves, avionics, actuators, and other high value components. Technology such as built-in-test and health monitoring is used to automatically perform vehicle checkout. (Fig 4)

We have also made the vehicle's basic design much simpler. By using parallel rather than serial stages, all engines can be ignited on the pad. By using launch pad hold-down, engines can be fully checked out before the vehicle is released and committed to flight. Even so, we have designed for full engine out capability from liftoff. These actions substantially improve mission reliability.

Parallel stages also permit a high degree of core and booster commonality. We use identical engines on both stages. Avionics, actuators, and fluid systems components are also identical. Identical propellant tank volumes and diameters on the core and booster provide a high degree of structural and fluid subsystem commonality.

Parallel stages also support a family of vehicles approach to accommodating future payload growth. Multiple liquid boosters (up to six) can be attached to the core to increase payload capability to approximately half-a-million pounds. This concept cost effectively supports Lunar return and Mars exploration initiatives. (Fig 5)

The family of vehicles concept also provides another interesting benefit. All ELVs have become performance driven because payload requirements have steadily grown to exceed "current" vehicle capability. This helps keep launch costs high because iterative vehicle modifications to accommodate steadily increasing payload demands is expensive. The ALS family of vehicles breaks this cycle: another more capable family member is readily available to handle heavier payloads.

Will these innovative concepts allow us to meet ALS goals? Based on the work performed thus far, YES! Changes in launch vehicle operations, made possible by a simpler cost-driven vehicle concept that capitalizes on mature technology, make our goals realizable. ALS offers an opportunity for the United States to be the major world class space transportation provider in the 21st century.

WHAT DOES THE AIR FORCE EXPECT OF LAUNCH VEHICLES TO SATISFY MISSION ASSURANCE?

A Launch Vehicle System that will Launch on Schedule

- Operability - 90% Confidence of Launch - 95% of the Time
- Resiliency - Fly Through Failures & Surge
- Dependability - Launch on Schedule
- Reliability - Placement of Payloads Greater than 98% of the Time
- Affordability - Goal of $300/Lb to Low Earth Orbit
- Flexible Capability - Satisfy a Wide Range of Mission Orbit Altitudes and Inclinations, Payload Sizes and Weights

Launch Vehicle Systems Must be Designed to Operational Criteria to Satisfy Their Mission Assurance Role

FIGURE 2

GENERAL DYNAMICS
Space Systems Division

GENERAL DYNAMICS' OPERATIONS CONCEPT

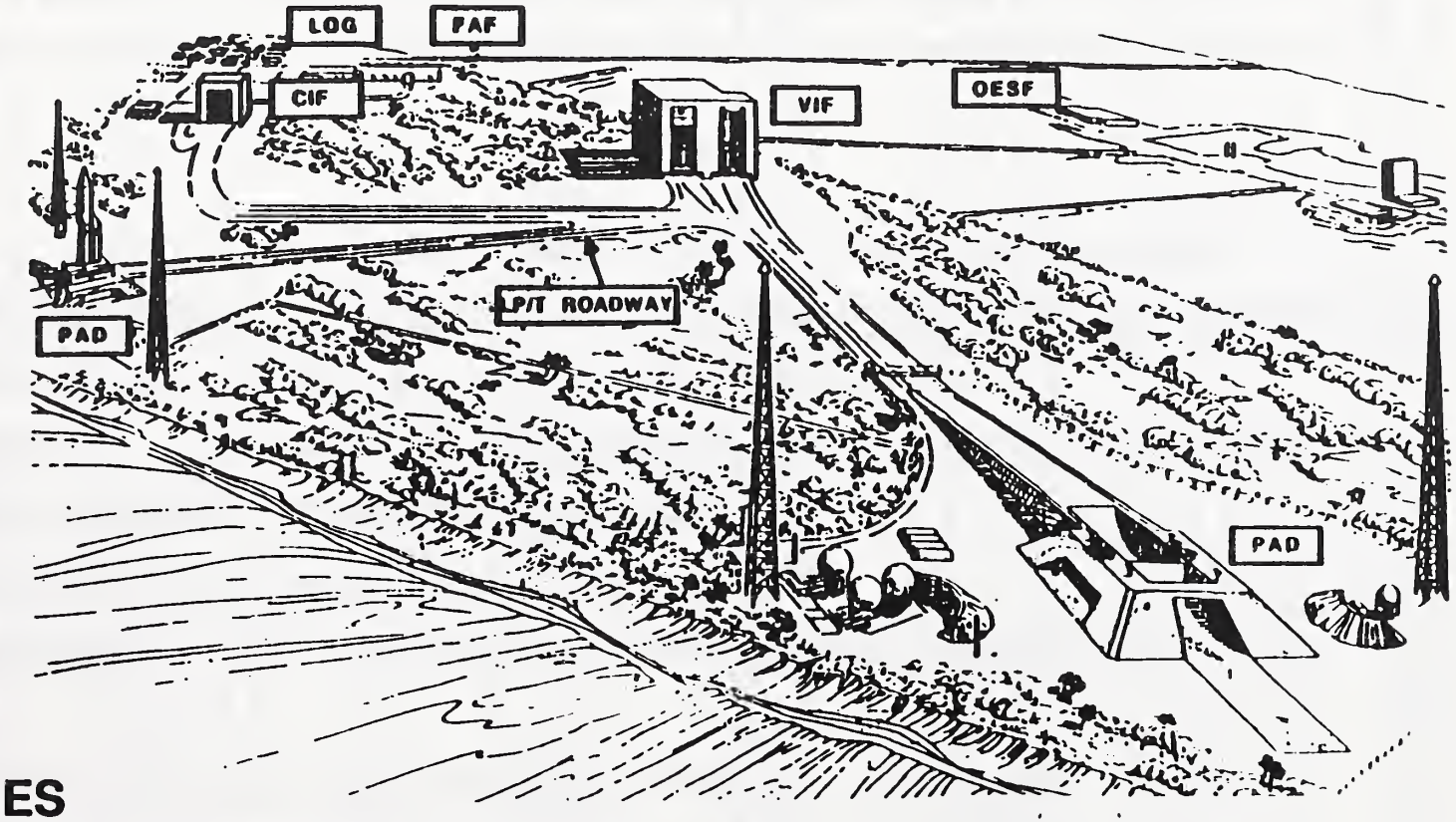

FEATURES

- Maximum Off-line Parallel Processing
- Reliability Allocated to Each Ground Processing Function
- Install & Checkout Through Rise-off Disconnects in Final Assembly Facility (FAF)
- Horizontal Processing to Vehicle Integration Facility
- Clean Pad - Only Fixed Service Connections
- Continuous Health Monitoring from FAF Through Launch

FIGURE 3

BIG DUMB BOOSTER APPROACH ADAPTED FOR ALS

GENERAL DYNAMICS
Space Systems Division

BDB APPROACH	ADOPTED IN ALS	REMARKS
• Structurally Stable Tanks	• Yes	
• Simple Structure	• Yes	
• Large Design Margins	• Yes	
• Design Simplicity	• Yes	
• Streamlined Operations	• Yes	
• Low $/lb to Orbit	• Yes	
• Ablative Nozzles	• Partially	• Nozzle Extensions
• Non-Gimballed Engines	• Backup Only	• For Solid Strap-ons
• Storable Propellants	• Clean LH2 & LO2	• Storable Propellants Not Environmentally Acceptable • LH2/LO2 Mature Technology
• Pressure-Fed Engines	• Low Cost Pump-Fed	• No Test Experience With Large Press.-Fed Engines *
• Not Included	• Engine-out from Lift-off	} Added Reliability & Reduced Life Cycle Cost
• Not Included	• All Engines Ignited before Release	

* Findings of OTA Report, Feb. 1989

WCS-F/W-003

FIGURE 4

GENERAL DYNAMICS
Space Systems Division

"BUILT-IN-TEST CAN REDUCE SYSTEM CHECKOUT COST BY 84%

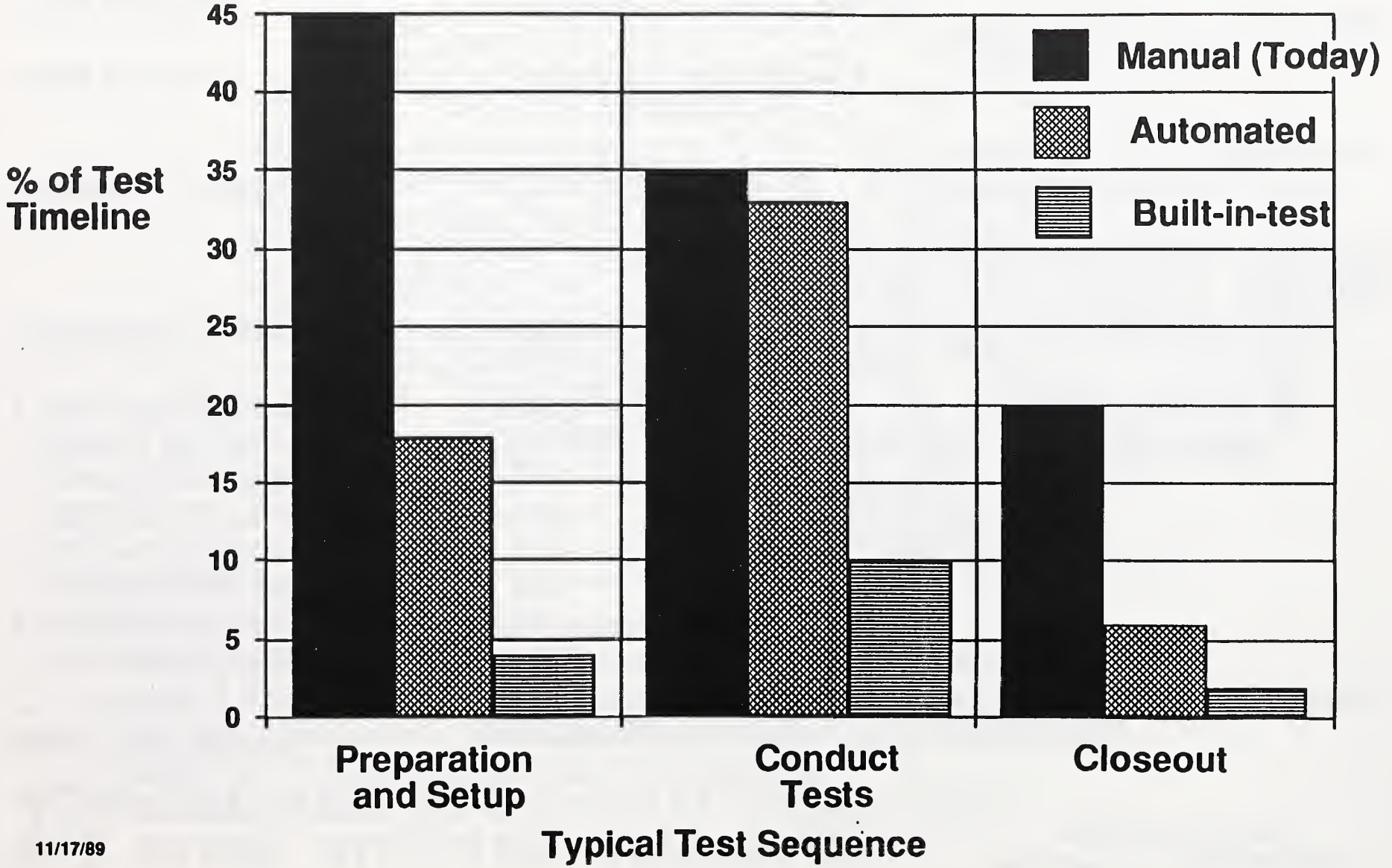

11/17/89

ALS FAMILY OF VEHICLES

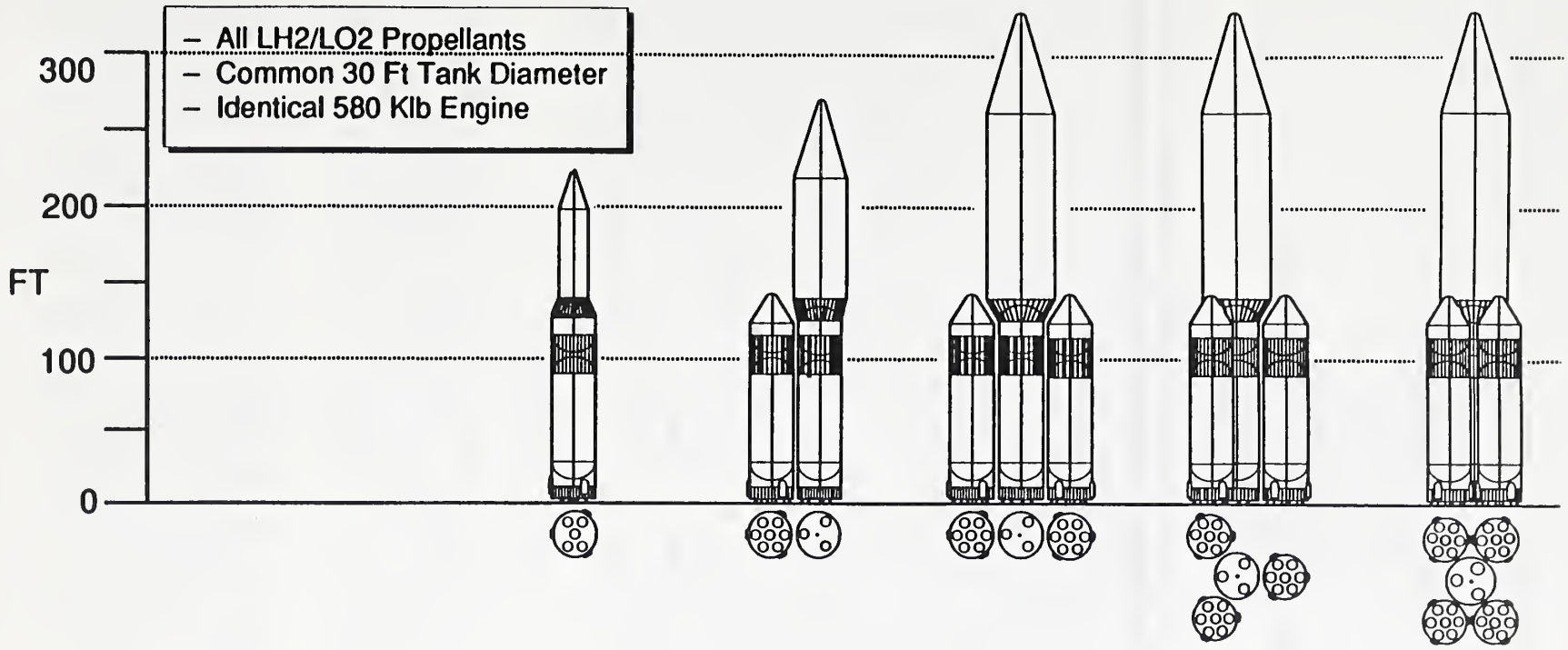

	ALS-C5	ALS-L	ALS-L2	ALS-L3	ALS-L4
DESIGN PAYLOAD	37 KLB	132 KLB	246 KLB	350 KLB	495 KLB
RATED PAYLOAD	34 KLB	120 KLB	224 KLB	318 KLB	450 KLB
GLOW	1.65 MLB	3.49 MLB	5.31 MLB	7.09 MLB	9.13 MLb
RELIABILITY	.991	.989	.984	.980	.978

Payload Sensors

Carl F. Schueler
Hughes Santa Barbara Research Center
75 Coromar Dr.
Goleta, CA 93117

PAYLOAD SENSORS

Carl F. Schueler
Hughes Santa Barbara Research Center
75 Coromar Dr.
Goleta CA 93117

ABSTRACT

Payload sensor costs are driven by a general trend of increasing performance requirements: better spatial, spectral, and radiometric coverage and resolution. This trend reflects the continuing science and operational need for better data from earth-orbiting satellites, and makes cost reduction a challenge. Advances in technology needed to meet new requirements inevitably have a price, as reflected in the non-recurring costs for new sensors, and in more broadly directed research and development efforts. On the other hand, without technology advancements, it may in many cases be impossible or at least impractical to build adequate sensors at affordable prices. Moreover, even when new technology is not needed, requirements changes create the need for new sensor design, and design changes represent new development costs that add to the cost of placing new sensors in orbit. Based on a representative class of sensors, this paper reviews the requirements and technology trends that drive cost, and points to some areas where changes in current practice may help to reduce those costs.

INTRODUCTION

A broad range of sensor technologies exists, which can be categorized into four classes of sensors: Active microwave, passive microwave, active optical, and passive optical sensors. Each comprises several sub-classes, including in general non-imaging and imaging sensors.

Active microwave sensors include non-imaging real-aperture radars (an acronym for RAdio Detection And Ranging) often termed "scatterometers," which are used to evaluate the surface roughness characteristics of ground or ocean features. Imaging radars, usually employing the synthetic aperture concept, produce high-quality radar images of the earth and ocean surfaces. Passive microwave devices rely on the emitted long-wave

radiation from the surface to produce either sounding profiles of the atmosphere (non-imaging) or images of the surface (imaging radiometers).

Active optical devices typically employ laser beams and time-of-flight measurements of the reflected light from a target, and are known as Lidars, an acronym for LIght Detection And Ranging, in analogy to radar. Passive electro-optical cameras, on the other hand, use reflected sunlight or emitted thermal radiation from the earth to construct sounding profiles of the atmosphere (non-imaging) or images of the earth surface (imaging radiometers).

All four classes of sensor, although quite distinct in their operation, are designed and built using common technologies and design principles. All utilize common mechanical design techniques, power systems and electronics, precision mechanical components, and various sensing elements. The design principles underlying their development are also held in common, including geometric and Fourier optics, dynamic structural analysis, and analog and digital signal processing and control techniques. Therefore, any one of the four classes of sensor technology can serve as the basis for the discussion of cost trends associated with sensors.

Santa Barbara Research Center (SBRC) specializes in the development of passive electro-optical space sensors, so these will be the basis of the rest of this paper. Cost control is important for such sensors, because they are used widely on a diverse range of government earth-observation missions. These include the upcoming Mission to Planet Earth, within which NASA's Earth Observing System is now being planned, as well as NOAA's Geo-platform missions planned for the next decade.

APPLICATIONS SPAN THE ENTIRE EARTH ENVIRONMENT

As illustrated in Figure 1, electro-optical sensors are needed to address meteorological measurements, ocean radiometry, and land imaging and mapping requirements.

Eos MODIS and HIRIS Illustrate Mission Design Complexity

The future missions for space-based earth observation include NASA's Earth Observing System (Eos) (Butler, et al, 1984; Bretherton, et al, 1988), with substantial growth in imaging capability for land and ocean measurements using sensors such as the Moderate Resolution Imaging Spectrometer (MODIS) which actually comprises two separate sensors, both being developed by

the NASA Goddard Space Flight Center (GSFC) (Salomonson, et al, 1989). A nadir viewing sensor (MODIS-N) emphasizes land applications, and ocean requirements are met with a ±50° fore-aft, off-nadir pointable (tilt) sensor (MODIS-T). While MODIS offers broad spatial survey capability (roughly a 1400 km swath) with daily repeat coverage of the globe in some forty visible and near infrared (VNIR), short wave infrared (SWIR), and thermal infrared (TIR) spectral channels, it has 500 meter or coarser spatial resolution. Fine resolution of spatial and spectral detail, as well as continuous spectral coverage throughout the VNIR and SWIR is also required to study specific areas of the land surface, particularly for ground feature identification.

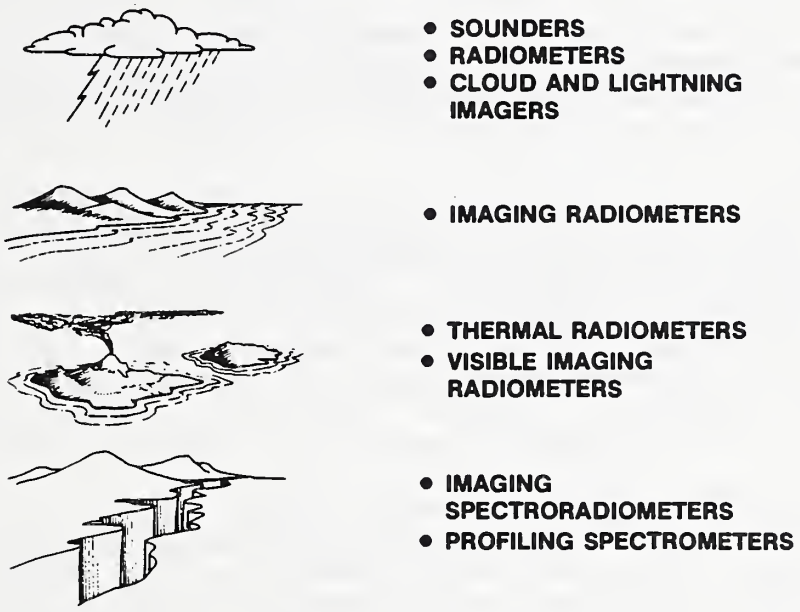

Figure 1 - Applications for Electro-optical sensors and example sensor types for the applications.

This latter Eos requirement is to be met using a finer spatial and spectral resolution instrument called the High Resolution Imaging Spectrometer (HIRIS), being developed by NASA's Jet Propulsion Laboratory (JPL) (Goetz and Herring, 1989). HIRIS offers 30 meter spatial resolution and 10 nm spectral bandwidths, as well as continuous spectral coverage from 0.4 to 2.5 μm. HIRIS is restricted to a 25 km swath, however, and is termed an "observatory" sensor in Eos parlance as opposed to the survey capability offered by MODIS. While MODIS and HIRIS are complementary so far as their use is concerned, with MODIS serving the scientist as a "search" or "detection" sensor, and HIRIS serving the scientist as the "examination" or "recognition" sensor, the two are incompatible from the standpoint of design.

That is, it would be hardly practical (though it is clearly possible in principle) to design one sensor that could perform both the MODIS and the HIRIS missions simultaneously.

Future Missions Challenge Technology Three Ways

Fundamental physical limitations in sensor performance form the foundation of sensor design in three performance modalities:

• Spatial - Fine imaging detail, typically for cartographic applicatons, requires excellent optics with instantaneous field of view from low Earth orbit (LEO) of roughly 7 μrad and rapid data collection capability.

• Spectral - Broad spectral coverage with continuous or nearly continuous and very narrow (< 10 nm) spectral windows for ground feature spectral signature matching requires advanced, flexible spectral filtering technology.

• Radiometric - Reflectance and emittance sensitivities of less than 0.5% NE$\Delta\rho$ (noise equivalent reflectance variation, where "ρ" denotes reflectance) and 0.1 K NEΔT (noise equivalent temperature variation) that are comparable to atmospheric degradation uncertainties and correction methods require sensitive, low noise detection and high dynamic range.

As for the MODIS/HIRIS example cited above, it is difficult in general to address all three modalities simultaneously. Consider first radiometric performance. A fundamental limitation to radiometric sensitivity is the signal-to-noise ratio, typically denoted SNR. There are several sources of noise that tend to degrade sensitivity by lowering the SNR. These include detector thermal noise, electronics noise, and quantization noise for a sensor with digital data readout. Although these noise sources are controllable to a point with extensive care in manufacture, one other noise source exists which is natural and cannot be controlled. This is photon noise, which adds uncertainty to the signal that is equal to the square root of the signal itself, measured in photons per second impinging on a detector element in the sensor.

The only way to reduce the relative effect of photon noise is to increase the signal level; every factor of four increase in signal, for example, results in an increase of a factor of two in photon SNR. By ensuring that the signal is large enough (or that non-photon noise sources are small enough) that the photon noise

swamps out the other noise sources, non-photon noise sources no longer substantially affect SNR. This "threshold" of radiometric performance is termed Background Limited Photon (BLIP) noise performance. A BLIP sensor's SNR is determined by the amount of signal collected by the optical aperture; and BLIP performance is often synonymous with radiometric sensitivity.

With a fixed optical design, the signal collected by the sensor entrance aperture cannot be increased, so that the only remaining ways to boost signal at the detector involve either increasing the size of the detector or broadening the spectral window through which light is collected. The former, while it will boost radiometric sensitivity, will also reduce spatial imaging performance by producing larger image pixels and a coarser image. The latter also boosts radiometric sensitivity without hurting spatial performance, but broader spectral bands degrade fine spectral structure recognition.

This design incompatibility among the three performance modalities forces engineering tradeoffs that must either balance the performance among the three modalities, or emphasize one over another. In many cases, missions can be categorized as having an emphasis in one or two modalities, and design trades will result in sensors that provide appropriate performance.

Mission Performance Requirements Trends

Eos and new NOAA geoplatform missions are major civil remote-sensing applications in the next five years (Bretherton, et al, 1988; Schenk, et al, 1987). Along with the HIRIS and MODIS sensors described earlier, the Eos program has defined some thirty other sensors, many of which are electro-optical, to address various aspects of the broad Eos mission (See the Eos Wall Chart, May 1989, available from Santa Barbara Research Center). The NOAA program promises enhancements in ocean and atmospheric measurements, as well. Some general performance trends drawn from Eos and from planned NOAA geoplatform missions are listed in Table 1.

Atmospheric science and even operational applications are moving towards finer vertical atmospheric profiling resolution, improved temperature accuracy, and gas species identification. Imaging radiometers and imaging spectro-radiometers are being driven towards high SNR and finer spectral resolution at the same time, while survey capability rather than fine spatial feature mapping can also be noted from Eos. Therefore, it appears that spectro-radiometric performance rather than

spatial resolution improvements are the focus of current applications efforts. This emphasis has key technology implications.

Table 1 - General Technology Implications for The Future

KEY SENSOR CATEGORY	KEY FUTURE REQUIREMENTS	TECHNOLOGY IMPLICATIONS
ATMOSPHERIC RADIOMETERS • TEMPERATURE SOUNDERS • GAS SPECTROMETER	• FINER VERTICAL RESOLUTION (1 km) • IMPROVED ACCURACY (<1°C) • IDENTIFY SPECIES	• FINE SPECTRAL RESOLUTION (0.1%) • SPECTROMETRY (<0.01%) • SNR
IMAGING RADIOMETERS	• HIGH RADIOMETRIC ACCURACY • FINER SPECTRAL RESOLUTION • BROAD SPECTRAL COVERAGE • SURVEY CAPABILITY	• HIGH SNR (200+ FOR MWIR/SWIR) • MANY DETECTORS (MULTILINEAR ARRAYS) • BAND-TO-BAND SPATIAL REGISTRATION
IMAGING SPECTRO-RADIOMETERS	• "CONTINUOUS" SPECTROMETRY • VERY FINE SPECTRAL RESOLUTION • HIGH RADIOMETRIC ACCURACY	• SPECTROMETRY • MANY² DETECTORS (AREA ARRAYS) • HIGH SNR • BAND-TO-BAND SPATIAL REGISTRATION

SPECTRO/RADIOMETRIC PERFORMANCE IMPROVEMENTS RATHER THAN SPATIAL RESOLUTION

TECHNOLOGY TRENDS

To appreciate the impact of the spectro-radiometric performance emphasis on electro-optical technology trends, consider the "generic electro-optical sensor" depicted in block diagram form in Figure 2. This diagram illustrates the four key subsystems of the sensor: mechanics, optics, focal plane, and electronics.

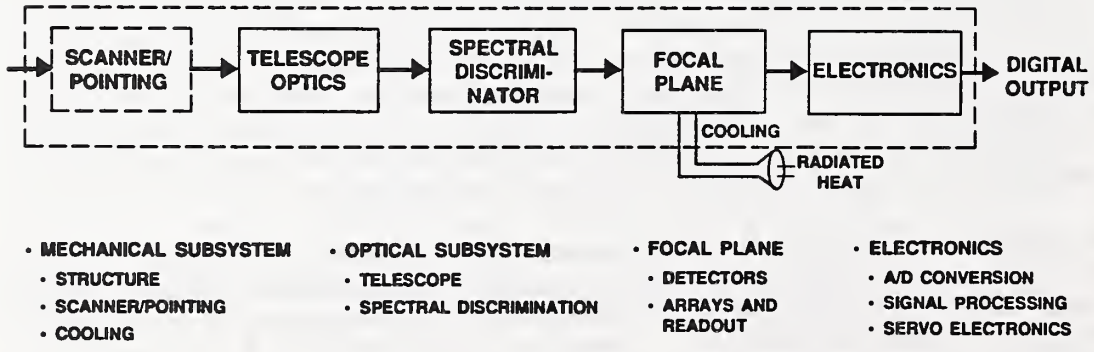

Figure 2 - Four Key Subsystems Comprise the Generic Electro-optical Sensor

The mechanical system provides the overall structural packaging that supports the optical system, as well as any pointing or mechanical scanning capability. The mechanical subsytem would also include cryogenic cooling capability for a sensor that employs detection in the longer wavelengths such as the thermal infrared where detection of low-energy photons competes with thermal noise processes. The optics includes the telescope and spectral filtering mechanisms that allow the sensor to discriminate signals in various spectral channels. The focal plane comprises the detection mechanism that converts photons into electrical signals that are processed by the electronics subsystem.

It should be noted that although the four subsystems have until now been physically separate functional units in the typical passive electro-optical sensor, the physical distinction is rapidly growing fuzzy. For example, new hybrid focal planes are now being developed that combine spectral discrimination, detection, and sophisticated digital signal processing all on one compact physical unit. Although the categorization of Figure 2 is still useful from a pedagogical point-of-view to describe even a sensor based on such an integrated design, the separate functional units depicted in Figure 2 is not an entirely accurate representation.

Optics Trends

Optical technology requirements are partially dictated by the spectro-radiometric emphasis indicated in Table 2. The broad spectral coverage into the thermal infrared, for example, dictates the use of reflective optics (mirrors) rather than refractive optics (lenses). The need for wide fields-of-view and high throughput for radiometric sensitivity for survey instruments dictates off-axis, aspherical elements in the optical system with excellent figure and alignment. Forms such as the Ritchey-Chretien design used in the Landsat Thematic Mapper, although workable for the Landsat mission, are inadequate partly because of the central aperture obscuration caused by the on-axis secondary in the optical chain. Instead, an approach such as the off-axis, three-mirror concept illustrated in Figure 3 is better.

This laboratory model, which is an actual working prototype built at Santa Barbara Research Center, shows the performance capability of modern optical design. It is an approach that until recently was impractical due to the precise alignment tolerances required of an off-axis form. Traditional mechanical alignment

methods are not capable of the precision of 1/20 wavelength at 0.55 μm that is available using computer-aided, real-time, optical interferometric alignment procedures. An example of the accuracy available is illustrated in Figure 3, which shows that with only four iterations of the alignment mechanism through the interferometric fringe matching procedure used, one can obtain better than 0.1 wavelength alignment out to +4/-2 degrees off-nadir. Moreover, the performance is nearly diffraction-limited out to 7.5 degrees off-nadir, which is equivalent to a 185 km swath from a 705 km orbit. That is, with this three-mirror concept, one can have the Thematic Mapper swath without a scan mirror.

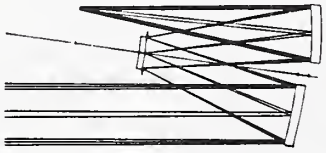

OPTICAL SCHEMATIC

- **ALIGNMENT TO 0.055 λ AT 0.55 μm**
- **NEARLY DIFFRACTION LIMITED PERFORMANCE OVER 15° FOV**
- **ADDRESSES KEY REQUIREMENTS TRENDS**

LABORATORY SCALE VERSION

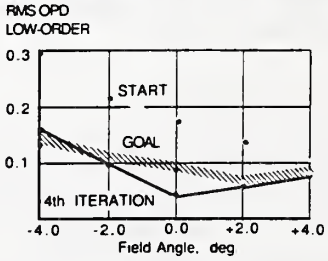

PERFORMANCE CURVES

Figure 3 - Improved Three Mirror Unobscured Design.

With the high throughput obtained by such an unobscured system, and using a line array of detectors extending across the entire field-of-view, one gains nearly a three orders-of-magnitude increase in dwell-time compared to a scanning system such as the Thematic Mapper. This increase in signal can then be used to reduce spectral bandwidth for improved spectrometry, and still obtain substantial improvement in SNR; yet without compromising spatial resolution. This is a major reason that the HIRIS sensor, for example, has been designed using a pushbroom optical approach.

Spectral discrimination of ground features is possibly the most important application of earth sensing using passive electro-optical instruments. One of the major improvements in remote sensing from the late 1970's to

the early 1980's, for example, was achieved by the addition of more spectral discrimination capability to the Landsat system. While the Multispectral Scanner (MSS) on Landsats 1, 2, and 3 offered useful data, the Thematic Mapper (TM) on Landsats 4 and 5 offers capability to discriminate ground features such as iron oxides from clay mineral compounds, and clouds from snow because of the short-wave infrared channels that were added to the TM sensor (Schueler and Salomonson, 1985). As is reported elsewhere in the literature, the acquisition of many narrow spectral channels across the spectrum from visible through thermal infrared is a major goal of future sensors such as HIRIS and MODIS (Goetz and Herring, 1989; Salomonson, et al, 1989).

To obtain continuous, narrow resolution spectral coverage requires advances not only in optical throughput as described above, but also in the spectral filtering technology that is used to define the spectral bands. Table 3 illustrates the range of technologies that are available now to accomplish this, with some general indications of the relative capabilities of the various approaches. There are essentially four major classes of spectral filtering methods shown. These include: (1) filters, such as the beamsplitter, filter wheel, and interference filters; (2) gratings and prisms; (3) Fabry-Perot interferometers; and (4) Michelson interferometer techniques.

Table 3 - Spectral Separation Technologies

APPROACH	SIMULTANEITY	TRANSMISSION	TUNABILITY	SPECTRAL RESOLUTION
DICHROIC BEAMSPLITTER	YES	MEDIUM TO HIGH (> 50%)	NO	COARSE (> 1%)
FILTER WHEEL	SEQUENTIAL	MEDIUM-HIGH	NO	MEDIUM-FINE
UNIFORM (STRIPE) INTERFERENCE FILTER	YES *	MEDIUM-HIGH	NO	MEDIUM FINE (0.1-1%)
DIFFRACTION GRATING 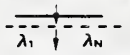 TRANSMISSIVE OR REFLECTIVE	OR SEQUENTIAL	LOW-MEDIUM (< 50%)	YES (IF SCANNED)	MEDIUM-FINE
DISPERSIVE PRISM	OR SEQUENTIAL	LOW-MEDIUM	YES (IF SCANNED)	MEDIUM-FINE
INTERFEROMETER • FABRY PEROT 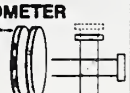 • FOURIER (MICHELSON)	• SEQUENTIAL • YES	MEDIUM	YES	COARSE TO VERY FINE (LIMITED BY OPD)

Table 3 is organized roughly in order of increasing technology sophistication and capability, as well as decreasing technology maturity. For example, tunability and spectral resolution both become better as we move from the top to the bottom of the Table. Transmission and capability to simultaneously (in a temporal sense) acquire data from different spectral bands are desirable attributes. (The asterisk next to the "YES" for spectral simultaneity for the stripe filter indicates that while the filters can acquire different spectral bands at the same time, they cannot in general acquire different spectral bands at the same spatial location on the ground.) From the last column, one can see that for HIRIS, the prism spectrometer becomes attractive due to the capability for fine spectral resolution and temporal/spatial spectral simultaneity.

Focal Plane Trends

Figure 4 illustrates the trends in focal planes. The Thematic Mapper, including the Enhanced Thematic Mapper (ETM) under development for Landsat 6, uses technology one step less advanced than the first generation technology illustrated, which is employed in the SPOT sensor, for example. While the TM sensor exploits 1970's discrete detector technology, with off focal-plane electronics, the first generation of integrated focal-plane uses line arrays of detectors fabricated on a single chip of substrate material.

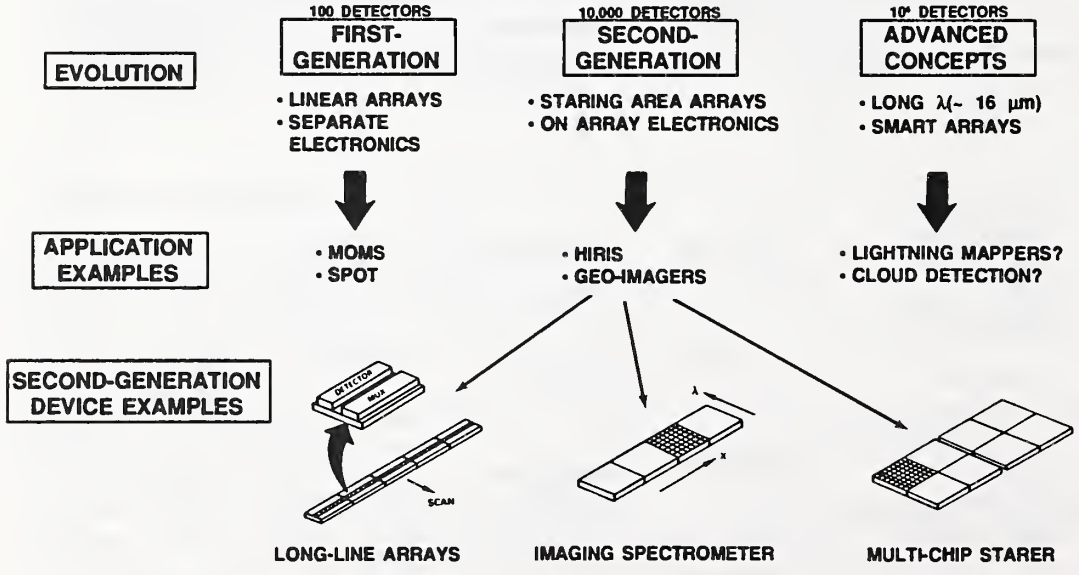

Figure 4 - Detection on Integrated Focal Planes

Newer sensors such as HIRIS will employ second-generation techniques with area arrays fabricated on a single chip of detector material. Here, the electronics, including read-out and analog-to-digital (A/D) signal conversion, is integrated into the focal-plane. Finally, advanced concepts are under development that will integrate much or all of the entire signal processing required to generate image products onto the focal-plane. These concepts are currently of primary interest to the DoD community, for which the imaging tasks are much more clearly delineated than are those for the science community represented by NASA Eos and NOAA.

Aside from the processing and integration advances that are being pursued, and possibly of more importance from the standpoint of real data utility, is the much more fundamental work in progress to improve detection. Radiometry is the key driver here, and efforts to improve SNR and long-wavelength performance are under way. Extended blue response approaching the ultraviolet, dynamic range exceeding four orders of magnitude, and low noise below 50 electrons are the goals in the visible and near infrared (0.4 to 1.0 μm). Development of photo-voltaic HgCdTe (Mercury Cadmium Tellurde) detectors with high quantum efficiency and operating temperatures exceeding 145 K are key goals in the short-wave infrared (1.0 to 2.5 μm). Photo-voltaic HgCdTe and InSb (Indium Antimonide) detectors of generally mature capability already exist in the middle infrared (3 to 5 μm), while longer cutoff wavelengths out to sixteen μm using photo-voltaic HgCdTe detector materials is the goal for the Thermal Infrared (from 8 μm up).

Electronics and Mechanical Trends

Commercial applications of advanced electronics abound, and these have resulted in rapid advances in both analog and digital signal processing in the past ten years. It is now possible and practical to perform not only on-board radiometric correction, but even much of the complex signal and image analysis can be accomplished in space that is currently typically done by large computers on the ground. On-board Fourier transforms can be computed "on-the-fly" by off focal plane processors, and spectral template matching as well as advanced data compression are available with very low-power and low-density electronics.

In the mechanical arena, probably the two greatest concerns are cooling for the long wave detectors, and pointing stability and knowledge. The choice of cryogenics is complicated by the details of sensor

configuration on the spacecraft, as well as by the amount of radiative heat transfer capability required to cool the detectors. If a clear view to cold space is available, and if the temperature requirement is not too low (T > 60K, for example, with a power dissipation level below 5 watts as a rule of thumb) then a passive radiator is typically the choice. This is because the passive radiator offers the maximum reliability and lightest weight compared to equivalent active coolers. Moreover, passive radiation requires no operating power.

If the clear view to cold space is not available, and the power dissipation and temperature requirements are too stringent for a passive radiator, then either passive cryogen systems (liquid or solid boil-off), or active mechanical refrigeration are the other two choices. If reliability is critical, sometimes the passive cryogen boil-off approach is appropriate, but the inherently limited life (until the cryogen is gone; months, typically) and the high mass can be quite restrictive.

Mechanical systems, as a result, have been the subject of a very substantial and long-term research program sponsored by several agencies, including NASA (Linear Stirling one-stage cooler with 65K, 5 watt performance) and the Strategic Defense Initiative (e.g., Hughes Vuillemier 3 stage cooler with a second stage operating at 15K and 2 watts). It is expected that within the next five to ten years, very reliable (up to ten years in orbit) and high performance coolers will be available. These will be able to supply the very low temperatures and high power dissipation requirements of very large arrays of short-wave IR and Thermal IR focal planes. Currently, while active refrigerators can already supply the performance, their reliability is such that life in excess of one or two years is not generally expected.

Finally, in the mechanical pointing and stability area, 100 µrad stability is the current norm using mechanical bearings and servo-motors for pointing. While 100 µrad performance, corresponding to about 70 meters from a 705 km orbit and about 4 km from geo-synchronous orbit, is adequate for many applications, future requirements for sub-kilometer pointing accuracy from geo-synchronous orbit are driving the technology toward a goal of 20 µrad pointing stability. It is anticipated that this goal can be reached in the next few years, without major technology advances, through increased reliance on magnetic bearings and improved servo control systems.

COST REDUCTION

The cost implications associated with the foregoing technology discussion are illustrated in Figures 5 and 6. Figure 5 illustrates the dependence of cost on both performance and orbit life. Clearly, the lower the performance requirements, and the less stringent the longevity requirement, the lower the cost. As performance increases, so does cost. For fixed performance, however, as the longevity requirement lengthens, the cost also grows. Although a sensor may become more expensive as mission life increases, it may still be cost-effective to demand long life to save the cost of building and launching replacements, even if the replacements are exact replicas of the first flight model sensor. Clearly, as launch costs drop in the future, the longevity requirements may be scaled back.

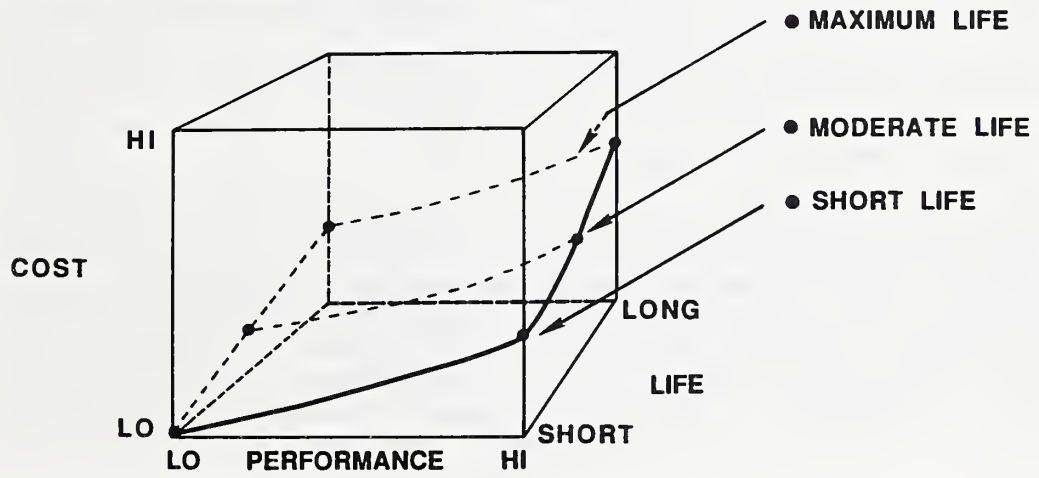

Figure 5 - Cost is Traded with Performance and Life

Figure 6 illustrates the dependence of cost on the growth of mission performance requirements. As discussed in detail above, mission requirements are advancing, and new technologies are necessary to meet them. Costs accordingly grow from one mission to the next as these requirements advance. In other cases, mission requirements are sufficiently stable to obtain the benefits of low recurring costs for mature designs. An example is the Japanese Geostationary Meteorological Satellite (GMS) series. Other than some minor improvements, the Japanese have not required significant changes in design from the first launch in the early 1970's to the current fifth mission.

An example of an evolutionary requirements growth trend is provided by the NOAA Geostationary Operational Enviromental Satellite (GOES) program. Requirements here have grown substantially enough that a new design

has been required in the transition from GOES to GOES Next in the 1990's, with attendant high cost.

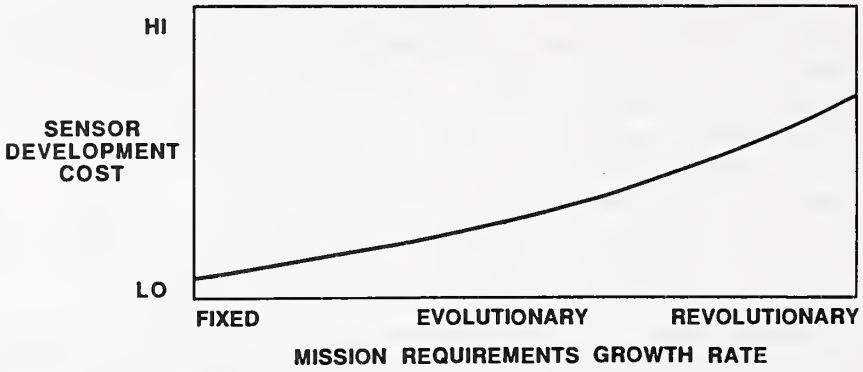

Figure 6 - Cost is Correlated to Requirements Evolution

Based on these sets of observations, a five-part "recipe" for cost control can be cited:

• Concise and stable specifications.

These should be based on substantial up-front negotiation with the contractor community to ensure that optimal mission specifications are developed and that they will not need changing based on some unforeseen contractor discovery after contract initiation. Stability of specifications is a particularly important cost reduction element, because changes generally stretch schedule and therefore add substantially to cost.

• Tailored sensor quality and reliability plans.

Transfer of boiler-plate plans from a previous program to a new one without modifications to account for either relaxation or tightening requirements can and probably will result in either excess cost or inadequate performance, respectively.

• On-site management authority.

This can be via a resident customer representative, or via some other mechanism. This expedites the flow of hardware through the fabrication and test cycle by providing rapid review and approval of quality and test data. The resulting schedule savings are directly reflected in lower costs.

• Streamlined program controls and documentation.

This can substantially reduce personnel overhead and cost on a contract. Again, program controls that may have worked well on one program may not be appropriate for another and these procedures should be reviewed carefully by appropriate personnel who are familiar with the specifics of the specific program of interest.

• When practical, return to "Skunk Works."

The simplest form of contract which has become known as the "skunk works" approach, should be used as appropriate. Here, the contractor is provided with specifications, a schedule, and a budget. He is then left alone until the end of the schedule, at which time the customer reviews the results. It is up to the contractor to internally monitor the contract to meet specifications, schedule and budget. This approach saves the customer money because a full retinue of customer personnel are not needed to monitor the contract, and it saves the contractor money because a correspondingly large staff is not needed to provide continuous feedback to the customer on contract progress. This technique carries some risks and requires an estraordinary degree of trust between the customer and his contractor, but the efficiencies are undeniable. One of the most important ingredients for the success of this approach is stable specifications stated at the highest possible functional level.

SUMMARY

The major technology trends described in this paper are in the areas of optics (telescope FOV to 15 degrees and improved spectrometry) for broad area coverage, feature discrimination, and vertical temperature sounding; the focal plane (longer wavelength photovoltaic detectors with improved noise characteristics at higher temperatures); and in improved cooling systems and better pointing capability to 20 μrad stability.

These improvements promise to favorably impact all areas of earth observation, from atmospheric sounding and gas spectrometry, to biological feature identification, ocean sea-surface temperature mapping and productivity analysis, as well as earth surface mineral identification. The improvements are driven by escalations in performance requirements, and make cost control challenging. Some specific contracting procedures can be implemented, however, to mitigate cost growth associated with improved performance.

REFERENCES

Bretherton, F., et al, 1988, (Earth System Sciences Committee of the NASA Advisory Council), Earth System Science - A Closer View, NASA, January.

Butler, D.M., et al, 1984, (Eos Science and Mission Requirements Working Group), Earth Observing System, NASA Technical Memorandum 86129, August.

Goetz, A.F.H., and M. Herring, 1989, "The High Resolution Imaging Spectrometer (HIRIS) for Eos," IEEE Trans. Geoscience and Remote Sensing, vol. 27, no. 2, pp. 136-144.

Salomonson, V.V., W.L. Barnes, P. W. Maymon, H.E. Montgomery, and H. Ostrow, 1989, "MODIS: Advanced Facility Instrument for Studies of the Earth as a System," IEEE Trans. Geoscience and Remote Sensing, vol. 27, no. 2, pp. 145-153.

Schueler, C.F., and V.V. Salomonson, 1985, "Landsat Image Data Quality Studies," Advances in Space Research, Vol. 5, no. 5, pp. 1-11.

Shenk, W. E., T. H. Vonderhaar, and W. L. Smith, 1987, "An Evaluation of Observations from Satellites for the Study and Prediction of Mesoscale Events and Cyclone Events," Bulletin of the American Meteorological Society, vol. 68, no. 1, pp. 21-35.

Cost Comparison Between the Space Flight and the Commercial Catalog Models of a Cesium Atomic Clock Module

Helmut Hellwig
National Institute of Standards and Technology
Gaithersburg, MD 20899

COST COMPARISON BETWEEN THE SPACE FLIGHT AND THE COMMERCIAL CATALOG MODELS OF A CESIUM ATOMIC CLOCK MODULE

Helmut Hellwig

National Institute of Standards and Technology
Gaithersburg, MD 20899

Abstract

The data reported is not based on work done at the National Institute of Standards and Technology but stems from the author's prior experience as president of an electronics firm involved in the research, design and manufacture of cesium clocks for civilian as well as military and aerospace applications. The cost comparison addresses the various cost elements that render the total cost of the space flight module twelve times that of the technically similar catalog item. The cost elements are quantified; it is concluded that technical and performance requirements of space flight boost cost by a factor of two whereas managerial, procedural and control requirements account for an additional factor of six. Therefore, in order to achieve substantial cost-reductions, the latter requirements are deserving primary attention.

INTRODUCTION

The cesium clock technology is a complex integration of sophisticated electronics and physics principles. A cesium atomic clock provides superb time-keeping and frequency control capabilities (1). Accuracy and stability performance of the

output signals approaches 10^{-13}; e.g., time signals vary only 10 nanoseconds during one day.

The clock is based on the resonance frequency of the cesium atom at about 9 GHz. This resonance is accessed by interrogating cesium atoms in an atomic beam with a microwave signal which is synthesized from a precision quartz crystal oscillator operating near 5 MHz. Servo electronics steers the quartz crystal oscillator frequency to track the cesium resonance. The high accuracy is a consequence of the fact that the cesium resonance is an invariant of nature.

The very high accuracy of this clock is needed for frequency control in communication and for time-keeping in navigation. For example, in electronic navigation, distances are determined via the speed of light; thus, 10 nanoseconds represent a distance of about 3 meters.

SPACE APPLICATIONS OF THE ATOMIC CLOCK

The Navstar satellites of the Global Positioning System (GPS) carry cesium clocks (2) which enable the GPS to offer absolute positioning fixes in three dimensions with accuracies measured in meters.

These cesium clocks have been manufactured by a firm which began to develop this technology in 1973. The pre-production model for GPS was qualified in 1979 (2). Qualification of the production model was completed in 1982. In 1978 the firm also began to produce a commercial version of the same design using a nearly identical cesium beam resonator. The block diagram of the

GPS (2) and the commercial clocks are identical and their overall physical dimensions as well as their performance as clock or frequency standard are the same.

SCOPE OF SPACE AND COMMERCIAL EFFORTS

Table 1 illustrates the non-recurring engineering requirements which had to be met for the GPS clock module as compared to the commercial module.

TABLE 1

NONRECURRING ENGINEERING REQUIREMENTS

- Performance Related Redesign
- Form/Fit/Function Related Redesign
- Reliability Prediction
- Parts Stress Analysis
- FMEA
- WCCA
- Qualification Testing
- Design Reviews

In this paper, no attention will be paid to the design and engineering development of the device. Nevertheless, it should be noted that the total effort expended by the firm for these requirements was about the same as that needed for the original design and engineering of the cesium clock itself.

In the mid-1980's commercial, militarized and GPS clock modules were produced in quantity; i.e., orders were received for

50-100 units in each category. This makes the following cost comparison (Table 2) meaningful in that it compares the different realizations of the same technology and design based on equal opportunities for economics of scale.

TABLE 2

COST OF HARDWARE COMPARISON

o	Commercial/Catalog	P
o	Military/Special	1.5 to 5P
o	Spaceflight	10 to 20 P

The remainder of this paper is an attempt to rationalize as to why the cost of the GPS clock is about twelve times that of the similar commercial clock module offered in the firm's product catalog[1].

Additional requirements for space flight:

In order to segregate the various cost-drivers one has to look at what requirements differentiate the space hardware from the catalog item (Table 3).

---

[1]The catalog price of the commercial module was around $30,000 in 1985.

TABLE 3

ADDITIONAL REQUIREMENTS FOR SPACE HARDWARE

- Physical Requirements
- Systems Requirements
- Manufacturing Requirements
- Production Control Requirements
- Test Requirements
- Procedural Requirements

Table 4 gives for each of these six categories the detailed requirement elements which the firm encountered. Listed are only those requirements which either were not part of the specifications or manufacturing practice of the commercial module or which significantly exceeded them or which were explicitly contractually prescribed.

COST ANALYSIS

Based on the analysis of Table 4, it is now possible to estimate the additional cost increments associated with each of the categories. It must be noted that the firm was neither organized nor was its cost control system designed to allow this type of cost collection. Therefore, for the estimates of Table 5, other measures were used such as staffing levels, average parts costs, project duration times, etc. The cost increments are entered in the column "actual" in terms of P, the cost of the catalog item. Thus, a cost increment of 1.1P means that this

TABLE 4

A. PHYSICAL REQUIREMENTS

- o Vacuum
- o Vibration
- o Acoustics
- o Radiation
- o Operate-Through/Survival
- o Reliability
- o weight
- o power (start-up, steady-state)

B. SYSTEMS REQUIREMENTS

- o Physical Dimensions
- o Electrical Interfaces
- o Command/Control
- o Monitors & Diagnostics
- o EMI
- o Hazards

C. MANUFACTURING REQUIREMENTS

- o Flight-Qualified Parts
- o Program-Approved Parts
- o Non-Standard Parts
- o Parts Screening
- o As-Built Configuration
- o Rework

D. PRODUCTION CONTROL REQUIREMENTS

- o Process Controls
- o Materials Controls
- o Vendor Controls
- o Quality Controls/ Inspection
- o Configuration Control
- o Calibration Control
- o Lot Control

E. TEST REQUIREMENTS

- o Acceptance Testing
- o Special Test Equipment (automation)
- o Test Plans & Procedures
- o Failure Analysis & Corrective Action

F. PROCEDURAL REQUIREMENTS

- o Customer (Prime Contractor) Witnessing/Audits
- o Government Witnessing/Audits
- o Proposal Preparation
- o Liaison/Customer Support
- o Customer & Government Source Inspection

increment alone would more than double the clock module's cost to 2.1P total. The second column gives the author's opinion of these cost elements that are technically required in order to achieve mission objectives. For example, the requirements of Table 4 A. and B. impose real demands which can only be met by adding parts or upgrading parts of the commercial unit. It must be noted that this is fully true for the requirements of Table 4 A.; as regard Table 4 B., it is assumed that the system designer has considered the given design of the commercially available module; therefore, systems requirements do not demand changes in the physical dimensions and monitor functions,

TABLE 5

COST-DRIVER ELEMENTS

Categories	Additional Cost Increments Actual	Technically Required
Physical Requirements	1.1P	0.3P (Parts)
Systems Requirements	1.1P	0.2P (Parts)
Manufacturing Requirements	2.8P	0
Production Control Requirements	2.2P	0
Test Requirements	2.0P	0.5P
Procedural Requirements	1.8P	0
Total Added Cost	11.0P	1.0P
Total Hardware Cost	12.0P	2.0P

and changes in electrical interfaces are limited to connector type and do not involve different supply voltages, etc.

Significantly extended testing is absolutely necessary for space flight; however, significant savings can be realized in several areas of current requirements including repetitive testing, failure analysis, inflexible test procedures, etc. In the areas of manufacturing, production control and procedural requirements, the additional requirements imposed on the space hardware are not likely to lead to a better performing or more reliable unit, nor to any other tangible benefit for the end user.

CONCLUSION

It may be concluded that the target cost for manufacturing (not engineering or designing) a reliable unit meeting all mission requirements could be as low as only twice that of its sister-unit found in the firm's catalog. Realizing even a fraction of such savings, however, would require substantial changes in buyer-vendor relations, procurement practices, in the interactions between the several tiers of contractors, and in the approach to testing and systems design. Many of these changes have been described in reference 3.

Finally, it should be noted that one of the firm's militarized cesium clocks (at a cost of below 2P) was successfully deployed in space and returned to earth as part of a West-German Spacelab navigation experiment (4).

References:

1. "Microwave Frequency and Time Standards", Chapter 10 of "Precision Frequency Control", E.A. Gerber and A. Ballato, editors, Academic Press, 1985, pp 114-175.

2. "Cesium Clocks Deployed in the Global Positioning System: Design and Performance Data", H. Hellwig and M. Levine, Proc. 38th Annual Symposium on Frequency Control, Institute of Electrical and Electronics Engineers, 1984, pp 458-463.

3. "Bolstering Defense Industrial Competitiveness", Report to the Secretary of Defense, Department of Defense, July 1988.

4. "Performance of Atomic Clocks Flown on the Space Shuttle Experiment NAVEX", J. Hammesfahr, H. Nau, and S. Starker, Proc. 19th PTTI Applications and Planning Meeting, U.S. Naval Observatory, Wash. D.C., 1987, pp 325-336.

Laser Propulsion Work at Livermore

Pulsed-Laser Propulsion for Low Cost, High Volume Launch to Orbit

Dr. Jordin Kare
LLNL
Mailstop L278, P.O. Box 808
LIvermore, CA 94550

and

Laser Propulsion and Possible Missions to Mars

Dr. Jordin Kare
LLNL
Mailstop L278, P.O. Box 808
LIvermore, CA 94550

Pulsed Laser Propulsion for Low Cost, High Volume Launch to Orbit

Jordin Kare

Lawrence Livermore National Laboratory
Livermore, CA

ABSTRACT

Pulsed laser propulsion offers the prospect of delivering high thrust at high specific impulse (500 - 1000 seconds) from a very simple thruster, using the energy of a remote ground-based laser to heat an inert propellant. Current analyses indicate that payloads of approximately 1 kg per megawatt of average laser power can be launched at a rate of one payload every 15 minutes and a marginal cost of $20 to $200 per kg. A 20 MW entry-level launch system could be built using current technology at a cost of $500 million or less; it would be capable of placing 600 tons per year into LEO.

The SDIO Laser Propulsion Program has been developing the technology for such a launch system since 1987. The Program has conducted theoretical and experimental research on a particular class of laser-driven thruster, the planar double-pulse LSD-wave thruster, which could be used for a near-term launcher. The double-pulse thruster offers several advantages, including extreme simplicity, design flexibility, and the ability to guide a vehicle remotely by precise control of the laser beam. Small-scale experiments have demonstrated the operation of this thruster at a specific impulse of 600 seconds and 10% efficiency; larger experiments now under way are expected to increase this to at least 20% efficiency. Systems-level issues, from guidance and tracking to possible unique applications, have also been considered and will be briefly discussed. There appear to be no fundamental obstacles to creating, in the next five to ten years, a new low-cost "pipeline to space".

Introduction

Most space power and space power transmission systems now being planned or discussed have power levels measured in kilowatts. We do not yet have space hardware that needs, or can handle, megawatts of electrical power; developing such hardware will require enormous technical development and capital investment. Yet very high powers and power densities are required for one space use: generating thrust for high acceleration, and particularly for launching payloads from Earth to orbit. Currently, these power levels can only be generated (with acceptable power-to-weight ratios) by chemical combustion: a modest solid rocket booster (10^6 newton thrust, 250 seconds I_{sp}) produces over 1 GW. Pulsed laser propulsion, unique among alternative thruster and power beaming technologies, can reach power levels and power densities comparable to chemical thrusters, with higher performance, and without requiring expensive flight hardware. A price is paid, of course, in complex hardware for generating and transmitting the laser beam, but that hardware can reside on the ground, indefinitely reusable and straightforward to build, test, and maintain.

Laser propulsion, as originally conceived by Kantrowitz [1], uses a large ground-based laser to supply energy to a small rocket vehicle. The laser beam heats an inert propellant, which is exhausted to provide thrust. Because the propellant exhaust velocity is not limited by its chemical energy content, specific impulses in excess of 1000 seconds can be achieved. Ground- or space-based CW lasers and space relay mirrors have been suggested as a way to power orbital maneuvering thrusters [2,3], but proposed CW-laser thruster designs have been relatively complex, using regeneratively-cooled nozzles and liquid hydrogen

propellant. Such systems are competitive with other advanced orbital-maneuvering concepts such as solar-electric or solar-thermal, but are not suitable for a small-scale Earth-to-orbit launcher.

If a pulsed laser is used, a thruster the engineering temperature limits of conventional thrusters do not apply. High I_{sp} is thus available from propellants much heavier (on an atomic scale) than hydrogen. Also, with appropriate design, no nozzle is needed to produce efficient thrust, and ideally, a thruster can consist of only a block of suitably-formulated solid propellant.

Since the spring of 1987, the U.S. Strategic Defense Initiative Organization (SDIO) has sponsored a research Program on Laser Propulsion, managed through the Lawrence Livermore National Laboratory. The Program has focussed on a particular type of laser propulsion thruster, the double-pulse planar thruster [4]. This thruster uses a solid propellant block composed of one of several inert materials, such as plastic or water ice, seeded with additives to control its optical and chemical properties. An "evaporation" laser pulse ablates a few-micron-thick layer of propellant, forming a thin layer of gas which is allowed to expand to roughly atmospheric density. A second laser pulse then heats this gas layer to approximately 10,000 K. The hot gas layer expands rapidly, producing thrust. The entire process takes a few microseconds, and is repeated at 10^2–10^3 Hz rates. This process is illustrated in Figure 1.

Because the hot gas layer is only a few millimeters thick, while a typical vehicle is two meters across, no nozzle is needed to confine the expanding gas. The expansion generates thrust uniformly across the flat base of the vehicle (hence the "planar" thruster). In addition to making the vehicle design extremely simple, this scheme has two other advantages. First, the thrust direction is independent of the laser beam direction; the vehicle can fly at an angle to the laser beam. Second, the thrust can varied across the base of the vehicle by controlling the beam profile. The vehicle can therefore be steered from the ground, and does not need its own guidance system.

Properties of a Ground to Orbit Launcher

Figure 2 illustrates the components of a minimum-size ground-to-orbit launch system which could be constructed in the next four to five years. The laser is a 20 MW average power electric-discharge CO_2 laser, producing 500 kJ, 2 microsecond pulses at 40 Hz. This would be a very large laser, but the technology for such large CO_2 lasers was well developed in the 1970's. Because of the physics of the double-pulse thruster itself, the 10 μm wavelegth is preferred over shorter wavelengths, although a laser propulsion system could operate at wavelengths as short as 1 μm. A high-power free electron laser (FEL) would be even better, offering higher electrical efficiency (20-25% vs. 15%) and possibly greater reliability. FEL technology is still new, however, and may not be available at competitive prices for several years. The laser requires roughly 150 MW of electricity, which can be obtained from the national power grid or produced locally, e.g., by diesel generators.

The laser beam is focussed by a 10 meter diameter beam projector telescope onto a two meter diameter vehicle. This combination gives a useful range of approximately 1000 km. The maximum payload mass is proportional to the system range (other factors being equal), but 1000 km approaches the maxixmum practical range, both because of limits on telescope and vehicle size, and because the vehicle must stay well above the laser's horizon during the launch. The telescope could be a variant of a conventional astronomical telescope, similar to the 10-meter Keck astronomical telescope now being built by Cal Tech and the University of California [5], or it could be a more specialized design, for example a phased array of smaller mirrors. An adaptive optics system is needed to correct for atmospheric turbulence and thermal blooming, but the combination of long wavelength and a cooperative vehicle (which can even telemeter back information about the beam profile) keeps the complexity of this system well within the state of the art. However, a mountaintop (3-km altitude) launch site is needed to reduce absorption of the laser beam by atmospheric water vapor and CO_2.

The vehicle consists of 120-150 kg of propellant, and 20 kg of payload, with a few kg of structural support, primarily a stiff baseplate to support the thin propellant block. A throwaway air-breathing stage improves performance by lifting the vehicle to 20 km or higher with a "laser pulse-jet". The vehicle then drops the air-breathing hardware and accelerates vertically to about 100 km, where it "turns over" and accelerates downrange to 400 - 500 km altitude and 1000 km range. At that point it runs out of propellant and enters a circular or elliptical orbit. The maximum acceleration is about 6 gees. The time from launch to entering orbit is 15 minutes or less.

Launcher Cost and Scaling

The cost of the 20-MW, 20-kg system described here is estimated at $450 million; this is roughly broken down in Table 1. The incremental cost of launching a single vehicle is simply the cost of the vehicle, propellant, and electricity; the electricity cost is some 30 to 40 thousand kWH or, at 4 cents/kWh, $1200 to $1600. Assuming a propellant cost of $10/kg and a vehicle cost of no more than $2000 (mostly sheet-metal structure, produced in quantity), the total incremental cost per launch could be below $5000; this would give a cost to orbit of $250/kg or less than $120/lb. However, the small payload size means the vehicle must remain cheap; even a few thousand dollars spent on, e.g., telemetry, could double the incremental costs.

The true cost to orbit requires amortizing the cost of the launcher itself, and its maintenance and manpower, and thus depends on how heavily the launcher is used. At one extreme, to reduce the true costs to $10,000/kg ($4500/lb, comparable to current expendable rockets) would require launching a minimum of 50,000 kg, or about 2500 launches, over the life of the system. At the other extreme, the launcher is capable of up to 100 launches per day, or more than 30,000 launches per year. That would put 600,000 kg, or more than 20 Space Shuttle loads, in orbit each year. This exceeds not only the capacity of the Shuttle fleet, but the total capacity of all existing US launch systems at current production rates [6]. Assuming a 5 year system life, and annual operating costs of 20% of the capital cost, the effective cost of the system would be $180 million per year, or $300 per kg launched. Including the incremental costs, the total launch cost would be approximately $550/kg, or $200/lb.

The 20-MW, 20-kg system described here is probably near the smallest size that can be built cost-effectively. This results from tradeoffs among vehicle size and structural mass, beam projector size, and laser properties. There is, however, no obvious limit to increasing the system size, and larger systems gain at least linearly in payload size vs. laser power, and considerably better than linearly in payload size vs. system cost.

Table 1: Approximate system cost breakdown

Laser:	$185 M	(approx. $8/watt + $25 M design cost)
Telescope:	$100 M	(based on Keck 10 meter astronomical telescope cost)
Adaptive Optics:	$ 15 M	
Tracking:	$ 50 M	
Power plant:	$ 50 M	(Diesel generators)
Structure:	$ 50 M	(roads, buildings, etc.)
Total	$450 M	

Applications

There is no fundamental upper limit to the size of payloads that could be launched with a laser. However, economic limits will restrict lasers to small payloads in the near future — a 1-GW laser could be built for perhaps $10 billion, much less than the amount that has been spent on the Space Shuttle, but at present there is literally no use for the 50,000 tons of payload that it could launch each year.

Even at 20 to 100 kg payload size, however, there are many possible payloads. So-called "lightsats" have been proposed for communications, remote sensing, and scientific applications; while these are usually thought of as weighing 100 to 1000 kg, some lighter satellites ("microsats") have already been flown [7]. Most of these satellites would be needed in small quantities, but cumulatively they could represent a market for several hundred launches per year. Some uses, such as packet-switching low-orbit communications networks, could involve hundreds or thousands of microsats. Obviously, there are also possible strategic defense applications, particularly in connection with recent suggestions for swarms of small space-based interceptors ("Brilliant Pebbles").

The number of applications grows enormously if some form of assembly in space is possible. It is currently impractical to assemble anything in space from 20-kg modules using either human or robotic labor; there is not even a practical way to collect such pieces and bring them together. However, the technology needed to build small autonomous spacecraft capable of rendezvous and docking maneuvers is

rapidly being developed. At the simplest level, satellites of moderate size could be launched as modules, starting with a maneuverable guidance and command unit. This unit could, over several days, collect and join together independent modules (power, communications, scientific experiment, booster) to form, for example, an interplanetary probe.

A larger-scale application of this concept would be efficient resupply of Space Station Freedom. Supplies (food, water, tools, spare parts, etc.) could be delivered to orbit perhaps 100 km from the Space Station (to keep the Station safe from both laser beams and packages at high relative velocity) A very small (<100 kg) retriever vehicle would collect these supply packages and return them to a suitable airlock on the Station. Astronaut time would be needed only to unpack and store the supplies, and perhaps to monitor the final approach of the retriever to the Station. Even chemical fuels, oxygen, and batteries could be delivered — a particularly direct way of "beaming" power, and one which could be used over arbitrary distances, since the laser can easily launch payloads to escape velocity.

The laser system cannot launch to a given non-equatorial orbit at any time; the laser is precisely in the orbital plane only twice a day. However, the laser has some crossrange capability — the vehicle can be steered in a "dogleg" trajectory which results in an orbit that does not pass over the laser. Even a 100 kilometer crossrange capability (out of a laser range of 1000 km or more) could allow at least eight payloads per day to reach the Space Station. Eight payloads per day would be over 50 tons — two Shuttle loads — per year. The limited size of each payload would be somewhat offset by the promptness of delivery; a tool or spare part could be delivered to the Station with, in many cases, less than a day's delay. As Federal Express has demonstrated, overnight delivery frequently commands a premium price, and is sometimes truly invaluable.

Uses for a Sub-Scale Laser Facility

Although a true launch-to-orbit system requires a 20-MW system, there are some propulsion applications for considerably smaller lasers. Perhaps the most important of these is orbital maneuvering propulsion. A laser as small as 1 to 2 MW can give considerable impulse to a satellite passing overhead. To keep the beam projector size and cost within reason, the satellite must deploy a crude reflector (essentially a beach umbrella of aluminized Mylar) to concentrate the laser beam. However, with such a concentrator, the satellite can get thrust with triple the specific impulse of solid rockets, or twice that of H_2/O_2 rockets, from a completely safe and stable block of inert propellant.

The laser can only track a given satellite in low orbit for a few minutes each day; exactly how much time depends on the details of the satellite's orbit and the laser range. (Orbiting mirrors would greatly increase this, but would cost much more than the laser system). That is sufficient to allow a 2-MW laser to maintain or raise the orbit an object as large as a Space Shuttle External Tank. It is also sufficient to push ton-sized satellites from low orbit to geosynchronous transfer orbit on time scales of weeks, while saving half to two thirds of the mass of a standard liquid or solid fuelled upper stage.

If a high enough laser flux can be achieved in orbit, the laser could also clear away space junk. Small bits of debris would be evaporated. The surface of larger pieces would ablate, producing enough thrust (at low specific impulse) to deflect the junk into orbits that re-enter the atmosphere.

A megawatt-scale laser facility is also a necessary step in developing a laser launcher. While not capable of putting anything in orbit, it could launch small "sounding rockets" to several hundred km altitudes, and provide detailed information on atmospheric absorption, turbulence, and blooming. It could also aid other space experiments, by providing very high levels of burst power to satellites passing overhead (although this function might be better served by a short wavelength laser whose light could be efficiently converted to electricity by ordinary solar cells).

Status of Laser Propulsion Research

The SDIO Laser Propulsion Program has conducted experiments at several industry and Federal laboratories, and both industry and university groups have done theoretical analysis and computer modelling of the double-pulse planar thruster and related schemes. We have demonstrated experimentally that the double pulse thruster concept works, producing higher thrust efficiency (exhaust kinetic energy/laser pulse energy) and higher specific impulse than can be achieved with single laser pulses under similar

conditions. This was done with single pairs of CO_2 laser pulses, with pulse energies of a few Joules and pulse widths of 50 to 100 ns. Specific impulses of 700 to 800 seconds have been demonstrated using both single and double pulses.

The actual thrust efficiencies achieved with double pulses are only about 10%, while the launch system specifications cited above assume an efficiency of 40%. However, theory and computer modelling suggest that substantially higher efficiencies will be obtainable with longer pulses. Several energy loss mechanisms involve characteristic time or distance scales comparable to the scale of the current experiments, and will be much reduced at larger scales. We are currently preparing for experiments using a 2 kJ, 1 μs laser at Avco Research Laboratory, in which we hope to demonstrate efficiencies of 20% or more. Note that varying the efficiency changes only the size of the laser needed to lift a given payload; even at 20% efficiency all of the applications described above are practical, although the launch system cost would be somewhat higher.

We have identified several promising propellant candidates, including lithium hydride and other light hydrides, water ice, and certain C-H-O plastics, notably polyacetals (trade names Delrin and Celcon). More important, we now understand many of the properties required of a good propellant, such as short optical absorption depth in the solid (for efficient evaporation during the first laser pulse) and at least one component with a low ionization potential (for efficient absorption of the second pulse, which is absorbed by electron-ion and electron-neutral interactions). We have demonstrated our ability to modify propellants to achieve desired properties, for exampe by mixing wavelength-sized metal flakes into a plastic propellant to serve as plasma ignition sites; these lower the flux needed to achieve efficient heating during the second laser pulse.

Finally, we have analyzed many of the critical systems-level problems involved in building an actual launcher. We have, for example, calculated the control-loop response involved in guiding a laser-driven vehicle from the ground, and demonstrated that such ground-based guidance is stable over a wide range of conditions.

If the planned tests with single pulse pairs at 2 kJ are successful, the Laser Propulsion Program will be ready to proceed to tests with a repetitively pulsed laser of significant average power. Unfortunately, few such lasers are available, and none provide our desired pulse format. The Program currently plans to modify the Humdinger CO_2 laser at Avco Research Laboratory, but we are still seeking other options. The Program will also begin work on tests using Nd:glass lasers at 1.06 μm, both to determine the wavelength scaling properties of the double-pulse thruster, and specifically to see how laser propulsion could be adapted to use the large 1.06 μm FEL's now under develoment by the SDIO.

Program for Laser Propulsion

There are several possible routes to a working laser launch system. Assuming continued development of large lasers by the SDIO, it is likely that lasers (and optics) sufficient for launch-to-orbit will be built in the next decade. If these can be adapted (primarily through extended run times and improved durability) to routine use, laser launching may be a major peacetime application of strategic defense technology.

Alternatively, a dedicated laser launcher using CO_2 technology could be built. This would require a modest expansion of the current research efforts to demonstrate higher efficiencies, select and optimize a propellant, and demonstrate sustained performance with repetitive pulses. This would be followed by the design and construction of a sub-scale launch facility with 1-2 MW average power and a 4-meter-class telescope; the laser in particular could serve as a prototype module for a larger modular laser. As noted above, this sub-scale system could find immediate practical applications in satellite maneuvering. It would also answer essentially all questions about the viability of a larger system, particularly with respect to transmitting a beam through the atmosphere.

Finally, using the engineering experience and proof-of-principle results from the sub-scale launcher, a full 20-MW launcher could be designed and built. The time required to do this depends on the priority given to the project, but an overall time scale of 5 years appears feasible.

Conclusions

A working ground-to-orbit laser launch system could be built by the middle of the coming decade. Such a launcher would be capable of launching tens of thousands of small (20 kg) payloads into low Earth orbit every year, at an incremental cost approaching $100/lb. The capital cost of the system, including development costs, would be approximately a half-billion dollars — comparable to the cost of a handful of Shuttle or expendable rocket launches, whose total payload the laser could launch in a few months.

Such a laser system could significantly lower the cost of many space operations, from Space Station resupply to launching of small communications satellites. It would also provide unique capabilities for prompt launch of, for example, emergency spares or small sensor satellites. Even a sub-scale laser system, costing roughly 1/10 as much, could provide new capabilities, notably for maneuvering satellites using thrusters with two to three times the specific impulse of chemical rockets.

The basic operation of a laser propulsion thruster has been demonstrated in the laboratory; larger scale tests which should demonstrate realistic thruster efficiencies are planned for the next few months. Although there is considerable development work to be done, no major advances in physics or technology are needed to build a launch system using CO_2 lasers; large FEL's offer even more possibilities in a slightly longer term. In either case, beamed laser energy and the uniquely simple flat-plate thruster offer the first real near-term competition to rockets for getting into space.

Acknowledgements

The author gratefully acknowledges extensive discussions with Arthur Kantrowitz, Dennis Reilly, Lowell Wood, and numerous laser propulsion researchers. This work is supported by the Directed Energy Office of the Strategic Defense Initiative Organization, and performed by the Lawrence Livermore National Laboratory under the auspices of the U. S. Department of Energy, contract No. W-7405-ENG-48.

References

[1] A. Kantrowitz, "Propulsion to Orbit by Ground-Based Lasers," *Astronautics and Aeronautics*, Vol. 10, May 1972, pp. 74-76.

[2] L. W. Jones and D. R. Keefer, "NASA's Laser-Propulsion Project," *Astronautics and Aeronautics*, Vol. 20, Sept. 1982, pp. 66-73.

[3] R. H. Frisbee, J. C. Horvath, and J. C. Sercel, "Space-Based Laser Propulsion for Orbital Transfer", JPL D-1919, Jet Propulsion Laboratory, December 1984.

[4] Details of the double-pulse thruster, and additional background information on laser propulsion, are included in the *Proceedings of the 1986 SDIO/DARPA Workshop on Laser Propulsion*, Kare, J. T., ed., LLNL CONF-860778, (Lawrence Livermore National Laboratory, August 1987), volumes 1 and 2.

[5] *The Design of the Keck Observatory and Telescope*, Keck Observatory Report No. 90, J. E. Nelson, T. S. Mast, S. M. Faber, eds., University of California and Californial Institute of Technology, January 1985.

[6] U.S. Congress, Office of Technology Assessment, *Launch Options for the Future: A Buyers Guide*, OTA-ISC-383 (U.S. Government Printing Office, July 1988), p. 20.

[7] *Proceedings of the Second Annual AIAA/Utah State University Conference on Small Satellites*, F. J. Redd, Chairman, Utah State University, September 1988.

Figure 1: Double-Pulse LSD-Wave* Thrust Cycle

A) "Metering" pulse evaporates a thin layer of propellant
$\tau_1 = 2 - 5\,\mu s$

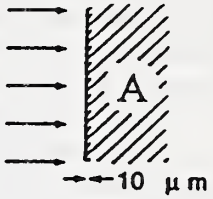

B) Gas expands to the desired density
$\tau_{1\text{-}2} = 0 - 5\mu s$

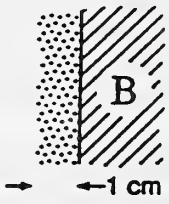

C) Main pulse passes through gas,
forms plasma at surface τ_{ign} = few ns

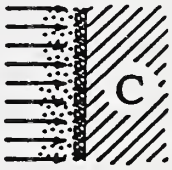

D) Plasma absorbs beam by inverse brems-strahlung; absorbing layer (LSD wave) propagates through gas $\tau_2 = 1\,\mu s$

E) Uniformly hot gas expands in 1-D,
producing thrust $\tau_{exp} = 3 - 10\,\mu s$

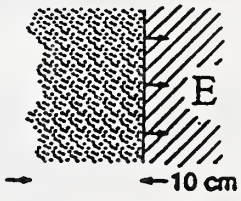

F) Exhaust dissipates; cycle repeats at 100 Hz - few kHz

Figure 2:
Components of a 20 MW/20 kg Laser Launch System

SDIO Laser Propulsion Program

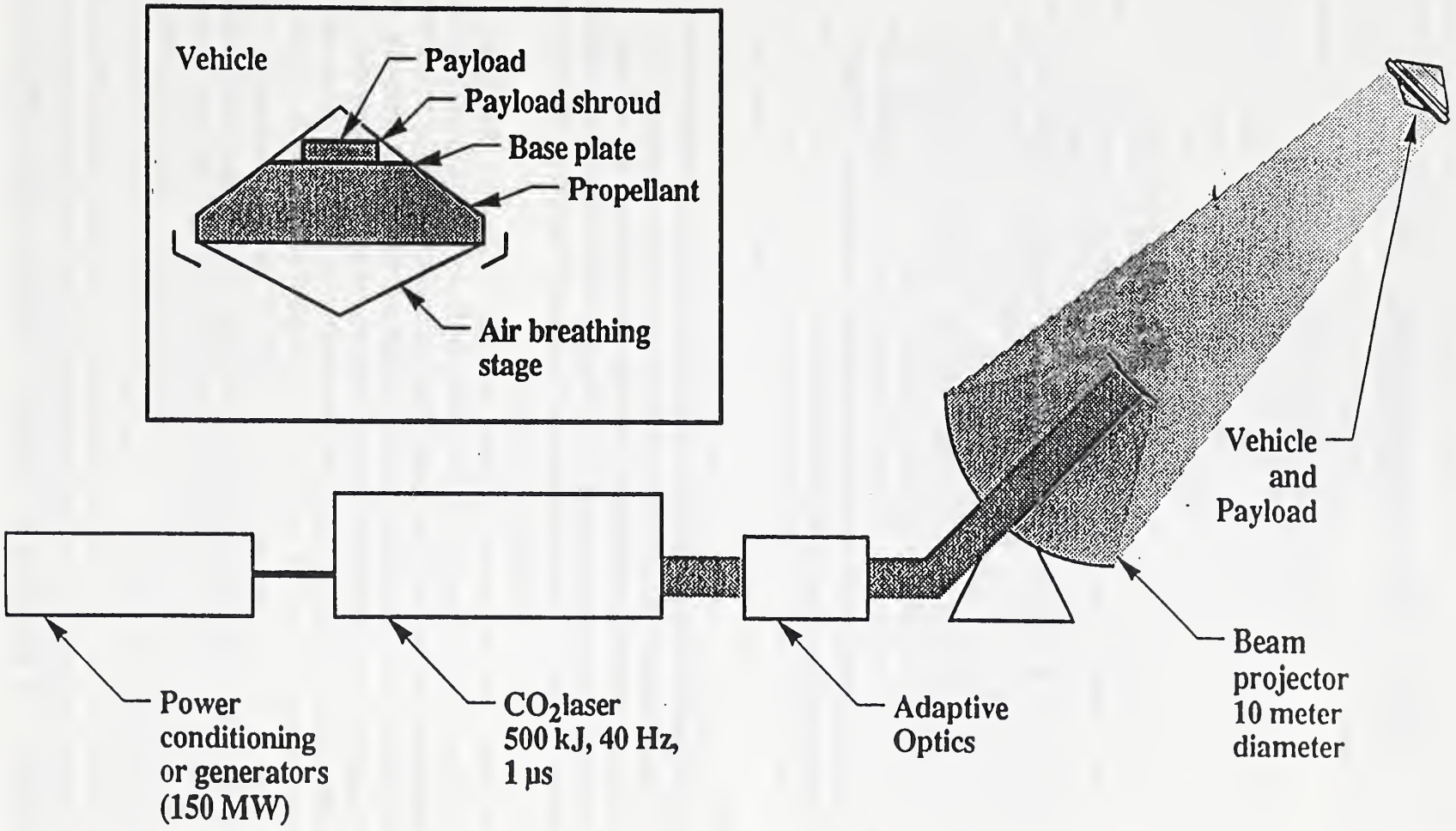

IIC 003 U 3425-002

Laser Propulsion and Possible Missions To Mars

Jordin T. Kare

Lawrence Livermore National Laboratory
Livermore, CA

ABSTRACT

Laser propulsion uses the energy of a large ground- or space-based laser to heat an inert propellant, producing high thrust at large specific impulse (500 - 2000 s) from a very simple thruster. Laser propulsion has until recently been considered largely for orbital transfer missions where high specific impulse and low thruster mass are critical; it remains a prime candidate for such missions. Recent developments, however, suggest that the major impact of laser propulsion will be in ground-to-orbit launching, where costs over an order of magnitude lower than those of proposed chemically-powered launch vehicles may be achievable within a decade. In this paper we summarize the likely capabilities of near-term laser propulsion, and discuss the capabilities -- and limits -- of laser propulsion as applied to possible missions to Mars.

I. Introduction

Laser propulsion systems use the energy of a high power laser beam to heat an inert propellant, producing thrust from the expansion of the propellant as in a chemical rocket. This separation of the energy source from the reaction mass allows the use of a much wider range of propellant materials and, subject to the limits of radiation losses, much higher exhaust temperatures and thus higher specific impulse. It also permits the use of very simple thrusters, and for many purposes simplicity is even more important than performance.

Laser propulsion was first proposed by Kantrowitz [1] in 1972, shortly after the advent of high power CO_2 lasers. Early proposals, however, invoked extremely large (gigawatt-scale) lasers to launch payloads from the surface of the Earth. These, and the related requirements for large telescopes and adaptive optics, were sufficiently far beyond the then state of the art that until recently laser propulsion has been viewed as a technology for orbital maneuvering only. Laser propulsion studies supported by NASA [2], DARPA, and the Air Force have concentrated on orbital maneuvering missions requiring high delta-vee but modest thrust levels corresponding to laser powers of order 10 MW or less. A 1984 study by JPL [3], for example, compared several possible space-based laser configurations (using very conservative technology outside of the laser itself) as an alternative for powering an Orbital Transfer Vehicle (OTV); their results indicated that even at the 1 MW level, such a laser system would be competitive with chemical or nuclear-electric OTV's for many mission models.

Laser propulsion can be done with either continuous (CW) or pulsed lasers. CW thrusters [4, 5] would resemble conventional liquid-fuel rocket engines, but with a single propellant, such as liquid hydrogen. The laser beam must enter the absorption chamber (analogous to a

*This work was performed under the auspices of the U.S. Department of Energy by Lawrence Livermore National Laboratory under contract No. W-7405-Eng-48.

combustion chamber) via a window (two-port design) or a reflective nozzle (single-port design) and is absorbed in a stable laser-supported plasma. Designs similar to solar-thermal rockets, which transfer energy to the propellant via a heat exchanger, are also possible. Pulsed laser thrusters can use a wider range of propellants, including solid materials. Since pulsed thrusters do not require an absorption chamber or a regenerative cooling system, very simple designs are possible. An excellent summary of work on laser propulsion up to 1984 is found in [6].

Recently, much progress has been made in the development of high power lasers, especially free electron lasers (FEL's) and in related technologies such as adaptive optics. This work, supported largely by the defense community, has led to the expectation that lasers (and optics) operating at a significant fraction of 1 GW average power will be demonstrated by the early 1990's. Both major FEL technologies, the induction linac FEL and the RF linac FEL, produce pulsed laser beams.

In the summer of 1986, a Workshop on Laser Propulsion was held at Lawrence Livermore National Laboratory [7]. The Workshop concluded that the technology needed for ground-to-orbit launch systems was within reach, and in early 1987, a program of research in laser propulsion was begun under the auspices of the SDIO. This Program has so far concentrated its efforts on a particularly simple variant of pulsed thruster that is compatible with the induction linac FEL in particular, and that offers great flexibility and the prospect of high performance at low cost: the double-pulse planar thruster.

In section II of this paper, we discuss the physics of the double-pulse thruster. In section III, Ground to Orbit Laser Launching, we describe a baseline launch system, using a 100 MW laser to launch 150 kg payloads, which could be built in the next 10 to 15 years. The capital and operating costs of this system are estimated in section IV, Launch Capacity and Cost.

Section V, Laser Propulsion for Missions to Mars, describes possible applications of the baseline launch system to missions beyond low Earth orbit. Section VI, Limits on Deep Space Propulsion, notes that expanding the baseline system to directly launch a Mars mission would be uneconomical; the best approach is to take advantage of the lowered cost to low orbit to build a more conventional vehicle. Finally, section VII gives a brief scenario for a Mars mission taking maximum advantage of near-term laser propulsion capabilities.

II. The Double-Pulse Planar Thruster

The double-pulse thruster was suggested originally by Reilly [8]. A prepulse, or metering pulse, evaporates a thin layer from the surface of a block of solid propellant. The resulting gas expands to some desired density, and then a separate power pulse heats it to high temperature by creating an absorbing plasma, or LSD wave, which propagates through the gas layer, as shown in figure 1.

As originally proposed, the double-pulse thruster would have used CO_2 laser pulses 10 to 20 microseconds long, and the resulting vehicle would have needed a skirt or nozzle a meter or more long to contain the expanding gas layer and generate thrust. However, in 1986 Kantrowitz [9] pointed out that with short (50 ns) FEL pulses, the expanding gas layer is so thin that expansion above a simple flat surface would be one-dimensional (except for narrow edge regions) and would generate thrust efficiently.

The planar thruster has additional advantages besides simplicity. Since the thrust is always normal to the thruster surface, independent of the direction of the laser beam, thrust can be

generated at a large (45 - 60 degree) angle to the beam. The double laser pulse provides many degrees of freedom (pulse shape, pulse spacing, ratio of energies), so that the thruster performance can be optimized and even adjusted, e.g., by varying the specific impulse in flight. A vehicle can be steered simply by varying the distribution of laser flux on the thruster base. Ideally, a complete launch vehicle can consist of nothing but solid propellant and payload, with all sensing and guidance functions performed from the ground. This "4-P" vehicle ("Let's leave everything on the ground except Payload, Propellant, and Photons. Period." — A. Kantrowitz, 1986), with a typical trajectory, is illustrated in Figure 2. The conical shape protects the sides of the vehicle from stray light, even when thrusting at an angle to the laser beam.

The performance of any laser propulsion thruster can be defined in terms of its effective specific impulse (or mean exhaust velocity) and a thruster efficiency η, defined as

$$\eta = \tfrac{1}{2}\dot{m}V_{exh}^2 / P_{laser}$$

(i.e. exhaust kinetic energy / laser energy). Based on initial computer modelling [10] and preliminary experimental results [11], we believe that efficiencies of 40% will be possible, with $I_{sp} >$ 800 seconds.

Because the double-pulse thruster is so simple, the main variable determining its performance is the composition of the propellant; the best propellants are likely to be complex composite materials. Some of the desirable properties of the propellant are:

Short absorption depth
: To minimize heating of the propellant block by the evaporation pulse.

Low heat of vaporization; low reflectivity (at the laser wavelength)
: To reduce the energy required in the evaporation pulse.

High heat of vaporization; high reflectivity (at other wavelengths)
: To minimize undesired evaporation ("dribbling" losses).

Low LSD-wave ignition threshold; low LSD-wave maintenance threshold
: To reduce the required laser flux in the main pulse.

High LSD-wave ignition threshold
: To prevent ignition of a plasma during the evaporation pulse, or during the main pulse away from the propellant surface.

Uniform ignition properties; closely spaced ignition sites
: To allow prompt formation of an LSD wave; delay or holes in the LSD wave will cause excessive dribbling losses.

Low dissociation energy and/or rapid chemical recombination
: To minimize the energy trapped in broken chemical bonds ("frozen flow") due to the rapid expansion of the exhaust gas.

Low mean atomic weight
: To allow high I_{sp} while keeping radiation losses small.

Mechanical strength

Low toxicity and flammability

Low cost

Obviously, some of these are contradictory, but by clever invention, undesirable compromises can be avoided. As an example, Reilly [12] has proposed the Tuned Ignition Array, using 5 micron wide conductive strips embedded in a dielectric propellant as ignition sites. These strips would act as resonant antennas at the laser wavelength, and would be selective in both wavelength and polarization, so that the LSD-wave ignition threshold could be varied between (and even within) pulses.

Current likely candidates for propellants include water ice, plastics, various C-H-O compounds, and light metal hydrides, the last having very low dissociation energies and thus low frozen flow losses. All of these would be combined with additives to control their absorption, ignition, and mechanical properties. There is extensive room for invention in propellant design, and much of the current effort of the SDIO Laser Propulsion Program is devoted to creating, testing, and characterizing such complex propellants.

III. Ground-to-Orbit Laser Launching

Table 1 lists the properties of a hypothetical 100 MW laser launch system, which we take as a reference in the following discussion. Smaller systems would be feasible, although practical considerations of vehicle design (especially in terms of aerodynamics) probably place a lower limit on useful launchers of a few tens of megawatts. There is no obvious upper limit to the launcher size; the cost and complexity would scale linearly at worst (the worst case being to simply build a second complete launch system adjacent to the first) while the payload capacity grows at least linearly with laser power.

The reference system includes a laser, which might be a single unit or a modular system of laser amplifiers phase locked to produce a single beam. Although an induction linac FEL is the laser of choice, other lasers, notably electric-discharge CO_2 lasers, could be used. The nominal laser wavelength is 10 microns, although many wavelengths between 1 and 10 microns could be used. At shorter wavelengths, correction for atmospheric turbulence becomes very difficult, and stimulated Raman scattering limits the laser flux that can be transmitted through the atmosphere. Although the optics needed become smaller, the flux required to initiate and maintain an LSD wave increases at short wavelengths, partly cancelling this gain; the optics must also be of higher quality. Long wavelengths are thus preferred; 10 microns is a somewhat arbitrary limit set by the wide availability of optics and coatings for the CO_2 laser wavelength of 10.6 microns, and by the fact that at much longer wavelengths the beam projector becomes excessively large.

The beam director for the reference system is a 10 meter diameter telescope. The Keck Ten-Meter Telescope, now under construction in Hawaii [13], demonstrates that such optics are feasible, although a beam director might use a very different geometry than an astronomical telescope. The specified range of 1000 km (for focusing the laser beam onto a 1 meter diameter vehicle) implies that the optical system will be capable of correcting for atmospheric turbulence and thermal blooming, producing a nearly diffraction limited beam. This is not trivial but, given the long wavelength and a cooperative vehicle, it appears to be well within the state of the art for adaptive optics systems using piezoelectrically driven "rubber mirrors".

The payload of this system is approximately 150 kg, based on fairly detailed trajectory simulations [14]. To first order, this payload size scales linearly with laser power, thruster efficiency, and range (a function of telescope size and other factors); a conservative rule of thumb is:

$$\frac{\text{Payload}}{1\text{kg}} = 2.5\eta \left(\frac{P_{laser}}{1\text{MW}}\right)\left(\frac{\text{Range}}{1000\text{km}}\right)$$

The trajectory sketched in figure 2 is typical for launches to LEO. The reference vehicle would be launched from the mountaintop launch site (chosen both to minimize atmospheric absorption of the laser and aerodynamic drag on the vehicle) by some launch mechanism such as a compressed-air catapult. It would climb slowly through the atmosphere, possibly using an air-breathing version of the planar thruster for the first few km. Once above the lower atmosphere, it would climb vertically to approximately 100 km, then "turn over" and accelerate downrange at an angle to the laser beam. At a range of approximately 1000 km, and an altitude of approximately 500 km, the vehicle would reach orbital velocity and enter a near-circular orbit. The peak acceleration of the vehicle would be about 5 gees, and τ_{launch}, the total time to orbit, would be about 750 seconds. (The time to orbit varies considerably with the specific impulse used, but reasonable values are 10 to 15 minutes.)

IV. Launch Capacity and Cost

This last number is, of course, the key to the value of laser propulsion. Although the individual payload size is small, the laser can operate essentially continuously; at one launch every 15 minutes, even our reference system launches 600 kg per hour, or 14,400 kg per day. Of course, the system would not be able to operate 100% of the time; maintenance, weather, limited launch windows for rendezvous, and other factors would restrict the operating times. But even at an overall duty cycle of 20%, operating less than 5 hours per day, the reference system can put over one million kilograms, or forty Space Shuttle payloads, in orbit every year.

The estimated capital cost of this reference system is $2 billion, or somewhat less than a single Shuttle orbiter. Half of this pays for the laser at $10/watt, which is conservative for large CO_2 lasers; the costs of large FEL's is uncertain. The remainder pays for the beam director, adaptive optics, tracking, launch site, etc. The cost of these can be estimated by comparison with the Keck Ten-meter Telescope, which is comparable to the beam director. The expected cost of the Keck telescope, including the observatory facility, is under $100 million.

The operating costs for the launch facility should be low; an appropriate reference is not a spacecraft, or even an aircraft, but a large particle accelerator. Operating costs for accelerators are typically 20% of capital cost per year, or $400 million per year for our reference system [15]. The cost per kilogram launched is thus less than $400 (about $180/lb), even for a 20% duty cycle. Propellant and power costs would be a fraction of this. Even the complex propellants under consideration would be inexpensive compared to advanced chemical fuels, as they would be inert and require no special handling; some possibilities would be cheap even compared to kerosene and liquid oxygen. With laser efficiencies of 20% (estimated to be well within reach of FEL's; CO_2 lasers are about 15% efficient) the overall "wallplug to orbit" energy efficiency of the system is greater than 1%, and the electricity needed to put 1 kg in orbit is less than 900 kWH, worth about $20 to $50 depending on rates. The total cost would therefore be below $500/kg ($220/lb). At a duty cycle of approximately 50%, the cost would fall below the magic number of $100/lb. More generally, once the facility is built and operating, the incremental cost of launching each additional payload is likely to be $100/lb. or less, until the system capacity is reached.

V. Laser Propulsion for Missions to Mars

The reference launch system described above is typical of laser propulsion systems that could be built in the next 10 to 20 years. Clearly, if such a system were built, the economics of spaceflight would change drastically. Fuels, consumables, structural materials, and even complex items like electronic subassemblies or optical mirror segments could be placed in orbit at

relatively low cost, provided they could be packaged within the weight and size limits of the launcher. The vibration and acceleration such payloads would experience would be comparable to that seen by Shuttle or expendable rocket payloads. The cost advantage of laser propulsion would be a strong incentive to break larger assemblies into modular units that could be assembled in space, either by astronauts (who would themselves cost less to maintain in space) or by robots or remote manipulator systems.

Given the small size of such units, and the cheapness and promptness with which a failed part or assembly could be replaced, the extreme reliability and performance constraints now placed on space hardware could be relaxed. Redundancy, modularity, robustness, and suitability for in-space repair would become the design criteria even for systems (such as Mars mission hardware) which would be out of reach of Earth for long periods, as spare parts would no longer be intolerably expensive to carry.

In addition to its effect on the economics and logistics of spaceflight in general, laser propulsion could have direct effects on interplanetary missions, and particularly on a manned mission to Mars. The simplest of these would be in launching individual payloads into interplanetary trajectories. Because of the high I_{sp} of laser propulsion thrusters, the penalty for launching payloads to escape velocity rather than Earth orbital velocity is modest. Provided the beam director is large enough, the payload to escape can nearly equal the payload to orbit, as the vehicle can stay in the laser beam longer without going over the laser's horizon or exceeding the desired velocity. Each launch simply takes a few minutes longer. Thus, our reference facility, with a slightly increased mirror size, can launch payloads massing up to 100 kg payloads directly to Mars. (Note that we have not done detailed trajectory calculations for Mars mission trajectories, so this and following mass numbers are strictly order-of-magnitude estimates.)

This capability can be used in at least two ways. First, a wide variety of miniaturized probes could be launched to assist in the preliminary exploration of Mars. Second, small payloads could be launched ahead of a manned mission to serve as "supply depots" along the way. This function would be limited by the need for the small laser-launched packages to rendezvous with the main mission ship; extremely compact on board thrusters and guidance would be needed.

A more general extended use of a laser launch facility is to accelerate vehicles already in orbit. Our reference system can produce thrust of approximately 10^4 newtons at I_{sp} = 800 s. Each pass over the laser can thus provide a total impulse of order 10^6 newton-seconds (assuming that the vehicle is accelerated for ≈100 seconds). If the laser is on the equator, and the vehicle is in equatorial orbit, this push can be given once per orbit; for inclined orbits, the push occurs at most twice per day. Thus vehicles heavier than a few hundred kilograms require many orbits to gain significant velocity, and cannot effectively be given escape velocity; the orbital period just before escape becomes very long.

This situation can be improved by equipping orbiting vehicles with a collecting mirror or concentrator. Such a concentrator must meet several criteria, including handling the laser power without overheating and accepting beams from a wide range of angles. A sample design for a concentrator designed expressly for a pulsed laser thruster in orbit has been presented by Chapman and Reilly [17].

With a 10 to 20 meter diameter concentrator, a vehicle can be powered by the reference system over a typical range of 10,000 km. The impulse delivered in a single pass over the laser is increased to over 10^7 N-s, or 1 km/s delta-vee for a 1000 kg vehicle, provided the vehicle stays

above the laser's horizon for the necessary time. This constraint is removed if one or more relay mirrors are available in appropriate orbits, typically at altitudes of a few thousand km. Although such mirrors would need to be large (10 meters being typical) to give adequate range at long laser wavelengths, the optical requirements would be reasonable because of the same long wavelengths. Again, a segmented mirror design (with segments lofted by the laser launcher) would be appropriate. With relay mirrors, the reference system could deliver thrust to any vehicle in near-Earth space at almost any time, producing several times 10^8 N-s of impulse per day (all at I_{sp}'s of 800 seconds or more). This would, for example, move a 10^4 kg vehicle from LEO to geosynchronous orbit in about a day; heavier vehicles would take proportionately longer. For the reference system's laser to provide useful thrust in geosynchronous orbit, it is sufficient to increase the diameter of the optics and vehicle concentrators to approximately 20 meters. However, still longer ranges would require exorbitantly large optics, or a major change in the system design, e.g., to a shorter wavelength laser.

VI. Limits on Deep Space Propulsion

An actual Mars mission would be likely to require fairly heavy vehicles, 10^5 kg or larger, and they would need to leave near-Earth space with considerable (several km/s) velocity. Because of this finite terminal velocity, the total time spent within range of the laser is limited. The reference system (with 20 meter mirrors and 20 meter vehicle concentrator) could launch only a few thousand kg at a time to Mars; the concentrator would probably be a large part of this. This mass limit can be increased by increasing the laser range, or by increasing the average laser power. As noted, increasing the range rapidly becomes difficult, although up to a point the vehicle concentrator can be made larger at modest cost. As the possible mass of the Mars-bound vehicle increases, it can afford to carry a larger concentrator; this means, for example, that in a simple model, the limiting mass increases as $P_{laser}^{3/2}$, rather than linearly.

However, the fundamental cost advantage of laser propulsion is based on its ability to operate steadily, with a high duty cycle. Unless other space traffic requires a higher power, longer range laser system, a Mars mission alone would be unlikely to justify any substantial investment. One must bear in mind that, given a laser capable of launching material into orbit for \$100/lb, even relatively crude technologies may become inexpensive: 200,000 kg of kerosene and liquid oxygen would suffice to launch a substantial Mars mission from Earth orbit, if it could be placed there at a cost of a few tens of millions of dollars. Also unlike laser propulsion, storable chemical propellants would be useful for entering Mars orbit, and could even power Mars landers and surface vehicles.

If near-Earth space traffic were sufficient to justify a larger laser launch facility than our reference facility, this picture might change. A 1 GW laser launch facility is sufficient to launch payloads in excess of 1000 kg from the ground; if combined with a larger beam projector, the payload could be several thousand kg. (In passing, we note that even larger payloads could be launched to suborbital velocities and picked up by one of several classes of orbital assist devices such as rotating tethers [18]. Orbital constraints would limit such launches to one or two per day, but this would still allow exceptional payloads considerably larger than the normal maximum. Such a facility could also conceivably be man-rated; the payload is comparable to the mass of a Mercury capsule, and the pipelined nature of laser launching would allow a large number ($> 10^3$) of unmanned test launches.) Such a large launch facility could directly launch 10^5 kg vehicles (with 100 to 200 meter concentrators) into Mars-bound trajectories.

Similarly, increased traffic to the Moon might warrant use of a shorter-wavelength laser and/or larger mirrors to allow laser propulsion to operate at lunar distances. This would increase the system range (and the Mars vehicle mass) another factor of 10. However, the capital cost of such large systems would be in excess of 10 billion dollars, and substantial increases in space traffic would be needed to justify such developments.

VII. Conclusion: A Scenario

Assuming laser propulsion is available only on the scale of our reference system available, then one can contemplate the following scenario: A Mars mission vehicle would be assembled in orbit, from a core of large sections lofted by expendable rockets or by the Shuttle. As much of the vehicle mass as possible, though, from hull plates and shielding to computer assemblies, would be brought up by laser in sections massing no more than a few hundred kilograms. The finished vehicle would include large disposable tanks for storable chemical propellants, and a small chemical thruster.

The fuel tanks would be filled, over a period of weeks, with propellants brought up from Earth, also by laser. (A lunar oxygen plant might or might not be operating, depending, in part, on whether a laser launch facility has been set up on the Moon). A large block of laser propellant "ice" would also be attached to the back of the vehicle, along with a standard laser OTV concentrator.

This composite vehicle would be boosted into a highly elliptical intermediate orbit over the course of a few weeks. This orbit would have nearly Earth-escape energy, and would be chosen to minimize the delta-vee needed to enter a trajectory to Mars. The crew (and a few radiation-sensitive components) would arrive in LEO via Shuttle, and would rendezvous with the mission vehicle in a laser-powered OTV which, being quite a bit lighter than the Mars vehicle, could match orbits with it in less than a day.

With crew on board, the Mars mission vehicle would ignite its chemical thruster for its last perigee passage, converting the elliptical orbit to a hyperbolic one. While en route to Mars, it would partially refuel by collecting a number of 1000-kg fuel tanks laser-launched from Earth orbit ahead of time on intersecting trajectories. After a comparatively short transit time (the extra delta-vee needed for a faster trajectory costs only a few million dollars) the vehicle would arrive at Mars. Data from a large number of small laser-launched probes, in orbit and on the surface, would be available in real time to help plan the exploration of the planet. The vehicle would use its chemical rocket to enter and, after a productive visit, leave Mars orbit. Finally, after additional refuelling on the trip home, the vehicle would re-enter an elliptical Earth orbit, possibly with the aid of aerobraking. A new laser propellant block would be brought up to rendezvous with the vehicle, and it would finally be parked in a convenient orbit for possible re-use — assuming, of course, that the new gigawatt laser system does not render it obsolete too soon.

References

1. A. Kantrowitz, "Propulsion to Orbit by Ground-Based Lasers, " *Astronautics and Aeronautics*, Vol. 10, May 1972, pp. 74-76.
2. L. W. Jones and D. R. Keefer, "NASA's Laser-Propulsion Project," *Astronautics and Aeronautics*, Vol. 20, Sept. 1982, pp. 66-73.
3. R. H. Frisbee, J. C. Horvath, and J. C. Sercel, "Space-Based Laser Propulsion for Orbital Transfer", JPL D-1919, Jet Propulsion Laboratory, December 1984.
4. H. Krier, J. Mazumder, T. J. Rockstroh, T. D. Bender, and R. J. Glumb, "CW Laser Gas Heating by Laser-Sustained Plasmas in Flowing Argon," *AIAA J*, Vol. 24, p.1656, Sept. 1986.
5. D. Keefer, R. Welle, and C. Peters, "Power Absorption Processes in Laser Sustained Argon Plasmas," AIAA Paper 85-1552, AIAA 17th Plasma Dynamics Conference, July, 1985.
6. R. J. Glumb and H. Krier, "Concepts and Status of Laser-Supported Rocket Propulsion," *Journal of Spacecraft and Rockets*, January, 1984, pp. 70-79.
7. —, *Proceedings of the 1986 SDIO/DARPA Workshop on Laser Propulsion*, J. T. Kare, ed., Lawrence Livermore National Laboratory CONF-860778, Vol. I, November, 1986.
8. P. K. Chapman, D. H. Douglas-Hamilton, and D. A. Reilly, "Investigation of Laser Propulsion," Vols. I and II, Avco Everett Research Laboratory, DARPA Order 3138, Nov. 1977.
9. A. Kantrowitz, "Laser Propulsion To Earth Orbit: Has Its Time Come?", *Proceedings of the 1986 SDIO/DARPA Workshop on Laser Propulsion*, J. T. Kare, Ed., Lawrence Livermore National Laboratory CONF-860778, Vol. II, April 1987.
10. R. A. Hyde, "1-D Modelling of a Two-pulse LSD Thruster,", *Proceedings of the 1986 SDIO/DARPA Workshop on Laser Propulsion*, J. T. Kare, Ed., Lawrence Livermore National Laboratory CONF-860778, Vol. II, April 1987.
11. Efficiencies of order 10% have been demonstrated by Spectra Technology (M. Hale, private communication) using double pulses on polyethylene, and by Physical Sciences, Inc. (C. Rollins, private communication) using double pulses on glass and single pulses on carbon composite materials. We anticipate improvements of at least twofold through adjustment of the laser pulse energies and pulse shape, and additional improvement through optimization of the propellant material and structure.
12. D. Reilly, "Advanced Propellant for Laser Propulsion", to be published in *Proceedings of the 1987 SDIO Workshop on Laser Propulsion*, in press.
13. J. E. Nelson, T. S. Mast, and S. M. Faber, eds., "The Design of the Keck Observatory and Telescope", Keck Observatory Report No. 90, January 1985.
14. J. T. Kare, "Trajectory Simulation for Laser Launching,", *Proceedings of the 1986 SDIO/DARPA Workshop on Laser Propulsion*, J. T. Kare, Ed., Lawrence Livermore National Laboratory CONF-860778, Vol. II, April 1987.
15. A. Kantrowitz, private communication.
16. P. K. Chapman and D. A. Reilly, "Orbital Maneuvering via Pulsed Laser Propulsion", *Proceedings of the 1987 SDIO Workshop on Laser Propulsion*, in press.
17. P. K. Chapman, "Cable Connected Satellites for Inter-Orbital Transfer", NASA Lewis Advanced Space Propulsion Award Prize Essay, 1981, available from author.

Figure 1: Double-Pulse LSD-Wave* Thrust Cycle

A) "Metering" pulse evaporates a thin layer of propellant
$\tau_1 = 2 - 5\ \mu s$

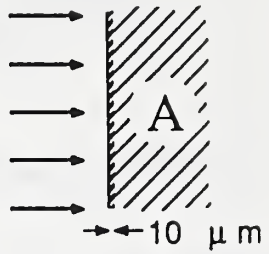

B) Gas expands to the desired density
$\tau_{1\text{-}2} = 0 - 5 \mu s$

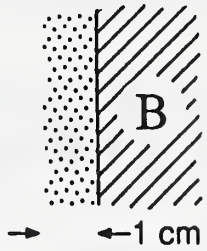

C) Main pulse passes through gas,
forms plasma at surface τ_{ign} = few ns

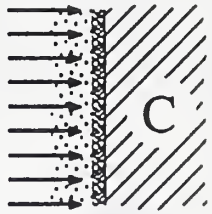

D) Plasma absorbs beam by inverse brems-strahlung; absorbing layer (LSD wave) propagates through gas $\tau_2 = 1 \mu s$

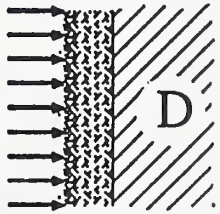

E) Uniformly hot gas expands in 1-D,
producing thrust $\tau_{exp} = 3 - 10 \mu s$

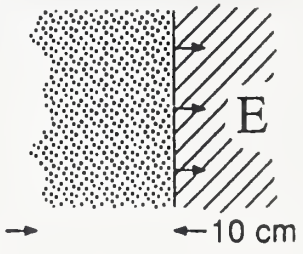

F) Exhaust dissipates; cycle repeats at 100 Hz - few kHz

Figure 2: Laser Propelled Vehicle and Trajectory

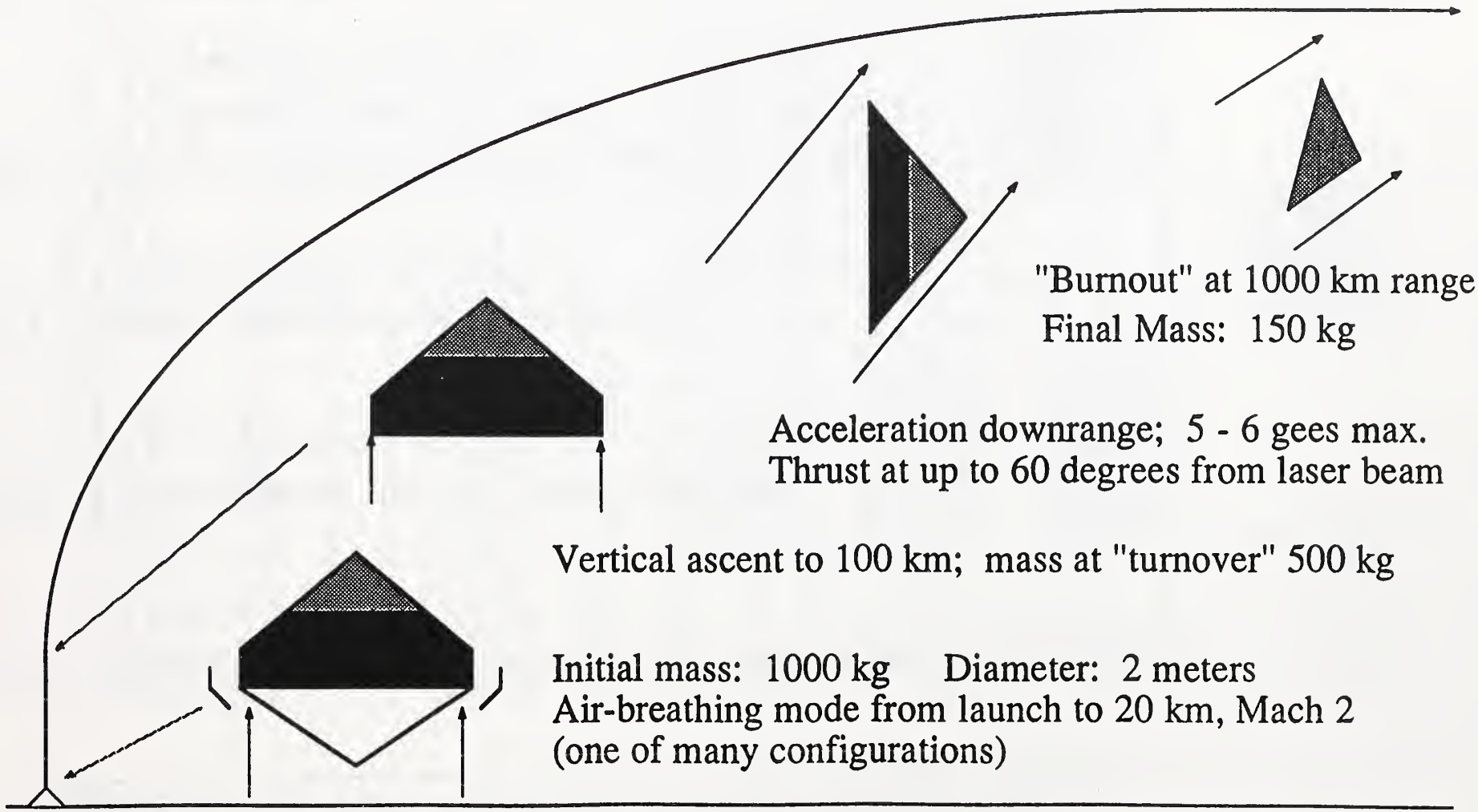
"Burnout" at 1000 km range
Final Mass: 150 kg
Acceleration downrange; 5 - 6 gees max.
Thrust at up to 60 degrees from laser beam
Vertical ascent to 100 km; mass at "turnover" 500 kg
Initial mass: 1000 kg Diameter: 2 meters
Air-breathing mode from launch to 20 km, Mach 2
(one of many configurations)

Table 1: Typical Characteristics of a 100 MW Laser Launch System

Laser average power	100 MW
Laser wavelength	10 μm
Laser pulse energy	1 MJ
Laser pulse width	1 μs
Beam director diameter	10 meters
Thruster specific impulse	800 seconds
Thruster efficiency	40%
Vehicle initial mass	1000 kg
(may include up to 200 kg of structure for air-breathing mode)	
Vehicle mass at burnout (Payload)	150 kg
Vehicle diameter	2 meters
Range at burnout	1000 km
Altitude at burnout	500 km
Velocity at burnout	7.8 km/second
Maximum acceleration	6 gees
Time to reach orbit	750 seconds

The Ram Accelerator as a Space Cargo Launcher

A. Hertzberg and A.P. Bruckner
Aerospace & Energetics Research Program
University of Washington
Seattle, WA 98195

ABSTRACT

The University of Washington has developed a new accelerator concept whereby chemical energy may be efficiently used to accelerate projectiles from velocities of approximately 600 m/sec to as high as 12 km/sec. This approach, called the "ram accelerator," lends itself very well to scaling, so that it is anticipated that payloads of several thousand kilograms may be fired directly into space. In view of the potential of this approach, the University initiated a study of this new accelerator technique as an economical direct launch system to lift the raw materials and resupply elements needed for the envisioned large-scale space station systems of the future. This technology is expected to provide an important supplement to enhance the effectiveness of conventional space transportation systems. The results of this study have proved extremely encouraging and indicate that payload launch costs between $100/kg and $500/kg are feasible.

PREFACE

The high cost of launch systems capable of carrying the raw materials and consumables required to construct and maintain a large space system infrastructure remains a serious barrier to the full exploration of our solar system. Much of this materiél, such as the components of large space structures, the various raw materials for space manufacturing, and hydrogen, oxygen, and other supply elements are capable of withstanding high launching stress. This stress insensitivity has attracted the attention of scientists and engineers over the years, and various mass launchers have been examined as methods of reducing prohibitively high launch costs. These have ranged from hypervelocity two-stage gas guns to various electrical accelerators. The relatively low efficiency of the former as well as the difficulty of controlling the acceleration level and the formidable problem of dealing with the management of the large pulsed electric loads of the latter have proved to be serious barriers to their implementation.

At the University of Washington a new method of efficiently accelerating projectiles to as high as 12 km/sec using chemical energy has been developed. Analytical and experimental studies carried out at the University since mid-1983 have led to a basic engineering understanding of this promising new technique, called the "ram accelerator." The basic principle involves an energy release process that travels with the projectile; unlike a rocket however, with this new concept there is no propellant on board the projectile. The projectile, which resembles the centerbody of a ramjet, travels through a stationary tube filled with a premixed gaseous fuel and oxidizer mixture which burns on or behind the projectile, establishing a pressure field which results in forward thrust. The ballistic efficiency remains high up to 12 km/sec, with an acceleration that can be maintained at a nearly constant level, and the concept can be scaled to projectile masses of several metric tons.

Preliminary studies indicated that the issues of feasibility can be addressed without extending current technology. The key questions then become the economic viability and the ease with which such a system might be implemented. Therefore, the main thrust of this effort was directed towards carrying out an engineering analysis in a conservative manner to establish the payload cost to orbit of an entire system. While it is easy to show that propellant costs are negligible, the nature of the cargo containers and their operational characteristics were examined so as to assure a reasonable prospect for an efficient launch system.

These problems were examined by the University of Washington (UW) and the United Technologies Research Center (UTRC) in a joint effort designed to make a systems analysis more meaningful. This work was carried out in a joint program funded by NASA under Grant No. NAG 1-746 in a brief program which was derived from a collaborative effort by the Univeresity of Washington. The system's definition lent itself to a number of possible models. In the early phases of program definition, one of the models was selected by the UW and used as the baseline for a point design to act as a guide for further, detailed engineering studies and economic analysis. Limitations on time required the UTRC group to stabilize early in the program on a specific scenario in order to examine the system parameters. While not as refined as the later design developed by the UW, particularly with respect to orbit circularization, the influence of system parameters was demonstrated. Due to the later findings of the UW, these findings by the UTRC group are considered to be conservative. Nonetheless, the UTRC study did report launch costs below $500 per kilogram. The more important results are reported below:

1. By proper scaling, earth orbit launch cost of $100-500/kg can be achieved. In view of recent studies at the UW concerning the advantages of an aerobraking reentry system in reducing the on-board propellant mass requirements for orbit circularization, this launch cost appears conservative.

2. Improving the ballistic coefficient, either by slender cone heat shield configurations or by increasing the mass of the vehicle, reduces on-board propellant requirements and increases the payload mass fraction, thus reducing costs.

3. The existing state of engineering art is adequate both for launch vehicle and launch facility design.

The authors feel that the results of this preliminary systems analysis are encouraging. Indeed, based on new experimental findings at the UW, which have shown that higher than anticipated ballistic efficiencies are achievable in the acceleration process, further reductions in payload costs may be possible. When operated in parallel with a conventional space transportation system, a ram accelerator facility will expand the capability of the system manyfold. The authors therefore feel that this study should be the precursor of more detailed systems analyses utilizing the latest experimental and theoretical data generated at the University of Washington, as well as more sophisticated models of foreseeable orbital and payload requirements.

For the convenience of the reader, the following section, Part 1, is a review of the status of the ram accelerator experiments and theory as carried out at the University of Washington under funding from the Air Force, ONR, and the Olin Corporation. This report identifies high efficiency operation up to 2.5 km/sec and has been used to demonstrate the various modes of operation that will be necessary to reach 10 km/sec. A computational fluid dynamics code with full chemistry has been used to demonstrate that efficient acceleration up to at least 9 km/sec can be achieved. Part 2 is adapted from an earlier report to NASA (Grant No. NAG 1-746) which presents a University study of the engineering problems associated with a ram accelerator space cargo launcher. The results of these studies have been very favorable from both the engineering technology standpoint and the capability of this device to achieve the level of performance necessary. At the present time, these studies are being continued with Air Force and NASA funds (USAF Contract No. FO8635-89-C-0196 and NASA Grant No. NAG 3-1061).

PART 1

EXPERIMENTAL AND THEORETICAL INVESTIGATIONS OF HIGH VELOCITY RAM ACCELERATOR MODES

A.P. Bruckner, A. Hertzberg, A.E. Kull, E.A. Burnham,
C. Knowlen, and S. Yungster

Aerospace and Energetics Research Program
University of Washington, FL-10
Seattle, Washington 98195

ABSTRACT

Recent high-velocity experiments with a ram accelerator are presented. The ram accelerator is a ramjet-in-tube projectile accelerator whose principle of operation is similar to that of a supersonic airbreathing ramjet. The projectile resembles the centerbody of a ramjet and travels through a stationary tube filled with a premixed gaseous fuel and oxidizer mixture. The tube acts as the outer cowling of the ramjet, and the combustion process travels with the projectile, generating a pressure field which produces forward thrust on the projectile. Different modes of combustion have been explored for accelerating projectiles of nearly identical geometry. Subsonic, thermally choked combustion theoretically allows a projectile to be accelerated to the Chapman-Jouguet (C-J) detonation speed of a particular gas mixture. In the superdetonative regime the same projectile is accelerated while always traveling faster than the detonation speed, and in the transdetonative regime (85-115% of detonation speed) the same projectile may transit smoothly from a subsonic to a superdetonative combustion mode. This paper examines operation in these three regimes of flow up to velocities approaching 2500 m/s in a 12.2 m long, 38 mm bore ram accelerator, using projectiles of 70 gm mass. Experimental evidence of acceleration in the transdetonative and superdetonative regimes is introduced. Also presented are the results of a computational fluid dynamics (CFD) code being developed for studying the flow, combustion, and performance of the ram accelerator, particularly in the superdetonative regime. The code solves the 2D, axisymmetric Euler equations with coupled chemical nonequilibrium processes, using a shock-capturing technique, and gives theoretical results which show that efficient acceleration of projectiles is possible through velocities as high as 9 km/sec.

INTRODUCTION

At the University of Washington experimental and theoretical research is being carried out on the acceleration of projectiles to ultrahigh velocities using a ramjet-in-tube concept called the "ram accelerator." [1-10] The projectile resembles the centerbody of a conventional ramjet and is accelerated by combustion through a stationary tube filled with a reactive gas mixture (see Figs. 1 and 2). There is no propellant on board the projectile. The pressure, composition, chemical energy density, and speed of sound of the mixture can be controlled to optimize the ballistic efficiency (defined here as the ratio of the rate of change of kinetic energy of the projectile to the rate of expenditure of chemical energy). The concept has the potential for a number of applications, such as hypervelocity impact studies,[11] direct launch to orbit of acceleration-insensitive payloads [12,13] and hypersonic testing.

Several modes of ram accelerator operation, which span the velocity range of 0.7-12 km/sec, have been proposed [1,2]. These include, among others, a thermally choked subsonic combustion mode, shown in Fig. 1, and two oblique detonation modes, one of which is shown in Fig. 2. The thermally choked subsonic combustion mode has been extensively studied experimentally by the authors,[1-8] and has attained velocities in excess of 2500 m/sec with 70 gm projectiles in a 12.2 m long 38 mm bore accelerator tube. In the oblique detonation modes the gasdynamic principles of the ram accelerator are similar to those of the Oblique Detonation Wave Engine (ODWE),[14,15] which has been proposed as an alternative to the scramjet engine for propelling hypersonic airbreathing vehicles such as the National Aerospace Plane (NASP).

To operate in the oblique detonation modes the projectile must fly at superdetonative speeds, i.e., speeds above the local Chapman-Jouguet (C-J) detonation speed of the gas mixture. The cone angle of the nose, the projectile velocity, and the speed of sound of the mixture are selected so that the first conical shock does not initiate combustion, but the reflected shock does. In operation the reflected shock becomes an oblique detonation wave. Theoretical studies by the authors and their colleagues have indicated that by judicious selection of gas mixtures the ram

accelerator will operate superdetonatively in the velocity range 2-12 km/sec. [4] In this paper we present experimental confirmation of superdetonative ram accelerator operation in the velocity range 2000-2500 m/sec, in an ethylene-based propellant mixture having a C-J detonation speed of 1650 m/sec.

In addition, it has been experimentally observed that while operating in the subdetonative regime, at velocities greater than 85% of C-J speed, the projectile often accelerates at a higher rate than is predicted by theoretical models for subsonic, thermally choked combustion. Further experiments have shown that in this transdetonative regime (85-115% of C-J speed), the projectile can accelerate smoothly from subdetonative to superdetonative speeds in a single gas mixture. These results may have interesting implications for any ramjet engine which must operate over a wide range of Mach numbers.

EXPERIMENTAL FACILITY

The ram accelerator facility (Fig. 3) consists of a light gas gun, ram accelerator section, final dump tank and projectile decelerator. The 38 mm bore, single-stage light gas gun is capable of accelerating the sabot and projectile combination (typical combined mass ~60-100 gm) to speeds up to approximately 1350 m/s. The muzzle of the gun is connected to a perforated-wall tube that passes through an evacuated tank which serves as a dump for the helium drive gas.

The ram accelerator section consists of seven steel tubes with a bore of 38 mm, an O.D. of 100 mm and an overall length of 12.2 m. There are a total of 32 pairs of diametrically opposed instrumentation ports disposed at 28 regular intervals along the accelerator tube. At four axial stations there are two pairs of opposing ports at right angles to each other, permitting the simultaneous use of four transducers. Piezoelectric pressure transducers are located at each of up to 20 observation ports. The remaining ports are used to mount electromagnetic velocity transducers (copper wire coiled around a lexan core) and fiber-optic light guides. A 20-channel, 1 MHz digital data acquisition system (DAS) is used to process the data. Multiplexing permits processing the 50 separate input signals currently being monitored.

The ram accelerator tube is designed to operate at propellant fill pressures up to 50 atm. Thin Mylar diaphragms are used to close off each end and to separate sections of the tube filled with different propellant mixtures. The fuel, oxidizer, and diluent gases are metered using sonic orifices, combined in a mixing chamber and directed to the appropriate section of the ram accelerator tube.

The end of the accelerator tube is connected by a 0.76 m long drift tube of equal bore to a 2.4 m long evacuated dump tank, where the projectile flies free. The tank has a pair of 25 cm dia. viewing ports for spark photography and two pairs of smaller ports for a two-beam laser velocity measuring system (Fig. 3). The free-flying projectile is brought to a stop in tightly packed rug remnants in an 18 cm I.D. x 1.8 m long tube attached to the far end of the dump tank.

Projectile Configuration

The basic projectile configuration that has been used in the majority of the experimental work to date is illustrated in Fig. 4. The projectile is fabricated from magnesium in two separate units: the nose cone and the body with integral fins. The nose and body are hollow. The fins serve only to center the projectile in the tube and the octagonal cross section of the body is simply a machining convenience. At the threaded joint between the nose and body is sandwiched a thin sheet of flexible magnetic material. A second magnet is affixed to the interior of the projectile at its base. These magnets interact with the electromagnetic transducers, providing time of flight data

from which the velocity history of the projectile can be determined. The projectile has a maximum diameter of 28.9 mm. In the 38 mm bore tube the resulting diffuser has a flow area ratio of 2.37.

Two variations of the basic projectile configuration have been experimented with extensively and are referred to in Fig. 4 as type A and type B. The differences between the two projectile geometries used lie in the angle of the nose (10° and 12.5°) and the length of the body (71 mm and 84 mm). The longer body is used with the 10° nose. The masses of the projectiles used have been in the range of 45 to 70 gm, depending on the external and internal configurations. The lexan launching sabot has a mass of 13 gm.

EXPERIMENTAL RESULTS

Thermally Choked Mode

Figure 5 illustrates typical transducer outputs obtained in the thermally choked combustion mode (subdetonative regime) in a tube segment containing $3.5CH_4 + 2O_2 + 6.5He$ at 25 atm. The projectile velocity and Mach number are 2020 m/s and 3.7, respectively. Time is measured from the instant of data acquisition system triggering, and pressure is measured in atmospheres. The pressure (middle) trace is typical of the thermally choked mode. The first pressure pulse is generated by the oblique shock system in the projectile diffuser section. There then follows a series of pulses which increase the pressure to a peak of approximately 430 atm, after which the pressure decays. The increase in pressure after the initial oblique shocks represents the normal shock, which is assumed to consist of a complex system of oblique and normal shocks similar to that observed in supersonic flow in long ducts. [16] The flow entering the combustion zone is subsonic. The decay in pressure following the peak is due to subsonic heat addition accelerating the flow to choking and the subsequent nonsteady expansion of the combustion products behind the choking point.

The upper trace in Fig. 5 displays the output of an electromagnetic transducer located at the same axial station as the pressure transducer. The zero crossing of the first signal identifies the passage by the sensor of the annular magnetic disk located at the projectile throat. The later zero crossing identifies the rear of the projectile. These signals provide convenient reference points from which the position of the shock system on the projectile can be determined. A profile of the projectile scaled to the local velocity is shown for reference.

The bottom trace in Fig. 5 shows the output from a fiber-optic probe located at the same station as the pressure and electromagnetic probes. The fiber-optic probes are used to examine the luminosity emitted as the projectile and combustion gases pass by the the probe. The primary radiation is assumed to be that from carbon particles generated by the fuel-rich combustion of methane and oxygen in the subsonic zone behind the projectile. The carbon particles emit blackbody radiation whose peak intensity occurs at the highest gas temperature.

As reported in earlier publications,[6,7] velocities up to 2500 m/s have been attained with the thermally choked mode of propulsion. Such performance has been achieved using a four-stage ram accelerator configuration, in which the accelerator tube is filled with succesive combustible gas mixtures whose acoustic speeds increases towards the muzzle. In this manner the projectile Mach number is kept within relatively narrow limts (~2.5-4.0) for maximum propulsive efficiency.

Transdetonative Regime

In the higher Mach number ranges of the thermally choked mode (typically 4-4.5), it has been observed from velocity vs. distance curves, such as the example shown in Fig. 6, that the experimentally measured velocities remain higher than theory predicts. The theoretical model, described in detail elsewhere,[2] is based on quasi-steady flow and predicts that the thrust on the projectile decreases as the projectile approaches the C-J detonation speed of the gas. This model further assumes that heat addition occurs only in the subsonic zone behind the projectile.

Accelerations much greater than that predicted by the thermally choked model are routinely observed when the projectiles attain velocities greater than 85% of the C-J speed of the propellant mixture. When close to the detonation velocity, the pressure waves on the rear half of the projectile often sweep forward through the projectile throat and unstart it. During this transient shock system activity the projectile velocity and acceleration increase abruptly before it unstarts. This behavior could be due to the initiation phase of a detonation wave at the rear of the projectile which gives it a boost before the wave completely washes over.

It was found that longer projectiles more closely approached the experimentally determined detonation speeds of the thermally choked mode propellant gases [8] and in some cases actually accelerated through and above the C-J detonation velocity. It is postulated that the frequent discrepancy between theory and experiment in this transdetonative regime (85%-115% of C-J speed) may be explained by different modes of propulsion which do not require a thermal choking point at full tube area to stabilize the driving pressure wave system on the projectile. Heat addition is believed to occur at least partially on the projectile body. Credence is given to this hypothesis by data from the light fiber probes showing luminosity emanating from the rear half of the projectile at the high Mach number ranges of thermally choked operation.

Transdetonative propulsion suggests that it may be possible for projectiles to transition smoothly from thermally choked to superdetonative operation in one mixture. Figure 7 is a velocity versus distance plot of an experiment wherein the projectile entered a mixture of $4.5CH_4 + 2O_2 + 2He$ at a speed of 1300 m/sec (Mach 2.8) and accelerated to 2250 m/s (Mach 5.0). The experimentally determined C-J speed for this mixture is 2050 m/s. The projectile had a mass of 65 grams and the tube fill pressure was 25 atm. The solid line is the theoretical profile for the experiment. It shows good agreement with experiment up to about 85% of C-J speed, after which the experimental results outpace theory. The projectile accelerated through the C-J detonation speed, exceeding it by 10%. Similar results have been obtained in argon-diluted mixtures with C-J speeds in the 1600 m/s range.

A pressure and an electromagnetic transducer trace from the transdetonative regime are displayed in Fig. 8. These data were taken from the same experimental run plotted in Fig. 7. The projectile velocity and Mach number were 2150 m/s and 4.8, respectively. Although thermally choked, subdetonative theory predicts that the projectile loses thrust as it approaches the C-J speed due to the shock wave moving back on the body, the figure clearly shows that the shock system is well-attached to the projectile body. Also because of the higher Mach number, the initial oblique shock system is narrower and much stronger than that of Fig. 5.

The details of propulsion in the transdetonative regime are the subject of current research at the University of Washington. The exact mechanism by which heat is released during transdetonative operation is believed to be a "combined cycle" in which some heat is released on the projectile body and some in the recirculation zone behind it. The heat released on the body may come from partial shock-induced combustion (possibly supersonic), or the combustion may be transitioning from a subsonic to a supersonic (SCRAM) mode. Regardless of the mechanism, the existence of transdetonative propulsion may allow the projectile to be accelerated over a wide Mach

number range -- from subdetonative to superdetonative -- in only one mixture. Transdetonative propulsion may also have applications for other ramjet engines that must operate over a broad Mach number range such as on the NASP.

Superdetonative Regime

In view of the excellent performance obtained in the transdetonative regime using a projectile shape designed for subdetonative operation, experiments were performed in which a high-speed projectile, operating in a thermally choked mode, abruptly entered a propellant mixture whose detonation speed was substantially lower than the projectile velocity. The projectile was observed to accelerate in this superdetonative regime.

In the current experiments the first 8.5 m of tube are configured into a three-stage thermally choked ram accelerator which accelerates the 70 gm projectile to the 2000-2200 m/sec range, using methane-based propellant mixtures at nominal fill pressures of 25-30 atm, as described in Refs. 6-8. The last 3.66 m of the accelerator are filled with a mixture of $0.6C_2H_4 + 2O_2 + 3.3CO_2$ at 16 atm, which has an experimentally measured C-J detonation speed of 1650 m/sec (theoretical C-J speed is 1550 m/sec, based on equilibrium combustion). The projectile thus enters the final mixture at a velocity 20-30% higher than the C-J speed.

Figure 9 displays the outputs from a pressure transducer and an electromagnetic sensor at a point 0.5 m from the entrance to the last stage, where the projectile is operating in the superdetonative regime. The projectile velocity and Mach number are 2070 m/sec and 7.1, respectively. The pressure trace, typical of superdetonative operation, is completely different from that observed in the thermally choked mode (Fig. 5). In the present case there is an abrupt rise in pressure to 800 atm, i.e., a pressure ratio of 50, followed by a series of pressure pulses of decreasing amplitude. Eventually, a steady pressure plateau of 500 atm is reached.

Figure 10 displays the outputs from a pressure transducer and a light emission probe located 0.3 m ahead of the instruments in Fig. 9; the data in Fig. 10 are taken from the same experimental run as those in Fig. 9. The projectile velocity and Mach number are 2040 m/sec and 7.0, respectively. The features of the pressure trace are similar to those in Fig. 9. The light emission data are radically different from those in the thermally choked mode (Fig. 5). Along with the pressure traces, the light emission data suggest that combustion occurs mainly on the projectile body in contrast to the thermally choked mode, where all combustion activity occurs behind the projectile. The light emission behind the projectile in Fig. 10 may be a result of recombination or the formation of carbon particles. Currently, the exact combustion mode which drives the projectile in the superdetonative regime remains somewhat speculative, though recent CFD modeling indicates that shock-induced combustion may be the thrust-producing mechanism. [9,10] Regardless of the exact mechanism, the gas pressure is seen to rise during the combustion process, indicating supersonic heat addition.

The velocity of the projectile down the tube was deduced from the distance-time history of the electromagnetic transducer signals. The data obtained are curve fit with the highest order polynomial (typically fifth- to seventh-order) that closely matches the experimental data without producing excessive oscillations in the distance-velocity history obtained by differentiation. Figure 11 shows the experimentally determined velocity as a function of distance in the entire ram accelerator, including the first three stages of thermally choked operation. The solid line is the theoretical velocity-distance curve for the corresponding experimental run. The theoretical curve is plotted only for the subdetonative, thermally choked combustion regime. A model of superdetonative operation is the subject of current work. The operating conditions and the gas mixtures are noted in the figure. The short, dashed horizontal lines denote the C-J detonation speeds of the various gas mixtures. In this case superdetonative operation was observed over the

velocity range 2180-2475 m/sec. The peak Mach number attained in the superdetonative regime was 8.4.

NUMERICAL RESULTS

A computational fluid dynamics (CFD) code is being developed for studying the flow, combustion, and performance characteristics of the ram accelerator concept operating in the superdetonative velocity range* . Due to space limitations, the numerical formulation will only be discussed in general terms here. The code solves the 2D, axisymmetric Euler equations coupled with chemical nonequilibrium processes using a shock-capturing technique. Real gas effects are taken into account by expressing the specific heats of the various species as a function of temperature. The corresponding expressions were obtained from the JANAF tables[17].

A combustion model for hydrogen/oxygen mixtures consisting of 8 reactions and 7 species, including 6 reacting species H, O, H_2O, OH, O_2, H_2, and an inert species such as Argon or Nitrogen, was selected for our computations.[18] The eight significant reactions assumed are:

$$H + O_2 \Leftrightarrow OH + O \qquad H_2 + X \Leftrightarrow 2H + X$$

$$O + H_2 \Leftrightarrow OH + H \qquad H_2O + X \Leftrightarrow OH + H + X$$

$$H_2 + OH \Leftrightarrow H + H_2O \qquad OH + X \Leftrightarrow O + H + X$$

$$2OH \Leftrightarrow O + H_2O \qquad O_2 + X \Leftrightarrow 2O + X$$

The forward and backward reaction rates, K_{fi} and K_{bi}, are given by expressions of the form $K_i = A_i T^{bi} e^{-Ci/T}$, and the reaction coefficients A and C were taken from Evans and Schexnayder[19].

The code employs a total variation diminishing (TVD)[20] time marching method to solve the complete Euler and species equations in a fully coupled manner. This method, known as the "point implicit TVD MacCormack" scheme was originally developed by Yee and Shinn[21]. This approach requires an implicit treatment of the chemical source term, due to the fact that the equation set is mathematically stiff. The degree of stiffness is determined by the Damköhler number, defined as the ratio of the characteristic convection time to the characteristic reaction time. High Damköhler numbers imply high levels of stiffness, and in general there will be a Damköhler number associated with each reaction in the chemistry model.

Besides solving the stiffness problem, this method has several desirable properties, such as high-order accuracy, robustness, and the ability to achieve high resolution of shock waves, without the spurious oscillations associated with the more classical high-order schemes. The main disadvantage of the method is, however, that the solutions are not in general time accurate, making the scheme suitable only for steady state calculations.

---

*It should be noted that the numerical model presented here is a departure from the CFD model presented at the 1987 ARA Meeting.[5] The earlier model was based on a global Arrhenius rate equation, with the Arrhenius constants determined from experimental ignition delay studies. The current model is more accurate in that it accounts for reaction kinetics. Nonetheless, the earlier results were encouraging in that they predicted superdetonative operation was possible.

Before applying this numerical scheme to a ram accelerator configuration, the code was tested by conducting numerical simulations of the "exothermic blunt body flow" problem.[9,10] This type of flow, which consists of blunt projectiles flying into detonable gas mixtures, covers a wide range of shock-induced phenomena; from decoupled and coupled shock-deflagration systems, to overdriven and oblique detonation waves. They were experimentally investigated in the mid 1960's[22,23] and early 1970's, most notably by a group of researchers at the Institut Franco-Allemand de Reserches de Saint-Louis.[24,25]

Figures 12 (a) and (b) show a comparison between experimental and computational results obtained by using the present numerical scheme, for a blunt, spherical nose projectile flying through a stoichiometric mixture of H_2/O_2 at a pressure of 186 torr, and at a superdetonative velocity U = 2705 m/s (Mach number M = 5.08). The experimental results were obtained from the work of Lehr.[25] This case, produced a combination of overdriven and oblique Chapman-Jouguet detonative waves. Although the detailed structure of the detonation cannot be resolved numerically, the overall effects such as the location of the overdriven portion of the detonation wave, and the angle and location of the oblique portion, are in close agreement with experiment.

Ram accelerator results are presented for the projectile configuration shown in Fig. 13, which has dimensions similar to the experimental projectile currently operating at the University of Washington. (Note that the CFD projectile geometry differs somewhat in that it has an afterbody which tapers to a point). The projectile is composed of two 14° half angle cones and a cylindrical section. The maximum projectile diameter is 2.9 cm and its length is 19 cm. The tube diameter is 3.8 cm. A typical propellant fill pressure of 20 atm. was selected for our calculations.

Figure 14(a) shows temperature contours for a mixture of $2H_2 + O_2 + 5He$ and at a flight velocity U = 5.9 km/s (M = 8). (For clarity the plot is magnified in the vertical direction by a factor of five). At this Mach number, a shock-induced combustion front is established behind the second shock reflection. The pressure distribution along the projectile surface and tube wall is shown in Fig. 14(b). Note that the pressure at the projectile tail is higher than that at the nose, and as a result, a positive thrust force is produced.

A non-dimensional thrust, Φ, can be defined as:

$$\Phi = \frac{F}{p_0 A_t}$$

where F is the thrust, p_0 is the fill pressure,and A_t is the tube area. For the M = 8 case, a non-dimensional thrust $\Phi = 3.27$ was obtained.

The combustion front remains behind the second shock reflection for a certain Mach number range. As the projectile accelerates inside the tube, the strength of the shock wave system increases and, at a given point, causes the combustion front to jump from the second shock reflection to the first. This situation is shown in Fig. 15(a) for a Mach number M = 9 (U = 6.7 km/s). Note that due to the effect of the second reflection, which tends to speed up the reactions, the combustion zone at the projectile surface is narrower than at the tube wall. The pressure distribution for this case is shown in Fig. 15(b). The nondimensional thrust in this case is Φ = 2.93.

Figure 16 shows the variation of ballistic efficiency as a function of projectile velocity for two different projectiles, one having nose and tail half angles of 12° and the other 14°. Ballistic efficiency is defined as the ratio of the rate of change of kinetic energy of the projectile to the rate of expenditure of chemical energy. The lowest velocity data point in each case corresponds to a

combustion front behind the second shock reflection, while the highest velocity corresponds to premature combustion at the bow shock. Note that the 12° projectile produces a very small positive thrust in the case of premature combustion. It is observed that higher efficiencies are obtained with the 12° nose projectile (up to 20%), however, it must operate at higher velocities and Mach numbers. In a given mixture, the operational Mach number range of the 12° projectile is approximately from M = 9 to M = 11 while that of the 14° is from M = 9 to M = 10. For a given projectile, the ballistic efficiency decreases with increasing velocity. This is due to the fact that the high pressure region behind the combustion zone is not very sensitive to changes in velocity, while the nose wave drag increases significantly as the projectile velocity increases.

CONCLUSION

Acceleration of projectiles by ram accelerator propulsive modes at velocities greater than the local C-J detonation speed has been experimentally demonstrated in both methane and ethylene-based propellant mixtures and has been theoretically investigated in hydrogen mixtures. Projectiles were accelerated through the velocity range of 2000 m/sec to near 2500 m/sec by an ethylene-oxygen-carbon dioxide propellant mixture having an experimentally determined detonation speed of 1650 m/sec. Theoretical investigations indicate that superdetonative operation may efficiently accelerate projectiles to near 9 km/s. Many propellant mixtures used in the thermally choked propulsive mode have demonstrated extraordinary accelerations when the projectiles have been allowed to approach the detonation velocity of the mixture, and in several methane based propellant mixtures the projectiles have been smoothly accelerated through the entire transdetonative regime (85%-115% C-J detonation speed). These experiments suggest that smooth acceleration from a low Mach number, subdetonative regime to a hypersonic, superdetonative regime may be possible in a single propellant mixture.

Acknowledgements

This work was supported in part by ONR Contract No. N00014-88-K-0565, by USAF Contract F08635-89-C-0196 and by a grant from the Olin Corporation. The authors are deeply indebted to Peter Kaloupis, Gilbert Chew and Erik Christofferson for their assistance in performing the experiments, and to Bill Lowe, Malcolm Saynor, and Dennis Peterson for their skillful fabrication of the projectiles.

References

1. Hertzberg, A., Bruckner, A., and Bogdanoff, D.W., "The Ram Accelerator: A New Chemical Method of Achieving Ultrahigh Velocities," Proceedings of the 37th Aeroballistic Range Association Meeting, Quebec, Canada, September 9-12, 1986.

2. Hertzberg, A., Bruckner, A.P. and Bogdanoff, D.W., "Ram Accelerator: A New Chemical Method for Accelerating Projectiles to Ultrahigh Velocities," AIAA Journal., Vol. 26, pp. 195-203, 1988.

3. Bruckner, A.P., Bogdanoff, D.W., Knowlen, C. and Hertzberg, A.,"Investigation of Gasdynamic Phenomena Associated with the Ram Accelerator Concept," AIAA Paper 87-1327, 1987.

4. Knowlen, C., Bruckner, A.P., Bogdanoff, D.W. and Hertzberg, A., "Performance Capabilities of the Ram Accelerator," AIAA Paper 87-2152, 1987.

5. Bruckner, A.P. and Hertzberg, A., "Development of the Ram Accelerator Hypervelocity Launcher," Proceedings of the 38th Aeroballistic Range Association Meeting, Tokyo, Japan, October 6-9, 1987.

6. Bruckner, A.P., Knowlen, C., Scott, K.A. and Hertzberg, A., "High Velocity Modes of the Thermally Choked Ram Accelerator," AIAA Paper 88-2925, 1988.

7. Knowlen, C., Scott, K.A., Bruckner, A.P., and Hertzberg, A., "Recent Developments in Ram Accelerator Technology," Proceedings of the 39th Aeroballistic Range Association Meeting, Albuquerque, NM, October 10-13, 1988.

8. Bruckner, A.P., Knowlen, C., Scott, K.A., Hertzberg, A., and Bogdanoff, D.W., "Operational Characteristics of the Thermally Choked Ram Accelerator," to be published in Journal of Propulsion and Power.

9. Yungster, S., Eberhardt, S. and Bruckner, A.P., "Numerical Simulation of Shock-Induced Combustion Generated by High-Speed Projectiles in Detonable Gas Mixtures," AIAA Paper 89-0673, 1989.

10. Yungster, S. and Bruckner, A.P., "A Numerical Study of the Ram Accelerator Concept in the Superdetonative Velocity Range," AIAA Paper 89-2677, 1989.

11. Hertzberg, A., Bruckner, A.P. and Mattick, A.T., "A Chemical Method for Achieving Acceleration of Macroparticles to Ultrahigh Velocities," Final Report, UWAERP/15, Department of Energy Grant No. DE FG06 85ER13382, Aerospace and Energetics Research Program, University of Washington, Seattle, WA, 1987.

12. Bruckner, A.P. and Hertzberg, A., "Ram Accelerator Direct Launch System for Space Cargo," IAF Paper 87-211, 1987.

13. Kaloupis, P. and Bruckner, A.P., "The Ram Accelerator: A Chemically Driven Mass Launcher," AIAA Paper 88-2968, 1988.

14. Ostrander, M.J., Hyde, M.F., Young, R.D. and Kissinger, R.D., "Standing Oblique Detonation Wave Engine Performance," AIAA Paper 87-2002, 1987.

15. Pratt, D.T., Humphrey, J.W. and Glenn, D.E., "Morphology of a Standing Oblique Detonation Wave," AIAA Paper 87-1785, June 1987.

16. Shapiro, A.H., The Dynamics and Thermodynamics of Compressible Fluid Flow, Vol I, John Wiley and Sons, New York, 1953, pp. 135-137.

17. Stull, D.R. and Prophet, H., "JANAF Thermochemical Tables," 2nd. Ed., NSRDS-Report 37, National Bureau of Standards, June 1971.

18. Moretti, G., "A New Technique for the Numerical Analysis of Nonequilibrium Flows," AIAA Journal, Vol. 3, Feb. 1965, pp. 223-229.

19. Evans, J.S. and Schexnayder, C.J., "Influence of Chemical Kinetics and Unmixedness on Burning in Supersonic Hydrogen Flames," AIAA Journal, Vol. 18, Feb. 1980, pp. 188-193.

20. Harten, A., "On a Class of High Resolution Total-Variation-Stable Finite-Difference Schemes," SIAM J. Num. Anal., Vol. 21, 1984, pp. 1-23.

21. Yee, H.C. and Shinn, J.L., "Semi Implicit and Fully Implicit Shock-Capturing Methods for Nonequilibrium Flows," AIAA Journal, Vol. 27, March 1989, pp. 299-307.

22. Ruegg, F.W. and Dorsey, W.W., "A Missile Technique for the Study of Detonation Waves," J. Res. Nat. Bur. Stand., 66C, January 1962, pp. 51-58.

23. Chernyi, G.G., "Supersonic Flow Around Bodies With Detonation and Deflagration Fronts," Astronautica Acta, Vol.13, 1967, pp. 464-480.

24. Behrens, H., Struth, W., and Wecken, F., "Shock-Induced Combustion in the Bow Waves of High-Speed Missiles," Deutsch-Französisches Forschungsinstitut, Rep. 2/66, Saint-Louis, France, 1966.

25. Lehr, H.F., "Experiments on Shock-Induced Combustion," Astronautica Acta, Vol. 17, 1972, pp. 589-597.

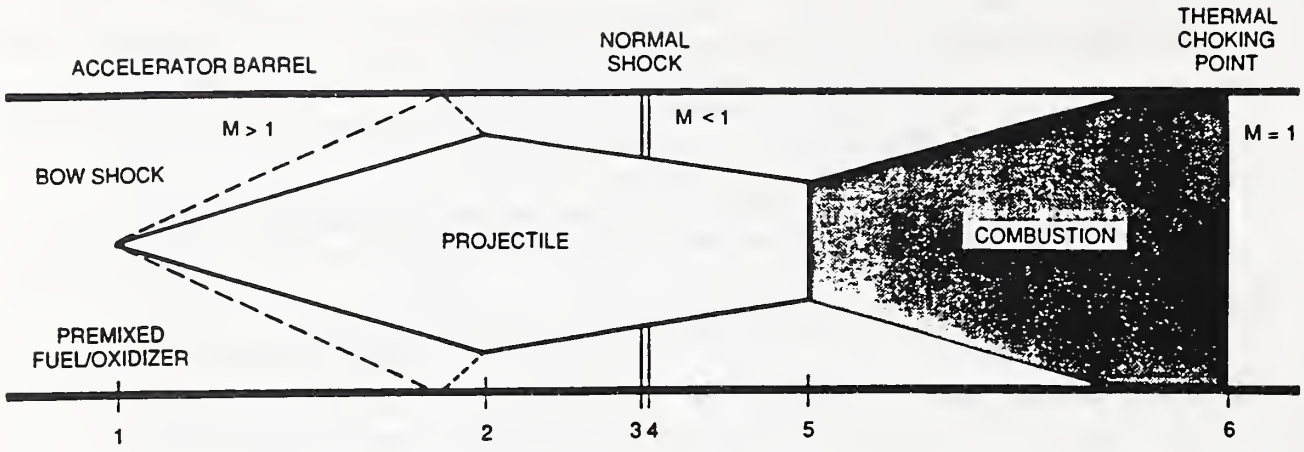

Fig. 1 Subsonic combustion thermally choked ram accelerator mode.

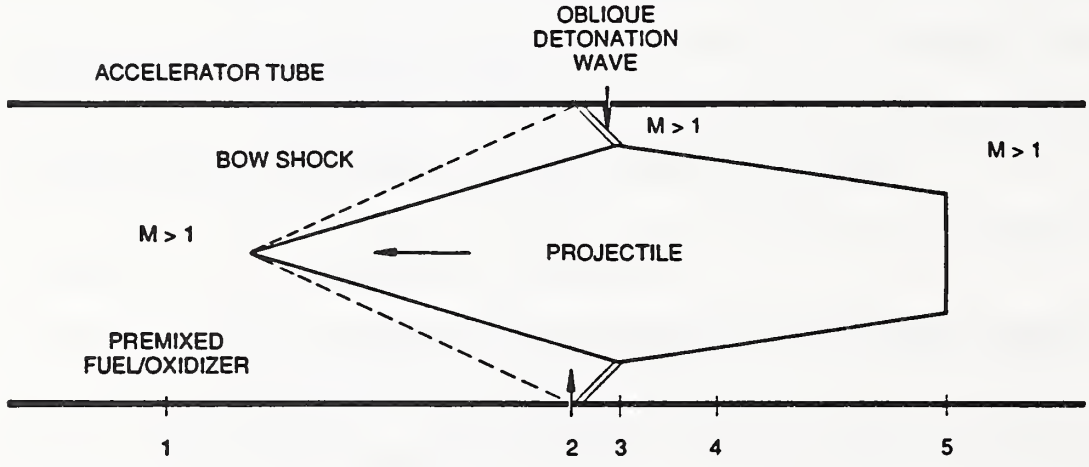

Fig. 2 Oblique detonation wave ram accelerator mode.

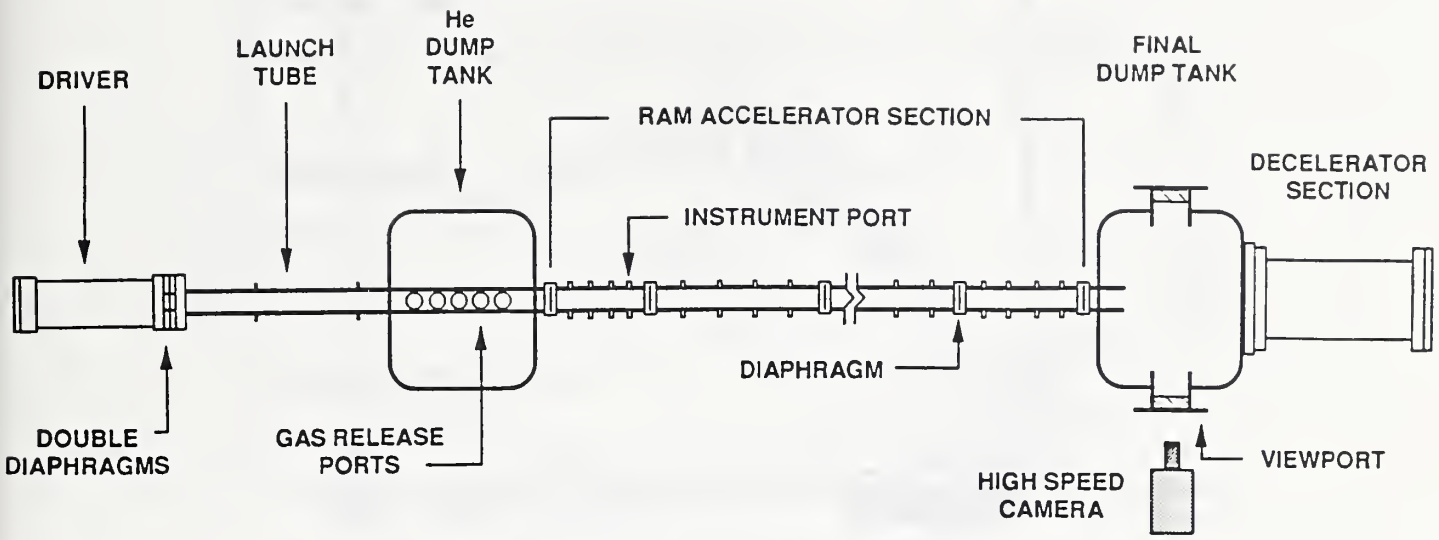

Fig. 3 Ram accelerator test facility.

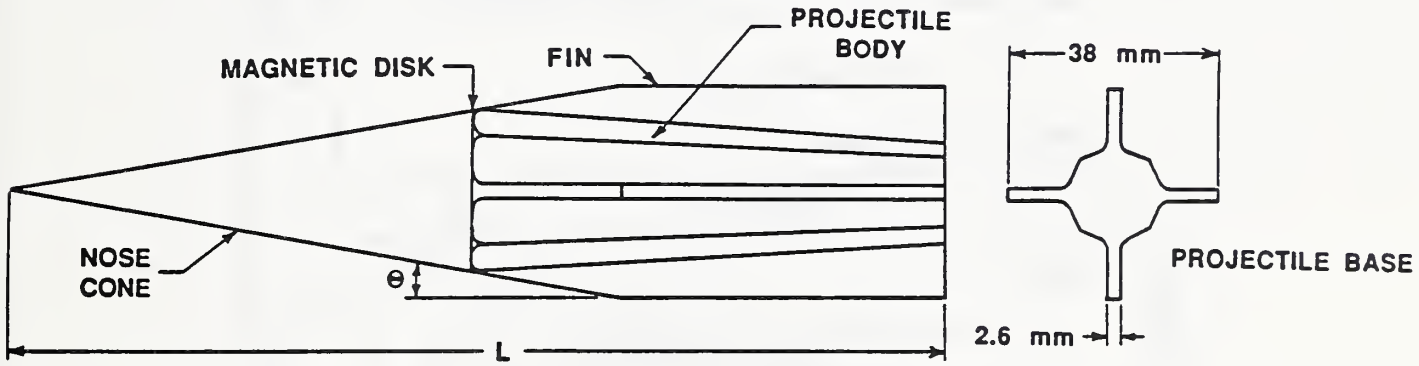

PROJECTILE

	TYPE A	TYPE B
L	138 mm	166 mm
θ	12.5°	10°

Fig. 4 Experimental projectile configuration.

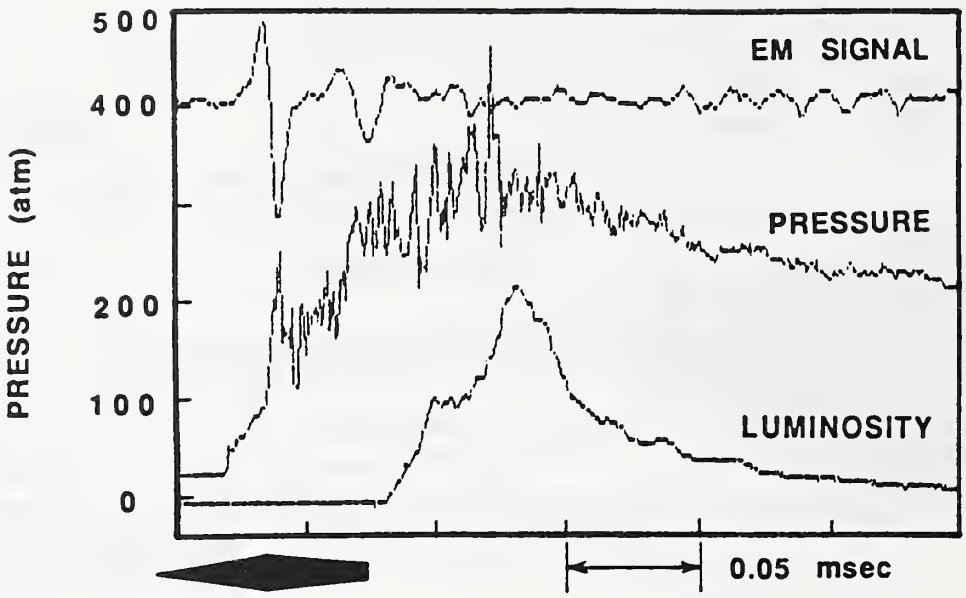

Fig. 5 Electromagnetic (EM), pressure and broadband luminosity signals in thermally choked ram accelerator operation. Propellant mixture $3.5CH_4 + 2O_2 + 6.5He$; fill pressure = 25 atm; U = 2020 m/s; M = 3.7; type B projectile.

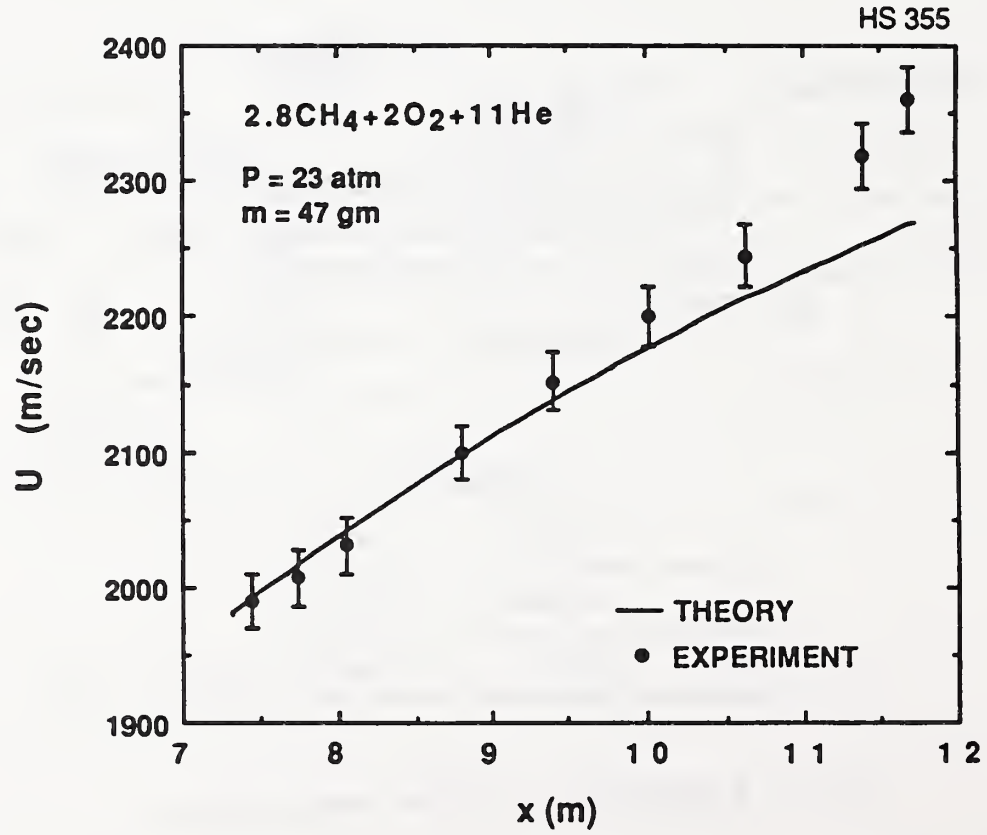

Fig. 6 Velocity profile in fourth stage of four-stage thermally choked ram accelerator. Type A projectile.

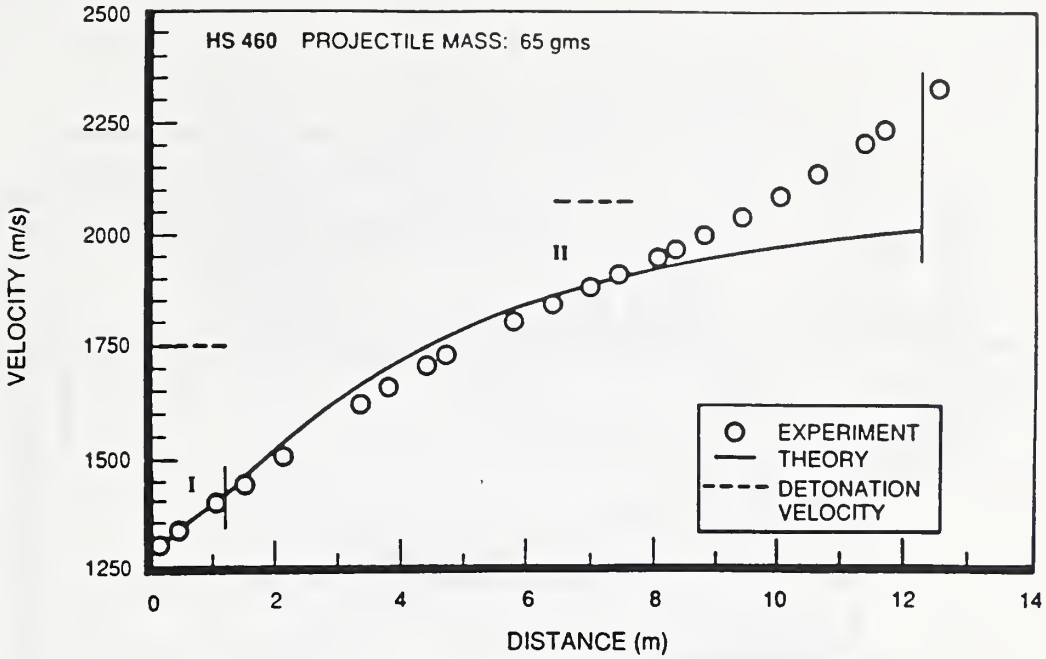

STAGE	MIX	SOUND SPEED	PRESSURE
I	2.6CH4 + 2O2 + 5.6N2	363 m/s	25 atm
II	4.5CH4 + 2O2 + 2He	448 m/s	25 atm

Fig. 7 Velocity profile in transdetonative ram accelerator operating regime.

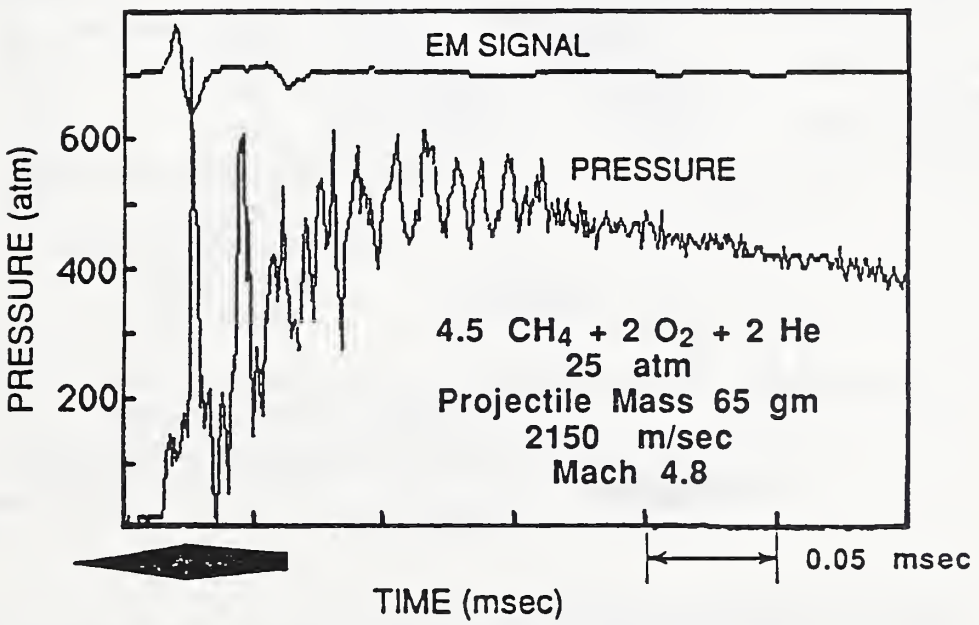

Fig. 8 Pressure and EM signatures in transdetonative ram accelerator operating regime.

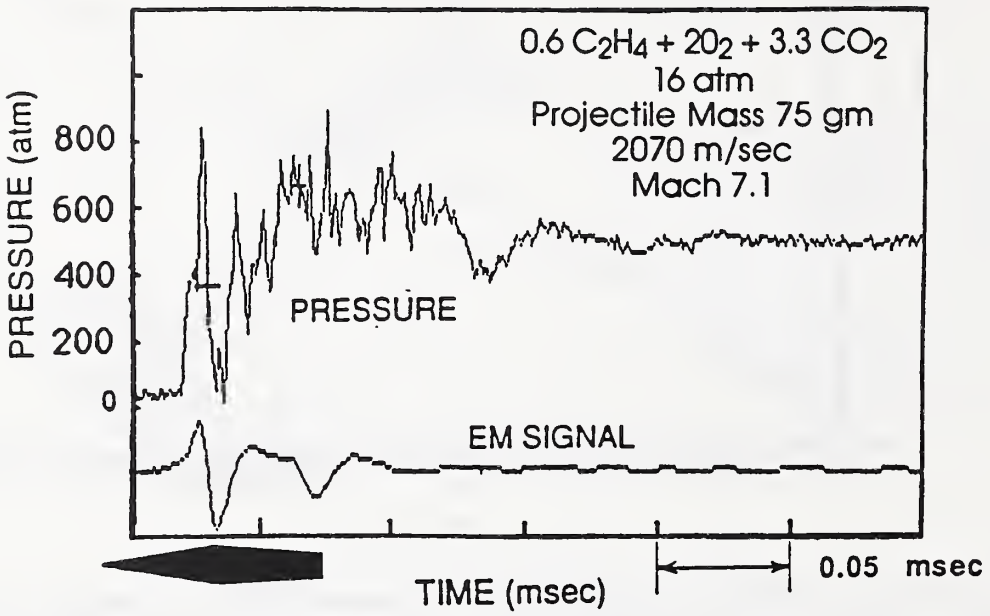

Fig. 9 Pressure and EM signatures in superdetonative ram accelerator operating regime.

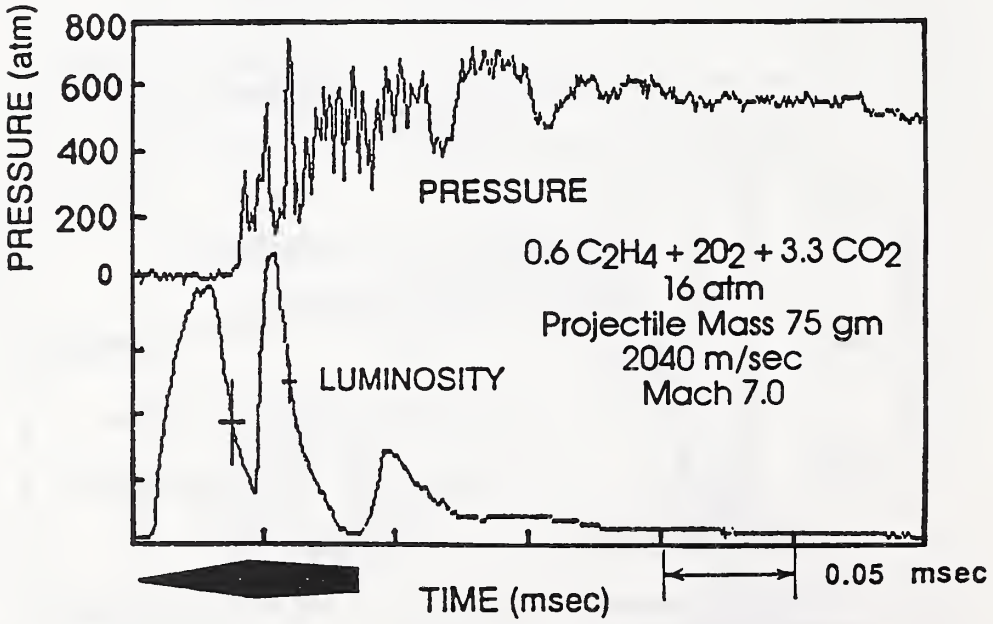

Fig. 10 Pressure and luminosity signatures in superdetonative ram accelerator operating regime.

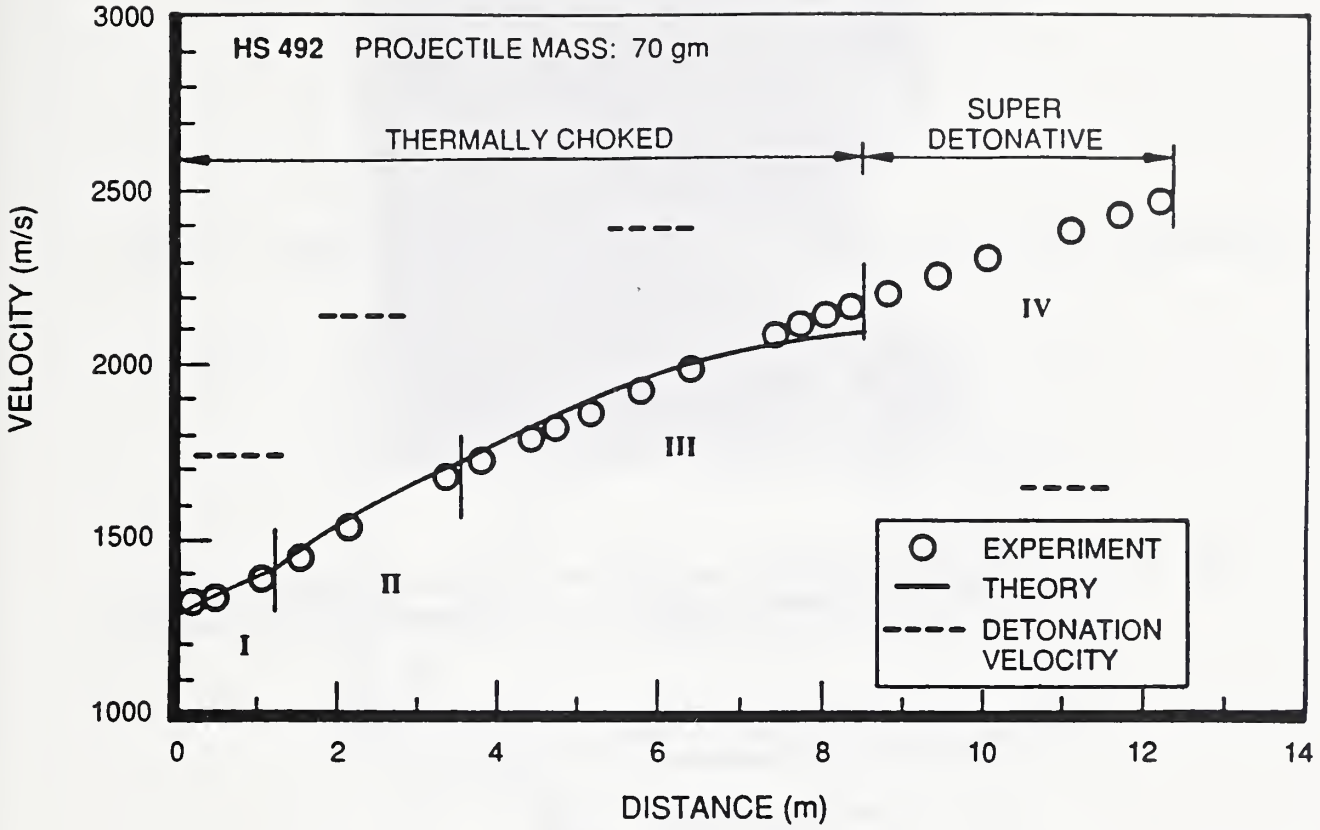

STAGE	MIX	SOUND SPEED	PRESSURE
I	2.6 CH_4 – 2O_2 – 5.6 N_2	363 (m/s)	31 atm
II	4.5 CH_4 – 2O_2 – 2 He	448 (m/s)	31 atm
III	3.5 CH_4 – 2O_2 – 6.5 He	544 (m/s)	31 atm
IV	0.6 C_2H_4 – 2O_2 – 3.3 CO_2	291 (m/s)	16 atm

Fig. 11 Velocity profile in thermally choked and superdetonative ram accelerator modes.

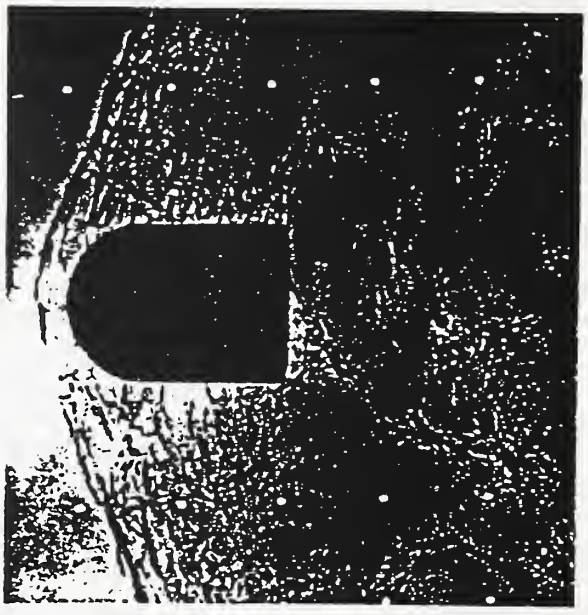

Fig. 12a Overdriven detonation and oblique Chapman-Jouguet detonation generated by a blunt projectile in a stoichiometric H_2/O_2 mixture at M = 5.08 (from Ref. 25).

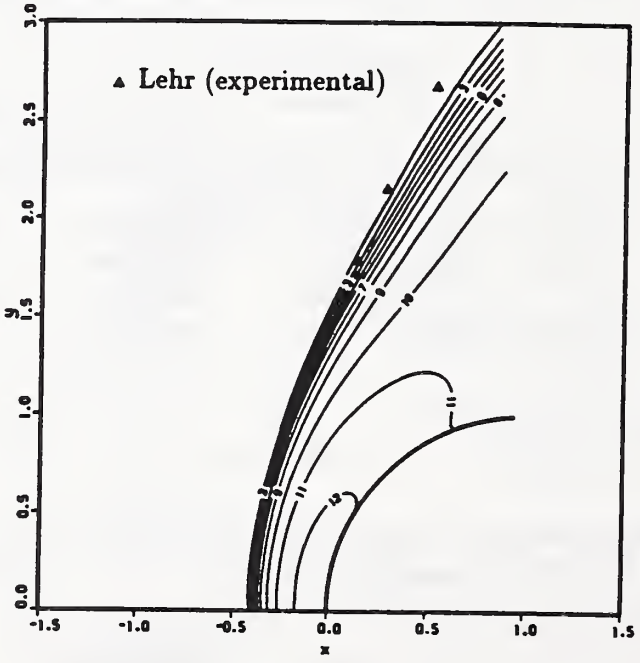

Fig. 12b Temperature contours (T/T_∞) for soichiometric H_2/O_2, M = 5.08 flow past a sphere. Experimental shock location obtained from Fig. 12a.

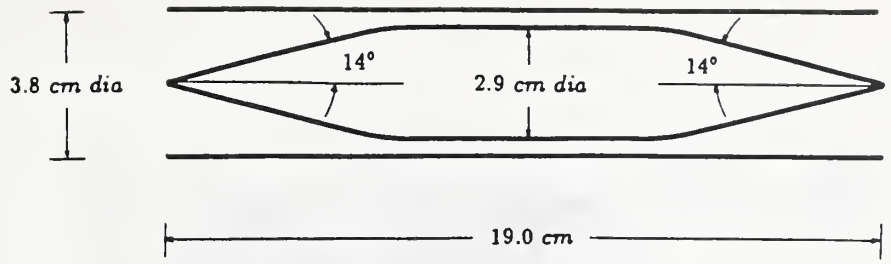

Fig. 13 Ram accelerator projectile configuration used in CFD computations.

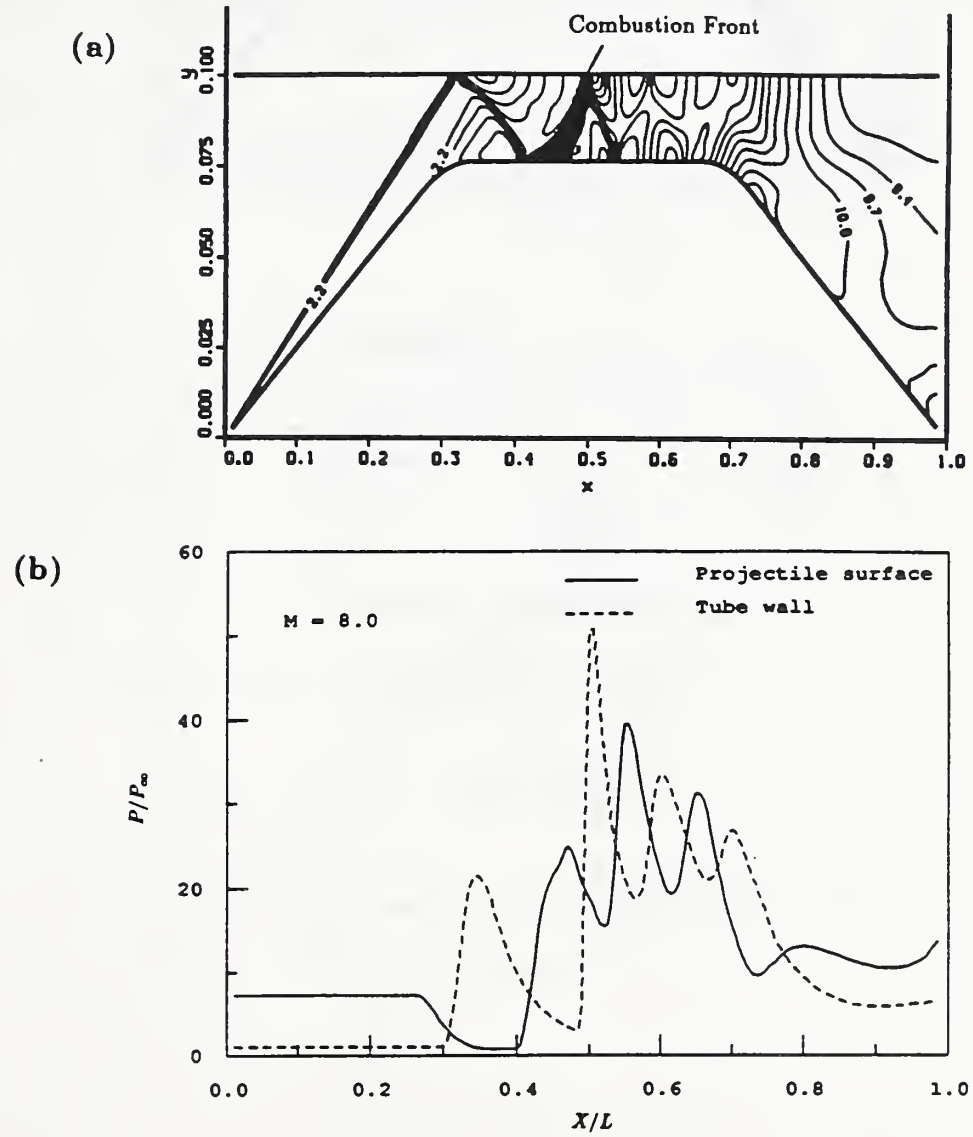

Fig. 14 (a) Temperature contours (T/T_∞); (b) pressure distribution; for a 14° projectile. U = 5.9 km/s (M = 8); mixture: $2H_2 + O_2 + 5He$. (In (a) vertical scale is magnified by factor of 5 for increased clarity).

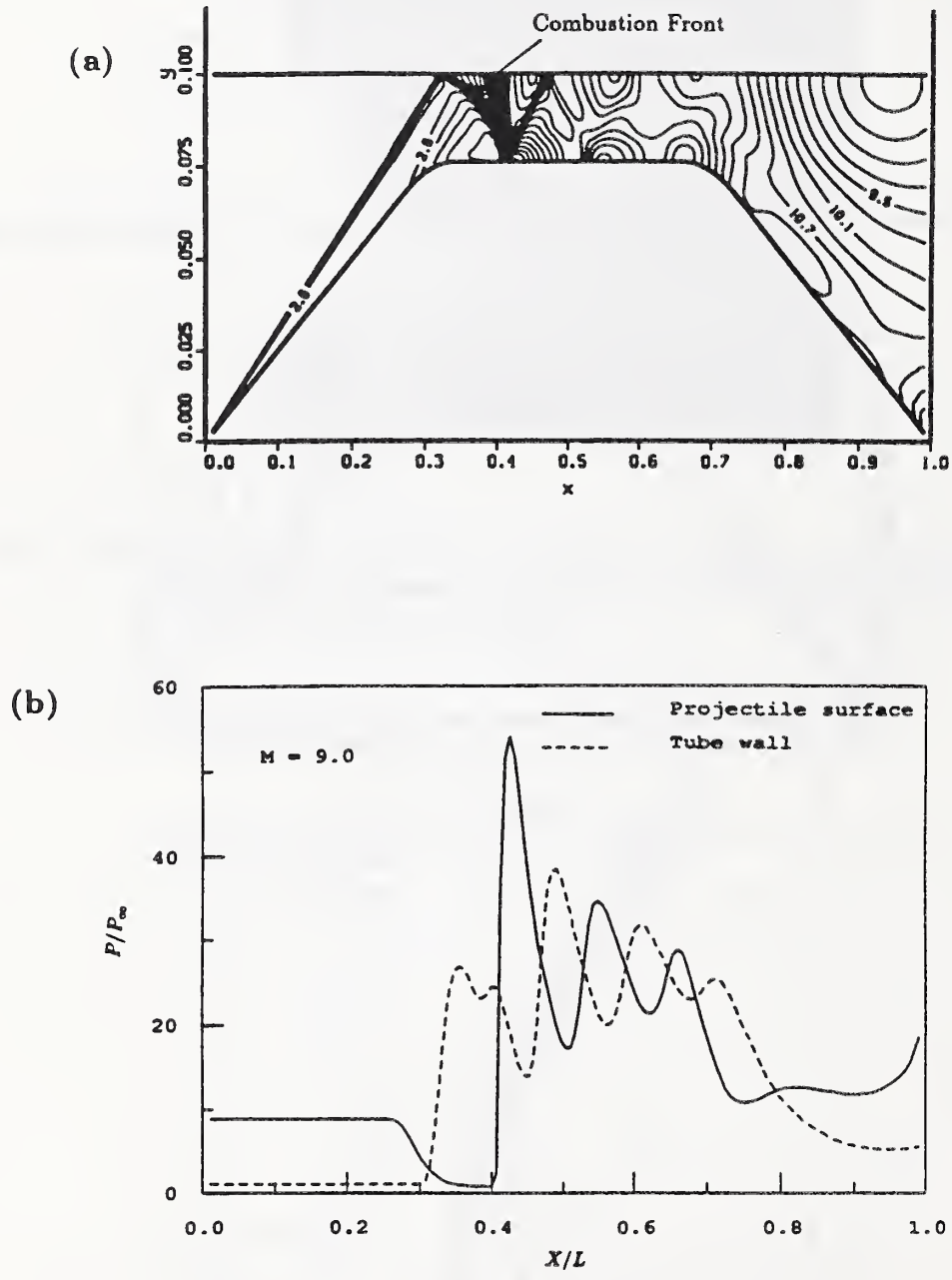

Fig. 15 (a) Temperature contours (T/T_∞); (b) pressure distribution for a 14° projectile. U = 6.7 km/s (M = 9); mixture: $2H_2 + O_2 + 5He$. (In (a) vertical scale is magnified by factor of 5 for increased clarity).

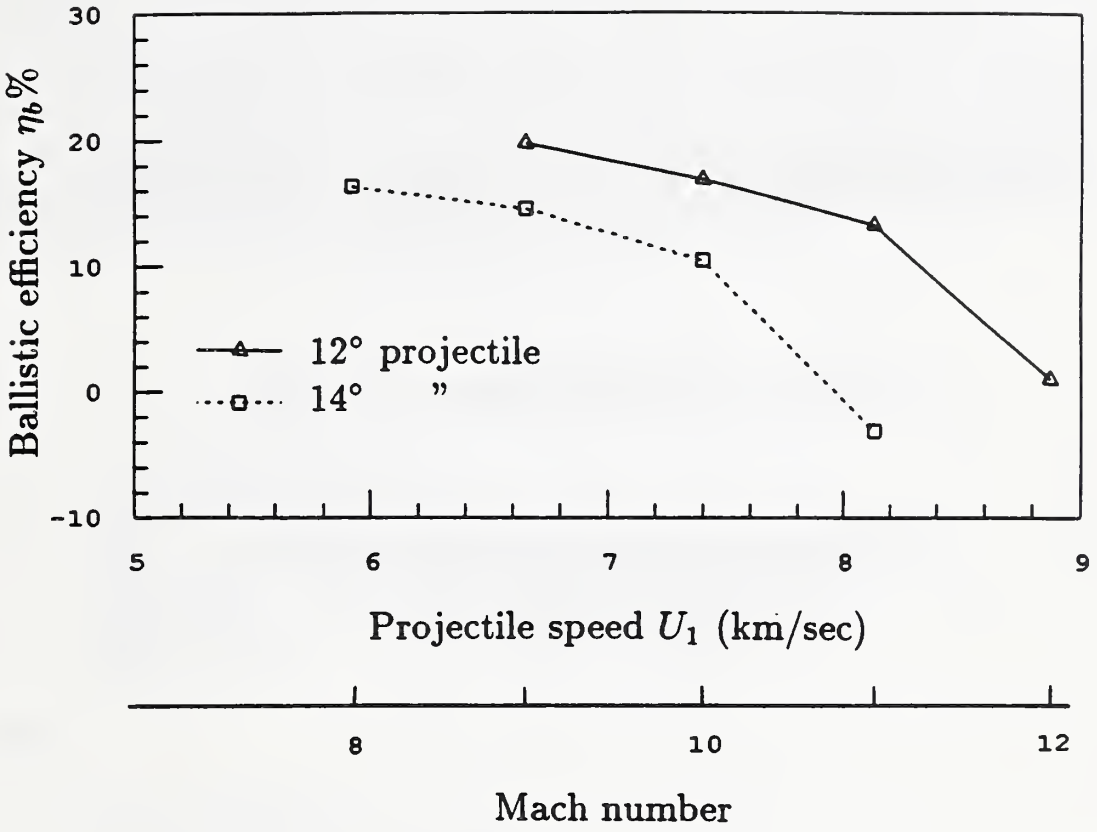

Fig. 16 Ballistic efficiency as a function of ram accelerator projectile speed and Mach number. Mixture: $2H_2 + O_2 + 5He$.

PART 2

EXPLORATORY STUDY OF A RAM ACCELERATOR MASS LAUNCH SYSTEM

P. Kaloupis, A.P. Bruckner, and A. Hertzberg

Aerospace and Energetics Research Program
University of Washington, FL-10
Seattle, Washington 98195

ABSTRACT

The ram accelerator, a chemically propelled mass driver, is presented as a viable new approach for directly launching acceleration-insensitive payloads into low earth orbit. The propulsion principle is similar to that of a conventional air-breathing ramjet. The cargo vehicle resembles the center-body of a ramjet and travels through a tube filled with a pre-mixed fuel and oxidizer mixture. The launch tube acts as the outer cowling of the ramjet and the combustion process travels with the vehicle. Two drive modes of the ram accelerator propulsion system are described, which when used in sequence are capable of accelerating the vehicle to as high as 12 km/sec. The requirements are examined for placing a 2000 kg vehicle into a 500 km orbit with a minimum of on-board rocket propellant for circularization maneuvers. It is shown that aerodynamic heating during atmospheric transit results in very little ablation of the nose. An indirect orbital insertion scenario is selected, utilizing a three step maneuver consisting of two burns and aerobraking. An on-board propulsion system using storable liquid propellants is chosen in order to minimize propellant mass requirements, and the use of a parking orbit below the desired final orbit is suggested as a means to increase the flexibility of the mass launch concept. A vehicle design using composite materials is proposed that will best meet the structural requirements, and a preliminary launch tube design is presented.

NOMENCLATURE

A_t	crossectional area of tube
C_p	specific heat at constant pressure
F	thrust
M	Mach number
p	static pressure
T	static temperature
y	altitude

Greek

γ	ratio of specific heats
Δq	heating value of propellant mixture
ρ	atmospheric density

Subscripts

1	conditions upstream of vehicle
6	conditions at thermal choking point

INTRODUCTION

A significant barrier to developing any large scale permanent space infrastructure designed for space manufacturing, or for the exploration and colonization of our solar system, is the high cost of launch systems capable of carrying the raw materials necessary to construct and maintain the large space systems required. Much of this materiél, such as the components of large space structures, the various raw materials required for space manufacturing, hydrogen, oxygen, water, and other consumables are capable of withstanding high accelerations. This stress insensitivity has attracted the attention of various investigators over the years, and a number of mass launch systems to carry out the function of direct launch have been proposed [1-14]. These have ranged from hypervelocity guns [1,2] to various electromagnetic accelerators [3-10] and beamed energy concepts [11-14]. The relatively low efficiencies of the gun concepts, the formidable problem of dealing with the large instantaneous electric loads in the electromagnetic systems, the problems of atmospheric beam propagation in the beamed energy systems, and the general problem of scaling these concepts to useful payloads have been serious impediments to their implementation.

At the University of Washington a ramjet-in-tube concept called the "ram accelerator" has been developed for efficiently accelerating relatively large masses (up to several metric tons) to as high as 12 km/sec using chemical energy [15-23]. The propulsive cycle of the ram accelerator is similar to the aerothermodynamic cycle that generates the thrust in a conventional ramjet; however, the device is operated in a different manner. The payload vehicle, which resembles the center-body of a conventional ramjet, travels through a tube filled with a combustible, premixed, gaseous fuel and oxidizer mixture (Figs. 1 and 2). The tube acts as the outer cowling of the ramjet, and the combustion process travels with the vehicle. Since the density, speed of sound, and chemical energy density of the propellant mixture can be controlled, the acceleration of the vehicle can be maintained nearly constant over the entire velocity range of operation. The concept is scalable for vehicle masses ranging from grams to thousands of kilograms, and thus offers the potential for impulsive launch of acceleration-insensitive payloads to low earth orbit [24-28].

Several modes of propulsion have been investigated for the ram accelerator. These differ primarily in the method of chemical heat release and velocity range of operation [15-20]. The two modes of interest for the direct launch system proposed here are illustrated in Figs. 1 and 2. The first mode (Fig. 1) uses thermally choked subsonic combustion behind the vehicle, and is suitable for the velocity range of 0.7-2.5 km/sec. The initial acceleration to the 0.7 km/sec required to start the first mode is accomplished by means of a conventional combustion-driven gas gun. The second mode (Fig. 2), which operates at superdetonative velocities (i.e., velocities exceeding the local speed of propagation of a Chapman-Jouguet (C-J) detonation wave), uses the heat release in the oblique detonation wave generated by a bump on the vehicle's surface to produce the forward thrust. In principle,this mode of propulsion is capable of efficiently accelerating the vehicle in the velocity range of 2.5-12 km/sec. Laboratory scale experiments performed at the University of Washington with a 45 gm projectile and 38 mm bore tube have achieved velocities in excess of 2.4 km/sec and accelerations of 30,000 g with the thermally choked mode [20]. The results have shown a remarkably close agreement between predicted performance and experimental results . More recent experiments have established the proof of principle of the superdetonative mode at velocities up to 2.5 km/sec with 70 gm projectiles [23].

A number of possible operating configurations for the ram accelerator mass launch system have been examined. A launch system capable of delivering a 2000 kg vehicle, with as high a payload mass fraction as possible, to a 500 km orbit was selected as a representative baseline case [26]. Launch velocities in the range of 8 to 10 km/sec have been considered. The peak permissible acceleration has been limited to 1000 g's as a compromise between limiting vehicle structural mass and limiting the length of the launch tube. Based on previous work [24] a launch tube inside diameter of 1.0 m and a vehicle diameter of 0.76 m were selected. The following key

issues are examined here: 1) the vehicle must be accelerated to a velocity of the order of the orbital velocity or higher (i.e. 8 to 10 km/sec); 2) the vehicle must survive the launch stresses during acceleration; 3) the vehicle must survive atmospheric transit and maintain its integrity with good thermal protection of the payload; 4) an on-board rocket system is required to accomplish the necessary orbital maneuvers with a minimum of on-board propellant.

The possible economic advantage of this concept was addressed only indirectly at the University of Washington. For example, in order to reduce costs, only currently available technology was invoked, cheap propellants were selected, and the potential reusability of the vehicle was explored. The economic issues were explored by the United Technologies Research Center under a subcontract to the University of Washington and are discussed in Ref. 28.

RAM ACCELERATOR DRIVE MODES

To achieve a launch velocity in the range of 8 to 10 km/sec two propulsive modes are required. These are the subsonic combustion, thermally choked mode (Fig. 1), and a mode which uses a stabilized oblique detonation wave for combustion (Fig. 2). These propulsion modes are similar to a ramjet cycle, and as such require an initial velocity to start the propulsion process. An initial accelerator is therefore required to accelerate the vehicle from rest to a starting velocity of 700 m/sec.

Initial Accelerator

The initial accelerator which imparts the necessary 700 m/sec velocity required to start the propulsion process is a combustion-driven gas gun of conventional design [26]. The gun uses a stoichiometric methane-air mixture at a fill pressure of 47 atm and at ambient temperature. The methane and air are premixed prior to injection into the combustion chamber. The combustion chamber and barrel have the same inside diameter as the diameter of the payload vehicle, 0.76 m. The length of the combustion chamber is 42 m, and the length of the barrel is 48 m. A muzzle blast relief section surrounded by a dump tank to the atmosphere provides for gas exhaust and recoil control, and couples the gas gun to the ram accelerator.

The constant volume combustion process in the gun is initiated by an electrically heated tungsten wire down the center-line of the combustion chamber. When the pressure reaches its peak value of 428 atm a petalling diaphragm, which separates the combustion chamber from the barrel, bursts open and the acceleration process begins. The peak acceleration of 1000 g's is experienced immediately. As the vehicle moves down the barrel, the vehicle base pressure decreases, thereby decreasing the acceleration. The average driving pressure is 222 atm and the piezometric pressure ratio is 1.93. The combustion chamber and the barrel could be constructed of a high strength steel alloy, such as AISI 4340 steel. For this choice of material, with a safety factor of 4 in yield, a tube wall thickness of 7.8 cm is required.

Although the initial accelerator is large compared to currently available combustion-driven gas guns [29], there does not appear to be any significant technical barrier to its implementation. At the NASA Ames Research Center a large, experimental combustion-driven shock tube with hydrogen as the fuel has been used routinely [30]. The combustion chamber of this device is 22.9 m in length, and its internal diameter is 0.43 m. These dimensions are more than half of those proposed here for the initial accelerator. In addition, during World War II, the German army employed a railway mounted artillery piece with a 0.80 m bore that was capable of accelerating a 7000 kg shell to a muzzle velocity of 700 m/sec [31].

The need for an initial accelerator could be circumvented by developing a means to start the ram accelerator process at zero vehicle velocity. Such a zero velocity start scheme, based on non-steady gasdynamic phenomena, has been proposed by the authors and is currently under investigation.

Subsonic Combustion Thermally Choked Ram Accelerator Mode

In the subsonic combustion mode (Fig. 1) the composition of the pressurized propellant mixture and the nosecone angle are chosen such that the oblique shocks in the diffuser are too weak to initiate combustion of the mixture. A normal shock located downstream of the throat renders the flow subsonic. This shock is also not of sufficient strength to ignite the gas mixture. Ignition of the propellant mixture behind the vehicle is accomplished by means of an external ignitor system developed at the University of Washington. The recirculation region at the base of the vehicle acts as a flameholding dump combustor and the premixed propellant mixture burns in the tube behind the vehicle. The normal shock is stabilized on the aft portion of the vehicle by the thermal choking of the flow in the full tube area. This propulsion mode has been experimentally verified at the University of Washington and has attained velocities exceeding 2.4 km/sec [15-20].

The subsonic combustion thermally choked mode can be modelled using a one-dimensional, inviscid, quasi-steady approach. This mode is amenable to a straightforward approach which results in a closed form analytical solution for the thrust on the vehicle [15, 16]:

$$\left(\frac{F}{P_1 A}\right) = \frac{\gamma_1 M_1}{\gamma_6}\left[2\left(\frac{\gamma_6^2-1}{\gamma_1-1}\right)\left[1+\frac{\gamma_1-1}{2}M_1^2+\left(\frac{\Delta q}{C_{p_1}T_1}\right)\right]\right]^{\frac{1}{2}} - \left(1+\gamma_1 M_1^2\right) \tag{1}$$

Implicit in this model is the assumption that the enthalpy both before and after combustion can be expressed in the form $h = C_pT$. Thus C_{p1}, γ_1 and γ_6 in the equations presented here represent average, not local, values. From Eq. 1 it can be seen that the thrust, and thus the acceleration, of the vehicle are determined by the propellant fill pressure in the launch tube, the amount of heat release during combustion, the vehicle Mach number, and the average properties of the propellant mixture before and after combustion. For a given propellant mixture the thrust is maximum at a Mach number given by:

$$M_1 = \left[\left(\frac{\gamma_6-1}{\gamma_1-1}\right)\left(1+\frac{\Delta q}{C_{p_1}T_1}\right)\right]^{\frac{1}{2}} \tag{2}$$

Typically this Mach number lies in the range between 2.3 and 2.8 for the propellant mixtures of interest.

The maximum thrust is given by:

$$\left(\frac{F}{P_1 A_t}\right)_{max} = \left[\frac{\gamma_1}{\gamma_6}\left(\frac{\gamma_6-1}{\gamma_1-1}\right)\left(1+\frac{\Delta q}{C_{p_1} T_1}\right)\right] - 1 \qquad (3)$$

This simple 1-D model predicts that the thrust decreases as the vehicle accelerates, reaching zero at a velocity corresponding to that of a C-J detonation wave propagating in the same mixture [15]. Optimum performance is thus obtained by keeping the vehicle Mach number within a narrow range, close to the Mach number corresponding to peak thrust. This can be accomplished by dividing the tube into several segments filled with different propellant mixtures whose speed of sound increases in the direction of travel [16, 20]. In the laboratory, velocities equal to and even exceeding the C-J velocity have been obtained [23]. The attainment of significant thrust at speeds above the C-J point is thought to be a result of unsteady gasdynamic effects and is under investigation by the authors. Although the thermally choked mode can, in principle, accelerate the vehicle to more than 3 km/sec, the velocity of 2.5 km/sec has been chosen for the transition to the superdetonative mode. This is because in the velocity range of 2.5 to 3 km/sec the superdetonative mode, in principle, provides for higher thrust and better efficiency than can be achieved by the thermally choked mode.

In order to accelerate the 2000 kg vehicle from 0.7 km/sec to 2.5 km/sec five different propellant mixtures at a fill pressure of 33 atm are needed [26], and a launch tube length of 345 m is required. Figure 3 shows a plot of vehicle acceleration versus velocity for the various propellant mixtures. The peak acceleration does not exceed the imposed limit of 1000 g, and the average acceleration is 857 g. The overall ballistic efficiency (the ratio of the change of kinetic energy to the available chemical energy) is ~14%.

Superdetonative Ram Accelerator Mode

The superdetonative mode (Fig. 2) requires a strong oblique shock to raise the propellant temperature high enough for combustion to occur. A small circumferential bump on the vehicle surface can be used to trigger and stabilize the detonation wave on the vehicle [15, 17]. This mode also requires that the bow shocks be too weak to ignite the combustible gas mixture. Consequently a slender nose is desired. A nosecone half-angle of 7° was found to be appropriate. The flow is supersonic throughout. Compression occurs across the diffuser and when the flow reaches the bump on the vehicle the oblique detonation wave greatly increases the pressure. The flow then expands over the rear portion of the vehicle providing the forward thrust. The oblique detonation wave mode operates at a vehicle velocity which exceeds the C-J wave velocity, hence the term "superdetonative".

The superdetonative mode is not amenable to a closed form solution; it was modelled using a quasi-one-dimensional analysis that assumes complete combustion and heat release take place instantaneously in a thin region immediately behind the oblique shock [17]. A two-dimensional CFD analysis [18] was used to confirm some of the 1-D results, but the increased computational time precluded its exclusive use. The CFD analysis predicted somewhat higher ballistic efficiencies. The results of the two methods were in good agreement however, and the quasi 1-D results were accordingly used for the present study. Experimental proof of principle of

superdetonative propulsion has recently been established by the authors and their colleagues at velocities up to 2.5 km/sec [23]. Expansion of the University's ram accelerator facility, currently under way, will permit the exploration of superdetonative operation up to velocities of ~4 km/sec.

The transition between the subsonic combustion thermally choked mode and the superdetonative mode is effected by a sudden change in propellant mixtures. At 2.5 km/sec the vehicle makes a transition from a high acoustic speed mixture to a low acoustic speed mixture, so that the Mach number jumps from approximately 4 to 7. The superdetonative mode is immediately established under these conditions [23].

The superdetonative mode requires four propellant mixtures to accelerate the vehicle from 2.5 to 10 km/sec [26]. Figure 4 shows the acceleration as a function of vehicle velocity at a fill pressure of 33 atm for the various propellant mixtures required for this mode. The average acceleration is 910 g. Each successive mixture has a higher speed of sound in order to maintain the Mach number within acceptable limits. In the final mixture the ballistic efficiency (hence the acceleration) drops significantly due to the necessary high dilution of the mixture by hydrogen. In order to keep the ballistic efficiency in this mixture at a reasonable value, the launch tube diameter is reduced from 1.0 m to 0.9 m in the final section. This increases the compression ratio of the propulsive cycle, leading to enhanced efficiency. The average ballistic efficiency of the superdetonative acceleration process from 2.5 to 10 km/sec is ~25%.

The in-tube velocity profile of the entire acceleration process is shown in Fig. 5. The overall length of the tube required to accelerate the vehicle from rest to 8 km/sec is 3.8 km. To accelerate the vehicle to 9 km/sec a tube length of 5.1 km is required, and to accelerate the vehicle to 10 km/sec a tube length of 6.7 km is required. Most of the overall length is required for the superdetonative mode of propulsion.

VEHICLE AND LAUNCH TUBE CONFIGURATION

Vehicle

The overall success of the ram accelerator concept depends ultimately on the successful design of a payload vehicle. Preliminary design of the vehicle yielded the two configurations shown in Fig. 6. The Type 1 configuration has the payload in the forward portion of the vehicle and Type 2 has it in the aft portion. The vehicle must be able to withstand a 1,000 g acceleration, and the high pressures and temperatures characteristic of ram acceleration. The total vehicle mass is 2000 kg, and it must accommodate an onboard propulsion system for circularization maneuvers and a set of attitude control thrusters. As noted earlier, the vehicle has a diameter of 0.76 m. The nosecone has a half-angle of 7° in order to meet the requirements of the in-tube propulsion cycles and to minimize drag losses during atmospheric transit. The base diameter of the vehicle is 0.38 m, or half the body diameter.

Pressure and temperature distributions obtained from computer simulations of the two propulsion modes were used to find the peak pressure and temperature to which the vehicle would be subjected. The highest pressure (1670 atm) and temperature (4100 °K) occurred in the superdetonative mode at 72% of the vehicle body length, where the circumferential bump that creates the oblique detonation wave is located. The vehicle must be able to withstand these conditions for less than 1 sec [26].

In order to select a vehicle configuration it is necessary to consider vehicle stability, which requires that the center of gravity be placed as far forward as possible. This would suggest the

configuration with the payload in the forward part of the vehicle, i.e., the Type 1 configuration in Fig. 6, since the payload is expected to comprise a significant fraction of the total vehicle mass. This would locate the rocket motor at the tail of the vehicle, with the propellant tanks situated between the rocket motor and the payload. The denser of the propellants would be located farthest forward.

To minimize vehicle structural mass, graphite/epoxy composites and titanium alloys were considered. Although titanium alloys are stronger than composites and result in thinner walls, their greater densities make the overall vehicle structure unacceptably heavier. Therefore titanium alloys were not considered viable. The specific graphite/epoxy composite selected was T300/5208, because it is approximately 50% stronger in transverse and longtitudinal compression than the high or ultra-high modulus composites [32]. A foreseeable limitation of the T300/5208 graphite/epoxy composite is its low temperature tolerance. This problem is overcome with the use of a standard carbon-carbon ablating material that is used to protect the tail of the vehicle. The mass of the ablator required given the total heat load at the tail is only 2.1 kg, resulting in a shield thickness of approximately 3 mm [26].

Assuming isotropic properties [32] based on a (0,90) ply layup, a first order structural analysis was performed. This resulted in an overall vehicle structural mass of 600 kg,and an overall length of 7.5 m. In order to improve the accuracy for the design of the vehicle, a finite element analysis using the computer code SUPERSAP [33] was performed using a quasi-isotropic layup. Since this code could not perform calculations for a fully anisotropic layup, an optimum ply layup was not determined. The code yielded a total vehicle structural mass of 625 kg, which compares favorably with the result of the preliminary analysis.

Launch Tube

For the point design discussed here the overall launch tube length required ranges from 3.8 km for a launch velocity of 8 km/sec to 6.7 km for a launch velocity of 10 km/sec. The tube material must be able to withstand the peak pressures imposed by each of the propulsion cycles. In each mode the heat and pressure pulse travels with the vehicle, distributing the load and the heat flux over the entire tube length. Consequently, the load seen by the launch tube is expected to result in very little tube wear. This has been confirmed experimentally by the authors.

The launch tube wall thickness was estimated by assuming that the peak cycle pressure in each propulsion mode must be contained in static loading. The peak pressure at the wall in the thermally choked mode is 1000 atm and in the superdetonative mode it is 1670 atm. AISI 4340 steel with a safety factor of 3 in yield was used for the calculations. The inside diameter of the tube is 1.0 m, therefore, a wall thickness of 12.7 cm is required for the thermally choked portion of operation. For the superdetonative mode a thickness of 27.6 cm is required for the first 2.3 km, and a thickness of 24.8 cm is required for the remainder, where the tube inside diameter is 0.9 m. This results in overall tube masses of approximately 32,000, 42,000, and 54,000 metric tons for 8, 9, and 10 km/sec launchers, respectively. Other tube materials, such as composites with steel liners, are also possible, however, the selection of a particular material for the launch tube is likely to be guided by economic considerations rather than by weight alone. The technology for fabricating and laying the launch tube (up the side of a mountain having the appropriate average slope) is similar to that developed for pipelines and should not present undue difficulties.

In order to contain the 33 atm propellant gas fill prior to launch, some form of closure is required at the entrance and the exit of the launch tube. These closures could be thin, petalling, Kevlar composite diaphragms or fast-acting mechanical shutters. The exit closure could be explosively removed as the vehicle arrives, since there would be no danger of igniting the combustible gas fill. A diaphragm is also required at the point of transition between the two

propulsive modes, and between successive propellant mixtures. These would be very thin, since they support no pressure difference. The propellant gases would be delivered to the various segments of the launch tube by turbine-driven pumps. It is expected that the necessary gases would be obtained on-site from the atmosphere, and from the pyrolysis of liquid hydrocarbons.

ATMOSPHERIC TRANSIT AND AERODYNAMIC HEATING

Once the desired launch velocity has been attained, the vehicle exits the launch tube and must transit the atmosphere. A high launch altitude is desirable in order to minimize aerodynamic drag and heating [25]. For the present case a launch altitude of 4000 m was selected. This choice is somewhat arbitrary, but can be achieved in many regions of the world. The launch angle was varied between 16° and 30° for the analysis. At exit velocities of 8 to 10 km/sec, which correspond to a Mach number range of 28 to 31 outside the launch tube, the aerodynamic heating will be severe. Even assuming equilibrium dissociation across the bow shock, the nosecone of the vehicle experiences temperatures of 9,000-13,000 °K at the stagnation region . The heating is predominantly convective [34]. Two methods of thermal protection have been considered - a transpiration cooled nosecone and an ablative carbon-carbon composite nosecone.

Transpiration Cooling

The method of transpiration cooling involves the injection of a coolant through a porous nosecone to keep the temperature constant at some low value. This method would leave the vehicle unharmed by atmospheric heating. The amount of coolant required is comparable to that of an ablative protection scheme [35], but the added mass of the delivery system, its complexity, and its cost, make it an unacceptable alternative.

Ablative Protection Scheme

An ablative nosecone will absorb the aerodynamic heat input and vaporize the carbon-carbon composite material without affecting the vehicle's integrity. Ablation, however, results in the blunting of the vehicle nose-tip and an increase of the drag coefficient. This results in a greater velocity decrement than would be incurred with a constant profile nose shape. This is a disadvantage of this method because it is important to maintain as high an atmospheric exit velocity as possible, in order to minimize the amount of onboard propellant that is required for the circularization maneuvers. However, the simplicity and low cost of this form of thermal protection, compared to other alternatives, make it the approach of choice

The analysis of the atmospheric heating was divided into two separate regions - the side-walls of the nose and body, and the stagnation region at the nose tip. The sidewall heating was found to be much smaller than at the stagnation region [26], thus only the convective heat input to the vehicle nose tip needed to be considered in detail. A mass loss due to heat input was calculated using standard aerodynamic heating models [36], and the resulting shape change was modelled as a cone with a spherical cap whose radius increases with mass loss. The tangent cone approximation was used to find the drag coefficient of the new shape.

The transit of the vehicle through the atmosphere was broken down into a series of small increments. The mass and velocity loss of the vehicle were determined at the beginning of each increment, and all parameters such as the drag coefficient, velocity, and local flow properties were kept constant over the increment. The steps were carried out from the 4000 m launch altitude to an altitude of 40 km, where the aerodynamic drag and heating become negligible. A two part

exponential curve fit based on experimental values available in atmospheric tables [37] was used. The first part covered the altitude range of 0 to 30 km:

$$r = 1.225 \exp(-y/7170) \quad (4)$$

and the other the altitude range of 30 to 100 km:

$$r = 1.3815 \exp(-y/6880) \quad (5)$$

Orbital mechanics calculations were used beyond the 40 km altitude to determine the vehicle trajectory and orbit circularization.

The results of the analysis for a launch velocity of 9 km/sec and launch angles between 16° and 30° are shown in Figs. 7 to 9. The results for 8 km/sec and 10 km/sec are very similar and are not shown here. Figure 7 shows the mass loss rate versus altitude for various launch angles. In each case it can be seen that the peak mass loss rate occurs at an altitude of approximately 10 km, and not at the launch tube exit where the atmospheric density is greatest. This interesting result arises from the fact that the surface area of the stagnation region increases with altitude due to the ablation, while the density decreases with altitude. These two factors work against each other to result in a maximum heat input at an altitude higher than at launch. The total mass loss versus altitude for various launch angles is shown in Fig. 8. The curves bear out the assumption that the sensible atmosphere ends at 40 km for these calculations.

Figure 9 shows the velocity retention as a function of launch angle. It is clearly seen that the vehicle retains more of its initial launch velocity at the higher launch angles, as would be expected since the vehicle is flying through less of the atmosphere.

For velocities of 8, 9, and 10 km/sec, at a launch angle of 16°, the mass loss is 40, 38, and 36 kg respectively. For a launch angle of 30° the corresponding mass losses are 13, 13, and 12 kg. In all cases as the launch angle is increased for a given launch velocity, the mass loss decreases. For increasing launch velocity at a given launch angle the mass loss also decreases. This surprising result is due to the fact that even though the velocity is higher and we expect higher heat transfer rates, the transit time for these velocities is less, and this results in a lower overall heat input to the vehicle. In any case, the mass loss due to ablation is a very small fraction of the vehicle mass, not exceeding 2% for any case considered.

In-tube Heating

The passage of the vehicle through the 33 atm propellant gas inside the launch tube could result in significant heating of the vehicle nose tip. Consequently the convective heat input to the vehicle's carbon-carbon composite nose tip was assessed. An analysis similar to that used for atmospheric transit was employed, using the conditions inside the tube. Since forced convection heating increases with Mach number, the calculations were carried out for the final section of the tube, where the velocity exceeds 7 km/sec and the Mach numbers are the highest. In this section the Mach number ranges from 7 to 12. In the preceding sections of tube the velocity and Mach number are sufficiently low that aerodynamic heating does not present a problem.

Results from a first order analysis indicate that ablation due to in-tube heating is minimal. For a launch velocity of 9 km/sec and a 3 cm initial nose tip radius the amount of mass ablated from the nose tip is only 0.23 kg. For a 10 km/sec launch velocity the ablated mass is only 1.4 kg, again a nearly negligible amount [26]. These increase with increasing nose tip radius, but only slightly. It is clear that if the nosecone is designed to survive atmospheric transit, no

additional thermal protection will be needed to protect the vehicle during the in-tube propulsion processes. The amount of mass ablated is so small that it does not present any problem to the in-tube propulsive modes.

Vehicle Stability

To examine the problem of stability and control during atmospheric transit the vehicle geometry and mass distribution must be defined. For the ram accelerator vehicle with a length of 7.5 m, a diameter of 0.76 m and a nosecone half-angle of 7° the center of gravity (CG) is ~5.3 m from the nose tip for the expected payload distribution. The center of pressure (CP), however, is 2.4 m from the nose tip. Since the CP is ahead of the CG, the vehicle is inherently unstable. Slender body small perturbation theory was used to obtain a rough estimate the magnitude of this instability [38].

The dynamic pressure on the vehicle varies by three orders of magnitude from the initial launch altitude of 4 km to 40 km, where atmospheric effects cease to play a role. Thus, the altitude is a dominant factor in the vehicle's dynamic response to perturbations. For a 1° incidence angle at 4 km altitude the angular acceleration is approximately 164 rad/sec^2, and at 40 km it is 0.16 rad/sec^2. In order to counter these angular accelerations active stability augmentation and/or spinning the vehicle is necessary. A more detailed investigation of this problem is clearly required, and possible stability augmentation devices need to be carefully considered.

The vehicle is also aerodynamically unstable during its flight through the launch tube. In order to keep the vehicle centered in the tube, it is proposed to use a set of three equally spaced guide rails attached to the bore of the tube. These rails would not interfere with the propulsion processes.

ORBITAL MECHANICS

Orbital Requirements

Once the atmospheric transit phase of the vehicle is successfully completed, the vehicle is in a ballistic trajectory, which, if left undisturbed, intersects the earth. Therefore, to place the projectile into low earth orbit (LEO), a circularization maneuver must be performed. This requires the use of an onboard propulsion system. In order to maximize the payload fraction of the vehicle, the amount of onboard propellant required for this maneuver must be minimized.

A major problem with any impulsive mass launch concept is that the time of launch from even an equatorial site is limited to specific intervals, so that the trajectory will intersect the desired final orbit when the space station or other space platform is in position to receive it. This limits the rate of launch and reception and therefore increases costs. The solution is to make use of a parking orbit.

To increase the flexibility of the ram accelerator launch concept, a parking orbit below that of the final orbit has been proposed [24, 25]. This orbit would be used to store vehicles until they are needed in the final orbit, at which time an orbital transfer would be performed. This allows for the continuous launching of vehicles without having to synchronize the vehicle launch with the orbital position of the space station. An equatorial orbit would be preferred, so that for frequent launches all the projectiles would be in the same orbital plane regardless of scheduling of launches.

Several launch sites in the vicinity of the equator have been identified which meet the necessary requirements for the ram accelerator mass launch concept [26]. One excellent possible site, which lies almost on the equator, is Mt. Kenya, in Africa. It provides the desired 4000 m launch altitude below the snow line, has a slope that can accommodate the proposed launch angles in the desired easterly direction, and is free of seismic disturbances.

Orbital Mechanics Scenario

Several possible methods of orbital insertion have been considered in the past [25]. Conventionally, a direct launch scheme would involve the launching of the vehicle at such an angle that the ballistic apogee would coincide with the altitude of the desired orbit. Another scheme that has been proposed involves launching to an initial apogee above the desired orbit, whereupon a burn is made to raise the perigee to coincide with the desired orbit. Both these methods have been shown to be more costly in terms of required onboard propellant mass than the one described below [25, 26].

The proposed scenario is shown in Fig. 10. It is a multistep maneuver that involves the use of an aerobraking pass through the upper atmosphere. This scenario offers the potential for the lowest onboard propulsion system mass. The vehicle is launched impulsively from the earth, traverses the atmosphere (Phase 1), and follows a ballistic trajectory to its first apogee (Phase 2). At this point a propellant burn is performed which increases the velocity of the vehicle so that it misses the earth (Phase 3a), but passes through the upper atmosphere (Phase 3b). Here the vehicle slows due to aerodynamic drag, i.e., aerobraking, and its apogee is lowered to coincide with the altitude of the desired parking orbit. Another burn is performed at that destination to circularize the orbit. From the parking orbit the vehicle can be transferred to the final desired orbit with a small burn at the appropriate time (Phase 5).

Of these maneuvers, the aerobraking is the most critical and requires the most analysis. For the range of launch velocities and angles considered the perigee altitude lies in the range of 30 to 50 km. At these altitudes the drag force on the vehicle is sufficient to perform the necessary velocity change without the use of special aerodynamic devices. At the same time this altitude range is sufficiently high that aerodynamic heating does not pose a problem for the vehicle.

A simple impulsive model was used to perform an initial assessment of the feasibility of aerobraking. It was first assumed that the aerobraking occurs over a small angular distance and is of short duration, so that the process could be considered to produce an impulsive velocity change at perigee. Although the model assumes an impulsive velocity change, it is based on the decrement of velocity across incremental steps of true anomaly in the orbital path. By summing the change in velocity over each increment it was possible to find a total velocity change for the process. The atmospheric model used was the same as that used for the atmospheric transit calculations, the two-part exponential given in Eqs. 4 and 5.

The major contribution of this preliminary model to the understanding of aerobraking was in finding the range of true anomaly over which aerobraking is significant. It was found that the velocity change outside of $+20^\circ$ and -20° is negligible, and that 98% of the velocity change occurs within $+10^\circ$ and -10° for the case of a launch at 9 km/sec at 20° [26]. The result is very similar for other launch angles and velocities, thus verifying the validity of the impulsive model as a first approximation. Using this information the actual flight path of the vehicle through the upper atmosphere was computed by numerical integration of the equations of motion. The drag coefficient used was that calculated at the end of the initial atmospheric transit following launch.

The aerobraking details are particularly dependent on the altitude of the first apogee, which is determined by the launch conditions. The apogee altitude for various launch angles and initial velocities is shown in Fig. 11. The perigee altitude, where the aerobraking occurs, is determined by the desired altitude of the parking orbit. The perigee altitude for various launch angles and launch velocities is shown in Fig. 12. If the launch angle is increased for a given launch velocity, or if the launch velocity is increased for a given launch angle, the perigee must dip lower into the earth's atmosphere. This is required because the vehicle must lose a greater amount of kinetic energy at perigee, in order that the vehicle's altitude at second apogee coincide with that of the desired parking orbit.

Figure 13 shows the total velocity change that the on-board propulsion system must impart to reach the desired 500 km final orbit for various launch angles and velocities. It is clearly seen that a minimum occurs at a specific launch angle for each launch velocity . Based on orbital considerations alone, the lower launch angles are preferred because the vehicle's initial flight path is more circular, which results in a lower ΔV requirement for the onboard rocket. At the lower launch angles, however, the vehicle travels through more of the dense atmosphere, which results in a greater velocity decrement due to drag, thus requiring a greater ΔV. At the higher launch angles the vehicle retains more of its initial velocity but, because its flight path is more eccentric, it requires a greater ΔV, which offsets the advantage of the greater velocity retention. Thus, a minimum occurs between the two extremes. For 8, 9, and 10 km/sec the optimum launch angles are 22°, 20°, and 18° respectively. These launch angles result in a minimization of the onboard propellant mass.

Final Hohmann Transfer

To conduct a Hohmann transfer between the parking and final orbits, the vehicle and the space station must be in the proper initial position if a rendezvous is to occur. The rate of transfer of vehicles to the space station is determined by the time it takes the space station and the vehicle to make the necessary initial relative angle. Table 1 lists the time to conjunction as a function of the number of vehicles in the parking orbit. If the rate of transfer of vehicles to a space station in equatorial orbit is assumed equal to the expected maximum rate of fire of the ram accelerator (approximately every two hours) the optimum steady state number of vehicles in the parking orbit is 69. Assuming a payload fraction of 50%, this rate of fire would permit delivering 12,000 kg of materials and supplies daily to a space station in equatorial orbit.

ONBOARD PROPULSION SYSTEM

The orbital requirements of the vehicle determine the necessary velocity change and performance characteristics of the onboard propulsion system. Both solid and liquid propellant systems were considered. Although desirable from the viewpoint of simplicity and low cost, solid motors were found to be impractical, as they are not robust enough to survive the 1000 g stress of launch and do not offer restart capability for orbital maneuvering. In addition, their performance characteristics were found to be inadequate, resulting in low payload mass fractions.

A system which appears to meet the necessary requirements is a bipropellant liquid rocket using monomethylhydrazine (MMH) and nitrogen tetroxide (NTO) as the fuel and oxidizer [39]. A schematic of the proposed system is shown in Fig. 14. The onboard propulsion system uses a pressurized propellant delivery system which employs a gas generator and diaphragm equipped

tank. This configuration can be easily expanded to incorporate the necessary attitude control thrusters required for the vehicle. The main engine operates at a chamber pressure of 20 atm and produces 10,000 N of thrust. The nozzle area ratio is 46, the throat diameter is 5.9 cm, and the exit diameter is 40 cm. The main engine and nozzle are designed to fit within the tail portion of the vehicle (see Fig. 6). A specific impulse of 297 sec is attained by this system. Figure 15 shows how the mass of the onboard propulsion system varies with the required amount of velocity change. For 8, 9, and 10 km/sec launch velocities at their respective optimum launch angles, the total mass of the onboard propulsion system, including the necessary propellants, is 980 kg, 630 kg, and 480 kg respectively.

PAYLOAD MASS FRACTION

From the results presented above, it is clear that the payload carrying capacity of the ram accelerator vehicle is strongly dependent on the initial conditions at launch and on the orbital mechanics scenario. As noted previously, the multi-step maneuver with aerobraking requires the least amount of onboard rocket propellant for the orbit circularization maneuver, for any feasible launch velocity. An optimum launch angle for each launch velocity considered was also found. The overall mass inventories and payload mass fractions for launch velocities of 8, 9, and 10 km/sec at their respective optimum launch angles are shown in Table 2.

Not surprisingly, the payload mass fraction increases with increasing launch velocity. Thus, for economic reasons, the highest possible launch velocity should be used. There is, however, a practical upper limit. Velocities much above 10 km/sec are not desirable for launch to low earth orbit. As the launch velocity is increased, the launch angle must be decreased. Thus, a larger percentage of the initial kinetic energy is lost to aerodynamic drag, resulting in an increased heat input to the vehicle. In addition, the velocity change requirements during aerobraking increase significantly, requiring the vehicle to dip lower into the earth's atmosphere, increasing the dynamic stability problems and increasing the aerodynamic heating to the point where it may no longer be neglected. Higher velocities also result in higher apogee altitudes, which lead to excessive travel times.

A launch velocity of 10 km/sec results in a payload mass fraction of 0.43 for the present vehicle design. It is likely that this fraction can be increased to 0.50, or more, by improving the structural design to reduce its mass and by increasing the specific impulse of the onboard propulsion system (specific impulses of approximately 320 should be attainable with the current selection of propellants through optimized design). Additional gains in the payload mass fraction may also be realized through further optimization of the orbit circularization maneuvers.

Refinements of the in-tube propulsion modes may also reflect favorably on the payload fraction. For example, if the peak acceleration is reduced, the peak cycle pressure also decreases and the vehicle structure can be made lighter. If the average acceleration is lowered, however, a longer launch tube will be required. This may offset the economic gains presented by a higher payload mass fraction. Further research clearly needs to be performed in the area of the possible economic tradeoffs of this launch system.

DISPOSITION OF SPENT VEHICLES

The disposition of the ram accelerator vehicles, once they have been intercepted and unloaded at the space station, presents several possible options: 1) discard them in orbit, 2) disassemble them and use the payload vessels to store materials at the space station, 3) use them as sources of material for space structures or other uses, 4) use tether techniques to send clusters of them back to earth on re-entry trajectories for refurbishment and re-use, 5) de-orbit the vehicles and allow them to burn up on re-entry. Clearly, option 1 must be ruled out because of the severe orbital clutter that would result. Options 2 and 3 are more desirable but place additional design constraints on the vehicles to optimize their adaptability to other uses and require some means of returning the salvaged onboard rockets to earth. Option 4 would require that the ablative shield be designed to also survive atmospheric re-entry, which would place a much more severe heat load on the vehicle than the initial upward leg of the journey. In addition, recovery and refurbishment operations would have to be implemented. Finally, option 5 does not appear to be acceptable because portions of the vehicles, such as the nose cones and tail sections might survive re-entry and reach the ground. Which of the feasible options turns out to be the most desirable will depend on their relative impacts on overall launch costs. This issue needs to be studied further.

CONCLUSIONS

The ram accelerator mass launch system was conceived as a means for economically launching acceleration-insensitive materials to low earth orbit. Using the release of chemical energy in a propulsive cycle similar to that of a conventional ramjet, a vehicle with a mass of the order of several metric tons can be accelerated in a stationary tube to velocities as high as 12 km/sec at a nearly constant acceleration. A point design case study of launching a 2000 kg vehicle into low earth orbit with current technology was carried out.

Two propulsive cycles are required to accelerate the vehicle to its desired launch velocity. The thermally choked mode accelerates the vehicle to 2.5 km/sec, at which point it makes a transition to the superdetonative mode which accelerates the vehicle to the desired final launch velocity (8-10 km/sec). A structural configuration integrating the payload vessel with the vehicle design was chosen and a graphite/epoxy composite was selected in order to withstand the high pressures and accelerations attendant to the launch process. A carbon-carbon ablating nosecone protects the vehicle from the aerodynamic heating which occurs during atmospheric transit. The ablative mass loss is shown to be very small, of the order of 1-2% of the vehicle mass. The vehicle requires stability augmentation devices, such as control surfaces to maintain dynamic stability during flight. A multi-step orbital mechanics scenario is proposed which incorporates an aerobraking maneuver. For orbital circularization and maneuvering, an onboard propulsion system using storable liquid propellants is proposed.

The payload mass fraction ranges from 19% for a launch velocity of 8 km/sec to 43% for a launch velocity of 10 km/sec. Judicious design and further refinements of this launch system are needed in order to increase the mass fraction. Methods for recycling the vehicles or for returning them to earth should also be investigated, and a detailed cost analysis of the mass launch system should be performed.

The ram accelerator mass launch system described here is not intended to replace other existing or proposed launch systems, but rather to complement them. For example, the ram accelerator would release both the Space Shuttle and the Advanced Launch System from the expensive burden of carrying the bulk of the acceleration-insensitive payloads to low earth orbit. It is envisioned that a spectrum of different launch systems will evolve as the space program matures,

each designed to be cost effective for a specific range of applications. A good analogy can be found in earth based transportation systems, which utilize specialized vehicles or systems to minimize costs and to maximize efficiency. For example, over distances exceeding a few hundred kilometers, airplanes are used to transport people; trains, trucks, and ships are used to transport bulk solid and liquid materials; and pipelines are used to transport bulk liquids and gases. The same philosophy will need to be applied to develop a cost-effective space transportation system. The ram accelerator mass launcher would play an integral role in such a system.

ACKNOWLEDGEMENTS

This work was supported by NASA Grant No. 1-746 and by the NASA/USRA Advanced Design Program. The authors are indebted to A. Berschauer, E. Christofferson, P. Clement, C. Rodriguez, S. Vaddey, J. Vickers, and L. Wolf for their assistance in performing the preliminary system analysis which formed the basis of this paper.

REFERENCES

1. Bruckner, A. P., "A Gun-Launched Satellite," Spaceflight, Vol. 7, 1965, pp. 118-121.

2. Eder, D., "A Low Cost Earth Based Launch System and its Effects on Space Industrialization," Space Manufacturing 4: Proceedings of the 5th Conference, Princeton, NJ, May 18-21, 1981, pp. 221-229.

3. O'Neill, G. K., "The Colonization of Space," Physics Today, Vol. 27, 1974, pp. 32-40.

4. Chilton, F., Hibbs, B., Kolm, H., O'Neill, G. K., and Phillips, J., "Electromagnetic Mass Drivers," Progress in Aeronautics and Astronautics, Vol. 57, 1977, pp. 37-61.

5. Barber, J. P., "Direct Launch Using the Electric Rail Gun," Proceedings of the JANAF Propulsion Meeting, Vol. 1, 1983, pp. 51-56.

6. Kolm, H., et al., "An Electromagnetic First Stage Space Cargo Launcher," Space Manufacturing 4: Proceedings of the 5th Conference, Princeton, NJ, May 18-21, 1981, pp. 231-233.

7. Hawke, R. S., Brooks, A. L., Fowler, C. A., and Peterson, D. R., "Electromagnetic Railgun Launchers: Direct Launch Feasibility," AIAA Journal, Vol. 20, July 1982, pp. 978-985.

8. Winterberg, F., "The Electromagnetic Rocket Gun," Acta Astronautica, Vol. 12, 1985, pp. 155-161.

9. Miller, L. A., Rice, E. E., Earhart, R. W., and Conlon, R. J., "Preliminary Analysis of Space Mission Applications for Electromagnetic Launchers," Final Technical Report, Contract No. NAS 3-23354, Battelle Columbus Laboratories, Columbus, OH, August 30, 1984.

10. Wilbur, P. J., Mitchell, C. E. and Shaw, B. D., "The Electro-thermal Ramjet," J. Spacecraft and Rockets, Vol. 20, Nov.-Dec. 1983, pp. 603-610.

11. Glumb, R. J., and Krier, H., "Concepts and Status of Laser Supported Rocket Propulsion," J. Spacecraft and Rockets, Vol. 21, Jan.-Feb. 1984, pp 70-79.

12. Huberman, M., et al., "Investigation of Beamed Energy Concepts for Propulsion," AFRPL-TR-76-66, Oct. 1976, p. 113.

13. Kare, J. T., ed., "Proceedings SDIO/DARPA Workshop on Laser Propulsion, Lawrence Livermore National Laboratory, 7-18 July 1986, Volume 1-Executive Summary," CONF-860778, Lawrence Livermore National Laboratory, CA, Nov. 1986.

14. Powers, M. V., Zaretsky, C., and Myrabo, L. N., "Analysis of Beamed Energy Ramjet/Scramjet Performance," AIAA Paper 86-1761, AIAA/SAE/ASME/ASEE 22nd Joint Propulsion Conference, Huntsville, AL, June 16-18, 1986.

15. Hertzberg, A., Bruckner, A. P., and Bogdanoff, D. W., "Ram Accelerator: A New Method for Accelerating Projectiles to Ultrahigh Velocities," AIAA Journal, Vol. 26, Feb. 1988, pp. 195-203.

16. Bruckner, A. P., Bogdanoff, D. W., Knowlen, C., and Hertzberg, A., "Investigation of Gasdynamic Phenomena Associated with the Ram Accelerator Concept," AIAA Paper 87-1327, AIAA 19th Fluid Dynamics, Plasma Dynamics and Lasers Conference, Honolulu, HI, June 8-10, 1987.

17. Knowlen, C., Bruckner, A. P., Bogdanoff, D. W., and Hertzberg, A., "Performance Capabilities of the Ram Accelerator," AIAA Paper 87-2152, AIAA/SAE/ASME/ASEE 23rd Joint Propulsion Conference, San Diego, CA, June 29-July 2, 1987.

18. Brackett, D. C. and Bogdanoff, D. W., "Computational Investigation of Oblique Detonation Ramjet-inTube Concepts," J. Propulsion and Power, Vol. 5, May-June 1989, pp. 276-281.

19. Hertzberg, A., Bruckner, A. P., Bogdanoff, D. W., and Knowlen, C., "The Ram Accelerator and its Applications: A New Chemical Approach for Reaching Ultrahigh Velocities," Proceedings of the 16th International Symposium on Shock Tubes and Waves, Aachen, West Germany, July 26-30, 1987.

20. Bruckner, A. P., Knowlen, C., Scott, K. A., and Hertzberg, A., "High Velocity Modes of the Thermally Choked Ram Accelerator Concept," AIAA Paper 88-2925, AIAA/SAE/ASME/ASEE 24th Joint Propulsion Conference, Boston, MA, July 11-13, 1988.

21. Yungster, S., Eberhardt, S., and Bruckner, A.P., "Numerical Simulation of Shock-Induced Combustion Generated by High Speed Projectiles in Detonable Gas Mixtures," AIAA Paper No. 89-0673, AIAA 27th Aerospace Sciences Meeting, Reno, NV, January 9-12, 1989. (Also accepted for publication in AIAA Journal).

22. Yungster, S. and Bruckner, A.P., "A Numerical Study of the Ram Accelerator Concept in the Superdetonative Velocity Range," AIAA Paper No. 89-2677, AIAA/ASME/SAE/ASEE 25th Joint Propulsion Conference, Monterey, CA, July 10-12, 1989.

23. Kull, A., Burnham, E.A., Knowlen, C., Bruckner, A.P., and Hertzberg, A., "Experimental Studies of Superdetonative Ram Accelerator Modes," AIAA Paper No. 89-2632, AIAA/ASME/SAE/ASEE 25th Joint Propulsion Conference, Monterey, CA, July 10-12, 1989.

24. Hertzberg, A., and Bruckner, A. P., eds., "The Ram Accelerator Concept: A Method of Direct Launch of Space Cargo to Orbit," Final Report, AA420/499, NASA/USRA Advanced Space Design Program, University of Washington, Seattle, WA, June 1987.

25. Bruckner, A. P., and Hertzberg, A., "Ram Accelerator Direct Launch System for Space Cargo," Paper IAF-87-211, 38th Congress of the International Astronautical Federation, Brighton, United Kingdom, Oct. 10-17, 1987.

26. Bruckner, A. P., and Hertzberg, A., eds., "Design of a Ram Accelerator Mass Launch System," Final Report, AA420/499, NASA/USRA Advanced Space Design Program, University of Washington, Seattle, WA, June 1988.

27. Kaloupis, P. and Bruckner, A.P., "The Ram Accelerator: A Chemically Driven Mass Launcher," AIAA Paper 88-2968, AIAA/SAE/ASME/ASEE 24th Joint Propulsion Conference, Boston, MA, July 11-13, 1988.

28. Hertzberg, A. and Bruckner, A.P., "Study of a Ram Cannon for a Space Cargo Launcher," Final Report, NASA Grant No. NAG 1-746, University of Washington, Seattle, WA, Oct. 1988.

29. Krier, H., and Summerfield, M., eds., Interior Ballistics of Guns: Progress in Aeronautics and Astronautics, Vol. 66, AIAA, New York, 1979.

30. Bogdanoff, D. W., NASA Ames Research Center, Moffet Field, CA, private communication, April 1988.

31. Hogg, I. V., The Guns 1939-45, Ballantine Books Inc., New York, 1970.

32. DOD, NASA, Advanced Composites Design Guide, Wright-Patterson Air Force Base, OH, 1983.

33. Algor Interactive Systems Inc., ALGOR SUPERSAP, Finite Element Analysis System, Pittsburgh, PA, 1988.

34. Allen, H. J., Seiff, A., and Winovich, W., "Aerodynamic Heating of Conical Entry Bodies in Excess of Earth Parabolic Speed," NASA TR R-185, 1963.

35. Ghosh, S., "A Study of Transpiration Cooling for Sharp Conical Bodies in Hypersonic Flow," M.S. Thesis, Department of Aeronautics and Astronautics, University of Washington, Seattle, WA, June 1988.

36. Schreier, S., Compressible Flow, John Wiley and Sons, New York, 1982, pp. 406-455.

37. NOAA, NASA, USAF, U.S. Standard Atmosphere, 1976, Washington, D.C., Oct. 1976.

38. Liepmann, H. W., and Roshko, A., Elements of Gasdynamics, GALCIT Aeronautical Series, John Wiley and Sons, New York, 1965, pp. 303-313.

39. Schmitz, B., Rocket Research Co., Redmond, WA, Private Communication, Feb. 1988.

TABLE 1. Time to Conjunction

Number of Vehicles	Angular Spacing (deg)	Time to Reach Conjunction (hrs)
1	360	138.1
5	72	27.62
10	36	13.8
25	14.4	5.52
50	7.2	2.76
69	5.22	2.0
100	3.6	1.38

TABLE 2. Vehicle Mass Inventory

Payload Launch Velocity (km/sec)	Optimum Launch Angle (deg)	Vehicle Structural Mass (kg)	Ablator Mass (kg)	Onboard Propulsion Mass (kg)	Payload Mass (kg)	Payload Mass Fraction
8	22	625	22	980	373	0.19
9	20	625	25	630	720	0.36
10	18	625	29	480	866	0.43

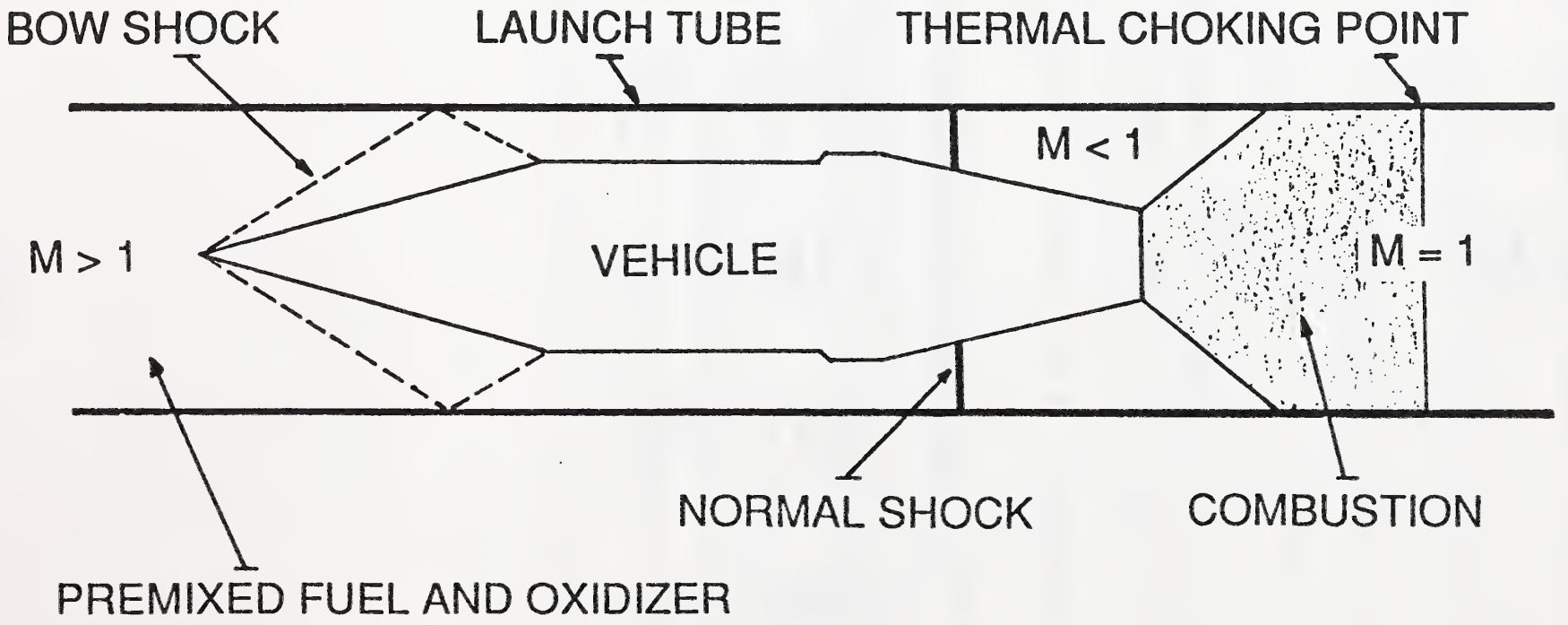

Fig. 1 Subsonic Combustion, Thermally Choked Mode of Operation

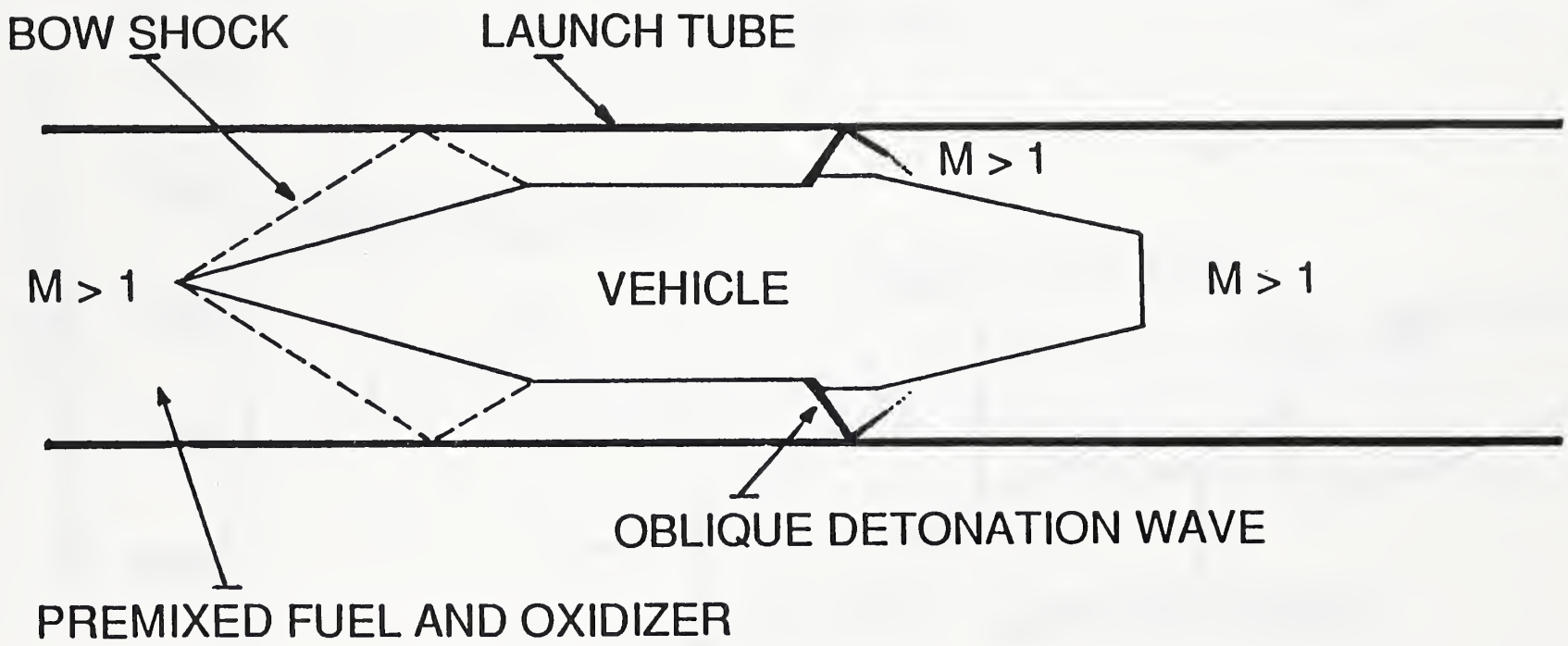

Fig. 2 Oblique Detonation Wave (Superdetonative) Mode of Operation

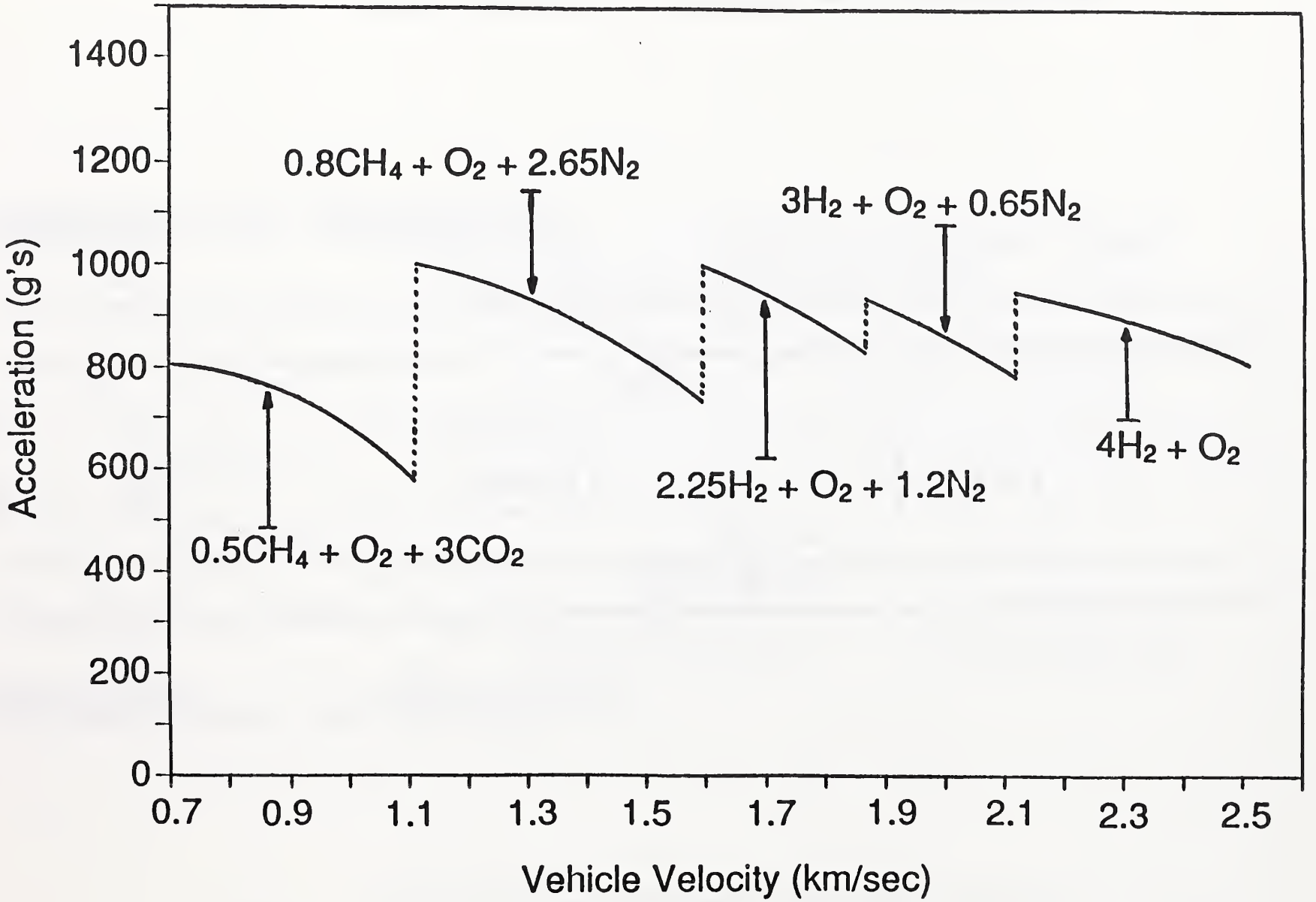

Fig. 3 Acceleration Profile of the Thermally Choked Mode of Operation Showing the Required Propellant Mixtures to Achieve 2.5 km/sec

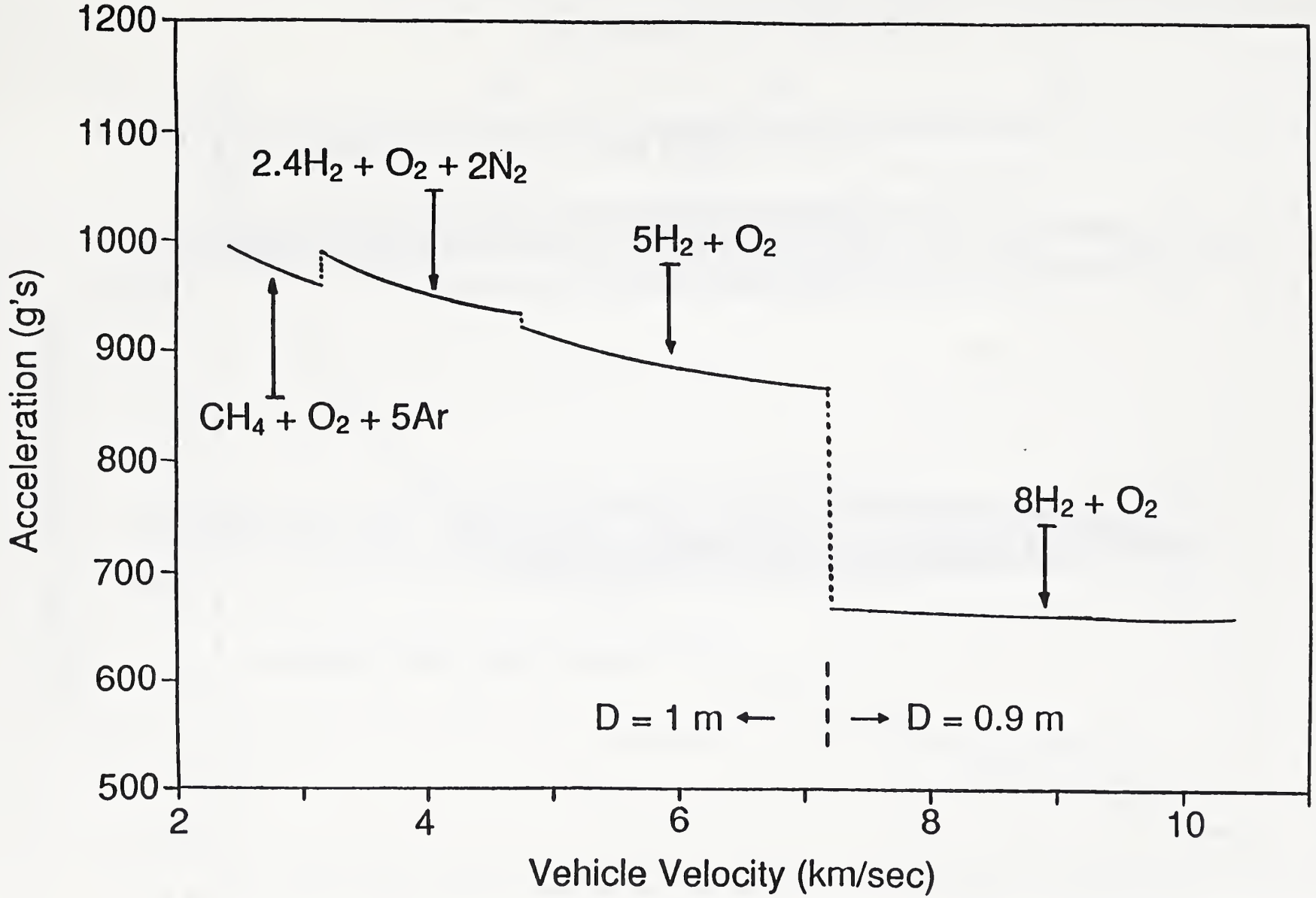

Fig. 4 Acceleration Profile of the Superdetonative Mode of Operation Showing the Required Propellant Mixtures to Achieve 10 km/sec

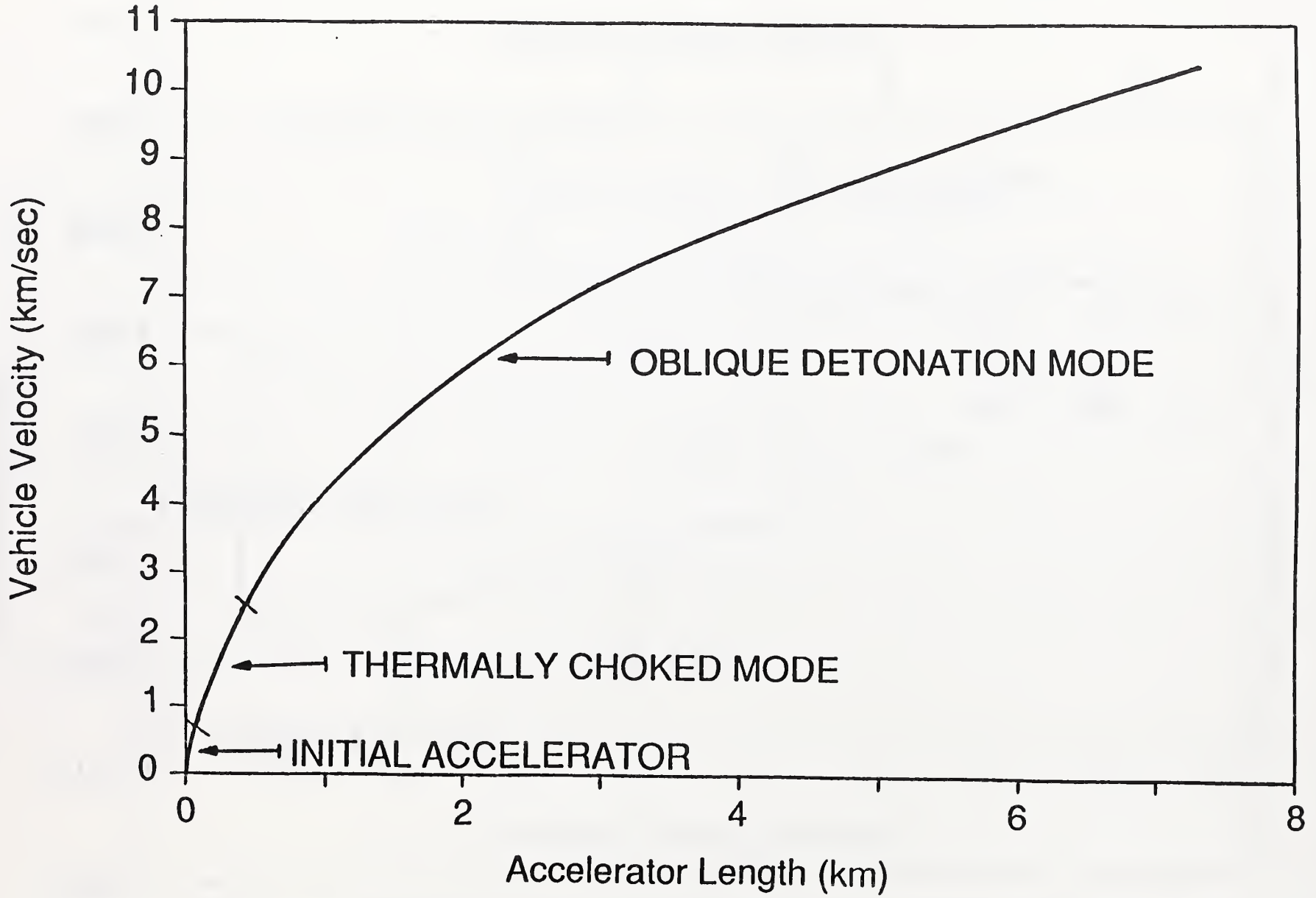

Fig. 5 In-Tube Velocity Profile for the Ram Accelerator Propulsion Modes

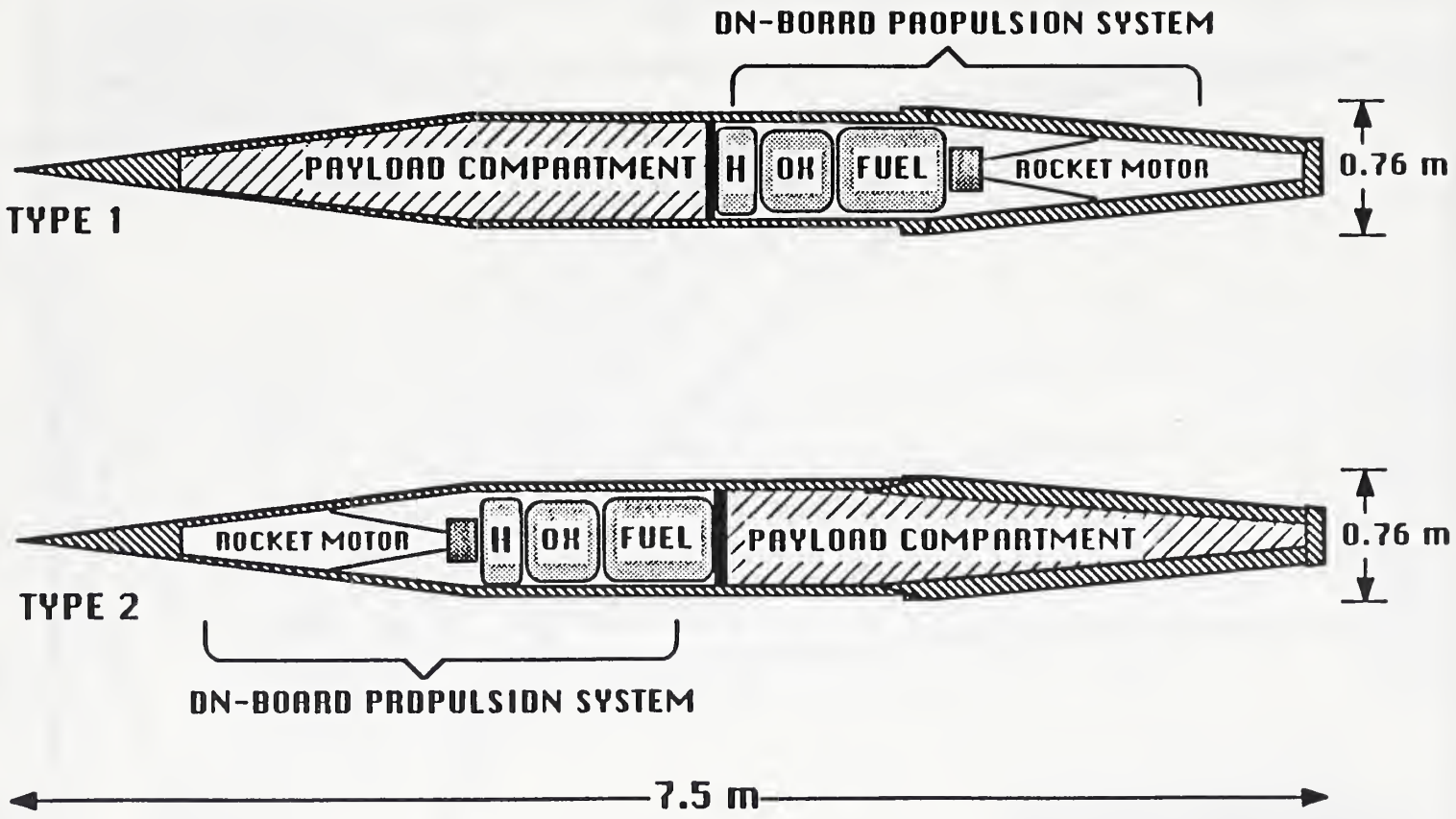

Fig. 6 Two Possible Vehicle Configurations

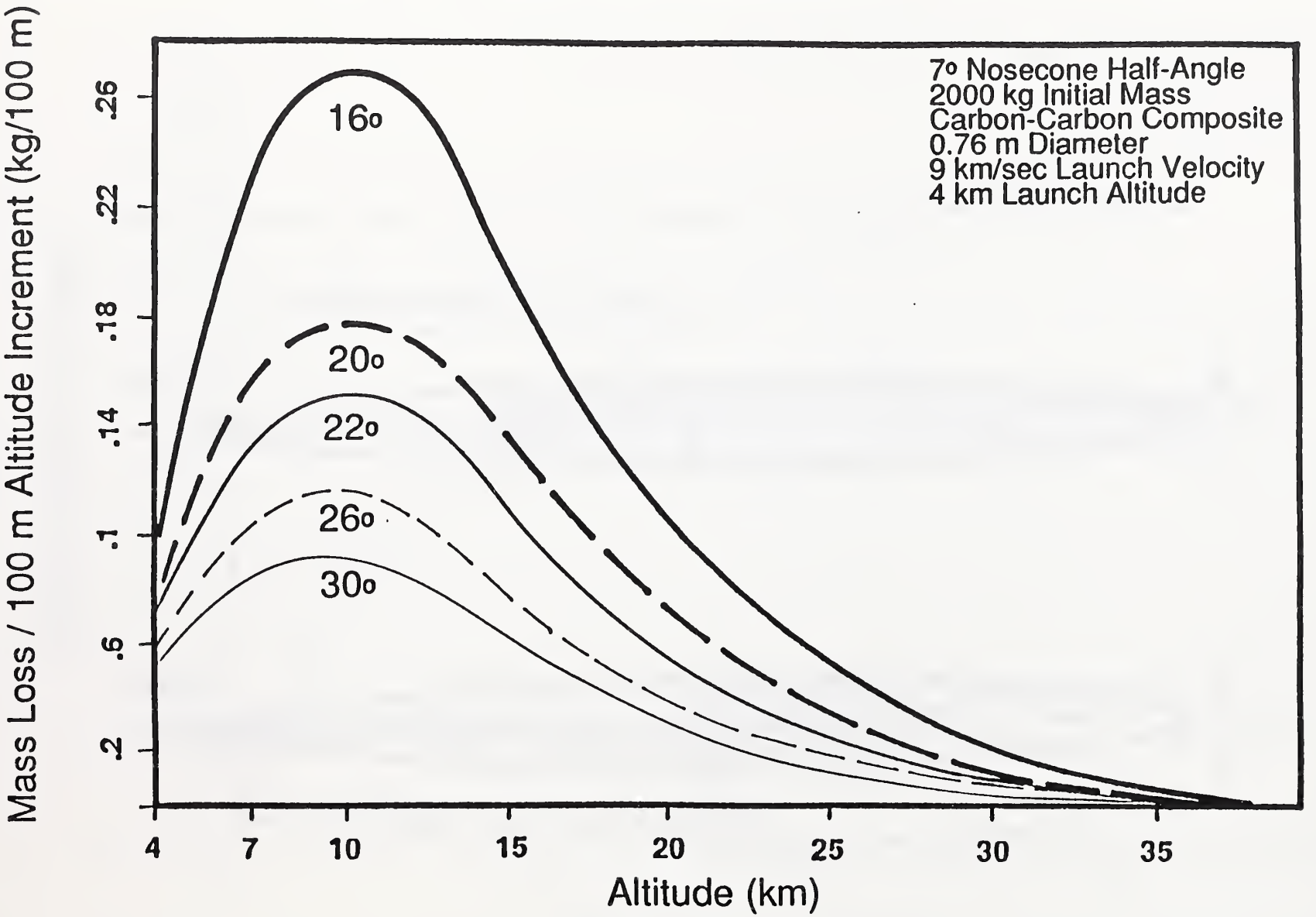

Fig. 7 Mass Loss Rate per 100 m Altitude Increment Versus Altitude for Various Launch Angles, for 9 km/sec Launch Velocity

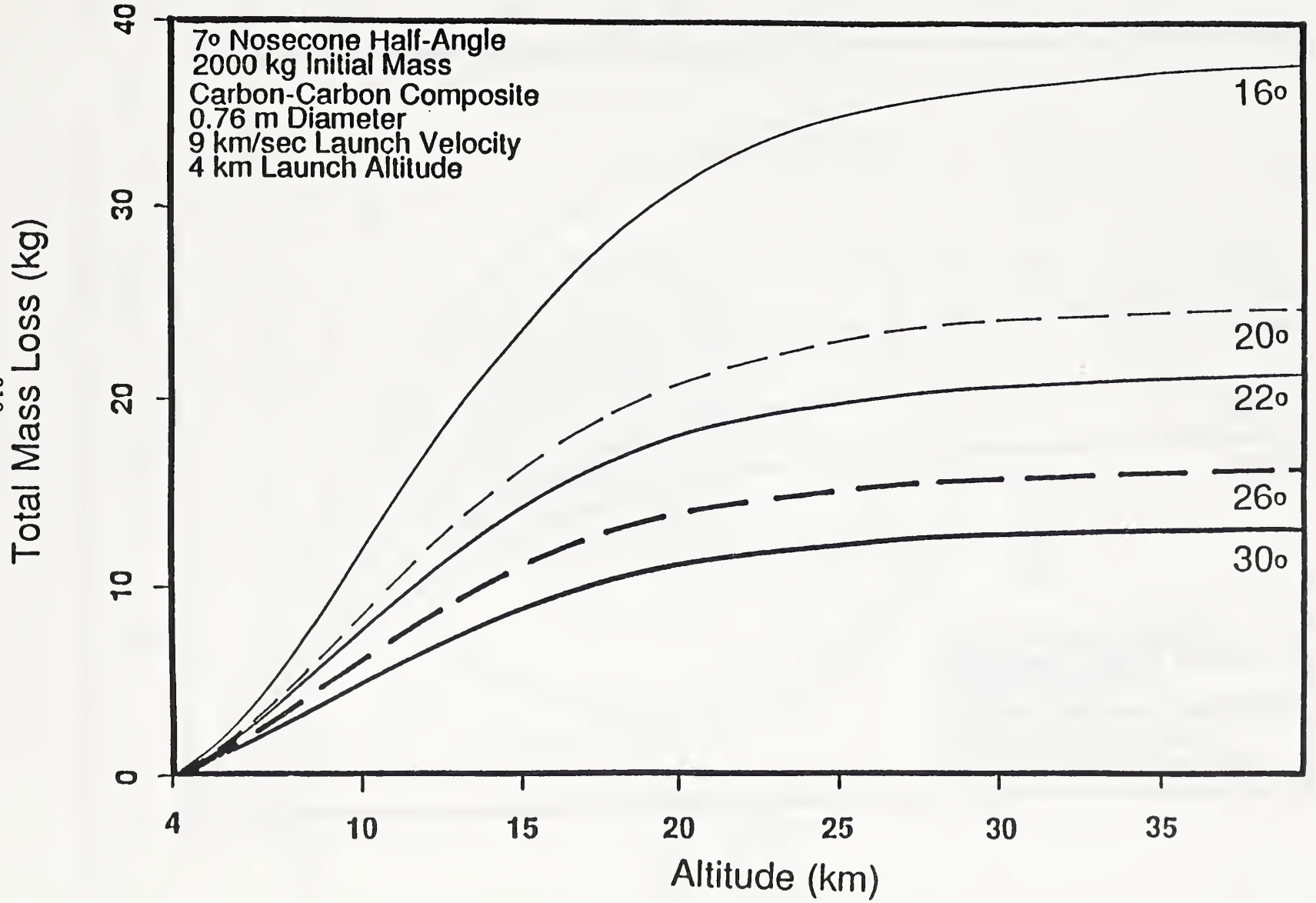

Fig. 8 Total Mass Loss Versus Altitude for Various LAunch Angles, for 9 km/sec Launch Velocity

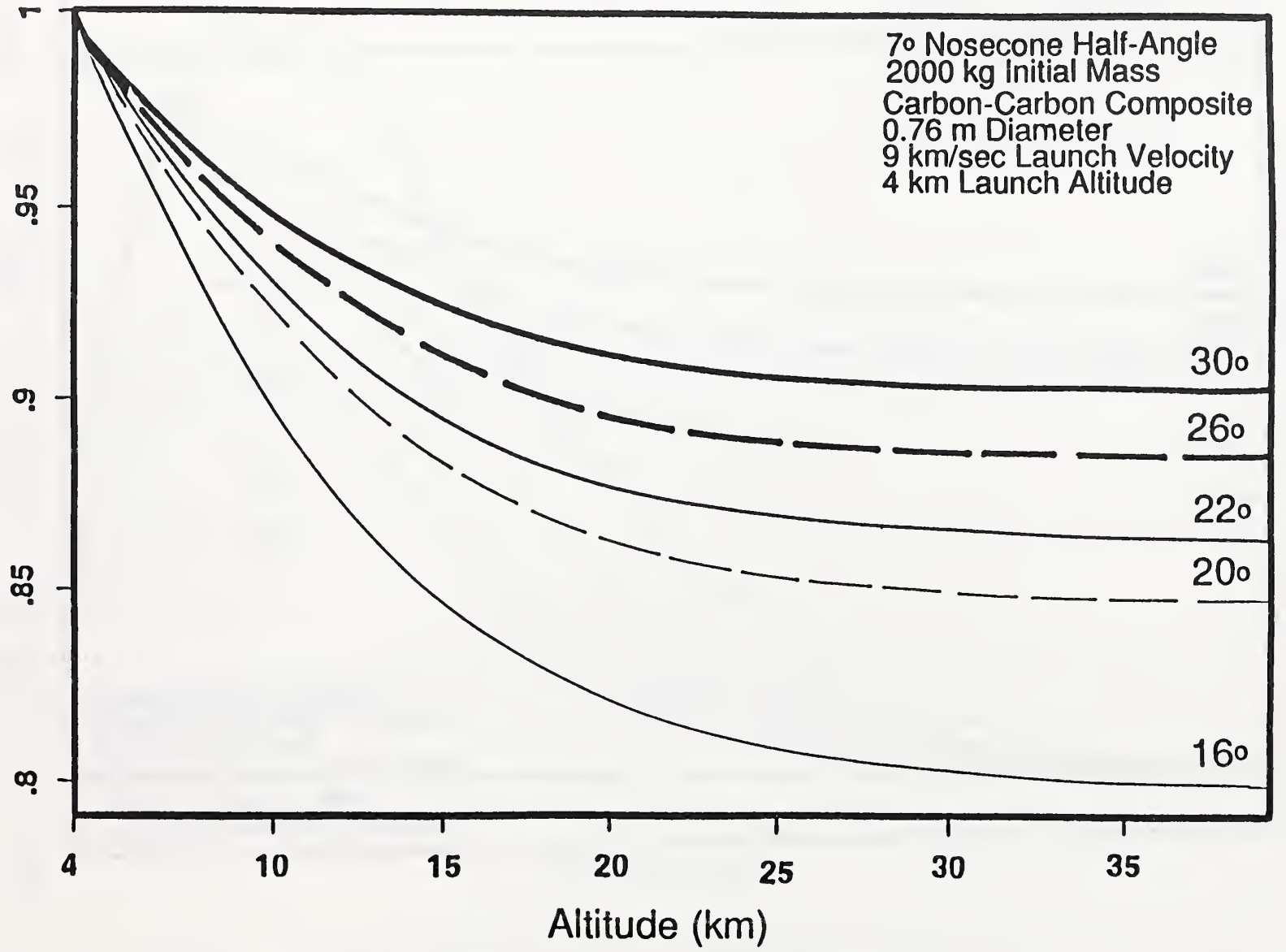

Fig. 9 Velocity Retention V/V_o Versus Altitude for Various Launch Angles, for 9 km/sec Launch Velocity

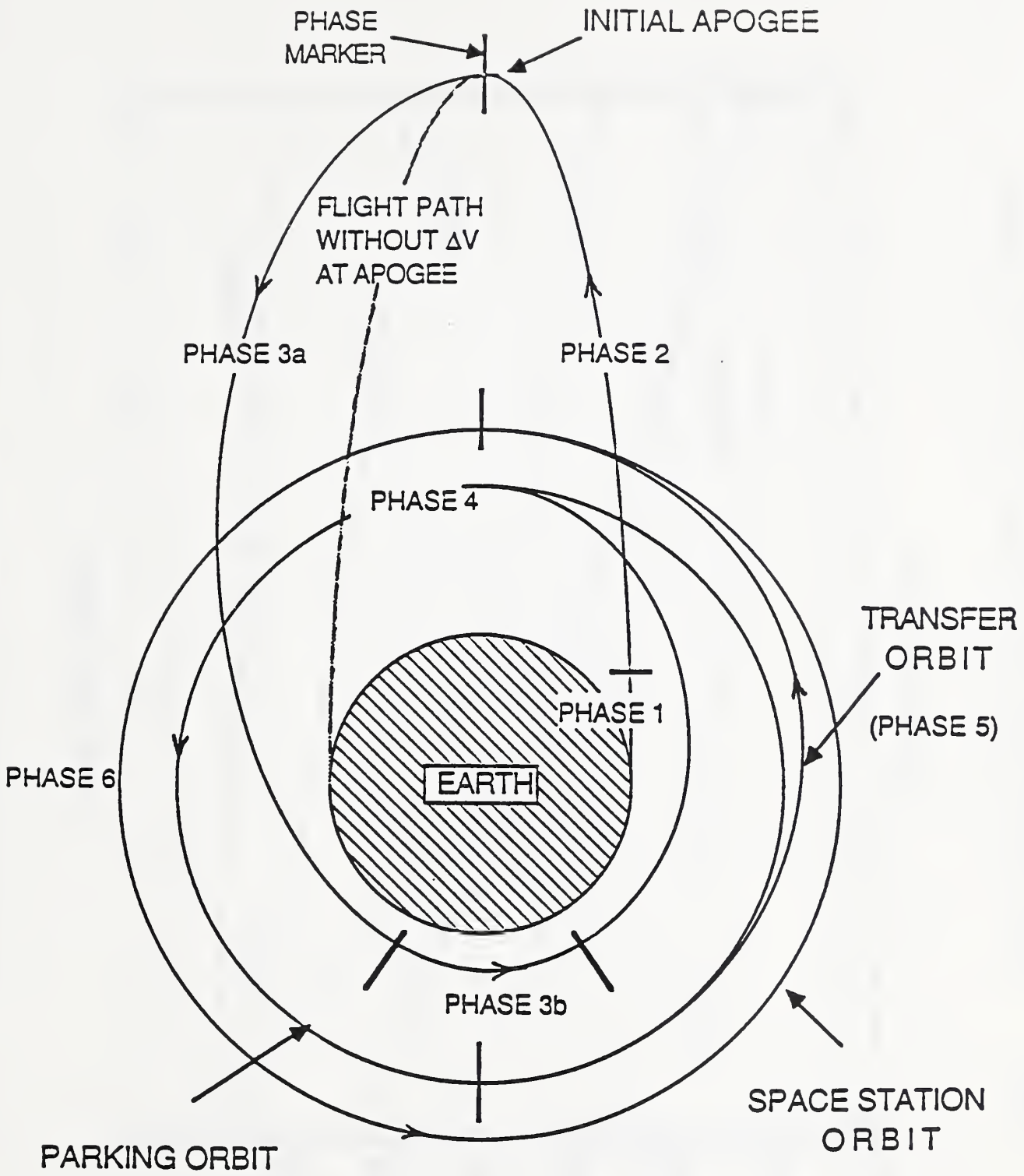

Fig. 10 Proposed Multistep Orbital Trajectory with Aerobraking Maneuver

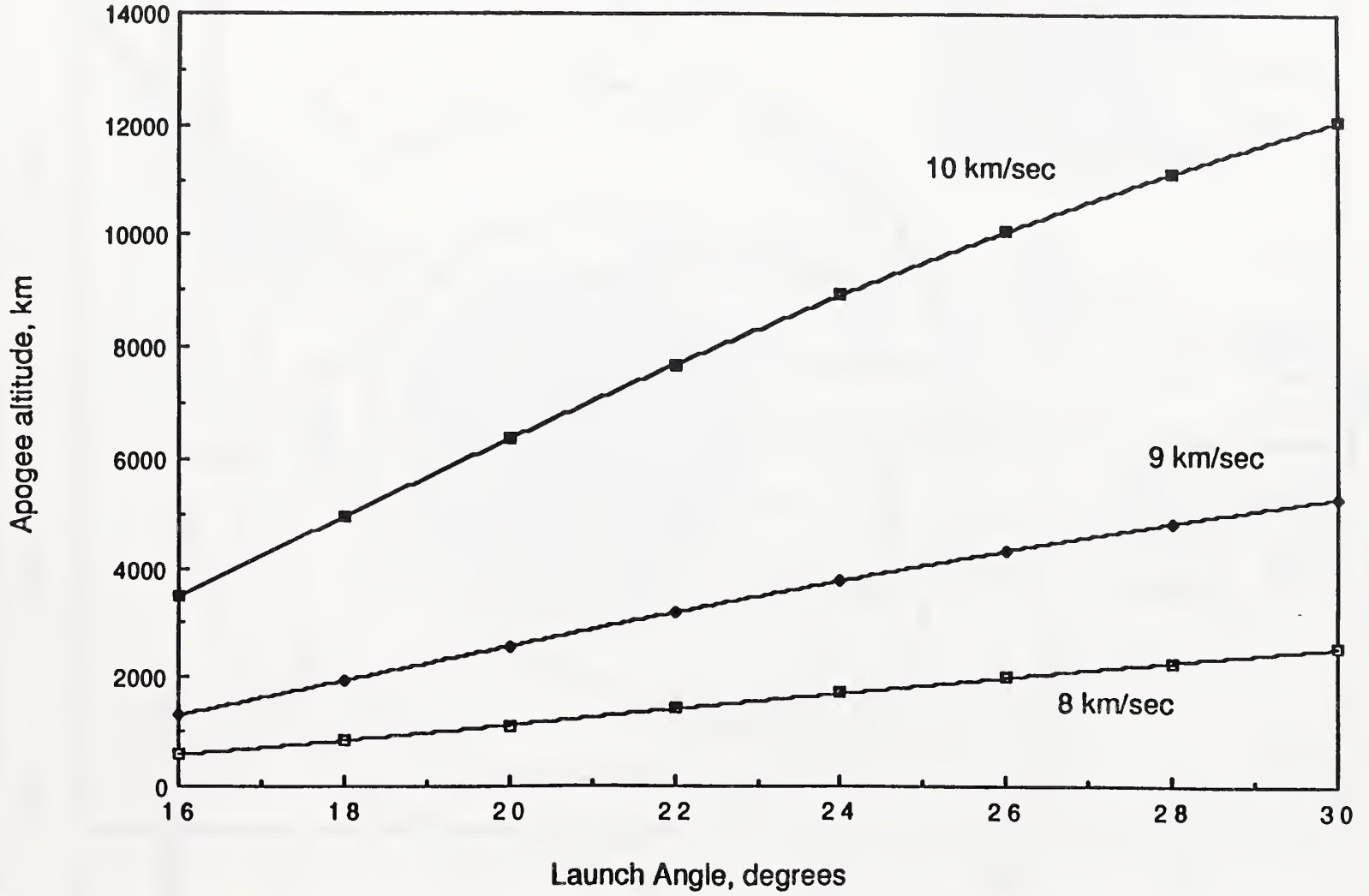

Fig. 11 Apogee Altitude Versus Launch Angle for Various Launch Velocities

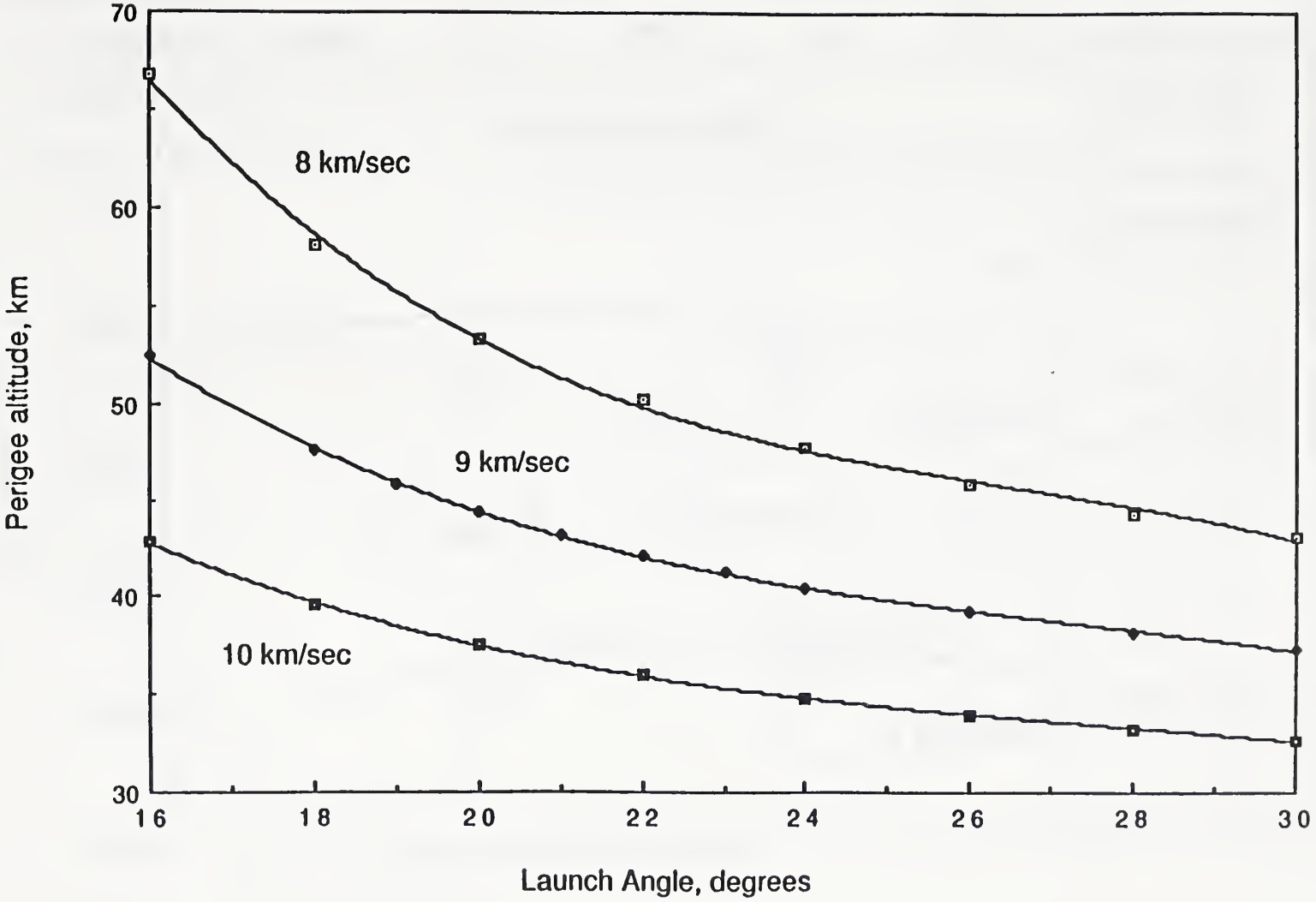

Fig. 12 Perigee Altitude Versus Launch Angle for Various Launch Velocities

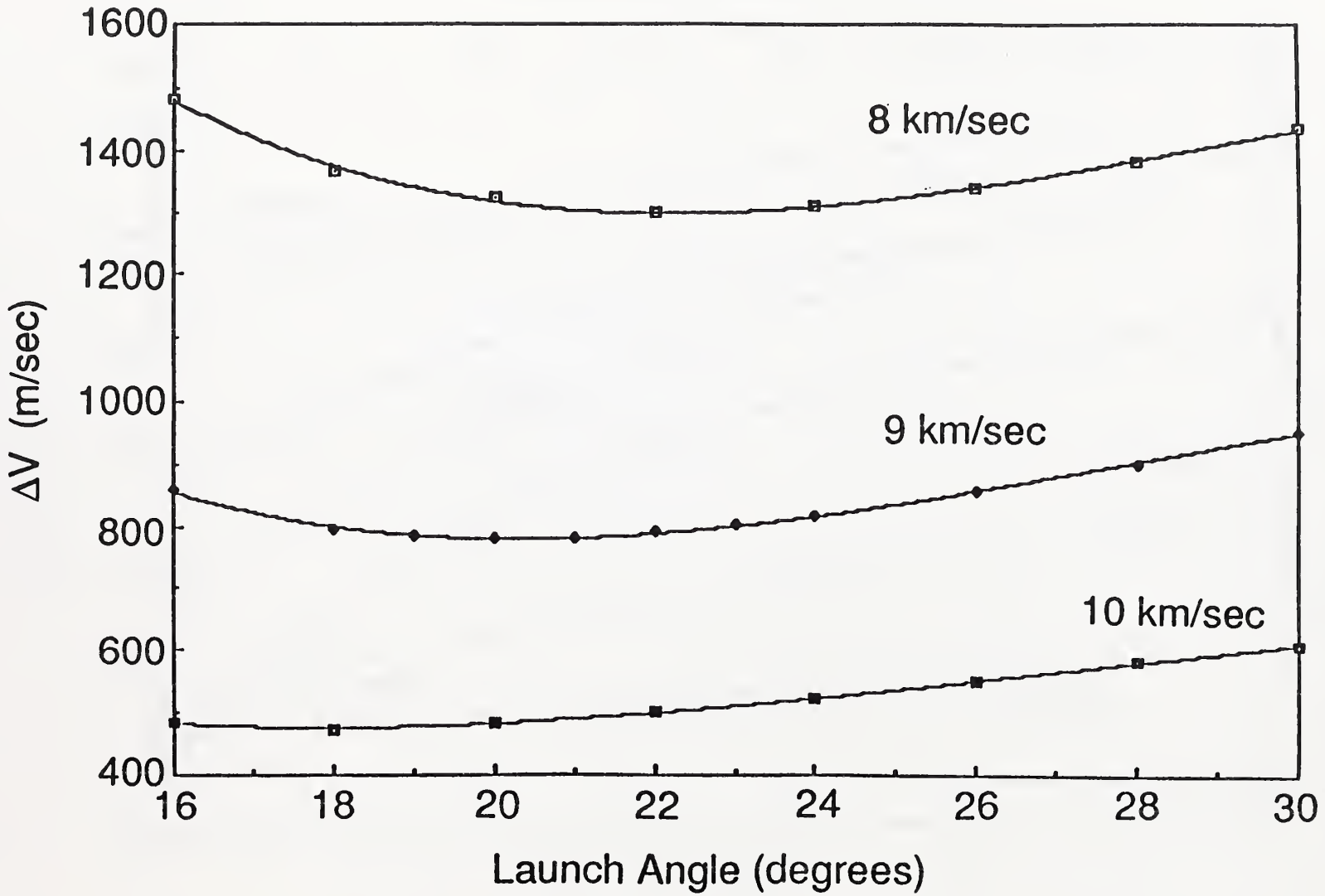

Fig. 13 Total ΔV Required from Onboard Propulsion System for Ram Accelerator Vehicle to Reach 500 km Orbit as a Function of Launch Angle for Various Launch Velocities.

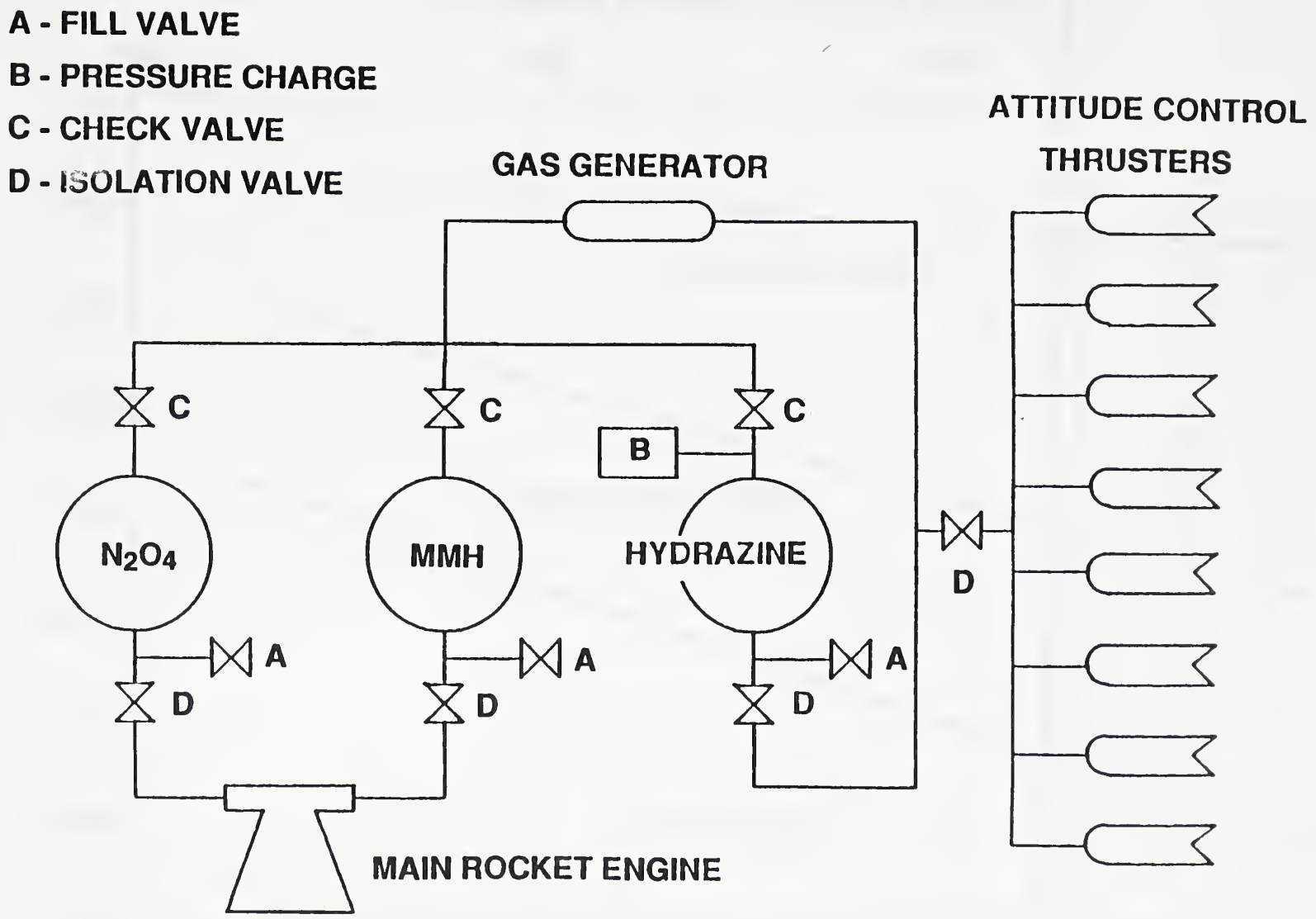

Fig. 14 Schematic of the Pressure Fed Onboard Liquid Propellant System, Showing the Delivery System and the Attitude Control Thrusters

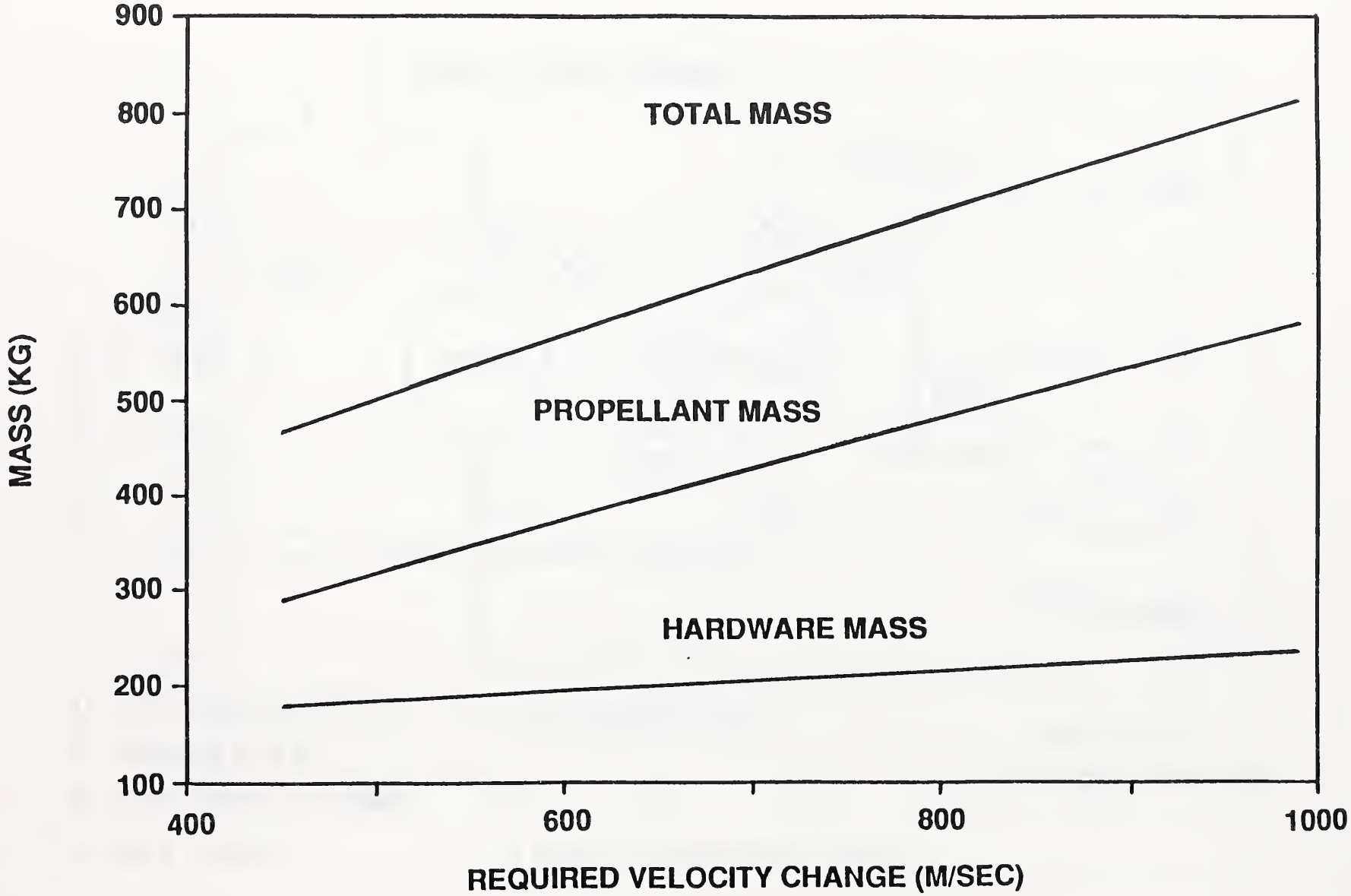

Fig. 15 Onboard Propulsion System Mass as a Function of Required Velocity Change

Appendix A: Final Attendance List

Final Attendance List

Reducing the Cost of Space Infrastructure and Operations

November 20-22,1989

National Institute of Standards and Technology
Gaithersburg, Maryland

Laura Ayres
Office of Space
Commerce
Depart. of Commerce
Room 7064, HCHB
Washington, DC 20230

Kevin Barquinero
NASA
600 Independ Ave. SW
Rm 536 MC ST
Washington, DC 20546

Greg Barr
1412 Potomac Ave SE
Washington, DC 20003

James Beggs
SpaceHab, Inc.
5408 Falmouth Rd.
Bethesda, MD 20816

Barry Beringer
US House of
Representatives
Washington, DC 20515

Ed Bock
General Dynamics
Space Division
3636 Mt. Laurence Dr
San Diego, CA 92117

M.P. Boland
IBM/SID-Houston
3700 Bay Area Blvd.
MC 3206B
Houston, TX 77058

John Cozzi
Carroon and Black
Inspace
3 Bethesda Metro Ctr
Suite 450
Bethesda, MD 20814

Rich Dalbello
Space Commerce, DOC
Room 7064
HCHB
Washington, DC 20230

Donald Dalton
US DOC
Main Comm HCHB
Rm 4882
Washington, DC 20230

Ralph J. Dornsife
Army Corps-CERL
PO Box 4005
USACE-CERL-EM
Champaign, IL 61824

Stanley Dorr
Westinghouse
1512 W. Pratt St.
Baltimore, MD 21223

Joe Engleberger
Transition Research
Corp.
15 Great Pasture Rd.
Danbury, CT 06810

Jim English
CanDive Services, Ltd.
1367 Crown St.
N. Vancouver, BC
V7J-1G4
Canada

Maxime Faget
Space Industries, Inc.
711 West Bay Area Bd
Webster, TX 77598

Chris Faranetta
Space Studies Institute
5 Cresent Ave.
Rocky Hill, NJ 08553

Walter Froehlich
Int'l Science Writers
5531 Warwick Pl.
Washington, DC 20815

Ed Gabris
NASA Headquarters
Code MD
600 Indep. Ave. SW
Washington, DC 20546

Cary Gravatt
NIST
Bldg. 101, 5th flr.
Gaithersburg, MD 20899

Joseph L. Gray
US DOC
8060-13th St.
Rm 820
Silver Spring, MD 20910

T. Brian Gray
Gray Matter Solutions
4611 Governors Dr.
#111
Huntsville, AL 35805

Joel Greenberg
Princeton Synergetics
900 State Road
Princeton, NJ 08540

Don Groves
IDA
1801 N. Beauregard
Street
Alexandria, VA
22311-1772

R. W. Hamilton
Hamilton Research, Ltd.
80 Grove St.
Tarrytown, NY
10591-4138

Carol Hammer
Energy Research Group
120 Fourth Ave.
Oakmont, PA 15139

C.S. Hatfield
IBM Corp
3700 Bay Area Blvd.
6220/MC6272
Houston, TX 77058-1199

Helmut Hellwig
NIST
Poly, A339
Gaithersburg, MD 20899

Abe Hertzberg
Univ. of Washington
Aero. & Energ. Proj.
MS SL-10
Seattle, WA 98195

Steve Höeser
General Research Corp.
145 Jeff. Davis Hgwy
Suite 601
Arlington, VA 22202

David A. Hornig
Carnegie Group, Inc.
Five PPG Place
Pittsburgh, PA 15222

Steven J. Isakowitz
Martin Marietta Astron
PO Box 179
G1600
Denver, CO 80201

Douglas Isbell
Washington Technology
1953 Gallows Rd.
#130
Vienna, VA 22182

Aleta Jackson
High Frontier
2800 Shirlington Rd.
#405 A
Arlington, VA 22206

Jordin T. Kare
LLNL
PO Box 808
L-278
Livermore, CA 94550

Jay Kniffen
AMROC
847 Flynn Rd.
Camrillo, CA 93010

Paula Korn
Independent Consultant
490 M St., SW
W305
Washington, DC 20024

Sam Kramer
NIST
Tech. B119
Gaithersburg, MD 20899

Robert Lindberg
Orbital Sciences Corp.
12500 Fair Lakes Cir
Fairfax, VA 22033

Curtis Lomax
NASA Ames Res Ctr
Moffett Field
239-15
Mtn. View, CA 94035

Paul Marshall
NASA
17019 Parkridge Blve
555
Reston, VA 22091

Mike Miller
Ctr. for Innovative Tech.
CIT Bldg, Suite 600
2214 Rock Hill Rd.
Herndon, VA 22070

Thomas Mininger
Computer Sciences Corp
1100 West St.
Rm 355
Laurel, MD 20708

Stephen L. Morgan
Center for Innov Tech
2214 Rock Hill Rd.
CIT Tower, Ste 600
Herndon, VA 22070

Mark Owensby
Office of Space Commerce
Depart. of Commerce
Room 7064, HCHB
Washington, DC 20230

Barbara Ragan
Coldwell Banker Res Affil
8608 Rolling Rd.
Springfield, VA 22153

Lon Rains
Space News
6339 Commercian Dr.
Springfield, VA 22159

Catherine Rawlings
US House of Represent.
US House of Rep.
Washington, DC 20515

Curt Reimann
NIST
Admin. A1134
Gaithersburg, MD 20899

Thomas F. Rogers
The Sophron Foundation
7404 Colshire Dr.
McLean, VA 22102

Carl Schueler
Hughes SBRC
75 Coromar Dr.
Goleta, CA 93117

Richard W. Scott
Space Services, Inc.
600 Water St., SW
Suite 207
Washington, DC 20024

Linda Shiner
Air & Space/Smithsonian
370 L'Enfant Prom,SW
Washington, DC 20024

Rand E. Simberg
Rockwell Int'l
12214 Lakewood Blvd.
Downey, CA 90241

Michael C. Simon
General Dynamics Space Sy
PO Box 85990
MZ C1-7106
San Diego, CA 92111

Joseph J. Snyder
Sea Power Magazine
2008 Ashley Dr.
Shepherdstown, WV 25443

Courtney Stadd
National Space Council
Exec. Off. of Pres.
Washington, DC 20500

Bill Stone
NIST
Bldg 226, B168
Gaithersburg, MD 20899

Jack Suddreth
SRS Technologies
1500 Wilson Blvd
Suite 800
Arlington, VA 22209

Robert Summersgill
Space Studies Institute
7718C Lexton Pl.
Springfield, VA 22152

William A. Swenson
American Cyanamid
124C Camp Hill Rd.
Pomona, NY 10970

David G. Tarbert
1234 Grouse Dr.
Pittsburgh, PA 15243

Glen Taylor
NOAA
Suite 805, WSC-5
6010 Executive Blvd.
Rockville, MD 20852

Jay S. Troetschel
Ichor
600 Grant St.
1410
Pittsburgh, PA 15219

Randolph Ware
ETCO/ UNADVCO
3300 Mitchell Lane
Boulder, CO 80301

Alison Watkins
The Egan Group
1701 K St., NW
12th Fl.
Washington, DC 20006

Mike Weeks
NASA Headquarters
Mail Code RN
600 Indep. Ave. SW
Washington, DC 20546

Eckards Weinrich
Arianespace
1747 Penn. Ave. NW
Washington, DC 20007

Jack Whitelaw
LTV Aerospace &
Defense
1725 Jeff Davis Hwy
Suite 900
Arlington, VA 22202

Ray Williamson
OTA
Congress of US
Washington, DC
20510-8025

Alfred J. Wolfson
EER Systems Corp
10289 Aerospace Rd.
Seabrook, MD 20706

Peter Wood
Space Cosultant
1250 S Washington St
#210
Alexandria, VA 22314

Dietmar Wurzel
DLR/German Aerospace
One Farragut Sq Sout
Suite 600
Washington, DC 20006